SECOND-ORDER STRUCTURAL IDENTIFICATION VIA STATE SPACE-BASED SYSTEM REALIZATIONS

by

KENNETH F. ALVIN

B. S., Iowa State University, 1983

M. S., University of Colorado, 1990

A dissertation submitted to the

Faculty of the Graduate School of the

University of Colorado in partial fulfillment

of the requirements for the degree of

Doctor of Philosophy

Aerospace Engineering Sciences

1993

This dissertation for the Doctor of Philosophy degree by

Kenneth F. Alvin

has been approved for the

Department of

Aerospace Engineering Sciences

by

_____

K. C. Park

_____

L. D. Peterson

Date _____

Alvin, Kenneth F. (Ph.D., Aerospace Engineering Sciences)
Second-Order Structural Identification
via State Space-Based System Realizations
Dissertation directed by Professor K. C. Park

The present study has focused on the estimation of normal modes and their mode shapes from experimental data. The determination of accurate undamped modal parameters from experimental data in the presence of damping is critical for the construction or reconciliation of structural dynamics models, in which the physical mass and stiffness properties are isolated from the dissipative effects of damping. The response functions measured from experimental data are generally approximated by finite-dimensional first-order difference equations in the time-domain using algorithms such as ERA. Such models, or *realizations*, do not directly determine the mass and stiffness matrices, except under special restrictions. This thesis develops a family of transformation-based methods for the construction of second-order structural dynamic models from first-order system realizations of experimental data. Transformations to a second-order canonical basis are effective for the systematic extraction of the normal modes from the first-order realizations.

Two separate transformations are developed: the Common Basis-Normalized Structural Identification (CBSI) procedure and the Uncoupled Nonproportional Damping (UNDAMP) procedure. CBSI transforms the first-order state space realizations to the well-known form of second-order proportionally-damped equations of motion. The resulting structural dynamics models are shown not only to yield the accurate normal modes for

proportionally damped cases, but also improved estimates of the normal mode shapes in the presence of nonproportional damping as compared to existing methods. The UNDAMP algorithm extends the CBSI method to a global transformation spanning up to the full space of the damped modes. As such, UNDAMP is capable of filtering out the contaminating attributes of nonproportional damping from the CBSI-determined normal modal parameters. Furthermore, UNDAMP is applicable to the extracting of nonproportional damping when the number of measured sensors is less than the number of identified modes.

Using normal modal parameters determined by CBSI or UNDAMP, a method for determining minimal-order mass and stiffness matrices is presented. The resultant model is an alternative second-order realization with measured physical variables as degrees of freedom, and the derived mass and stiffness matrices are shown to have asymptotic equivalence to Guyan-reduced and/or Craig-Bampton-synthesized structural models.

The efficiency and accuracy of the present transformation methods are demonstrated through simulated numerical examples and experimental data. In particular, the present methods are used to reconstruct frequency response functions and applied to damage detection in truss structures. Finally, the implications of these analytical techniques for structural system identification and directions for future research are also discussed.

Dedicated to my wife Carol and to my parents

for their love and support.

ACKNOWLEDGEMENTS

The author is pleased to acknowledge the contributions of his advisor Professor K. C. Park. His technical insights, encouragement, and skills in all aspects of computational dynamics have proven invaluable throughout the author's graduate study. Professor Park's patient and trustful guidance have allowed this author the freedom he needed to accomplish this work. The author is also greatly indebted to Assistant Professor L. D. Peterson for his keen technical direction and enthusiasm. Dr. Peterson's outstanding knowledge of system identification and modal testing has played a fundamental role in the evolution of this research, and the author could not have completed this work without his contributions. Finally, the author would like to personally thank Dr. W. K. Belvin of NASA Langley for his feedback on the early development of this research and in particular pointing out the importance of addressing the problem of nonproportional damping.

The author would like to thank the many other individuals who directly or indirectly helped to shape the content of this research. The author acknowledges the support of his Advisory Committee; Professor C. A. Felippa, Associate Professor C. Farhat, Associate Professor R. Y. S. Pak and Professor T. L. Geers. Also, the help provided by those associated with the Structural Dynamics and Controls Laboratory; S. Doebling, S. Bullock and M. Barlow. The author would particularly like to thank F. Hemez for his invaluable help in the area of model correlation and damage detection. The financial support provided by a grant from NASA Langley Research Center

(number NAG-1-1200) is gratefully acknowledged. Support for the Structural Dynamics and Controls Laboratory was provided by grants from the McDonnell Douglas Foundation and Shimizu Corporation.

Many colleagues at the University of Colorado and Harris Corporation have made significant contributions to the author's work and career development. Thanks in particular to S. Alexander, B. Haugen, J. Schuler, L. Crivelli and J. Chiou at CU-Boulder. Thanks also to M. Carroll, T. Yost, F. Bourne and F. Arthur at Harris. To all his friends and colleagues, past and present, many many thanks.

Finally, this author wishes to thank his wife, parents and family, for more than words can express.

CONTENTS

CHAPTER

I. INTRODUCTION 1

1.1 Modal Testing, System Identification and Model Validation 1

1.2 Motivation for the Present Work 11

1.3 Survey of Previous and Related Work 15

1.4 The Present Structural Identification Research 19

1.5 Outline of the Dissertation 23

II. STATE SPACE REALIZATION FOR STRUCTURAL IDENTIFICATION 27

2.1 State Space Formulations of Structural Dynamics 27

2.1.1 General State Space Realizations 29

2.1.2 State Space Realizations for Structural Dynamics: Physical Variables 32

2.1.3 State Space Realizations for Structural Dynamics: Normal Modal Variables 33

2.1.4 State Space Damped Modal Realizations 35

2.1.5 Displacement-Output Equivalent Realizations 38

2.2 Frequency Domain Modal Testing and Data Analysis 40

2.2.1 Frequency Domain Characterization of Structures 42

2.2.2 Determining Response Functions from Modal Tests 42

2.3 The System Realization Problem and ERA 44

2.3.1 Discrete-Time Models and System Realization 46

2.3.2 The Eigensystem Realization Algorithm (ERA) 48

2.3.3 Determining the Damped Modal Realization from ERA 52

2.4 Concluding Remarks 54

III. COMMON BASIS-NORMALIZED STRUCTURAL IDENTIFICATION 56

3.1 Introduction 56

3.2 Normal Mode Estimation from Damped Modes 58

3.2.1 Traditional Approximation Methods 59

3.2.2 McMillan Normal-Form Transformation 62

3.3 Transformation to Canonical Variables 63

3.4 The CBSI Algorithm 66

3.4.1 Basic CBSI for Proportional Damping 67

3.4.2 Least-Squared CBSI for General Viscous Damping 70

3.4.3 A Symmetrical CBSI Method 75

3.4.4 Summary of CBSI Algorithm 78

3.5 Numerical Examples 80

3.5.1 Mode Shape Collinearity Indicators 80

3.5.2 3-DOF Spring-Mass System with Proportional Damping 81

3.5.3 3-DOF Spring-Mass System with Nonproportional Damping 86

3.5.4 36-DOF Planar Truss with Light Nonproportional Damping 89

3.6 Concluding Remarks 94

IV. EXTRACTION OF NORMAL MODAL PARAMETERS FOR NONPROPORTIONAL DAMPING 96

4.1 Introduction 96

4.2 The Inverse Damped Vibration Problem 99

4.3 The UNDAMP Basis Correction Algorithm 102

4.3.1 Global UNDAMP Transformation to Second-Order Basis 102

4.3.2 Solution of $\mathbf{V}_d$ for Well and Overdetermined Constraint 106

4.3.3 Solution of $\mathbf{V}_d$ for Underdetermined Constraint 107

4.3.4 Displacement Consistency Criterion for $\mathbf{V}_d$ 108

4.4 Computational Considerations for Determining $\mathbf{V}_d$ 111

4.4.1 Underdetermined Solution via Augmented Outputs ... 112

4.4.2 Optimization-Based Underdetermined Solution 113

4.4.3 Two-Stage Iterative SQP Procedure for $\mathbf{S}_{nn}$ 115

4.5 Summary of Damping Correction Algorithm 117

4.5.1 Well-Determined Transformation Constraint 117

4.5.2 Over-Determined Transformation Constraint 118

4.5.3 Under-Determined Transformation Constraint 118

4.6 Numerical Examples for the UNDAMP Algorithm 119

4.6.1 3-DOF Spring-Mass System
with Nonproportional Damping 119

4.6.2 36-DOF Planar Truss with
Light Nonproportional Damping 123

4.7 Concluding Remarks 126

V. MINIMAL-ORDER
MASS AND STIFFNESS DETERMINATION 128

5.1 Introduction 128

5.2 Reduced Mass and Stiffness from
Normal Modal Parameters 131

5.3 Minimum-Order Mass and Stiffness from
Normal Modal Parameters 136

5.4 Numerical Examples 140

5.4.1 3-DOF Undamped Spring-Mass System 140

5.4.2 36-DOF Planar Truss with Light Nonproportional Damping 141

5.5 Conclusions 145

VI. IMPLEMENTATION AND APPLICATIONS 147

6.1 Implementation of Present Procedures 147

6.1.1 Description of *ModalID* Data Blocks 148

6.1.2 SSI Toolbox Functions 150

6.2 Numerical Example of FRF Reconstruction 153

6.3 FRF Reconstruction for Experimental Data 157

6.3.1 Modal Testing and Data Collection 157

6.3.2 System Realization and Normal Modal Estimation 160

6.3.3 Results of FRF Reconstruction using Experimental Data 162

6.4 Damage Detection Using Experimentally Measured Stiffness 174

6.4.1 Inverse Connectivity Algorithms 175

6.4.2 Numerical Example: Planar Truss Structure 182

6.4.3 Application of Damage Detection to the MUDDE Testbed Structure 182

VII. CONCLUSIONS 189

7.1 Summary of Work 189

7.2 Directions for Future Research 192

7.2.1 System Realization 192

7.2.2 Second-Order Models and Normal Modes Estimation 192

7.2.3 Applications of Structural System Identification 193

REFERENCES. 194

TABLES

TABLE

3.1 Notation Used in Example Problems 83

3.2 Comparison of Normal Mode Shape Estimates for 3-DOF Nonproportionally Damped Model 88

3.3 Comparison of Normal Mode Shape Estimates for 36-DOF Nonproportionally Damped Truss 91

4.1 Comparison of Modal Assurance Criteria for Normal Modes Estimates on Nonproportionally-Damped Planar Truss 124

6.1 Discrete Impulse Response Accuracy Indicators for Second-Order Model Estimates of MUDDE Structural Dynamics 171

FIGURES

FIGURE

1.1 The central role of structural testing 2

1.2 Damped Modal Parameter Estimation from Modal Testing 4

1.3 Normal Modal Parameter Determination from Finite Element Modeling and Analysis 7

1.4 Finite Element Model Correlation Process 9

1.5 The Real Influence of Nonproportional Damping on the Displacement Response of Two Closely-Space Modes 10

1.6 Missing Links in Parameter Equivalence Between Test and Analysis Models 12

2.1 Components of the Frequency Response Function for Proportional and Nonproportional Damping 38

3.1 Spring-Mass Example Model 82

3.2 Planar Truss Example Model Showing Input Force and Output Displacement Locations 90

3.3 Modal Damping Matrix for Truss Example 91

3.5 Complex Mode Shape with High Phase Collinearity 92

3.5 Complex Mode Shape with Poor Phase Collinearity 92

3.7 Comparison of Estimated Normal Mode Shapes for Planar Truss, Mode 23 93

3.7 Comparison of Estimated Normal Mode Shapes for Planar Truss, Mode 27 93

4.1 Reduction in Quadratic Constraint Violation using the Minimization Method for Under-determined Problems 125

4.2 UNDAMP-derived Nondiagonal Damping Matrix for Nonproportionally Damped Planar Truss Problem 125

4.3 Improvement in Estimated Normal Mode Shape Using UNDAMP 126

5.1 Measured Reduced Stiffness of Planar Truss 142

5.2 Minimal-Order Measured Stiffness of Planar Truss 142

5.3 Minimal-Order Measured Mass of Planar Truss 143

5.4 Singular Values of the Residual Stiffness 144

5.5 Convergence of the Reduced Stiffness Matrix 144

5.6 Convergence of Reduced Element Stiffnesses in Planar Truss 145

6.1 Hierarchical Organization of the SSI Toolbox 151

6.2 FRF Reconstruction for Planar Truss: ST vs. CBSI 155

6.3 FRF Reconstruction for Planar Truss: ST vs. CBSI, Expanded View of Midrange Frequencies 155

6.4 FRF Reconstruction for Planar Truss: CBSI vs. UNDAMP . 156

6.5 FRF Reconstruction for Planar Truss: CBSI vs. UNDAMP, Expanded View of Midrange Frequencies 156

6.6 MUDDE Structure at the McDonnell Douglas Structural Dynamics and Controls Laboratory, University of Colorado 158

6.7 Tri-Axial Accelerometer Configuration on the MUDDE Structure 160

6.8 Complex Mode Shapes for MUDDE Modal Test Realization . 163

6.9 FRF Reconstruction for Experimental Data: CBSI-SYM vs. ST, Point Inertance for Input 3 165

6.10 FRF Reconstruction for Experimental Data: CBSI-SYM vs. ST, Expanded View of Low-Midrange Frequencies 166

6.11 FRF Reconstruction for Experimental Data: CBSI-SYM vs. ST, Expanded View of Midrange-High Frequencies 167

6.12 FRF Reconstruction for Experimental Data: CBSI-SYM vs. ST, Inertance from Input 3 to Input 2 168

6.13 FRF Reconstruction for Experimental Data: CBSI-SYM vs. ST, Expanded View of Low-Midrange Frequencies 169

6.14 FRF Reconstruction for Experimental Data: CBSI-SYM vs. ST,

Expanded View of Midrange-High Frequencies 170

6.15 FRF Reconstruction for Hex Truss Experimental Data: CBSI-SYM vs. ST 173

6.16 Structural Segmentation into Identified DOF, Boundary DOF, and DOF within a Damaged Substructure 176

6.17 Convergence of Undamaged Element Stiffness for Numerical Planar Truss Example 183

6.18 Convergence of Damaged Element Stiffness for Numerical Planar Truss Example 183

6.19 Convergence of Element Stiffness Changes for Numerical Planar Truss Example 184

6.20 Convergence of Undamaged Longeron Stiffness for MUDDE Truss Modal Test 186

6.21 Convergence of Damaged Longeron Stiffness for MUDDE Truss Modal Test 186

6.22 Resultant Changes in Longeron Stiffness for the MUDDE Structure: 173 Modes in Damaged Model 187

6.23 Resultant Changes in Longeron Stiffness for the MUDDE Structure: 140 Modes in Damaged Model 187

CHAPTER I

INTRODUCTION

1.1 Modal Testing, System Identification and Model Validation

The experimentally validated modeling of complex structures subjected to dynamic loading and active controls has been a subject of intense research for the last decade. While the variety and efficiency of finite element modeling and analysis tools have undergone enormous growth over the same period, systematic improvements in the accuracy and reliability of finite element analysis for structural dynamics have proven much more difficult to achieve. This is due in part to the governing assumptions of linearity in the analysis, the statistical variance in the properties of structural components due to fabrication tolerance, and the increased heterogeneity of the structures being modeled. It is also true, however, that much of the limitation of model accuracy is due to the ever-growing complexity of lightweight structures, including articulating joint designs and the introduction of new hybrid materials. Even a high degree of modeling precision cannot compensate for a lack of experience with the real measured behavior of complex structures.

Test-validated finite element models have therefore played a key role in the design of high performance and high reliability structures. Even as testing validates current analysis methodologies, it stimulates an enhanced understanding of complex dynamic behavior. Model validation testing is particularly critical in the design qualification of structures. This is because

verification of structural strength and dynamic performance, even under extensive environmental testing, remains strongly dependent on the choice of analytical models. For example, the specification of test load levels for design qualification and the determination of appropriate test boundary conditions depend on a reasonably accurate finite element model of the tested subsystem. Correlation of finite element models is therefore a necessary component of progress in the design and optimization of structures subject to dynamic excitation. Figure 1.1 illustrates the central role which structural dynamic model validation testing plays in the design philosophy of advanced structural systems.

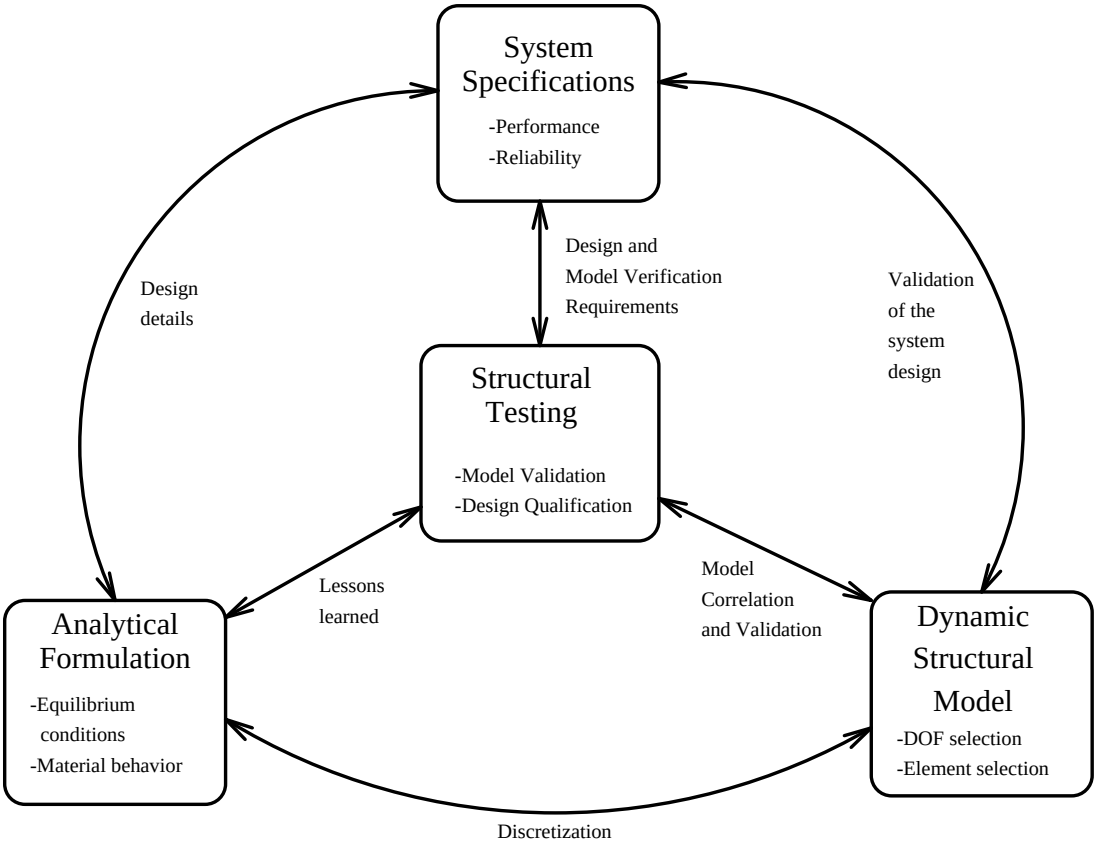

Figure 1.1: The central role of structural testing

Modal testing [1] is perhaps the most versatile form of structural model validation testing. It is also the most problematic because, unlike mass property measurements or static influence coefficient testing, modal tests attempt to measure or characterize mass, damping and stiffness behavior simultaneously. The general purpose of modal testing is the measurement or identification of the dominant modes of vibration of the structure [2]. For simple systems with well-isolated, lightly damped vibrational modes, it is possible to directly excite and accurately measure each mode individually using sine dwell excitation methods [3]. Such an approach, however, is time-consuming and costly, and, in the case of complex structures with a high modal densities, often fails to characterize modes which are not anticipated by analytical models. For this reason, structural tests began using wideband excitations coupled with signal analysis techniques to discern all the modes of vibration which participate in the measured response. With the development of digital signal processing (DSP) techniques, and in particular the Fast Fourier Transform (FFT), frequency domain methods in modal testing became competitive with sine dwell methods for characterizing the modal properties of structures [4].

The identification or extraction of modal parameters from the measured force inputs and sensor outputs is a complex process as illustrated in Figure 1.2. In order to determine the damped modal parameters, the frequency response functions (FRFs), which relate each input force to each output measurement in the discrete frequency domain, must be effectively fit to an equivalent curve defined as the superposition of numerous modal response functions. This is generally referred to in the modal testing community as modal parameter estimation or system identification, although

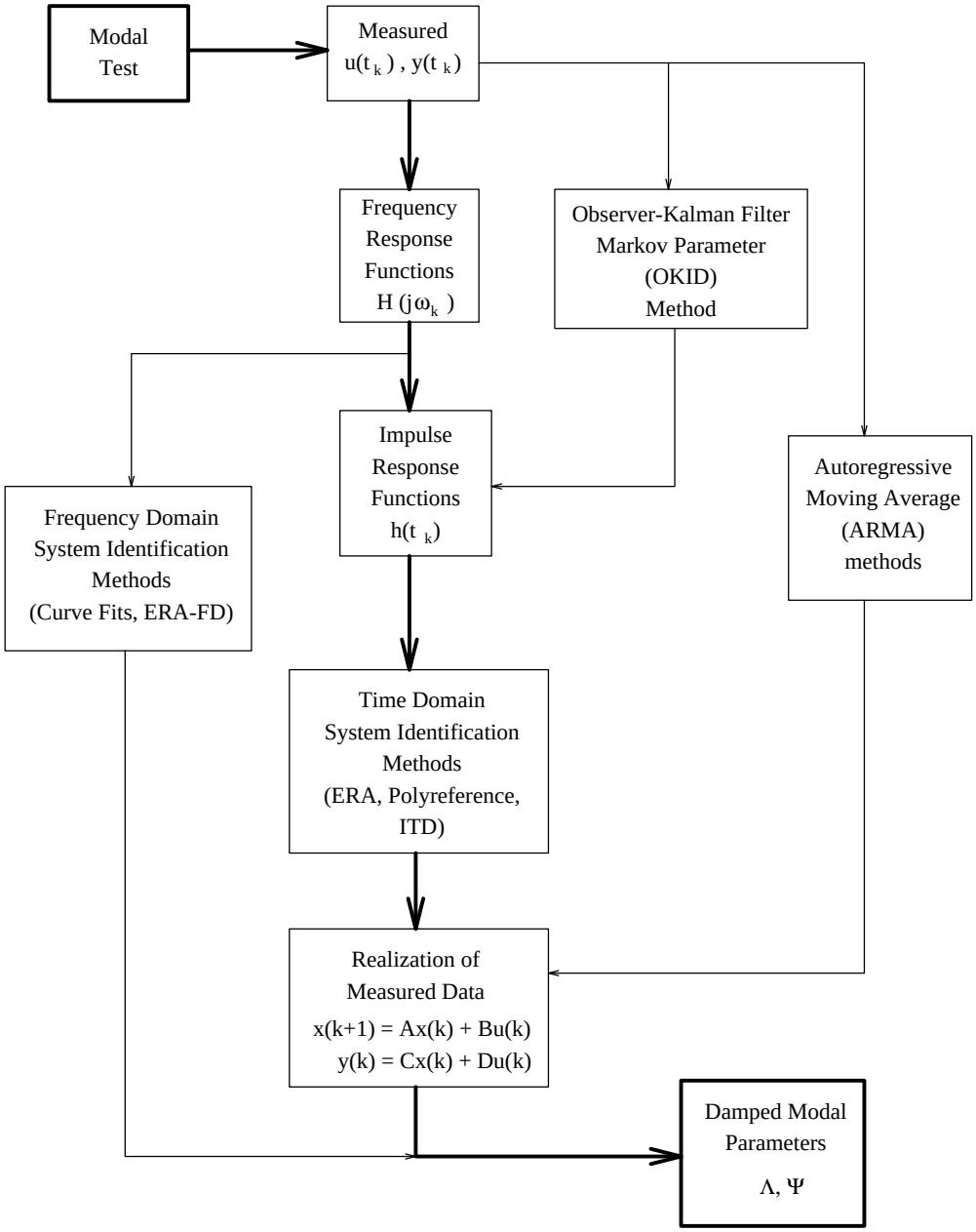

Figure 1.2: Damped Modal Parameter Estimation from Modal Testing

for clarity in this work it is termed *model estimation* in order to distinguish the model identification problem from the problem of extracting particular modal parameters of the structure.

There are numerous methods which can be applied to discrete FRFs or their associated impulse response functions (Markov parameters) in the time domain [5-9]. These methods have varying performance characteristics depending on the organization and condensation of data, methods of determining model size, ability to use multiple inputs and detect repeated modal frequencies, etc. While there is not a general consensus in the modal testing community about which model estimation method is superior, progress has been made towards unified formulations of the existing methods, both in terms of system realization theory [10] and matrix polynomials [11].

Notable amongst model estimation techniques is the Eigensystem Realization Algorithm (ERA) [8]. While most model estimation methods determine approximate models which fit the given measured data, the system realization theory that ERA is based on renders a minimum model order realization in the absence of noise. This characteristic enhances the application of ERA to the systematic identification needs of complex structures. System realization theory has been developed within the framework of linear dynamic systems analysis and control (see [12], for example). Realizations of linear systems are models which accurately express the system dynamics inherent in the transfer functions relating the system inputs and outputs [13-15]. State space realizations are relevant to modal testing because the first-order form encompasses all linear system behavior, including damped structural dynamics. Furthermore, the result of any model estimation method can be cast as a system realization of the measured data.

Literature on system realization theory and its recent application to modal testing is extensive (see Bibliography in [10] and [13-18], among others). Specifics of system realization theory, ERA, and its development for model estimation will be covered in depth in Chapter II.

There are two fundamental types of modal parameters of interest in linear structural dynamics: normal modes and damped modes. Normal modes, alternatively referred to as undamped or classical modes, are intrinsic properties of the conservative system, i.e., they are the eigensystem characterized by the mass and stiffness matrices. The undamped eigenvalues $\mathbf{\Omega}$ and their mode shapes $\mathbf{\Phi}$ can be predicted through finite element modeling and analysis as shown in Figure 1.3. Although damping always exists in real systems, in general it cannot be accurately modeled or predicted. The normal modes, therefore, are of primary interest in model validation and structural analysis because they are the dynamic response components which are direct expressions of the system mass and stiffness without the influence of unmodeled damping. Complex modes, on the other hand, are the intrinsic modes of the damped structure, also referred to as damped or complex damped modes. The term complex modes refers to the complex roots of a first-order system of equations, which can be transformed into the vibrational characteristics of a damped structure [19]. The damped eigenvalues $\mathbf{\Lambda}$ and their damped mode shapes $\mathbf{\Psi}$ are complex quantities, and in general the real and imaginary components of the mode shapes are not linearly dependent [20, 21].

The solution provided by model estimation methods determines the damped modes and complex mode shapes, but does not determine the normal modal parameters of the associated conservative structure. If the real and

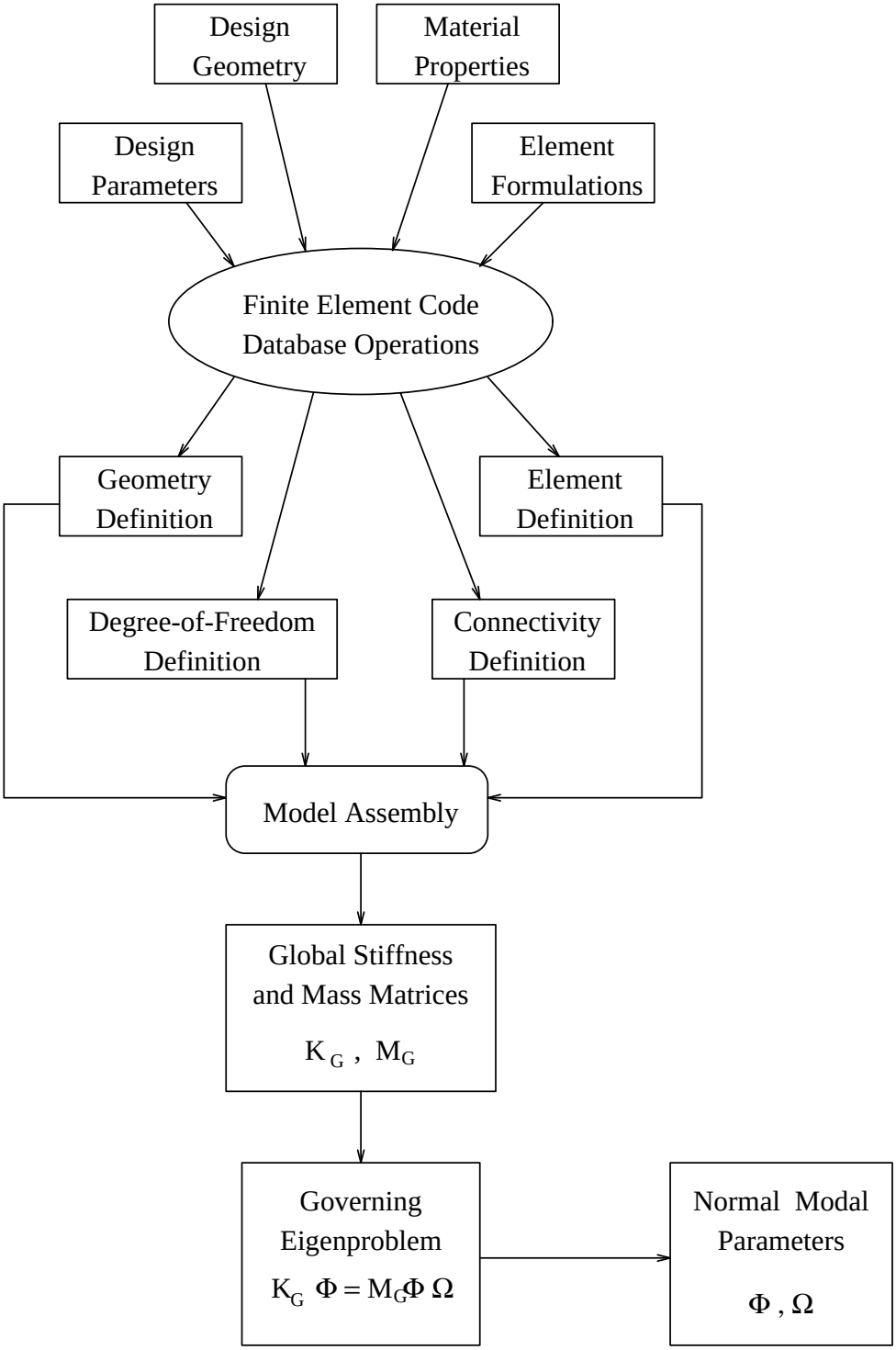

Figure 1.3: Normal Modal Parameter Determination from Finite Element Modeling and Analysis

imaginary components of the damped mode shapes are collinear (i.e. linearly dependent), the system is said to be proportionally or classically damped. In this particular case, the complex modes are also collinear with the normal mode shapes, and the complex and normal modal parameters are easily related to one another, mode by mode. Therefore, for proportional damping, the normal modal parameters are obtained directly from the damped modal parameters, thereby providing the necessary modal data for finite element model correlation. The model validation or correlation analysis then proceeds by evaluating the normal modes of the finite element model and, if necessary, changing the model at the element level or global matrix level to improve the correlation between the normal modes of the model and of the test. This process is illustrated in Figure 1.4. Convergence of this correlation process depends upon the algorithm employed and the relative number of model variables and normal modes being considered.

Generally, however, the damping is nonproportional or nonclassical and the normal modes which uncouple the mass and stiffness matrices do not simultaneously uncouple the physical damping matrix. The equivalence between the damped and normal modes is therefore lost, and the modal parameters resulting from the finite element analysis are no longer directly comparable to the modal parameters obtained from dynamic testing. Figure 1.5 shows the displacement response of a simple spring-mass system with nonproportional damping. The proportionally-damped system used for comparison has equivalent apparent frequencies, damping ratios and mode shapes. Note that, apart from the beating phenomenon caused by closely-spaced frequencies, the response exhibits a simple exponential decay. The nonproportional damping response, on the other hand, is more complex in its

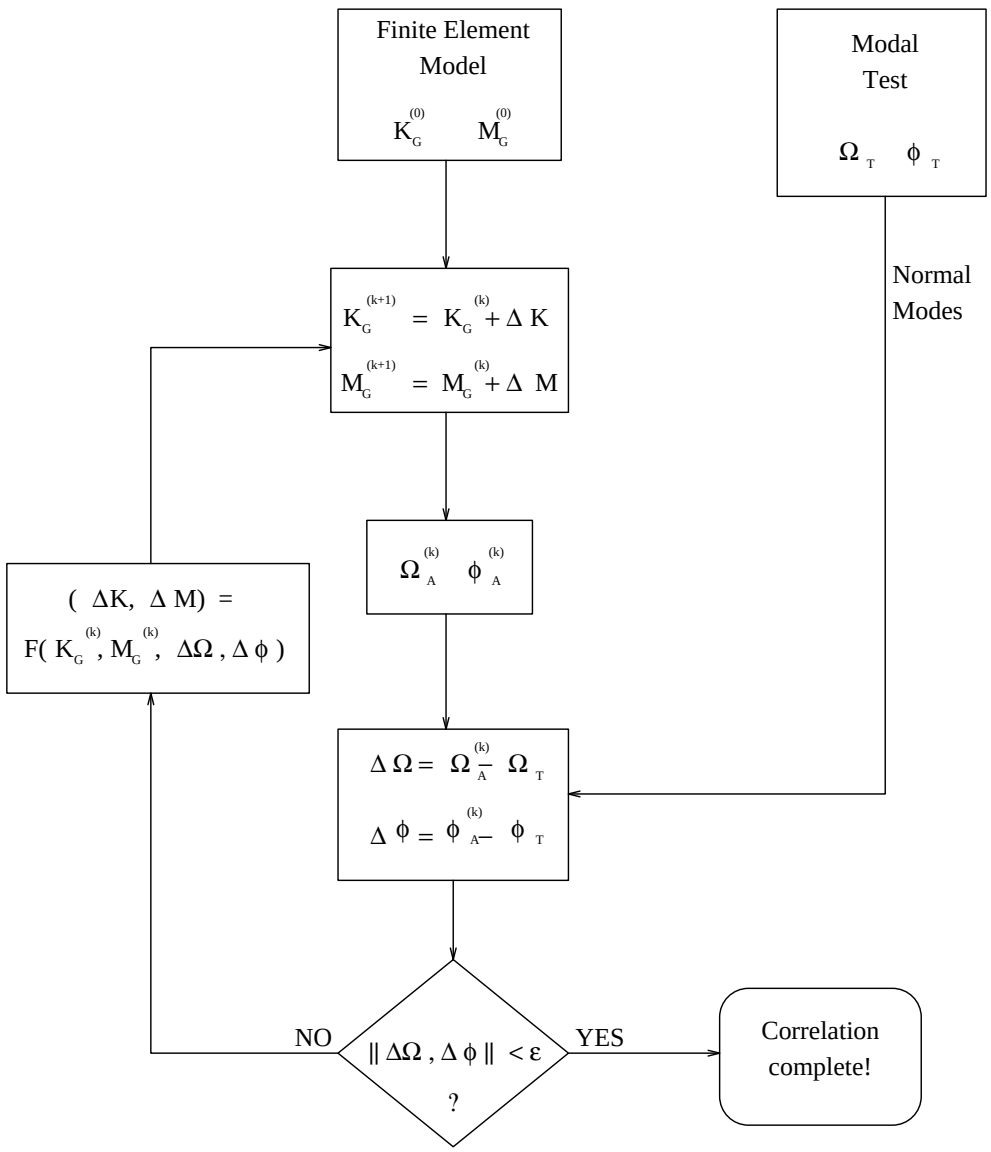

Figure 1.4: Finite Element Model Correlation Process

behavior, exhibiting not only the beating effect, but also a non-exponential decay envelope. The full difference in the response is due to the nonproportional nature of the damping, and this difference can lead to errors in the estimation of the normal modal parameters required for model correlation analyses.

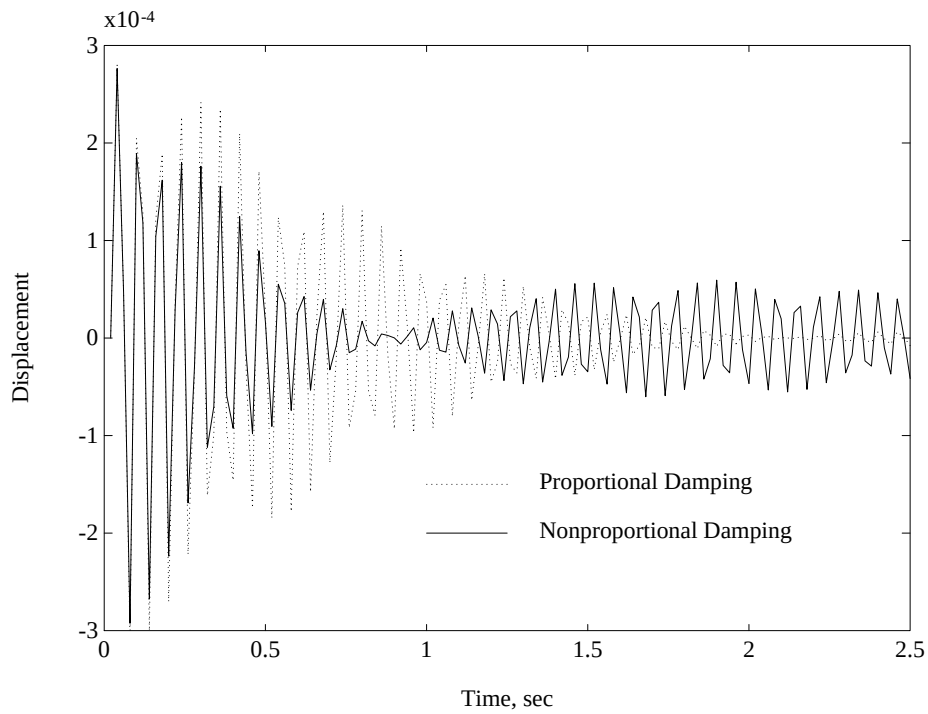

Figure 1.5: The Real Influence of Nonproportional Damping on the Displacement Response of Two Closely-Space Modes

Therefore, there is a missing link between the intrinsic damped modes $\mathbf{\Lambda}$ and $\mathbf{\Psi}$ of the tested structure as obtained through modal testing and model estimation, and the intrinsic undamped modes $\mathbf{\Omega}$ and $\mathbf{\Phi}$ of the finite element model. This dilemma is illustrated in Figure 1.6. In a physical sense, the missing link is the damping, which is not accurately predicted from the finite element model, nor isolated by the system realization of the measured modal test data. The solution to this dilemma is to transform the

state space-based system realizations which are characterized by $\mathbf{\Lambda}$ and $\mathbf{\Psi}$ to an equivalent second-order canonical basis. The equivalent second-order realization is significant in that it isolates the influence of damping into a damping matrix which can be used in finite element simulations, and simultaneously yields the undamped modal parameters $\mathbf{\Omega}$ and $\mathbf{\Phi}$ of the structure for use in model correlation, controls design and damage detection.

1.2 Motivation for the Present Work

The present research involves the development of transformation methods for structural system identification. The *system identification* problem is generally stated as the construction of mathematical models from observed data which can best fit the input-ouput relations without regard to physical interpretations [22]. *Structural system identification* involves the determination of physical models of structures from observed data, for example modal test data, such that the resulting physical models not only best fit the input-output relations but more importantly delineate the intrinsic structural parameters such as normal modes, mode shapes and the nature of damping. The primary motivation for the present research into structural system identification is the need for direct and systematic transformation procedures for system realizations of experimental test data which separately identify the normal modal characteristics of the structural system and the inherent proportional or nonproportional damping. The goal of the present research has been to exploit developments in modal testing and system realization theory to systematically and accurately develop physically-relevant models of structural dynamic systems directly from test. The expression of the measured damped dynamics, either as complex modes or as a general

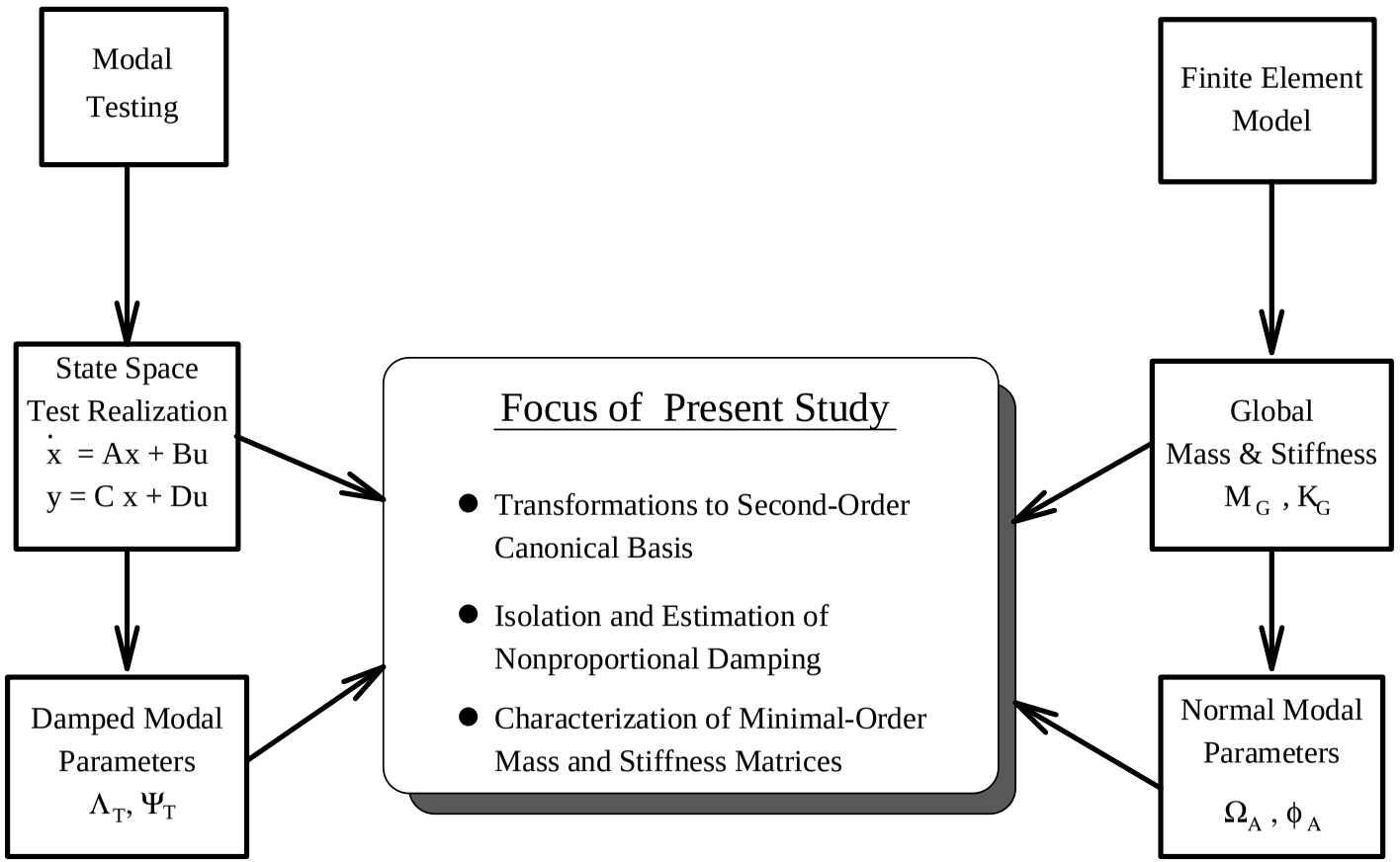

Figure 1.6: Missing Links in Parameter Equivalence Between Test and Analysis Models

state space realization, is insufficient for application to the validation of mass and stiffness models and detection of physical property variations because of the dissipative effects of unmodeled damping.

By determining an equivalent second-order realization of the measured data, however, the influence of damping is effectively isolated and the normal modal parameters more accurately predict the correct undamped structural response. It is known, for example, that structures characterized by symmetry (e.g. radial symmetry) possess modes with identical or closely spaced modal frequencies. In the presence of nonproportional damping, these modes can become highly coupled, as evidenced by a significant spatial distribution of phase components in the damped mode shapes. For such structural modes, estimates of the normal modal parameters are highly sensitive to the coordinate basis in which the estimated normal modes are defined. The success of control strategies or model correlation using moderately to highly complex modes will depend on the accurate estimation of the normal modes.

Another motivation for the current research is the recognition of converging trends in space structures design and dynamic testing. As higher precision is required for space structures, the frequency spectrum which can be tested and measured is broadening. Furthermore, modern system realization algorithms and their implementation via high-speed workstations and supercomputers allow model realizations which possess vast numbers of global and localized vibrational modes from a relatively smaller number of sensor locations. The integration of high-bandwidth data collection, modern efficient realization algorithms and high-speed computations will enable identifications of experimental data which can address the immediate needs

of high precision space structures technology. In order to exploit these technical advances, however, structural system identification must also mature from the classical problem of identifying the frequency and mode shapes of a small number of intrinsic modes with many sensors in a modal testing environment, to modern challenge of real-time identification for structural systems possessing large numbers of observable modes from a small number of sensors. For example, the primary truss structure design of Space Station Freedom will currently accommodate only 33 accelerometers to monitor on-orbit dynamic behavior. While modern system identification algorithms can fit accurate models to this limited form of data in a relatively systematic way, existing methods for determining the correct normal modes from the generally-damped modes of the identified model can not accommodate this condition.

Existing methods for determining physical coordinate models via correlation with finite element models are computationally intensive and can typically consider only a small subset of the modes inherent in the system realization. Representing the structural dynamics in terms of the physical mass, damping and stiffness is attractive because the influence of boundary conditions and element property variations is more locally and clearly expressed by the physical mass and stiffness matrices than by the normal vibration modes. Furthermore, the determination of physical coordinate realizations enable the synthesis of identified models using displacement-based modeling techniques. Unfortunately, the updating of large-order finite element models involves incomplete modal data, both less modes and less sensors than the number of model degrees of freedom. Therefore, the model update problem usually lacks a unique solution and the solutions which are

found may be highly sensitive to algorithmic details and the skill of the user. Similarity transformation-based determination of physical models, on the other hand, does not rely on a pre-existing model for correlation, and so the lack of uniqueness of the model update problem is avoided. The uniqueness of the solution follows from the definition of the physical variables as the sensor DOFs and the uniqueness of the normal modal parameters. The problem of incomplete spatial data in this direct solution to the inverse vibration problem, however, has remained a challenge. Because of the aforementioned trends in modal testing leading to measured systems possessing more modes than sensors, there is a need to address this form of incomplete spatial data, and how it relates to the physical model parameters.

1.3 Survey of Previous and Related Work

The use of system realization theory as a framework for modal testing analysis is a relatively new development, and hence there has been relatively little attention paid to the problem of mode shape estimation. In the original ERA development [8], it is noted that the damped roots and residues (i.e. mode shapes) are directly obtained from an equivalent realization from which the state transition matrix $\mathbf{A}$ is diagonal. In developing accuracy indicators from the system realized modes, it was suggested through use of a Modal Phase Collinearity (MPC) measure that modes with significant non-normal phase components are poorly identified and inaccurate. In subsequent work [23], accuracy measures including MPC were refined and studied, and it was noted that poor MPC's can be obtained for accurate modes due to the real influence of nonproportional damping. Further study of ERA and noise

modes [24] has largely ignored mode shape phase measures in favor of magnitude indicators such as Modal Singular Value (MSV), which considers the modal contribution to the measured response. Thus, there is a recognition of the need to retain identified modes which possess non-normal phase components unless those modes are demonstrated otherwise to have been poorly identified.

There are two general approaches to the problem of determining or realizing normal mode shapes in the presence of nonproportional damping. One family of methods, which can be classified as *mode shape estimation*, uses each complex mode individually to determine an associated normal mode estimates. Thus, there is a one-to-one assumed relationship between the decoupled damped modes and the normal modes, and the resulting modal parameters are in effect a proportionally-damped estimate of the realized system. Mode Shape Estimation is characteristically straightforward, but the modal parameters cannot maintain system dynamics exactly equivalent to the complex modes model. A recent survey [25] summarizes the common practice in mode shape estimation of using just the modulus of the complex modes and dismissing the non-normal phase information, which was referred to as the *standard technique* (ST). A new iterative approach is introduced to maximize the Modal Assurance Criterion (MAC) between the damped modes and normal modes estimates. Another recent approach [26] refers back to the measured peaks of the FRFs to extract real mode shape estimates using the eigenvalues (i.e. frequencies and damping rates) from Polyreference or ERA.

In [27], an equivalent realization was shown for which the continuous-time ERA state space $\mathbf{A}$ matrix is rotated to a real form representative of second-order dynamics, termed the McMillan normal form. This transformation-based approach provides real-valued mode shape estimation but does not account for the sensitivity to non-normal phase components in the complex modes. In other words, when the damping is nonproportional, the mode shape estimates will be dependent on the complex scaling of the damped modes, which is not generally defined in a physically-relevant or optimal sense. Hence, it is only accurate for proportional damping, for which the standard technique is adequate.

An alternative family of methods, which can be classified as *mode shape-damping decoupling*, involves global transformations which attempt to fully uncouple the damping matrix in order to obtain the real modes [28-36]. These methods can correctly account for the nature of nonproportional damping, and generally compute both real mode shapes and revised damping and frequency estimates. The revised modal damping matrix is characteristically nondiagonal, and the generalized form of the new modal parameters make it possible to maintain exact system equivalence with the initial complex damped modal parameters. In [37], a solution for the mass, damping and stiffness matrices in terms of the ERA system realization is given when the number of sensors, actuators, and identified modes are all equal. This method also accomplishes a mode shape-damping decoupling, though it is not a central point of the algorithm. An important limitation of all the existing methods for the mode shape-damping decoupling problem is that they require as many sensors as identified modes in order to uniquely define the required coordinate transformations.

The determination of normal modal parameters is a necessary precursor to the inverse vibration problem, whereby the measured or estimated vibrational modes are related back to the physical parameters of mass and stiffness [38]. Solution of this inverse problem is critical to many applications of structural identification involving physical parameters because the influence of changes in physical parameters are more highly localized with respect to physical displacement variables. In addition, physical matrices can be manipulated through displacement-based operations such as the imposing of boundary conditions, spatially-distributed applied loadings, substructure synthesis and assembly, etc. Most approaches to the inverse problem involve the updating of analytical mass and stiffness matrices, usually obtained from large-order finite element models as shown in Figure 1.4. Since the size of the matrices involved are typically much larger than the number of identified modes and sensors, the update problem lacks a unique solution. Optimal-matrix update procedures [39-42] determine updated global mass and stiffness matrices by minimizing some measure of the change in the model while constraining symmetry, positive definiteness, and possibly sparsity or connectivity. Sensitivity-based model update methods [43-45] determine changes in specified physical parameters (such as element properties) by determining sensitivity derivatives of the modal parameters. This generally requires projection of the test-measured mode shapes into the larger space of the finite element model coordinates, introducing additional uniqueness issues [46].

An alternative to algorithmic model updating or model correlation is the direct calculation of mass and stiffness operators from the identified normal modal parameters [47-48]. A unique transformation from any coordinate basis to a basis of measured physical variables is possible when the

number of measurements is equal to the number of identified modes, as in [37]. One important application of physical matrices obtained via model updating methods or direct computations is in the detection of structural damage. Recent work has focused on model update methods [49-54], whereby analytical models are correlated to the FRFs or more typically normal modal parameters of a nominal and damaged system. The physical parameters of the correlated nominal and damaged models are then examined to deduce information about the location and extent of changes in the structural properties. Localization of model update changes is a critical issue in damage detection, due to the indeterminacy of the update problem.

1.4 The Present Structural Identification Research

The current research effort builds on the assumption that model estimation methods such as ERA can determine a complex damped-mode model to a high degree of accuracy, and thus the realization problem and mode shape determination problem can be addressed separately. Then, assuming the measured structural system exhibits linear, time-invariant behavior and is free of nonreciprocal effects, such as gyroscopic damping, the complex modes emanate from symmetrical mass, damping and stiffness matrices, where the damping is not generally proportional. As discussed previously, the prevailing approaches to mode shape estimation either dismiss the non-normal mode shape phase components or seek an optimal solution without maintaining equivalence to the existing damped modes. In this thesis, a new mode shape estimation method, termed the *Common Basis-Normalized Structural Identification* (CBSI) algorithm [55], has been developed to systematically determine optimal normal mode shape estimates through state

space similarity transformations. Like other mode shape estimation techniques (e.g. [25]), CBSI assumes a one-to-one relationship between the damped and undamped modes, and so will not affect a true decoupling of nonproportional damping.

An important feature of CBSI is that it employs an objective definition of the model basis through a minimization of the quantities which do not fit the form of a proportionally-damped second-order model. This leads to a unique mode shape estimate independent of the complex scaling of the associated damped mode. In the case of proportional or zero damping, the CBSI procedure determines exactly the desired normal modal parameters and the associated residual quantities are zero. For nonproportional damping, CBSI determines an objective *pseudo-normal* modal basis, and the non-zero residual quantities are a direct measure of the magnitude and spatial characteristics of the nonproportional component of the damping. The standard technique, on the other hand, does not lead to an equivalent realization because it lacks a consistent transformation basis. Finally, CBSI independently accounts for the scaling of the normal mode shapes, and allows for mass normalization using driving point (i.e. collocated input-output) measurements.

The equivalent model determined by CBSI is a convenient basis for examining the mode shape-damping decoupling problem. Using the state space model form and the equivalence properties of nonsingular (i.e. similarity) transformations, a new *Uncoupled Nonproportional Damping* (UNDAMP) algorithm has been developed [56]. The purpose of UNDAMP is to optimally incorporate the residual quantities of the CBSI model into the estimated normal modes through an equivalent basis transformation. For n

identified modes, an order-n basis perturbation is uniquely defined for n sensor degrees of freedom, and is directly proportional to the CBSI model residual quantities. Therefore, when the damping is proportional with respect to the given sensors, the perturbation is null and the UNDAMP algorithm does not alter the CBSI-derived modal parameters.

The theoretical development of UNDAMP leads to consistency criterion which governs the damping decoupling problem. This consistency criterion is determined by considering the key characteristics of second-order structural models, including the reciprocal behavior of self-adjoint systems and the nature of the continuous impulse response functions for physical measurements. This allows for the physical consistency of the identified realization to be evaluated. The consistency criterion ensures that the phase quantities being incorporated into the physical model through the transformation are actually consistent with the underlying physics of linear structural dynamics, i.e. the second-order dynamics of the mass, damping and stiffness model. Existing methods for mode shape-damping decoupling fail to address these physical consistency issues, which govern not just the UNDAMP algorithm but the general technique of using the measured degrees of freedom as an equivalent physical model basis, which is the common feature of all global damping decoupling methods.

Constraining the UNDAMP algorithm to transformations within a subspace consistent with the second-order dynamics is an effective approach for determining physically-relevant solutions when the number of identified modes is either less than, equal to, or greater than the number of spatial measurements. When the number of modal states used in the algorithm is less or equal to the number of measured sensors, the algorithm can normally

determine a direct solution which implicitly satisfies the displacement consistency criterion. When the number of modal states is greater than the number of measured physical variables, the second-order transformation problem becomes under-determined. Using UNDAMP, however, solutions which account for the known sensor residual quantities are found either by constrainting the unmeasured spatial domain to appear proportionally-damped, or by minimizing a component of the basis perturbation. In these under-determined solutions, the displacement consistency criterion plays a crucial role in obtaining a physically-consistent solution.

A new physical basis transformation is also developed for the direct computation of minimal-order mass and stiffness matrices from the test-derived normal modal parameters given an arbitrarily large number of modes and a small number of sensors [57]. The method, which requires mass-normalized mode shapes, is based on static condensation [58] and component mode synthesis methods such as Craig-Bampton [59], whereby large-order mass and stiffness properties are represented approximately or very accurately in a smaller physical basis. The computed properties are in fact asymptotically equivalent to Guyan-reduced and Craig-Bampton mass and stiffness models as the full modal spectrum is identified. The transformation-based approach exactly preserves the normal modal parameters from test by augmenting the physical degrees of freedom measured by sensors with generalized degrees of freedom which together span the observable modes. The CBSI, UNDAMP, and minimal-order mass and stiffness methods have been implemented for use in modal test analysis through development of a Structural System Identification Toolbox for MATLAB^{TM} [60]. The functional

organization of the MATLAB program allows for a high-level algorithmic interface, and flexible command of the manipulated data. Of particular interest is a general command function, labeled `era2mdk`, which will transform an ERA-identified discrete time realization through the discrete-to-continuous time conversion, CBSI modal parameter extraction, UNDAMP transformation and mass and stiffness computation to directly compute mass and stiffness measures of the given system realization. The toolbox functions are designed for interfacing with the MODALID [61] package.

The application of CBSI and the minimal-order mass and stiffness method to the problem of structural damage detection has been studied using both numerical tests and experimental data from the Structural Dynamics and Controls Laboratory (SDCL) at the University of Colorado, Boulder. Two methods of deriving structural element stiffness sensitivity from the experimentally measured stiffness matrices have been developed [62]. Both the Pull Test (PT) and the Reduced Element Stiffness Test (REST) enable the analyst to compare undamaged and damaged data and compute element stiffness variations which clearly identify damage location. The asymptotic property of the reduced stiffness definition allows the convergence of the relevant stiffness parameters to be studied as a function of the system identification algorithm.

1.5 Outline of the Dissertation

The dissertation is organized as follows. Chapter II reviews system realization concepts for model identification. Chapters III and IV address

the determination of normal modal parameters through the CBSI and UNDAMP algorithms. Chapter V develops the minimal-order mass and stiffness method for direct computation of physical models. Chapter VI presents the implementation and application of the structural identification transformation methods to experimental data examples, including the problem of structural damage detection.

In Chapter II, the specifics of system realization theory and its application to structural identification are presented. The governing equations of motion for structural dynamics and the definition of normal modes is detailed. Then model estimation techniques are covered, culminating in the development of system realization methods and ERA through the definition of Markov parameters and Hankel matrices. The specifics of ERA are contrasted with other time-domain estimation methods, and the motivations for using system realization in model estimation are given.

The CBSI method is detailed in Chapter III. A modal displacement velocity canonical form of second-order structural dynamics is presented and a key observation is made about the uniqueness of this model form. Then, the objective basis definition is developed, and solutions which optimize various measures of the model residuals are derived. Numerical examples of undamped, proportionally-damped, and nonproportionally-damped systems are presented to illustrate the essential features of the algorithm.

In Chapter IV, the UNDAMP algorithm for decoupling mode shapes and nonproportional damping is developed from the CBSI model basis. The general solution to the inverse damped vibration problem is briefly

reviewed as a theoretical foundation for the modal-physical basis transformation employed in UNDAMP. Well-determined and over-determined solutions are presented, and the displacement consistency criterion is developed. Then the under-determined problem is studied in light of the known transformation constraints. Two solutions are determined through additional physical constraint and optimality considerations. Numerical examples of nonproportionally-damped systems are presented which demonstrate both well-determined and under-determined solutions.

The determination of minimal-order mass and stiffness matrices is presented in Chapter V. The direct solution to the normal modes inverse vibration problem is studied, and an equivalence is shown between partitions of the inverse stiffness matrix expressed in terms of the physical degrees of freedom and the full modal spectrum. This leads to the definition of a reduced stiffness matrix as measured from the available modal test-identified parameters which has an asymptotic equivalence to the Guyan-reduced stiffness well-known in finite element methodology. An extension of the reduced stiffness determined from modal test data is then found by applying system equivalence and component mode synthesis concepts, leading to the minimal-order mass and stiffness matrices. The essentials of the algorithm are demonstrated though numerical and experimental examples.

In Chapter VI, the implementation and application of the structural system identification methods developed herein are detailed. The MATLAB^{TM} Structural System Identification Toolbox is summarized and demonstrated on experimental data. The structural identification methods are then applied to damage detection in a suspended scale model truss structure. It is demonstrated that, through selection of model coordinate bases,

modal and physical parameters from modal test data can be efficiently and systematically determined, and can provide insight into the intrinsic properties of the measured structure without the use of a pre-existing analytical finite element model.

Finally, Chapter VII summarizes the contributions of this work, their relevance to modal testing and system realization methods, and their implications for the development of intelligent structural systems. Directions for future research motivated by this work are also discussed.

CHAPTER II

STATE SPACE REALIZATION FOR STRUCTURAL IDENTIFICATION

This chapter reviews the theoretical basis of structural system identification. To this end, we introduce the equations of motion for structures and their transformation to state space canonical forms. The state space or first-order equation form is important because the generally-damped behavior of the structural system can only be uniquely expressed from model realizations of experimental data in terms of the modal parameters of a first-order system of equations. A review of frequency-domain modal testing is then presented, followed by a detailed presentation of system realization concepts and the Eigensystem Realization Algorithm (ERA). Finally, the determination of the damped modal parameter realization from ERA is reviewed, which links the modal testing and model estimation developments back to the state space formulations presented for structural dynamics.

2.1 State Space Formulations of Structural Dynamics

Typically, the equilibrium conditions for linear time-invariant continuum mechanics are discretized through spatial displacement interpolation to a finite number of variables (e.g. finite element methods), resulting in the familiar n-dimensional set of second-order linear differential equations

$$\begin{aligned} \mathbf{M}\ddot{\mathbf{q}}(t)+\mathcal{D}\dot{\mathbf{q}}(t) + \mathbf{K}\mathbf{q}(t) &= \hat{\mathbf{B}}\mathbf{u}(t) \\ \mathbf{y}(t) = \mathbf{H}_d\mathbf{q}(t) + \mathbf{H}_v\dot{\mathbf{q}}(t) + \mathbf{H}_a\ddot{\mathbf{q}}(t) \end{aligned} \tag{2.1.1}$$

where $\mathbf{M}$, $\mathcal{D}$ and $\mathbf{K}$ are the mass, damping and stiffness matrices, respectively; $\mathbf{q}$ is the n-displacement state vector; $\mathbf{u}$ is a m-input force vector; $\mathbf{y}$ is a l-sensor output vector, either displacement, velocity, or acceleration; $\hat{\mathbf{B}}$ is the input-state influence matrix, and $\mathbf{H}_d$, $\mathbf{H}_v$ and $\mathbf{H}_a$ are state-output influence matrices for displacement, velocity, and acceleration, respectively . The undamped portion of this second-order system can be decoupled through an eigenvector change-of-basis $\mathbf{q}(t) = \mathbf{\Phi}\eta(t)$, resulting in

$$\begin{aligned} \ddot{\eta}(t) + \mathbf{\Phi}^T\mathcal{D}\mathbf{\Phi}\dot{\eta}(t) + \mathbf{\Omega}\eta(t) &= \mathbf{\Phi}^T\hat{\mathbf{B}}\mathbf{u}(t) \\ \mathbf{y}(t) &= \mathbf{H}_d\mathbf{\Phi}\eta(t) + \mathbf{H}_v\mathbf{\Phi}\dot{\eta}(t) + \mathbf{H}_a\mathbf{\Phi}\ddot{\eta}(t) \end{aligned} \tag{2.1.2}$$

where $\mathbf{\Phi}$ is the mass-orthonormalized eigenvector basis for the generalized undamped eigenproblem

$$\mathbf{K}\mathbf{\Phi} = \mathbf{M}\mathbf{\Phi}\mathbf{\Omega}$$

such that

$$\begin{aligned} \mathbf{\Phi}^T\mathbf{M}\mathbf{\Phi} &= \mathbf{I}_{n\times n} \\ \mathbf{\Phi}^T\mathbf{K}\mathbf{\Phi} &= \mathbf{\Omega} = diag\{{\omega_{ni}}^2, i = 1, \ldots, n\} \\ \mathbf{\Phi}^T\mathcal{D}\mathbf{\Phi} &= \mathbf{\Xi} \end{aligned} \tag{2.1.3}$$

where ω_{ni} is the undamped natural frequency for mode i. In the case of Rayleigh damping ($\mathcal{D} = \alpha\mathbf{M} + \beta\mathbf{K}$ or more generally $\mathcal{D} = \alpha\mathbf{M}^p + \beta\mathbf{K}^r$ [19]), this transformation will decouple the damped second-order system, and the *modal damping matrix* $\mathbf{\Xi}$ is given as

$$\mathbf{\Xi} = diag\{2\zeta_i\omega_{ni}, i = 1, \ldots, n\} \tag{2.1.4}$$

Here ζ_i is the *modal damping ratio* for mode i, which varies from 0% for undamped vibration to 100% for critically-damped vibration, at which point the system response for the mode becomes non-oscillatory.

Systems (2.1.1) and (2.1.2) possess different coordinate bases but are equivalent second-order *realizations* of the dynamical problem. To examine the concept of model equivalence, let us consider the general solution to (2.1.1). Using the Laplace transform

$$\begin{aligned} \left[\mathbf{M}s^2 + \mathcal{D}s + \mathbf{K}\right] \mathbf{q}(s) &= \hat{\mathbf{B}}\mathbf{u}(s) \\ \left[\mathbf{H}_d + \mathbf{H}_v s + \mathbf{H}_a s^2\right] \mathbf{q}(s) &= \mathbf{y}(s) \end{aligned} \tag{2.1.5}$$

Therefore, the input/output relations of(2.1.1) in the s-domain are expressed in matrix form as $\mathbf{y}(s) = \mathcal{H}(s)\mathbf{u}(s)$ where

$$\begin{aligned} \mathcal{H}(s) = (\mathbf{H}_d + \mathbf{H}_v s + \mathbf{H}_a s^2) \left[\mathbf{M}s^2 + \mathcal{D}s + \mathbf{K}\right]^{-1} \hat{\mathbf{B}} \\ \mathbf{u}(s) = \int_0^\infty \mathbf{u}(t)e^{-st}dt \\ \mathbf{y}(s) = \int_0^\infty \mathbf{y}(t)e^{-st}dt \end{aligned} \tag{2.1.6}$$

and $\mathcal{H}(s)$ is the transfer function matrix from input u to output y. The transfer function relationship can also be determined from the modal coordinate model (2.1.2), viz.

$$\begin{aligned} \mathbf{y}(s) &= (\mathbf{H}_d + \mathbf{H}_v s + \mathbf{H}_a s^2)\mathbf{\Phi} \left[\mathbf{\Phi}^T(\mathbf{M}s^2 + \mathcal{D}s + \mathbf{K})\mathbf{\Phi}\right]^{-1} \mathbf{\Phi}^T \hat{\mathbf{B}}\mathbf{u}(s) \\ &= (\mathbf{H}_d + \mathbf{H}_v s + \mathbf{H}_a s^2) \left[\mathbf{M}s^2 + \mathcal{D}s + \mathbf{K}\right]^{-1} \hat{\mathbf{B}}\mathbf{u}(s) \\ &= \mathcal{H}(s)\mathbf{u}(s) \end{aligned} \tag{2.1.7}$$

Thus, by *model equivalence* it is implied that the same input/output relationship exists, regardless of the definition of the internal dynamical states, in these cases the second-order model variables $\mathbf{q}$ and η.

2.1.1 General State Space Realizations

It is also possible to retain model equivalence while transforming the equations of motion from second-order to first-order differential form. The general form of a linear, time-invariant state space realization is

$$\begin{aligned} \dot{\mathbf{x}}(t) &= \mathbf{A}\mathbf{x}(t) + \mathbf{B}\mathbf{u}(t) \\ \mathbf{y}(t) &= \mathbf{C}\mathbf{x}(t) + \mathbf{D}\mathbf{u}(t) \end{aligned} \tag{2.1.8}$$

where $\mathbf{x}$ is the $N \times 1$ state vector, $\mathbf{A}$ is the $N \times N$ state transition matrix, $\mathbf{B}$ is the $N \times m$ input-state influence matrix, $\mathbf{C}$ is the $l \times N$ state-output influence matrix, and $\mathbf{D}$ is the $l \times m$ matrix corresponding to direct input/output feedthrough. For structural dynamics, $\mathbf{u}(t)$ are generally externally applied forces as in (2.1.1) and $\mathbf{B}$ is an array which maps the physical locations of the input forces to the internal variables of the realization. Similarly, $\mathbf{y}(t)$ are physical sensor measurements such as displacement, velocity or acceleration and $\mathbf{C}$ is an array which constructs these physical quantities from the internal variables $\mathbf{x}(t)$. For example, if $\mathbf{x}(t)$ is a vector of physical displacements and velocities which include as a subset those degrees of freedom driven by $\mathbf{u}$ or measured by $\mathbf{y}$, then $\mathbf{B}$ and $\mathbf{C}$ are typically binary arrays (i.e. values of 0 or 1). The state space formulation of structural dynamics requires $N = 2n$ states to equivalently represent the second-order system (2.1.1). Specific state space realizations for structural dynamics will be presented later in this section.

One important property relevant to model equivalence is that of the *similarity transformation.* Let the *state basis* $\mathbf{x}$ be defined in terms of an alternate basis $\mathbf{v}$, viz.

$$\mathbf{x} = \mathbf{T}\mathbf{v} \tag{2.1.9}$$

where $\mathbf{T}$ is a nonsingular matrix. Then (2.1.8) is given as

$$\begin{aligned} \mathbf{T}\dot{\mathbf{v}} &= \mathbf{A}\mathbf{T}\mathbf{v} + \mathbf{B}\mathbf{u} \\ \mathbf{y} &= \mathbf{C}\mathbf{T}\mathbf{v} + \mathbf{D}\mathbf{u} \end{aligned} \tag{2.1.10}$$

or equivalently as

$$\begin{aligned} \dot{\mathbf{v}} &= \mathbf{T}^{-1}\mathbf{A}\mathbf{T}\mathbf{v} + \mathbf{T}^{-1}\mathbf{B}\mathbf{u} = \mathcal{A}\mathbf{v} + \mathcal{B}\mathbf{u} \\ \mathbf{y} &= \mathcal{C}\mathbf{v} + \mathbf{D}\mathbf{u} \end{aligned} \tag{2.1.11}$$

where

$$\begin{aligned} \mathcal{A} &= \mathbf{T}^{-1}\mathbf{A}\mathbf{T} \\ \mathcal{B} &= \mathbf{T}^{-1}\mathbf{B} \\ \mathcal{C} &= \mathbf{C}\mathbf{T} \end{aligned} \tag{2.1.12}$$

Thus (2.1.11) is a new realization of (2.1.8) in terms of the state definition $\mathbf{v}$. The coordinate transformation $\mathbf{T}$ is termed a similarity transformation because the eigenvalues of the realization λ which satisfy

$$|\lambda\mathbf{I} - \mathbf{A}| = 0$$

are invariant under this transformation. Because these are the eignenvalues of $\mathbf{A}$ and $\mathcal{A}$, the two matrices are said to be *similar*. Another important property of the similarity transformation is that it preserves the transfer function $\mathcal{H}$ from $\mathbf{u}$ to $\mathbf{y}$. Applying the Laplace transform to (2.1.11),

$$\begin{aligned} \mathbf{y}(s) &= \mathcal{C}\left(s\mathbf{I} - \mathcal{A}\right)^{-1}\mathcal{B}\mathbf{u}(s) \\ &= \mathbf{C}\mathbf{T}\left(s\mathbf{T}^{-1}\mathbf{T} - \mathbf{T}^{-1}\mathbf{A}\mathbf{T}\right)^{-1}\mathbf{T}^{-1}\mathbf{B}\mathbf{u}(s) \\ &= \mathbf{C}\left(s\mathbf{I} - \mathbf{A}\right)^{-1}\mathbf{B}\mathbf{u}(s) \end{aligned} \tag{2.1.13}$$

Thus, the similarity transformation (2.1.12) leads to an equivalent model realization. From this development, it can be stated that there are an infinite

number of equivalent realizations of (2.1.8) which can be determined from similarity transformations utilizing nonsingular coordinate (basis) transformations such as $\mathbf{T}$.

2.1.2 State Space Realizations for Structural Dynamics: Physical Variables

A family of state space realizations of (2.1.1) can be expressed through a generalized momentum variable $\mathbf{v}$ (see [63]). Define $\mathbf{v}$ as

$$\mathbf{v}(t) = \mathbf{E}_1\mathbf{M}\dot{\mathbf{q}}(t) + \mathbf{E}_2\mathbf{q}(t) \tag{2.1.14}$$

and the state space basis as

$$\mathbf{x}(t) = \begin{Bmatrix} \mathbf{q}(t) \\ \mathbf{v}(t) \end{Bmatrix} \tag{2.1.15}$$

Rather than determining the general state space equations for $\mathbf{x}$, two special basis choices will be considered:

$$\begin{aligned} I. \qquad & \mathbf{E}_1 = \mathbf{M}^{-1}, \quad \mathbf{E}_2 = \mathbf{0} \\ II. \qquad & \mathbf{E}_1 = \mathbf{I}, \quad \mathbf{E}_2 = \mathcal{D} \end{aligned} \tag{2.1.16}$$

For Case I, since $\mathbf{v} = \dot{\mathbf{q}}$ the state space basis can be termed a *physical displacement-velocity (PDV)* model. The resultant model is given by

$$\begin{aligned} \dot{\mathbf{x}}_I(t) &= \mathbf{A}_I\mathbf{x}_I(t) + \mathbf{B}_I\mathbf{u}(t) \\ \mathbf{y}(t) &= \mathbf{C}_I\mathbf{x}_I(t) + \mathbf{D}\mathbf{u}(t) \end{aligned} \tag{2.1.17}$$

where

$$\begin{aligned} \mathbf{A}_I &= \begin{bmatrix} \mathbf{0} & \mathbf{I} \\ -\mathbf{M}^{-1}\mathbf{K} & -\mathbf{M}^{-1}\mathcal{D} \end{bmatrix} \\ \mathbf{B}_I &= \begin{bmatrix} \mathbf{0} \\ \mathbf{M}^{-1}\hat{\mathbf{B}} \end{bmatrix} \\ \mathbf{C}_I &= [\,\mathbf{H}_d \quad 0\,] + [\,\mathbf{H}_v \quad 0\,]\,\mathbf{A}_I + [\,\mathbf{H}_a \quad 0\,]\,\mathbf{A}_I^2 \\ &= [\,\mathbf{H}_d - \mathbf{H}_a\mathbf{M}^{-1}\mathbf{K} \quad \mathbf{H}_v - \mathbf{H}_a\mathbf{M}^{-1}\mathcal{D}\,] \\ \mathbf{D} &= \mathbf{H}_a\mathbf{M}^{-1}\hat{\mathbf{B}} \end{aligned} \tag{2.1.18}$$

Similarly, for case II, $\mathbf{v} = \mathbf{M}\dot{\mathbf{q}} + \mathcal{D}\mathbf{q}$ are the generalized momenta of $\mathbf{q}$ and the state basis definition (2.1.15) results in a *physical displacement-momentum (PDM)* model. The canonical equations for Case II are

$$\begin{aligned} \dot{\mathbf{x}}_{II}(t) &= \mathbf{A}_{II}\mathbf{x}_{II}(t) + \mathbf{B}_{II}\mathbf{u}(t) \\ \mathbf{y}(t) &= \mathbf{C}_{II}\mathbf{x}_{II}(t) + \mathbf{D}\mathbf{u}(t) \end{aligned} \tag{2.1.19}$$

where

$$\begin{aligned} \mathbf{A}_{II} &= \begin{bmatrix} -\mathbf{M}^{-1}\mathcal{D} & \mathbf{M}^{-1} \\ -\mathbf{K} & \mathbf{0} \end{bmatrix} \\ \mathbf{B}_{II} &= \begin{bmatrix} \mathbf{0} \\ \hat{\mathbf{B}} \end{bmatrix} \\ \mathbf{C}_{II} &= [\,\mathbf{H}_d \quad 0\,] + [\,\mathbf{H}_v \quad 0\,]\,\mathbf{A}_{II} + [\,\mathbf{H}_a \quad 0\,]\,\mathbf{A}_{II}^2 \\ \mathbf{D} &= \mathbf{H}_a\mathbf{M}^{-1}\hat{\mathbf{B}} \end{aligned} \tag{2.1.20}$$

The equivalence of (2.1.17)-(2.1.20) to (2.1.1) is easily verified as follows. Again, using Laplace transforms, the transfer function for (2.1.17) can be found as

$$\begin{aligned} \mathcal{H}(s) &= \mathbf{D} + \mathbf{C}_I\,(s\mathbf{I} - \mathbf{A}_I)^{-1}\,\mathbf{B}_I \\ &= \mathbf{D} + \mathbf{C}_I\left(\frac{1}{s} + \frac{1}{s^2}\mathbf{A}_I + \frac{1}{s^3}\mathbf{A}_I^2 + \cdots\right)\mathbf{B}_I \\ &= \mathbf{D} + \frac{1}{s}\mathbf{C}_I\mathbf{B}_I + \frac{1}{s^2}\mathbf{C}_I\mathbf{A}_I\mathbf{B}_I + \frac{1}{s^3}\mathbf{C}_I\mathbf{A}_I^2\mathbf{B}_I + \cdots \end{aligned} \tag{2.1.21}$$

Then, substituting the expressions for $\mathbf{A}_I$, $\mathbf{B}_I$, $\mathbf{C}_I$ and $\mathbf{D}$ from (2.1.18) and simplifying,

$$\begin{aligned} \mathcal{H}(s) &= \left[\mathbf{H}_d + \mathbf{H}_v s + \mathbf{H}_a s^2\right](\mathbf{M}^{-1}s^{-2} - \mathbf{M}^{-1}\mathcal{D}\mathbf{M}^{-1}s^{-3} - \\ &\qquad (\mathbf{M}^{-1}(\mathbf{K} - \mathcal{D}\mathbf{M}^{-1}\mathcal{D})\mathbf{M}^{-1})s^{-4} + \cdots)\hat{\mathbf{B}} \\ &= (\mathbf{H}_d + \mathbf{H}_v s + \mathbf{H}_a s^2)\left[\mathbf{M}s^2 + \mathcal{D}s + \mathbf{K}\right]^{-1}\hat{\mathbf{B}} \end{aligned} \tag{2.1.22}$$

Thus, the state vector definition for physical variables (2.1.15) spans the second-order dynamics, and the resultant physical variable realizations (2.1.17)-(2.1.20) lead to fully-equivalent state space realizations of (2.1.1).

2.1.3 State Space Realizations for Structural Dynamics: Normal Modal Variables

Equivalent state space models can also be developed analogously from the second-order modal equations (2.1.2). In this case, the generalized variable $\mathbf{v}$ is defined as

$$\mathbf{v}(t) = \mathbf{E}_1\dot{\eta}(t) + \mathbf{E}_2\eta(t) \tag{2.1.23}$$

and the state basis as

$$\mathbf{x}(t) = \begin{Bmatrix} \eta(t) \\ \mathbf{v}(t) \end{Bmatrix} \tag{2.1.24}$$

Two additional state space models are then defined as special cases of this general form, viz.

$$\begin{aligned} &III. \qquad \mathbf{E}_1 = \mathbf{I}, \quad \mathbf{E}_2 = \mathbf{0} \\ &IV. \qquad \mathbf{E}_1 = \mathbf{I}, \quad \mathbf{E}_2 = \mathbf{\Xi} \end{aligned} \tag{2.1.25}$$

Case III results in a *modal displacement-velocity (MDV)* model, while case IV can be termed a *modal displacement-momentum (MDM)* model, as both are related to the physical first-order models defined by cases I and II through the modal change of basis $\mathbf{\Phi}$. The model forms are the same as (2.1.17) with

$$\begin{aligned} \mathbf{A}_{III} &= \begin{bmatrix} \mathbf{0} & \mathbf{I} \\ -\mathbf{\Omega} & -\mathbf{\Xi} \end{bmatrix} \\ \mathbf{B}_{III} &= \begin{bmatrix} \mathbf{0} \\ \mathbf{\Phi}^T\hat{\mathbf{B}} \end{bmatrix} \\ \mathbf{C}_{III} &= [\,\mathbf{H}_d\mathbf{\Phi} \quad 0\,] + [\,\mathbf{H}_v\mathbf{\Phi} \quad 0\,]\,\mathbf{A}_{III} + [\,\mathbf{H}_a\mathbf{\Phi} \quad 0\,]\,\mathbf{A}_{III}^2 \\ &= [\,\mathbf{H}_d\mathbf{\Phi} - \mathbf{H}_a\mathbf{\Phi}\mathbf{\Omega} \quad \mathbf{H}_v\mathbf{\Phi} - \mathbf{H}_a\mathbf{\Phi}\mathbf{\Xi}\,] \\ \mathbf{D} &= \mathbf{H}_a\mathbf{\Phi}\mathbf{\Phi}^T\hat{\mathbf{B}} = \mathbf{H}_a\mathbf{M}^{-1}\hat{\mathbf{B}} \end{aligned} \tag{2.1.26}$$

for Case III and

$$
\begin{aligned}
\mathbf{A}_{IV} &= \begin{bmatrix} -\boldsymbol{\Xi} & \mathbf{I} \\ \boldsymbol{\Omega} & \mathbf{0} \end{bmatrix} \\
\mathbf{B}_{IV} &= \begin{bmatrix} \mathbf{0} \\ \boldsymbol{\Phi}^T \hat{\mathbf{B}} \end{bmatrix} \\
\mathbf{C}_{IV} &= [\, \mathbf{H}_d \boldsymbol{\Phi} \quad 0 \,] + [\, \mathbf{H}_v \boldsymbol{\Phi} \quad 0 \,]\, \mathbf{A}_{IV} + [\, \mathbf{H}_a \boldsymbol{\Phi} \quad 0 \,]\, \mathbf{A}_{IV}^2 \\
&= [\, \mathbf{H}_d \boldsymbol{\Phi} - \mathbf{H}_v \boldsymbol{\Phi} \boldsymbol{\Xi} + \mathbf{H}_a \boldsymbol{\Phi} \boldsymbol{\Xi}^2 - \mathbf{H} \boldsymbol{\Phi} \boldsymbol{\Omega} \quad \mathbf{H}_v \boldsymbol{\Phi} - \mathbf{H}_a \boldsymbol{\Phi} \boldsymbol{\Xi} \,] \\
\mathbf{D} &= \mathbf{H}_a \boldsymbol{\Phi} \boldsymbol{\Phi}^T \hat{\mathbf{B}} = \mathbf{H}_a \mathbf{M}^{-1} \hat{\mathbf{B}}
\end{aligned}
\tag{2.1.27}
$$

for Case IV. The model equivalence of (2.1.2) and (2.1.17)-(2.1.20) applies also to cases III and IV, resulting in a family of state space and second-order models, each of which has particular advantages for simulations, controls design, and system identification (e.g. see [64]).

2.1.4 State Space Damped Modal Realizations

As noted previously, for systems with Rayleigh damping, or where $\mathcal{D} = \alpha \mathbf{M}^p + \beta \mathbf{K}^r$, the modal equations (2.1.2) are decoupled, as $\boldsymbol{\Xi}$ is diagonal. This form of damping is referred to variously as diagonal, modal, classical, or proportional damping. When $\boldsymbol{\Xi}$ is not diagonal, the damping is termed non-classical or nonproportional, due to the fact that $\mathcal{D}$ cannot be expressed as a proportional combination of $\mathbf{M}$ and $\mathbf{K}$. One physical interpretation of this type of damping is that the modes which decouple the system equations are now complex, such that there are phase relationships between the various physical displacements of the structure within each mode. Another interpretation is that the classical undamped modes of the structure are energy-coupled through the off-diagonal terms of $\boldsymbol{\Xi}$.

Because the second-order equations of motion for nonproportionally-damped systems cannot be decoupled by the normal modes of $\mathbf{M}$ and $\mathbf{K}$, the

governing eigenproblem for nonproportional damping must be formulated from equivalent first-order equations of motion. To this end, the PDV model (2.1.17)-(2.1.18) with displacement sensing is rewritten in a symmetrical companion form as

$$\begin{bmatrix} \mathcal{D} & \mathbf{M} \\ \mathbf{M} & 0 \end{bmatrix} \begin{Bmatrix} \dot{\mathbf{q}} \\ \ddot{\mathbf{q}} \end{Bmatrix} = \begin{bmatrix} -\mathbf{K} & 0 \\ 0 & \mathbf{M} \end{bmatrix} \begin{Bmatrix} \mathbf{q} \\ \dot{\mathbf{q}} \end{Bmatrix} + \begin{bmatrix} \hat{\mathbf{B}} \\ 0 \end{bmatrix} \mathbf{u}$$
$$\mathbf{y}_d = [\,\mathbf{H}_d \quad 0\,] \begin{Bmatrix} \mathbf{q} \\ \dot{\mathbf{q}} \end{Bmatrix} \tag{2.1.28}$$

which leads to the symmetric generalized eigenproblem

$$\begin{bmatrix} -\mathbf{K} & 0 \\ 0 & \mathbf{M} \end{bmatrix} \begin{bmatrix} \mathbf{X} \\ \mathbf{X}\mathbf{\Lambda} \end{bmatrix} = \begin{bmatrix} \mathbf{D} & \mathbf{M} \\ \mathbf{M} & 0 \end{bmatrix} \begin{bmatrix} \mathbf{X} \\ \mathbf{X}\mathbf{\Lambda} \end{bmatrix} \mathbf{\Lambda} \tag{2.1.29}$$

such that

$$\begin{bmatrix} \mathbf{X} \\ \mathbf{X}\mathbf{\Lambda} \end{bmatrix}^T \begin{bmatrix} \mathbf{D} & \mathbf{M} \\ \mathbf{M} & 0 \end{bmatrix} \begin{bmatrix} \mathbf{X} \\ \mathbf{X}\mathbf{\Lambda} \end{bmatrix} = \mathbf{I}$$
$$\begin{bmatrix} \mathbf{X} \\ \mathbf{X}\mathbf{\Lambda} \end{bmatrix}^T \begin{bmatrix} -\mathbf{K} & 0 \\ 0 & \mathbf{M} \end{bmatrix} \begin{bmatrix} \mathbf{X} \\ \mathbf{X}\mathbf{\Lambda} \end{bmatrix} = \mathbf{\Lambda} \tag{2.1.30}$$
$$\mathbf{\Lambda} = diag\{\sigma_i \pm j\omega_i, i = 1, \ldots, n\}$$
$$\mathbf{X} = \lfloor \ldots, \Re(\mathbf{X}_i) \pm j\Im(\mathbf{X}_i), \ldots \rfloor$$

An equivalent *normalized damped modal* realization is then given by

$$\dot{\mathbf{z}}_n = \mathbf{\Lambda}\mathbf{z}_n + \mathbf{X}^T\hat{\mathbf{B}}\mathbf{u}$$
$$\mathbf{y}_d = \mathbf{H}_d\mathbf{X}\mathbf{z}_n \tag{2.1.31}$$

Here the columns of $\mathbf{X}$ are the complex damped mode shapes normalized with respect to the physical properties of the structure, and possibly possessing phase relationships within each decoupled mode between spatially distinct points. The symmetry of the damping matrix and the resultant generalized eigenproblem is important because they imply reciprocal behavior between spatially-distinct points. This property of self-adjoint structural systems is

useful for identification because it allows the sensor mode shapes and the modal participation factors of the input forces to be treated as equivalent. For systems possessing gyroscoping damping, for example, it is necessary to apply input forces at every sensor degree of freedom in order to discern the structural properties. This is because the right and left eigenvectors of (2.1.29) are no longer equivalent.

In the case of proportional damping, complex mode shapes and eigenvalues are still obtained when posing the first order eigenproblem as above, but the complex and real modal quantities are directly related to one another for each mode i as

$$\begin{aligned} \sigma_i &= -\zeta_i \omega_{n\,i} \\ \omega_i &= \omega_{n\,i}\sqrt{1-\zeta_i^2} \\ \Re(\mathbf{X}_i) &= \frac{1}{2\sqrt{\omega_i}}\phi_i \\ \Im(\mathbf{X}_i) &= -\frac{1}{2\sqrt{\omega_i}}\phi_i \end{aligned} \tag{2.1.32}$$

where ϕ_i and $\mathbf{X}_i$ are normalized as in (2.1.3) and (2.1.30), respectively. Figure 2.1 illustrates the contributions of the real and imaginary parts of the frequency domain transfer function to a typical displacement response in the case of two closely spaced modes for both proportional and nonproportional damping.

Thus, the intrinsic modes for nonproportional damping are different from those of classically-damped systems. The preceding discussion points out both the distinctions between the undamped and damped eigenproblems and their respective modal parameters, and the importance of the first-order (or state space) form in the behavior of damped structural dynamics. In the next section, some traditional and modern methods for modal testing and

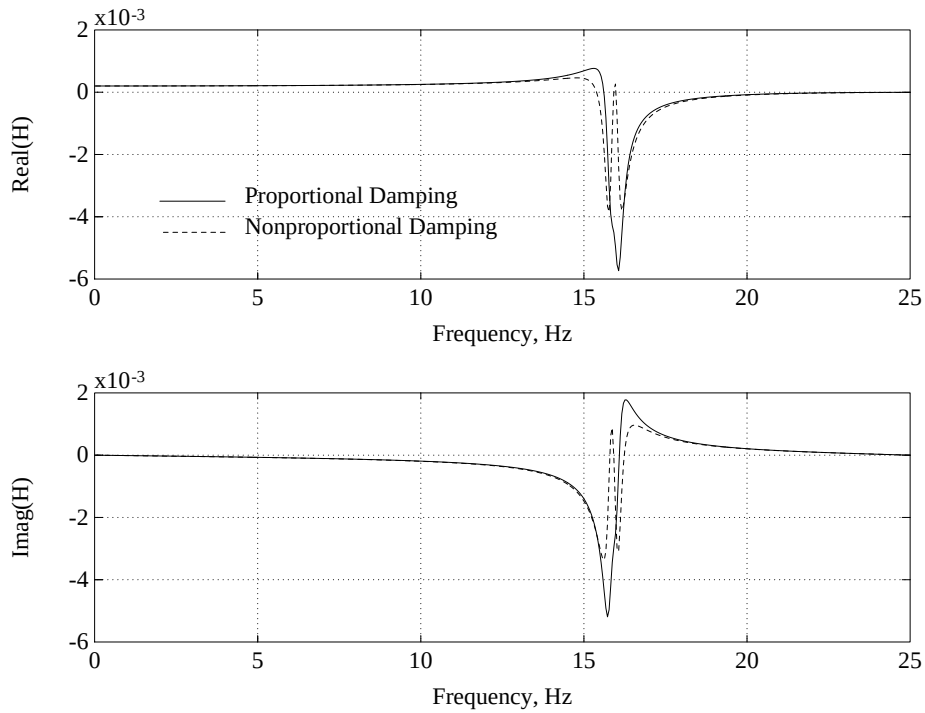

Figure 2.1: Contributions of Real and Imaginary Components of the Frequency Response Function for Proportional and Nonproportional Damping

data analysis will be reviewed and contrasted with the theoretical development of modal parameters.

2.1.5 Displacement-Output Equivalent Realizations

Although the state space models forms developed in the preceding sections are general enough to accommodate displacement, velocity and acceleration sensing, the most convenient form for structural system identification is displacement sensing. This is because the influence matrices for force inputs and displacement outputs in the various physical or modal bases previously studied are identically scaled. This leads to a number of "dual" relationships to be exploited in the following chapters. Fortunately, it is not necessary in theory to utilize displacement sensing in order to apply

identification methods for structural dynamics. Realizations utilizing velocity and acceleration sensing can be effectively "integrated" to determine displacement-equivalent realizations. These realizations possess equivalent damped eigenvalues and eigenvectors (except for scaling), hence there is no loss of accuracy and generality by developing structural identification methods for the displacement-output equivalent realizations. The form is adopted here for simplicity in deriving and presenting second-order identification procedures. Note that this does not imply using acceleration and displacement sensing in model estimations (i.e. realizations) of experimental data is equivalent. The model estimation or realization of experimental data is never exact, hence the specific algorithm employed, and the nature of the parameters matched or the error norms, will affect the results, leading to different identifications of displacement and acceleration output data.

A state space realization of a structural dynamic system is given with displacement outputs $\mathbf{y}_d(t)$ as

$$\begin{aligned} \dot{\mathbf{x}}(t) &= \mathbf{A}\mathbf{x}(t) + \mathbf{B}\mathbf{u}(t) \\ \mathbf{y}_d(t) &= \mathbf{C}_d\mathbf{x} \end{aligned} \tag{2.1.33}$$

Then differentiating $\mathbf{y}_d(t)$ in time, corresponding velocity and acceleration outputs $\mathbf{y}_v(t)$ and $\mathbf{y}_a(t)$ at the same physical degrees of freedom are given as

$$\begin{aligned} \mathbf{y}_v(t) = \dot{\mathbf{y}}_d(t) &= \mathbf{C}_d\dot{\mathbf{x}}(t) \\ &= \mathbf{C}_d\mathbf{A}\mathbf{x}(t) + \mathbf{C}_d\mathbf{B}\mathbf{u}(t) \\ &= \mathbf{C}_v\mathbf{x}(t) + \mathbf{D}_v\mathbf{u}(t) \\ \mathbf{y}_a(t) = \ddot{\mathbf{y}}_d(t) &= \mathbf{C}_d\mathbf{A}\dot{\mathbf{x}}(t) + \mathbf{D}_v\dot{\mathbf{u}}(t) \\ &= \mathbf{C}_d\mathbf{A}^2\mathbf{x}(t) + \mathbf{C}_d\mathbf{A}\mathbf{B}\mathbf{u}(t) + \mathbf{D}_v\dot{\mathbf{u}}(t) \\ &= \mathbf{C}_a\mathbf{x}(t) + \mathbf{D}_a\mathbf{u}(t) + \mathbf{D}_v\dot{\mathbf{u}}(t) \end{aligned} \tag{2.1.34}$$

However, from the underlying physics, acceleration is directly proportional to force but not to derivatives of force, viz.

$$\mathbf{D}_v = \mathbf{C}_d\mathbf{B} = 0 \tag{2.1.35}$$

The displacement, velocity, and acceleration outputs are thus related as

$$\begin{aligned} \mathbf{y}_d(t) &= \mathbf{C}_d\mathbf{x}(t) \\ \mathbf{y}_v(t) &= \mathbf{C}_v\mathbf{x}(t) \\ \mathbf{y}_a(t) &= \mathbf{C}_a\mathbf{x}(t) + \mathbf{D}_a\mathbf{u}(t) \end{aligned} \tag{2.1.36}$$

where

$$\begin{aligned} \mathbf{C}_d &= \mathbf{C}_v\mathbf{A}^{-1} = \mathbf{C}_a\mathbf{A}^{-2} \\ \mathbf{D}_a &= \mathbf{C}_d\mathbf{A}\mathbf{B} = \mathbf{C}_a\mathbf{A}^{-1}\mathbf{B} = \mathbf{H}\mathbf{M}^{-1}\hat{\mathbf{B}} \end{aligned} \tag{2.1.37}$$

Therefore, the displacement-equivalent output influence matrix $\mathbf{C}_d$ can be obtained from a given velocity or acceleration output influence matrix by "integrating" once or twice respectively though multiplication of $\mathbf{A}^{-1}$ as shown in (2.1.37a). The relationship (2.1.37b) is furthermore an indicator of the consistency of the acceleration feedthrough term $\mathbf{D}_a$ with respect to the dynamics of $\mathbf{A}$, $\mathbf{B}$ and $\mathbf{C}_d$, which together are assumed to be the equivalent representation of a second-order force-input, displacement output structural dynamic system. It can be verified that all state space realizations of structural dynamics, i.e. derived from and equivalent to (2.1.1), satisfy (2.1.35)-(2.1.37).

2.2 Frequency Domain Modal Testing and Data Analysis

As mentioned in the introductory chapter, modal tests may employ either narrowband or broadband excitation. The purpose of narrowband excitation, as is typical in tuned sine dwell testing, is the direct steady-state measurement of the modal parameters. The narrowband excitation is employed to excite one mode of vibration at a time. Damping estimates are obtained by the degree of force input required to maintain the modal excitation in a steady-state condition, i.e. the energy input which balances the energy loss from damping. The major problems with tuned sine dwell testing are the expense and time required to perform a full modal survey of a complex structure, ability to discern repeated modal frequencies, the appropriation of multiple actuator forces necessary to accurately tune modes, and the implicit dependence on analytical models to predict where to tune or search for significant modes. Although problematic, much valuable troubleshooting of structural designs has been traditionally accomplished through sine dwell tests.

In the preceding section, various equivalent forms for structural dynamics were presented using both first and second-order equation forms. It was shown that, although these models possess differing matrix coefficients and variable bases, the underlying dynamics as represented by the input-output transfer functions remain invariant. Measurement of the system transfer functions in the frequency domain is then exploited in frequency domain modal testing. The use of broadband testing was first motivated by the need to observe and measure an entire spectrum of vibrational response so as to discern modes which might not have been predicted by analytical modeling. The mathematical foundations of signal analysis through Fourier

transforms predates the use of broadband modal testing. The advent of digital signal processing, however, has enabled broadband testing to become widely utilized. We now briefly review the theory and equations related to frequency domain structural characterization and its relationship to modal parameter estimation.

2.2.1 Frequency Domain Characterization of Structures

The foundation of frequency domain characterization of structures is the *Fourier transform*, defined mathematically as

$$X(f) = \mathcal{F}\left[x(t)\right] = \int_{-\infty}^{\infty} x(t)e^{-j2\pi ft}dt \tag{2.2.1}$$

where $x(t)$ is some continuous function of t and $X(f)$ is the corresponding Fourier transform and a continuous complex function of the cyclical frequency f. In the case of structural dynamics, t is generally the variable for time, and $x(t)$ is a real function relating the change in a parameter to time. Similarly, the *inverse Fourier transform* is given as

$$x(t) = \mathcal{F}^{-1}\left[X(f)\right] = \int_{-\infty}^{\infty} X(f)e^{j2\pi ft}df \tag{2.2.2}$$

In the frequency domain, just as with the Laplace transform, the transforms of the input and output functions $\mathbf{u}$ and $\mathbf{y}$ are related through the transfer function, here termed the *Frequency Response Function* (FRF), and given by

$$\mathbf{Y}(f) = \mathcal{H}(f)\mathbf{U}(f) \tag{2.2.3}$$

where, for linear second-order structural dynamics

$$\mathcal{H}(f) = \left(\mathbf{H}_d + j2\pi f\mathbf{H}_v - 4\pi^2 f^2\mathbf{H}_a\right)\left[-4\pi^2 f^2\mathbf{M} + j2\pi f\mathcal{D} + \mathbf{K}\right]^{-1}\hat{\mathbf{B}} \tag{2.2.4}$$

2.2.2 Determining Response Functions from Modal Tests

The digital counterparts to the Fourier transform and its inverse transform are generally termed *discrete Fourier transforms* (DFT) and are given as

$$\begin{aligned} \bar{X}(f_k, N) &= \Delta t \sum_{n=0}^{N-1} x(n\Delta t)\, e^{-j2\pi nk/N} \qquad k = 0, 1, \ldots, N/2 \\ f_k &= \pm \frac{k}{N\Delta t} \end{aligned} \tag{2.2.5}$$

where bar notation is used to denote the discrete nature of the transform. The *Fast Fourier Transform* (FFT) [65] is a particularly efficient algorithm for computing DFTs when the data record length N is a factor of 2. In modern modal testing and data reduction, digital signal processing utilizing FFTs is the normal procedure for determining discrete FRFs.

In order to obtain the FRFs of the system input-output pairs from the discrete Fourier transforms of the input $\mathbf{u}_j$ and output $\mathbf{y}_j$, the one-sided (i.e. $f_k \geq 0$) auto spectral and cross spectral densities are typically employed [66], viz.

$$\begin{aligned} G_{u_i y_j}(f_k) &= \frac{2}{N} E\left[\mathbf{U}_i(f_k, N)^* \mathbf{Y}_j(f_k, N)\right] \\ G_{u_i u_i}(f_k) &= \frac{2}{N} E\left[\mathbf{U}_i(f_k, N)^* \mathbf{U}_i(f_k, N)\right] \\ G_{y_j y_j}(f_k) &= \frac{2}{N} E\left[\mathbf{Y}_j(f_k, N)^* \mathbf{Y}_j(f_k, N)\right] \end{aligned} \tag{2.2.6}$$

where the operator E denotes averaging of the spectral densities over multiple test trials. From the auto spectral and cross spectral densities, the FRFs and the *coherence function* are computed as

$$\begin{aligned} \mathcal{H}_{u_i y_j}(f_k) &= \frac{G_{u_i y_j}(f_k)}{G_{u_i u_i}(f_k)} \\ \gamma^2_{u_i y_j}(f_k) &= \frac{|G_{u_i y_j}(f_k)|^2}{G_{u_i u_i}(f_k) G_{y_j y_j}(f_k)} \end{aligned} \tag{2.2.7}$$

The model estimation problem may be solved either in the frequency domain using the discrete FRFs as defined above, or in the time-domain. In this case, the FRFs must be transformed using an inverse FFT into the discrete impulse response functions, otherwise known as *Markov parameters*. The Markov parameters are invariant properties of the system dynamics which though discrete convolution relate the forced response of the outputs to the input time history, viz.

$$\mathbf{y}(k) = \sum_{i=0}^{k} \bar{\mathbf{h}}(k-i)\mathbf{u}(i) \tag{2.2.8}$$

where

$$\bar{\mathbf{h}}(t_n) = IDFT(\bar{\mathbf{H}}(j\omega_k))$$

and IDFT symbolizes the inverse of the discrete Fourier transform (2.2.5) as implemented using the FFT-based algorithm. The model estimation problem will now be reviewed, whereby a finite-dimensional model is fit in the frequency or time domain to the FRFs or Markov parameters, leading to the extraction of the damped modal parameters.

2.3 The System Realization Problem and ERA

Generally the measured data obtained from modal testing, typically in the form of discrete FRFs or impulse response functions for each input-output pair, is not utilized directly in model correlation analyses, vibration control design or damage detection algorithms. It is necessary instead to determine a small number of intrinsic modal (hopefully normal mode) parameters which equally represent the large quantity of redundant response samples in the FRFs.

The earliest approaches to model estimation involved circle-fitting methods (e.g. [1]), which yields the estimated frequencies mode shapes and damping for a single FRF (i.e. a single input-output pair). More systematic and rigorous approaches for the Single-Input-Multiple-Output (SIMO) model estimation problem was eventually developed, starting with the *Ibrahim Time Domain* (ITD) [5] and complex exponentials [6], both of which operate in the time domain on the impulse response functions and determine least-squares solutions. It is not possible, however, to distinguish modes with close or identical frequencies using these methods, and so a Polyreference method [7], which determines a solution for the Multiple-Input-Multiple-Output (MIMO) model estimation problem, was developed. The damped modal characteristics are then determined from the poles and residues of the estimated model. Polyreference is similar to the least-square methods except for its multiple-input characteristics, and reduces to the complex exponential method in the case of a single input.

A key characteristic of these methods is that the model order, or the number of intrinsic modes, is not determined systematically by the model estimation solution. The estimated model will typically retain a higher order so that the modes of interest are identified accurately. Then the roots of the estimated model must be studied to determine which are structural and which are residual modes due to the high order of the model. Thus, in terms of linear systems theory, the estimated models lack properties such as model order minimization and model uniqueness. By formally addressing these properties through system realization theory, modern methods of model estimation have been developed which are advantageous for determining minimal-order realizations of MIMO systems. We will now briefly

review the concept of system realization for discrete-time systems and its implementation via the Eigensystem Realization Algorithm (ERA) for the time-domain estimation of modal test models.

2.3.1 Discrete-Time Models and System Realization

The various state space forms discussed previously for a linear time-invariant system are recast in a general form as

$$\begin{aligned} \dot{\mathbf{x}}(t) &= \mathbf{A}\mathbf{x}(t) + \mathbf{B}\mathbf{u}(t) \\ \mathbf{y}(t) &= \mathbf{C}\mathbf{x}(t) + \mathbf{D}\mathbf{u}(t) \end{aligned} \tag{2.3.1}$$

The general state solution of (2.3.1) is

$$\mathbf{x}(t) = \mathbf{h}(t)\mathbf{x}(0) + \int_0^t \mathbf{h}(t-\tau)\mathbf{B}\mathbf{u}(\tau)d\tau \tag{2.3.2}$$

where

$$\mathbf{h}(t) = e^{\mathbf{A}t}$$

is the continuous-time impulse response function.

Now consider a sampled data system with a zero-order hold; that is, the input $\mathbf{u}$ is held constant at the value $\mathbf{u}(k\Delta t)$ over the time $k\Delta t \leq t \leq (k+1)\Delta t$, where Δt is the sampling rate of the input/output data. Then, (2.3.2) at time $t = k\Delta t$ can be expressed as

$$\begin{aligned} \mathbf{x}(k\Delta t) &= \mathbf{h}(k\Delta t)\mathbf{x}(0) + \int_0^{k\Delta t} \mathbf{h}(k\Delta t - \tau)\mathbf{B}\mathbf{u}(\tau)d\tau \\ \mathbf{x}((k+1)\Delta t) &= \mathbf{h}(k\Delta t + \Delta t)\mathbf{x}(0) + \int_0^{k\Delta t} \mathbf{h}(k\Delta t + \Delta t - \tau)\mathbf{B}\mathbf{u}(\tau)d\tau \\ &\quad + \int_{k\Delta t}^{k\Delta t + \Delta t} \mathbf{h}(k\Delta t + \Delta t - \tau)\mathbf{B}\mathbf{u}(\tau)d\tau \\ &= \mathbf{h}(\Delta t)\mathbf{x}(k\Delta t) + \{\int_0^{\Delta t} \mathbf{h}(\Delta t - \hat{\tau})\mathbf{B}d\hat{\tau}\}\mathbf{u}(k\Delta t) \end{aligned} \tag{2.3.3}$$

The corresponding discrete-time (sampled data) model with a zero-order hold and a sampling rate of Δt is therefore given by

$$\begin{aligned} \mathbf{x}(k+1) &= \bar{\mathbf{A}}\mathbf{x}(k) + \bar{\mathbf{B}}\mathbf{u}(k) \\ \mathbf{y}(k) &= \mathbf{C}\mathbf{x}(k) + \mathbf{D}\mathbf{u}(k) \end{aligned} \tag{2.3.4}$$

where

$$\begin{aligned} \bar{\mathbf{A}} &= \mathbf{h}(\Delta t) = e^{\mathbf{A}\Delta t} \\ \bar{\mathbf{B}} &= \int_0^{\Delta t} \mathbf{h}(\Delta t - \tau)\mathbf{B}d\tau = \int_0^{\Delta t} e^{\mathbf{A}(\Delta t - \tau)}\mathbf{B}d\tau \\ \mathbf{x}(k) &= \mathbf{x}(k\Delta t) \\ \mathbf{u}(k) &= \mathbf{u}(k\Delta t) \\ \mathbf{y}(k) &= \mathbf{y}(k\Delta t) \end{aligned} \tag{2.3.5}$$

For an initially-relaxed system ($\mathbf{x}(0) = \mathbf{0}$), the solution for the output $\mathbf{y}(k)$ is given by

$$\begin{aligned} \mathbf{y}(k) &= \mathbf{D}\mathbf{u}(k) + \mathbf{C}\bar{\mathbf{B}}\mathbf{u}(k-1) + \mathbf{C}\bar{\mathbf{A}}\bar{\mathbf{B}}\mathbf{u}(k-2) + \cdots + \mathbf{C}\bar{\mathbf{A}}^{k-1}\bar{\mathbf{B}}\mathbf{u}(0) \\ &= \sum_{i=0}^{k} \mathbf{Y}(k-i)\mathbf{u}(i) \end{aligned} \tag{2.3.6}$$

where $\mathbf{Y}(i)$ are the discrete-time impulse response functions, otherwise known as the *Markov parameters*, defined as

$$\begin{aligned} \mathbf{Y}(0) &= \mathbf{D} \\ \mathbf{Y}(i) &= \mathbf{C}\bar{\mathbf{A}}^{i-1}\bar{\mathbf{B}} \qquad i = 1, \ldots, \infty \end{aligned} \tag{2.3.7}$$

Extending the concept of model equivalence discussed previously, the Markov parameters characterize the unit impulse input/output relationships of the system and as thus are unique for the system. Any equivalent realization of the system must therefore preserve the Markov parameters; in

particular, all nonsingular state basis transformations $\mathbf{x}(k) = \mathbf{P}\mathbf{z}(k)$ lead to equivalent models, as the new model is given by

$$\begin{aligned} \mathbf{z}(k+1) &= \mathbf{P}^{-1}\bar{\mathbf{A}}\mathbf{P}\mathbf{z}(k) + \mathbf{P}^{-1}\bar{\mathbf{B}}\mathbf{u}(k) \\ \mathbf{y}(k) &= \mathbf{C}\mathbf{P}\mathbf{z}(k) + \mathbf{D}\mathbf{u}(k) \end{aligned} \tag{2.3.8}$$

and the Markov parameters are then

$$\begin{aligned} \mathbf{Y}(0) &= \mathbf{D} \\ \mathbf{Y}(i) &= \mathbf{C}\mathbf{P}\left(\mathbf{P}^{-1}\bar{\mathbf{A}}\mathbf{P}\right)^{i-1}\mathbf{P}^{-1}\bar{\mathbf{B}} = \mathbf{C}\bar{\mathbf{A}}^{i-1}\bar{\mathbf{B}} \end{aligned} \tag{2.3.9}$$

The *system realization problem* is: given a sequence of Markov parameters $\mathbf{Y}(i)$ of the system (2.3.4), determine a realization $[\bar{\mathbf{A}}_0, \bar{\mathbf{B}}_0, \mathbf{C}_0]$ which best approximates the given Markov sequence according to some measure of accuracy, viz.

$$\begin{aligned} \mathbf{x}_0(k+1) &= \bar{\mathbf{A}}_0\mathbf{x}_0(k) + \bar{\mathbf{B}}_0\mathbf{u}(k) \\ \mathbf{y}(k) &= \mathbf{C}_0\mathbf{x}_0(k) + \mathbf{D}_0\mathbf{u}(k) \end{aligned} \tag{2.3.10}$$

such that

$$\mathbf{D}_0 = \mathbf{Y}(0)$$

$$\mathbf{C}_0\bar{\mathbf{A}}_0^{i-1}\bar{\mathbf{B}}_0 \approx \mathbf{Y}(i), \qquad i = 1, 2, \ldots$$

where $\mathbf{x}_0$ is the resultant state vector and $\mathbf{u}$ and $\mathbf{y}$ are the system inputs and outputs. Clearly, there are an infinite number of equivalent realizations for the given data; that is, any set $[\mathbf{P}^{-1}\bar{\mathbf{A}}_0\mathbf{P}, \mathbf{P}^{-1}\bar{\mathbf{B}}_0, \mathbf{C}_0\mathbf{P}]$ is an equivalent realization, where $\mathbf{P}$ is a nonsingular basis transformation $\mathbf{x}_0(k) = \mathbf{P}\mathbf{x}_p(k)$. Solution of the realization problem concerns issues of model order, uniqueness, noise, model measures to be fitted, etc.

2.3.2 The Eigensystem Realization Algorithm (ERA)

As an example of practical system realization for structural identification, the *Eigensystem Realization Algorithm* (ERA) [8] is presented herein. This technique provides a systematic approach to model order determination for a given accuracy, and the derivation of the discrete state space model. The algorithm itself was developed by Ho and Kalman [13] and uses the discrete-time shift of the Markov parameters, which are used to form a *Hankel matrix*, defined as follows.

$$\mathbf{H}_{qd}(k) = \begin{bmatrix} \mathbf{Y}(k+1) & \mathbf{Y}(k+2) & \cdots & \mathbf{Y}(k+d) \\ \mathbf{Y}(k+2) & \mathbf{Y}(k+3) & \cdots & \mathbf{Y}(k+d+1) \\ \cdot & \cdot & \cdot & \cdot \\ \cdot & \cdot & \cdot & \cdot \\ \cdot & \cdot & \cdot & \cdot \\ \mathbf{Y}(k+q) & \mathbf{Y}(k+q+1) & \cdots & \mathbf{Y}(k+q+d-1) \end{bmatrix} \tag{2.3.11}$$

We also define the order-q observability and order-d controllability matrices in terms of the desired system matrices $[\bar{\mathbf{A}}_0, \bar{\mathbf{B}}_0, \mathbf{C}_0]$ as

$$\mathbf{V}_q = \begin{bmatrix} \mathbf{C}_0 \\ \mathbf{C}_0\bar{\mathbf{A}}_0 \\ \cdot \\ \cdot \\ \cdot \\ \mathbf{C}_0\bar{\mathbf{A}}_0^{q-1} \end{bmatrix} \qquad \mathbf{W}_d = [\, \bar{\mathbf{B}}_0 \quad \bar{\mathbf{A}}_0\bar{\mathbf{B}}_0 \quad \cdots \quad \bar{\mathbf{A}}_0^{d-1}\bar{\mathbf{B}}_0 \,] \tag{2.3.12}$$

Then, the Hankel matrix (2.3.11) is directly related to the unknown realization, as

$$\mathbf{H}_{qd}(k) = \mathbf{V}_q\bar{\mathbf{A}}_0^k\mathbf{W}_d \tag{2.3.13}$$

Juang and Pappa [8] introduced the use of the *singular value decomposition (SVD)* of $\mathbf{H}_{qd}(k)$ to generalize the Ho-Kalman algorithm to structural system

identification when noise is present. Thus, for ERA, the measured Hankel matrix is expressed as

$$\mathbf{H}_{qd}(k) = \mathbf{P}\mathbf{S}\mathbf{Q}^T = \sum_{i=1}^{N_{max}} s_i \mathbf{p}_i \mathbf{q}_i^T \tag{2.3.14}$$

where $\mathbf{P}$ and $\mathbf{Q}$ are orthonormal $q \times q$ and $d \times d$ matrices composed of column vectors $\mathbf{p}_i$ and $\mathbf{q}_i$, respectively, $\mathbf{S}$ is a $q \times d$ matrix with the singular values s_i of $\mathbf{H}_{qd}(k)$ on the main diagonal and zeros elsewhere, and N_{max} is the minimum of q and d. Minimum model order is determined by minimizing the matrix norm between the measured and realized Hankel matrices $\mathbf{H}_{qd}(k)$ and $\hat{\mathbf{H}}_{qd}(k)$, viz.

$$\min \|\mathbf{H}_{qd}(k) - \hat{\mathbf{H}}_{qd}(k)\|$$

$\hat{\mathbf{H}}_{qd}(k)$ can be determined by truncating the SVD series expansion given in (2.3.14), that is determining N such that $s_{N+1} \leq \epsilon \approx 0$. Therefore, using the measured Hankel matrix $\mathbf{H}_{qd}(0)$, the realized Hankel matrix $\hat{\mathbf{H}}_{qd}(0)$ is

$$\hat{\mathbf{H}}_{qd}(0) \approx \sum_{i=1}^{N} s_i \mathbf{p}_i \mathbf{q}_i^T = \mathbf{P}_N \mathbf{S}_N \mathbf{Q}_N^T \tag{2.3.15}$$

where

$$\mathbf{P}_N = \mathbf{P}(1:q, 1:N) \qquad \mathbf{S}_N = \mathbf{S}(1:N, 1:N) \qquad \mathbf{Q}_N = \mathbf{Q}(1:d, 1:N) \tag{2.3.16}$$

Then, having properly determined N, let

$$\hat{\mathbf{W}}_d = \mathbf{S}_N^{1/2} \mathbf{Q}_N^T \qquad \hat{\mathbf{V}}_q = \mathbf{P}_N \mathbf{S}_N^{1/2} \tag{2.3.17}$$

and derive $\bar{\mathbf{A}}_0$ using $\mathbf{H}_{qd}(k)$, viz.

$$\mathbf{H}_{qd}(k) = \hat{\mathbf{V}}_q \bar{\mathbf{A}}^k \hat{\mathbf{W}}_d = \mathbf{P}_N \mathbf{S}_N^{1/2} \bar{\mathbf{A}}^k \mathbf{S}_N^{1/2} \mathbf{Q}_N^T \tag{2.3.18}$$

$$\bar{\mathbf{A}}_0^k = \mathbf{S}_N^{-1/2}\mathbf{P}_N^T\mathbf{H}_{qd}(k)\mathbf{Q}_N\mathbf{S}_N^{-1/2} \tag{2.3.19}$$

Specifically, $\bar{\mathbf{A}}_0$ is generally found using $\mathbf{H}_{qd}(1)$ since this allows the maximum values for q and d given a finite length data set, does not require any further computation to find $\bar{\mathbf{A}}_0$, and is least sensitive to the effects of noise. Thus

$$\bar{\mathbf{A}}_0 = \mathbf{S}_N^{-1/2}\mathbf{P}_N^T\mathbf{H}_{qd}(1)\mathbf{Q}_N\mathbf{S}_N^{-1/2} \tag{2.3.20}$$

Finally, $\bar{\mathbf{B}}_0$ and $\mathbf{C}_0$ are given directly by matrix partitions of $\mathbf{V}_q$ and $\mathbf{W}_d$, respectively,

$$\bar{\mathbf{B}}_0 = \hat{\mathbf{W}}_d(1:N, 1:m) \qquad \mathbf{C}_0 = \hat{\mathbf{V}}_q(1:l, 1:N) \tag{2.3.21}$$

and $\mathbf{D}_0$, which is invariant to the state basis definition, is given by

$$\mathbf{D}_0 = \mathbf{Y}(0) \tag{2.3.22}$$

There are an infinite number of equivalent realizations obtainable using the Hankel-based formulation shown above. This particular realization, however is distinctive in the following ways. First and foremost, it is a minimal-order realization in the absence of noise or for a defined accuracy because of the singular value decomposition (i.e. generalized pseudo-inverse) formulation of $\hat{\mathbf{V}}_q$ and $\hat{\mathbf{W}}_d$. Secondly, it is a balanced realization due to the equal distribution of the singular values of $\mathbf{H}_{qd}(0)$ in the definitions of $\hat{\mathbf{V}}_q$ and $\hat{\mathbf{W}}_d$.

This is the basic development and approach for modern time-domain model realization using ERA, though a number of theoretical and computational variations exist [17-18]. This family of identification algorithms share a common aspect, that of requiring as input the discrete system Markov parameters, which can be obtained through discrete Fourier transforms and

spectral analysis as detailed in Section 2.2. A recent development also allows derivation of the Markov parameters in the time domain, with a side benefit of providing filter gains of an asymptotically stable observer model [67]. This approach is related to the use of *auto regressive moving average* (ARMA) methods known in classical system identification [22].

2.3.3 Determining the Damped Modal Realization from ERA

Using the resultant system realization provided by ERA, the damped modal parameters are obtained as follows. Using the eigenvectors $\mathbf{\Psi}$ of $\bar{\mathbf{A}}$, defined as

$$\bar{\mathbf{A}}_0 \mathbf{\Psi} = \mathbf{\Psi} \bar{\mathbf{\Lambda}} \tag{2.3.23}$$

the damped mode shapes $\mathbf{C}_z$ and continuous-time complex eigenvalues are

$$\begin{aligned}
\bar{\mathbf{\Lambda}} &= \mathbf{\Psi}^{-1} \bar{\mathbf{A}}_0 \mathbf{\Psi} \\
\mathbf{\Lambda} &= \frac{\ln \bar{\mathbf{\Lambda}}}{\Delta t} = diag\{\sigma_i \pm j\omega_i, i = 1, \ldots, n\} \\
\mathbf{C}_z &= \begin{cases} \mathbf{C}_0 \mathbf{\Psi} & \text{for displacement sensing} \\ \mathbf{C}_0 \mathbf{\Psi} \mathbf{\Lambda}^{-1} & \text{for velocity sensing} \\ \mathbf{C}_0 \mathbf{\Psi} \mathbf{\Lambda}^{-2} & \text{for acceleration sensing} \end{cases} \\
\mathbf{C}_z &= \lfloor \ldots, \Re(\mathbf{C}_{z\,i}) \pm \Im(\mathbf{C}_{z\,i}), \ldots \rfloor \quad i = 1, \ldots, n
\end{aligned} \tag{2.3.24}$$

and the *damped modal* realization for displacement output, equivalent to (2.3.10) in continuous-time, is given by

$$\begin{aligned}
\dot{\mathbf{z}} &= \mathbf{\Lambda} \mathbf{z} + \mathbf{B}_z \mathbf{u} \\
\mathbf{y}_d &= \mathbf{C}_z \mathbf{z}
\end{aligned} \tag{2.3.25}$$

where

$$\mathbf{B}_z = \mathbf{\Psi}^{-1} \mathbf{B}_0 \tag{2.3.26}$$

and $\mathbf{B}_0$ is the continuous-time transform of $\bar{\mathbf{B}}_0$.

The damped modal realization (2.3.25) is one of the primary model realizations sought in structural system identification, as it is equivalent to the normalized damped modal realization (2.1.31) to within an arbitrary complex scaling of the state basis. As noted previously, when driving-point measurements (from sensors collocated with the forcing inputs) are available, the symmetry of the input and output matrix coefficients in (2.1.31) can be exploited to determine the complex scaling relating $\mathbf{C}_z$ and $\mathbf{X}$, and thus determine the "mass-normalized" damped mode shapes $\mathbf{X}$.

Note that, for a collocated actuator J and sensor K, $\mathbf{H}_K = \hat{\mathbf{B}}_J$. Thus, in the displacement output realization, the force-state input influence array and the state-output influence arrays are transposes of one another. This provides a criterion for physically-based normalization of the damped mode shapes such that they can be interpreted as the normalized damped mode shapes $\mathbf{X}$ without *a priori* knowledge of $\mathbf{M}$, $\mathbf{D}$ and $\mathbf{K}$. The correct physically-based normalization of the damped modal realization is as follows. The damped modal states $\mathbf{z}$ and their normalized counterparts $\mathbf{z}_n$ are related by a complex scaling transformation $\mathbf{F}_n$, viz.

$$\mathbf{z}_n = \mathbf{F}_n \mathbf{z} \tag{2.3.27}$$

where $\mathbf{F}_n$ is diagonal. Applying the similarity transformation $\mathbf{F}_n$ to the damped modal realization (2.3.25) with displacement output, the normalized damped modal realization is given by

$$\begin{aligned} \dot{\mathbf{z}}_n &= \mathbf{\Lambda} \mathbf{z}_n + \mathbf{F}_n \mathbf{B}_z \mathbf{u} \\ \mathbf{y}_d &= \mathbf{C}_z \mathbf{F}_n^{-1} \mathbf{z}_n \end{aligned} \tag{2.3.28}$$

The normalization of the damped mode shapes $\mathbf{X}$ implies that, for a collocated force input J and displacement output K, the normalized force-state influence matrix $\mathbf{F}_n\mathbf{B}_z$ is the transpose of the state-output influence matrix $\mathbf{C}_z\mathbf{F}_n^{-1}$. Therefore, for each state z_i,

$$\begin{aligned} f_i B_{ziJ} &= \frac{C_{ziK}}{s_i} \\ \Rightarrow f_i &= \sqrt{\frac{C_{ZiK}}{B_{ziJ}}} \\ \mathbf{F}_n &= diag\{f_i, i = 1, \ldots, 2n\} \end{aligned} \tag{2.3.29}$$

Thus, the normalized mode shapes $\mathbf{HX} = \mathbf{C}_z\mathbf{F}_n^{-1}$ can be determined from the unscaled damped modal realization (2.3.25) using driving point measurements. If the driving point sensor measures acceleration, then recalling (2.1.37) the output influence matrix in the $\mathbf{z}$ basis $\mathbf{C}_0\mathbf{\Psi}$ can be effectively integrated by postmultiplying with $\mathbf{\Lambda}^{-2}$ and then treated as the damped displacement mode shapes $\mathbf{C}_z$ thereafter.

2.4 Concluding Remarks

In this chapter, a number of equivalent second-order and state space realizations of structural dynamics have been reviewed, concluding with the damped modal realization which expresses the intrinsic modal parameters of the generally damped structural system. A brief discussion of discrete frequency domain characterization of structures was also given, focusing on the definition of response functions and their determination using broadband modal testing and digital signal processing techniques. Finally, the model estimation problem was reviewed and its solution via system realization, and in particular ERA, was presented in detail. It was shown how the ERA

realization can be transformed into the damped modal realization which yields the damped modal parameters $\mathbf{\Lambda}$ and $\mathbf{C}_z$.

Thus, the damped modal parameters of (2.1.1) are derivable in a general sense from broadband modal testing and system realization methods. As discussed in Chapter I, however, these modal parameters still implicitly contain the influence of system damping, and are thus only directly applicable to physical parameter derivation and model correction when the damping can be accurately characterized independently of the structure's mass and stiffness. Unfortunately, damping is usually the least understood or accurately known physical quantity. Thus, the normal modes, which express the undamped system behavior, are the desired modal quantities for model updating and physical parameter determination. In the next chapter, methods for estimating normal modal parameters from $\mathbf{\Lambda}$ and $\mathbf{C}_z$ will be reviewed, and a new method based on similarity transformations will be presented for approximating the normal modal parameters from the damped modal parameters $\mathbf{\Lambda}_i$ and $\mathbf{C}_{zi}$ of individual damped first-order modes.

CHAPTER III

COMMON BASIS-NORMALIZED STRUCTURAL IDENTIFICATION

3.1 Introduction

This chapter presents a procedure for transforming the system theory-based realization models into corresponding normal modal coordinate-based structural models. Since a key idea employed in the development of the present procedure is a common basis which is objectively oriented and normalized, it is designated as a *common basis-normalized structural identification* (CBSI) procedure. The resultant model is a uniquely-defined realization for a given sequence of Markov parameters, which in turn are uniquely determined for a linear structure with given inputs and outputs. Thus, the CBSI method leads to a unique estimation of the normal modal parameters for a given measure of the system dynamics. That is, regardless of the model estimation algorithm used, and the rotation and scaling of the damped modes which results, CBSI can transform equivalent realizations of the system to the same objectively-defined normal modal coordinate definition and thus will recover identical normal modal parameters.

The transformations employed by CBSI are determined and applied on each damped mode individually, and thus CBSI is a normal mode estimation technique. That is, because CBSI does not account for the coupling

effects of nonproportional damping, which violates the one-to-one correspondence between the damped and normal modal vectors, it is not possible in general to capture the true normal modal parameters, and thus the relevant partitions of the CBSI-transformed realization contains estimates of the normal modes. However, because of the transformation procedure approach used, the state space realization obtained using CBSI is fully equivalent to the damped modes. The equivalence of the CBSI state space realization is useful in that the residuals of the normal mode estimates, that is the partitions of the realization not fitting the MDV basis form, can be used to directly quantify the effects of estimating the system dynamics using proportionally-damped normal modal parameters.

There are several by-products that the present procedure provides, primarily due to the common basis normalization employed in the procedure. First, the present transformation procedure allows the integration of different realized models with varying actuator and sensor locations if they arise from the same structure. Second, each sensor/actuator pair or groups of sensors and actuators can be processed in parallel and combined concurrently or sequentially for the construction of a global model. From a structural dynamics point of view, the transformation to an objective basis provides a state space model coinciding with the canonical form of the second-order equations of motion, thus extracting the classical real-valued parameters of interest to modal testing, mass-normalized normal modes and a diagonal modal damping matrix, while maintaining the system equivalence properties of the state space form.

This Chapter is a more formal treatment of the CBSI method presented previously in [55]. That work has been extended to correctly determine objective bases in general symmetrically-damped multiple-input-multiple-output (MIMO) systems. This is accomplished by minimizing partitions of either the **B** or **C** arrays through an optimization-based formulation, which leads effectively to a least-square solution for the transformation parameters. In addition, an alternate symmetrical formulation of CBSI, which is alluded to in [56], is formally developed, leading to a symmetrical companion form realization. The symmetrical CBSI requires driving point measurements in order to correctly rotate the damped mode shapes, as opposed to a rotation of the real mode estimates as in [55]. The least-square CBSI does not specifically require this normalization, although a mass normalization of the mode shapes can be effectively found using driving point measurements with any of the CBSI algorithm variants.

The normal mode estimation problem is presented in Section 3.2, including a brief theoretical review of existing methods. In Section 3.3, a transformation theory for obtaining a second-order canonical basis is developed. It is then shown that the procedure applied in [27] for mode shape identification does not recover a second-order basis. The CBSI procedure is then presented in Section 3.4, which develops a second transformation for the McMillan normal form realization of [27] such that the correct second-order canonical basis is obtained. Finally, the symmetrical CBSI method is presented as an alternative to the similarity transformation-based methods of the basic CBSI. Numerical examples of the CBSI procedures are given in Section 3.5.

3.2 Normal Mode Estimation from Damped Modes

As discussed in Chapter I, the normal mode estimation problem is a subclass of the general normal mode determination problem. In normal mode estimation, the normal mode shapes are determined individually from each decoupled damped mode, so that the resultant normal modes are assumed to be related one-to-one with the damped modes. Recalling (2.1.32), the damped and normal modal quantities for proportional damping are directly related to one another for each mode i as

$$\begin{aligned} \sigma_i &= -\zeta_i \omega_{ni} \\ \omega_i &= \omega_{ni}\sqrt{1-\zeta_i^2} \\ \Re(\mathbf{X}_i) &= \frac{1}{2\sqrt{\omega_1}}\phi_i \\ \Im(\mathbf{X}_i) &= -\frac{1}{2\sqrt{\omega_1}}\phi_i \end{aligned} \tag{3.2.1}$$

where ϕ_i and $\mathbf{X}_i$ are the mass-normalized normal and damped mode shapes, respectively, σ_i and ω_i are the real and imaginary parts of the first-order eigenvalues, respectively, ω_{ni} is the undamped natural frequency, and ζ_i is the modal damping ratio. This condition only holds completely for proportionally-damped systems, or in the limit as the degree of damping goes to zero. Hence, in the more general damping case, the mode-by-mode approach to normal modal parameter estimation is an approximation. The alternate approach to normal mode determination requires the damping to be completely decoupled from the normal modal parameters through a general transformation which spans the full state space of the realization. This problem, termed mode shape-damping decoupling, is studied in Chapter 4.

3.2.1 Traditional Approximation Methods

The traditional approach to normal mode estimation is based on the expression of proportionally-damped behavior in the first-order damped or complex modes. Using (3.2.1), the undamped frequency and damping ratio are found as

$$\begin{aligned} {\omega_n}_i^2 &= \sigma_i^2 + \omega_i^2 \\ \zeta_i &= -\frac{\sigma_i}{\omega_{ni}} \end{aligned} \tag{3.2.2}$$

The above result is unambiguous and common to most normal mode estimation methods, including CBSI, because it is the only result which holds correctly for the exact case, i.e. when the damping is proportional. Note, however, that (3.2.2) does not hold for the nonproportional damping case. Hence, the existence of nonproportional damping affects not only the accuracy of estimated normal mode shapes, but also the estimated natural frequency and modal damping ratio.

The problem of normal mode shape estimation, however, is not as well determined. Ignoring the scaling of the vector, the correct normal mode shape can be determined by any combination of the real and imaginary components of the damped mode shape in the case of proportional damping. The Standard Technique (ST) (e.g. see Imregun and Ewins [25]) is evolved from interpreting the complex mode shape for mode i as vectors of magnitudes $\bar{X}_{ij}$ and phase angles α_{ij} at spatial points j such that

$$\begin{aligned} \Re(X_{ij}) &= \bar{X}_{ij} \cos \alpha_{ij} \\ \Im(X_{ij}) &= \bar{X}_{ij} \sin \alpha_{ij} \end{aligned} \quad \Longleftrightarrow \quad \begin{aligned} \bar{X}_{ij} &= \sqrt{\Re(X_{ij})^2 + \Im(X_{ij})^2} \\ \alpha_{ij} &= \tan^{-1}\left(\frac{\Im(X_{ij})}{\Re(X_{ij})}\right) \end{aligned} \tag{3.2.3}$$

For proportional damping, the phase angles α_{ij} are given as

$$\alpha_{ij} - \alpha_{0\,i} = (\mathrm{sgn}_j)\frac{\pi}{2} \tag{3.2.4}$$

where α_0 is an arbitrary angle dependent on the complex scaling of $\mathbf{X}_i$ and (sgn_j) is the sign function which is equal to $+1$ or -1 and varies with spatial location j. The components X_{ij} are said to be purely in-phase or out-of-phase if (3.2.4) holds. In the case of modes which are close to proportionally damped, the phase angles are clustered about $\alpha_{0\,i} \pm \frac{\pi}{2}$, viz.

$$\alpha_{ij} - \alpha_{0\,i} = (\mathrm{sgn}_j)\frac{\pi}{2} + \epsilon_j \tag{3.2.5}$$

The standard technique for normal mode shape estimation is then to neglect the variation ϵ_j in non-normal phase components, i.e. let $\epsilon_j \approx 0$. Thus, the normal mode estimates are given as

$$\phi_{ij} = \bar{X}_{ij}(\mathrm{sgn}_j) \tag{3.2.6}$$

Here, (sgn_j) is generally found by determining $\alpha_{0\,i}$ through a linear regression of the complex mode shape

$$\alpha_{0\,i} = \tan^{-1}\frac{\Re(\mathbf{X}_i)^T\Im(\mathbf{X}_i)}{\Re(\mathbf{X}_i)^T\Re(\mathbf{X}_i)} - \frac{\pi}{2} \tag{3.2.7}$$

Then the sign function is given as

$$(\mathrm{sgn}_j) = \begin{cases} -1 & \sin(\alpha_{ij} - \alpha_{0\,i}) < 0 \\ +1 & \sin(\alpha_{ij} - \alpha_{0\,i}) > 0 \end{cases} \tag{3.2.8}$$

While the standard technique is straightforward, it lacks a basis in the context of model equivalence previously discussed. That is, the relationship between the damped modal coordinates, and thus back to the original states

of the estimated model, is lost. An alternative to the standard technique is to utilize similarity transformations such that a new realization of the dynamics is obtained which is fully equivalent to the original realization but which directly expresses the modal parameters sought by the normal mode estimation problem. This alternative approach is explored in the next section.

3.2.2 McMillan Normal-Form Transformation

Transformation-based methods generally begin from the solution for the frequencies and damping ratios given by (3.2.2), coupled with the MDV state space model form presented in Chapter 2. Recalling (2.1.18), the aim of the transformation-based normal mode estimation method is to determine a change-of-basis transformation $\mathbf{V}_i$ for mode i such that the resultant equivalent realization is given in the MDV form as

$$\begin{aligned} \begin{Bmatrix} \dot{\eta}_i(t) \\ \ddot{\eta}_i(t) \end{Bmatrix} &= \begin{bmatrix} 0 & 1 \\ -\omega_{n\,i}^2 & -2\zeta_i\omega_{n\,i} \end{bmatrix} \begin{Bmatrix} \eta_i(t) \\ \dot{\eta}_i(t) \end{Bmatrix} + \begin{bmatrix} 0 \\ \phi_i^T \hat{\mathbf{B}} \end{bmatrix} \mathbf{u}(t) \\ \mathbf{y}_d(t) &= \sum_{i=1}^{n} [\, \mathbf{H}_d \phi_i \quad 0 \,] \begin{Bmatrix} \eta_i(t) \\ \dot{\eta}_i(t) \end{Bmatrix} \end{aligned} \tag{3.2.9}$$

For clarity, (3.2.9) is written for a system with displacement sensing, but the results throughout this chapter are easily extendible to velocity and acceleration sensing by integrating the outputs as detailed in Chapter II, Section 2.1.5. The form of the $\mathbf{A}$ matrix in this realization is sometimes referred to as the McMillan normal form (e.g. see Longman and Juang [27]). The transformation is determined from the damped modal basis (see (2.3.25)), given for each mode i as

$$\begin{aligned} \begin{Bmatrix} \dot{z}_i(t) \\ \bar{z}_i(t) \end{Bmatrix} &= \begin{bmatrix} \sigma_i + j\omega_i & 0 \\ 0 & \sigma_i - j\omega_i \end{bmatrix} \begin{Bmatrix} z_i(t) \\ \bar{z}_i(t) \end{Bmatrix} + \begin{bmatrix} \mathbf{b}_{z\,i}^T \\ \bar{\mathbf{b}}_{z\,i}^T \end{bmatrix} \mathbf{u}(t) \\ \mathbf{y}_d(t) &= \sum_{i=1}^{n} [\, \mathbf{C}_{z\,i} \quad \bar{\mathbf{C}}_{z\,i} \,] \begin{Bmatrix} z_i(t) \\ \bar{z}_i(t) \end{Bmatrix} \end{aligned} \tag{3.2.10}$$

where $\bar{z}_i(t)$, $\bar{\mathbf{b}}_i^T$ and $\bar{\mathbf{C}}_{z\,i}$ are complex conjugates of the complex quantities $z_i(t)$, $\mathbf{b}_i^T$ and $\mathbf{C}_{z\,i}$, respectively. In [27], a solution for $\mathbf{V}_i$ was given as

$$\begin{aligned} \mathbf{V}_{i1}^{-1} &= \begin{bmatrix} 1 & 1 \\ \sigma_i + j\omega_i & \sigma_i - j\omega_i \end{bmatrix} \\ \mathbf{V}_{i1} &= \frac{j}{2\omega_i} \begin{bmatrix} \sigma_i - j\omega_i & -1 \\ -\sigma_i - j\omega_i & 1 \end{bmatrix} \end{aligned} \tag{3.2.11}$$

such that

$$\mathbf{V}_{i1}^{-1} \begin{bmatrix} \sigma_i + j\omega_i & 0 \\ 0 & \sigma_i - j\omega_i \end{bmatrix} \mathbf{V}_{i1} = \begin{bmatrix} 0 & 1 \\ -\omega_{n\,i}^2 & -2\zeta_i\omega_{n\,i} \end{bmatrix} \tag{3.2.12}$$

As will be shown in the next section, however, this transformation does not correctly transform the damped modal coordinates $z_i(t)$ to a second-order canonical basis, as in the MDV model (3.2.9). The CBSI algorithm does provide a correct solution to the transformation-based normal mode estimation problem.

3.3 Transformation to Canonical Variables

The CBSI method is based on a consistent transformation which correctly satisfies the conditions for a second-order canonical state basis. That is, in order for the resultant system realization to match or coincide with the characteristics of second-order equations of motion, the basis transformation must be specifically constrained. In this section, the criteria for transformations to the second-order canonical form are developed and the McMillan normal form transformation, which was defined in the preceding section, is evaluated in accordance with the second-order transformation criteria.

A second-order canonical realization of the system dynamics is one for which the basis definition can be written as

$$\mathbf{x}(t) = \begin{Bmatrix} \mathbf{p}_d(t) \\ \dot{\mathbf{p}}_d(t) \end{Bmatrix} \tag{3.3.1}$$

where $\mathbf{p}_d(t)$ is a second-order state variable such that the first-order basis definition $\mathbf{x}(t)$ spans the state space of the original realization. If a given realization of arbitrary basis definition is given by

$$\begin{aligned} \dot{\mathbf{x}}_0(t) &= \mathbf{A}_0\mathbf{x}_0(t) + \mathbf{B}_0\mathbf{u}(t) \\ \mathbf{y}(t) &= \mathbf{C}_0\mathbf{x}_0(t) + \mathbf{D}_0\mathbf{u}(t) \end{aligned} \tag{3.3.2}$$

then an order-n state variable $\mathbf{p}(t)$ can be defined in terms of the order-$2n$ state vector $\mathbf{x}_0(t)$, viz.

$$\mathbf{p}_d(t) = \mathbf{P}\mathbf{x}_0(t) \tag{3.3.3}$$

Differentiating (3.3.3), the time derivative of the second-order state $\mathbf{p}_d(t)$ is given as

$$\begin{aligned} \dot{\mathbf{p}}_d(t) &= \mathbf{P}\dot{\mathbf{x}}_0(t) \\ &= \mathbf{P}\mathbf{A}_0\mathbf{x}_0(t) + \mathbf{P}\mathbf{B}_0\mathbf{u}(t) \end{aligned} \tag{3.3.4}$$

Now, define a new state basis and transformation as

$$\begin{Bmatrix} \mathbf{p}_d(t) \\ \mathbf{p}_v(t) \end{Bmatrix} = \mathbf{V}^{-1}\mathbf{x}_0(t) \tag{3.3.5}$$

where

$$\mathbf{V}^{-1} = \begin{bmatrix} \mathbf{P} \\ \mathbf{P}\mathbf{A}_0 \end{bmatrix} \tag{3.3.6}$$

Combining (3.3.4)-(3.3.6), $\mathbf{p}_v(t)$ and $\dot{\mathbf{p}}_d(t)$ are related as

$$\dot{\mathbf{p}}_d(t) = \mathbf{p}_v(t) + \mathbf{P}\mathbf{B}_0\mathbf{u}(t) \tag{3.3.7}$$

Therefore, for the new state basis given in (3.3.5) to be equivalent to the second-order canonical basis (3.3.1), the constraint

$$\mathbf{P}\mathbf{B}_0 = 0 \tag{3.3.8}$$

must be satisfied. The transformation $\mathbf{V}$ in (3.3.6) which satisfies the constraint (3.3.8) leads to an new state space realization which is equivalent to n second-order equilibrium equations augmented by n identity equations

$$\dot{\mathbf{p}}_d(t) = \mathbf{p}_v(t)$$

Note that the transformation $\mathbf{P}$ can be arbitrarily scaled without violating the constraint condition. Thus, satisfying the constraint $\mathbf{P}\mathbf{B}_0 = 0$ does not uniquely define the transformation $\mathbf{P}$. Generally, some scaling for $\mathbf{P}$ must also be chosen in order to objectively define the resultant second-order basis $\mathbf{x}$. It will be seen that in applying this transformation theory to the problem of normal mode estimation, various scaling choices affect only the real scaling of the normal mode shapes.

To apply the general transformation theory to the problem of normal mode estimation, the initial realization basis chosen is the individual damped modal displacements $z_i(t)$ and $\bar{z}_i(t)$ from (3.2.10). Therefore, a second-order variable $\eta(t)$ can be defined as

$$\eta(t) = \mathbf{P}_i \begin{Bmatrix} z_i(t) \\ \bar{z}_i(t) \end{Bmatrix} = d_i \begin{bmatrix} 1 & e_i \end{bmatrix} \begin{Bmatrix} z_i(t) \\ \bar{z}_i(t) \end{Bmatrix} \tag{3.3.9}$$

Using (3.3.5)-(3.3.6), the definition for the required transformation is

$$\begin{Bmatrix} \eta(t) \\ \dot{\eta}(t) \end{Bmatrix} = \mathbf{V}_i^{-1} \begin{Bmatrix} z_i(t) \\ \bar{z}_i(t) \end{Bmatrix} = d_i \begin{bmatrix} 1 & e_i \\ \sigma_i + j\omega_i & e_i\,(\sigma_i - j\omega_i) \end{bmatrix} \begin{Bmatrix} z_i(t) \\ \bar{z}_i(t) \end{Bmatrix} \tag{3.3.10}$$

with the constraint from (3.3.8)

$$\mathbf{P}_i\mathbf{B}_{zi} = \mathbf{b}_{z\ i}^T + e_i\bar{\mathbf{b}}_{z\ i}^T = 0 \tag{3.3.11}$$

Thus e_i is specifically defined by the constraint, while d_i is an arbitrary real scalar quantity.

Note that letting $d_i = 1$ and $e_i = 1$ leads to the McMillan normal form solution $\mathbf{V}_{i1}$ from [27] for $\mathbf{V}_i$. Evaluating the constraint, however, results in

$$\Re(\mathbf{b}_{z\ i}^T) = 0 \tag{3.3.12}$$

Thus, in order for the McMillan normal form transformation (3.2.11) to yield a canonical basis, the damped modal coordinates $z_i(t)$ must be rotated using an arbitrary complex scalar such that (3.3.12) holds. Correcting the complex normalization of the damped modes is one approach for determining a correct canonical basis. Another approach, which is used by the basic CBSI algorithm, simply applies a second transformation to the McMillan realization obtained by letting $d_i = 1$ and $e_i = 1$. The CBSI algorithm is presented in the next section.

3.4 The CBSI Algorithm

Although it is possible to correctly determine a transformation which yields a second-order canonical basis from the damped modal realization (3.2.10), it is also possible to use the McMillan normal form realization as a starting point since it is a fully equivalent realization. This is the approach

for the basic CBSI algorithm. Thus, applying $\mathbf{V}_{i1}$ from (3.2.11) to (3.2.10), the McMillan normal form realization is found as

$$\begin{aligned} \dot{\mathbf{z}}_{ri}(t) &= \begin{bmatrix} 0 & 1 \\ -\omega_{ni}^2 & -2\zeta_i\omega_{ni} \end{bmatrix} \mathbf{z}_{ri}(t) + \begin{bmatrix} \mathbf{b}_{i1}^T \\ \mathbf{b}_{i2}^T \end{bmatrix} \mathbf{u}(t) \\ \mathbf{y}_d(t) &= \sum_{i=1}^{n} [\, \mathbf{c}_{i1} \quad \mathbf{c}_{i2} \,] \, \mathbf{z}_{ri}(t) \end{aligned} \tag{3.4.1}$$

where $\mathbf{b}_{i1}$, $\mathbf{b}_{i2}$, $\mathbf{c}_{i1}$ and $\mathbf{c}_{i2}$ are real-valued partitions of the transformed input and output arrays, respectively, and $\mathbf{z}_{ri}$ is the real-valued basis resulting from the McMillan transformation and corresponding to the complex modal basis z_i and its complex conjugate.

Therefore, in order to transform (3.4.1) to a correct second-order basis, define the normal modal displacement $\eta(t)$ as

$$\eta(t) = d_i \, [\, 1 \quad e_i \,] \, \mathbf{z}_{ri} \tag{3.4.2}$$

and the transformation is given as

$$\begin{aligned} \mathbf{V}_{i2}^{-1} &= d_i \begin{bmatrix} 1 & e_i \\ -e_i(\sigma_i^2 + \omega_i^2) & 1 + 2\sigma_i e_i \end{bmatrix} \\ \mathbf{V}_{i2} &= \frac{1}{\bar{d}_i} \begin{bmatrix} 1 + 2\sigma_i e_i & -e_i \\ e_i(\sigma_i^2 + \omega_i^2) & 1 \end{bmatrix} \\ \bar{d}_i &= d_i \left(1 + 2\sigma_i e_i + (\sigma_i^2 + \omega_i^2) e_i^2\right) \end{aligned} \tag{3.4.3}$$

with the constraint

$$\mathbf{b}_{i1} + \mathbf{b}_{i2} e_i = 0 \tag{3.4.4}$$

This is the fundamental theoretical development for the basic CBSI algorithm. Two variants of method focus on the solution for e_i in the cases of proportional and nonproportional damping.

3.4.1 Basic CBSI for Proportional Damping

In determining a solution to the transformation constraint equation (3.4.4), it is first necessary to consider whether such a solution exists. In the case of proportional damping, it must be true that the vectors $\mathbf{b}_{i1}$ and $\mathbf{b}_{i2}$ are collinear, since both are linear combinations of the real and imaginary parts of the damped mode shape which are collinear. Therefore, the constraint is satisfied exactly for a single value e_i. From (3.4.4), e_i is determined by

$$e_i = \frac{-\mathbf{b}_{i1}^T \mathbf{b}_{i2}}{\mathbf{b}_{i2}^T \mathbf{b}_{i2}} \tag{3.4.5}$$

Furthermore, the vectors $\mathbf{c}_{i1}$ and $\mathbf{c}_{i2}$ are also linear combinations of the real and imaginary parts of the damped mode shape, and hence must also be collinear. In fact, they can be shown to satisfy

$$e_i \mathbf{c}_{i1} = \mathbf{c}_{i2} \tag{3.4.6}$$

Thus, applying (3.4.3) to (3.4.1), the CBSI realization is given as

$$\begin{aligned} \begin{Bmatrix} \dot{\eta}_i(t) \\ \ddot{\eta}_i(t) \end{Bmatrix} &= \begin{bmatrix} 0 & 1 \\ -\omega_{ni}^2 & -2\zeta_i\omega_{ni} \end{bmatrix} \begin{Bmatrix} \eta_i(t) \\ \dot{\eta}_i(t) \end{Bmatrix} + \begin{bmatrix} 0 \\ \phi_{ui}^T \end{bmatrix} \mathbf{u}(t) \\ \mathbf{y}_d(t) &= \sum_{i=1}^{n} \begin{bmatrix} \phi_{yi} & 0 \end{bmatrix} \begin{Bmatrix} \eta_i(t) \\ \dot{\eta}_i(t) \end{Bmatrix} \end{aligned} \tag{3.4.7}$$

where

$$\begin{aligned} \phi_{ui} &= d_i \mathbf{b}_{i2} + d_i e_i \left(2\sigma_i \mathbf{b}_{i2} - (\sigma_i^2 + \omega_i^2)\mathbf{b}_{i1}\right) \\ \phi_{yi} &= \frac{1}{\bar{d}_i}\mathbf{c}_{i1} + \frac{e_i}{\bar{d}_i}\left(2\sigma_i \mathbf{c}_{i1} + (\sigma_i^2 + \omega_i^2)\mathbf{c}_{i2}\right) \end{aligned} \tag{3.4.8}$$

By inspection, (3.4.7) is a correct second-order canonical realization for mode i. In order to provide a common basis normalization for ϕ_{ui} and ϕ_{yi}, some scaling definition independent of the particular model realization is needed.

For example, the modal participation factor ϕ_{uij} of some input $\mathbf{u}_j$ could be normalized to 1.0, viz.

$$d_i = \frac{1}{\mathbf{b}_{ij2} + e_i\left(2\sigma_i \mathbf{b}_{ij2} - (\sigma_i^2 + \omega_i^2)\mathbf{b}_{ij1}\right)} \tag{3.4.9}$$

If the system damping is proportional, it is also possible in some cases to normalize such that the mode shape data extracted from ϕ_{yi} is mass-normalized, provided there exists at least one collocated actuator and sensor pair. This allows ϕ_{ui} and ϕ_{yi} to be scaled as follows. For displacement sensing, collocation requires that,

$$\mathbf{H}_d = \hat{\mathbf{B}}^T$$

Therefore, for each mode i, $\phi_{ui} = \phi_{yi}$ for collocated input-output pairs, and d_i is found as

$$d_i^2 = \frac{\mathbf{c}_{i1} + e_i\left(2\sigma_i \mathbf{c}_{i1} + (\sigma_i^2 + \omega_i^2)\mathbf{c}_{i2}\right)}{\left(1 + 2\sigma_i e_i + (\sigma_i^2 + \omega_i^2)e_i^2\right)\left(\mathbf{b}_{i2} + e_i\left(2\sigma_i \mathbf{b}_{i2} - (\sigma_i^2 + \omega_i^2)\mathbf{b}_{i1}\right)\right)} \tag{3.4.10}$$

It can be proven that CBSI exactly captures the correct normal modes in the case of proportional damping. Recalling (2.1.30)-(2.1.32) and (3.2.10), the realization of a proportionally-damped system in the normalized damped modal basis is given as

$$\begin{aligned} \begin{Bmatrix} \dot{z}_i \\ \dot{\bar{z}}_i \end{Bmatrix} &= \begin{bmatrix} \sigma_i + j\omega_i & 0 \\ 0 & \sigma_i - j\omega_i \end{bmatrix} \begin{Bmatrix} z_i \\ \bar{z}_i \end{Bmatrix} + \frac{1}{2\sqrt{\omega_i}} \begin{bmatrix} (1-j)\phi_i^T \hat{\mathbf{B}} \\ (1+j)\phi_i^T \hat{\mathbf{B}} \end{bmatrix} \mathbf{u} \\ \mathbf{y}_d &= \sum_{i=1}^{n} \frac{1}{2\sqrt{\omega_i}} \begin{bmatrix} (1-j)\mathbf{H}_d\phi_i & (1+j)\mathbf{H}_d\phi_i \end{bmatrix} \begin{Bmatrix} z_i \\ \bar{z}_i \end{Bmatrix} \end{aligned} \tag{3.4.11}$$

Applying (3.2.11), a McMillan normal form realization of (3.4.11) is determined, viz.

$$\begin{aligned} \dot{\mathbf{z}}_{ri} &= \begin{bmatrix} 0 & 1 \\ -\omega_{ni}^2 & -2\zeta_i\omega_{ni} \end{bmatrix} \mathbf{z}_{ri} + \frac{1}{\sqrt{\omega_i}} \begin{bmatrix} \phi_i^T \hat{\mathbf{B}} \\ (\sigma_i + \omega_i)\phi_i^T \hat{\mathbf{B}} \end{bmatrix} \mathbf{u} \\ \mathbf{y}_d &= \sum_{i=1}^{n} \frac{1}{\omega_i^{3/2}} \begin{bmatrix} (\sigma_i + \omega_i)\mathbf{H}_d\phi_i & -\mathbf{H}_d\phi_i \end{bmatrix} \mathbf{z}_{ri} \end{aligned} \tag{3.4.12}$$

Therefore, from (3.4.5) and (3.4.3) the CBSI parameters for mode i are

$$\begin{aligned} e_i &= \frac{-1}{\sigma_i + \omega_i} \\ \bar{d}_i &= \frac{2d_i\omega_i^2}{(\sigma_i + \omega_i)^2} \end{aligned} \tag{3.4.13}$$

and applying (3.4.5), the CBSI realization is found as

$$\begin{aligned} \begin{Bmatrix} \dot{\eta}_i \\ \ddot{\eta}_i \end{Bmatrix} &= \begin{bmatrix} 0 & 1 \\ -\omega_{ni}^2 & -2\zeta_i\omega_{ni} \end{bmatrix} \begin{Bmatrix} \eta_i \\ \dot{\eta}_i \end{Bmatrix} + \frac{2d_i\omega_i^{3/2}}{\sigma_i + \omega_i} \begin{bmatrix} 0 \\ \phi_i^T \hat{\mathbf{B}} \end{bmatrix} \mathbf{u} \\ \mathbf{y}_d &= \sum_{i=1}^{n} \frac{\sigma_i + \omega_i}{2d_i\omega_i^{3/2}} \begin{bmatrix} \mathbf{H}_d\phi_i & 0 \end{bmatrix} \begin{Bmatrix} \eta_i \\ \dot{\eta}_i \end{Bmatrix} \end{aligned} \tag{3.4.14}$$

In order to mass-normalize the normal mode shapes, (3.4.10) provides

$$d_i = \frac{\sigma_i + \omega_i}{2\omega_i^{3/2}} \tag{3.4.15}$$

and (3.2.9) is exactly derived. Note also that (3.4.8) is exactly satisfied, as was previously claimed.

3.4.2 Least-Squared CBSI for General Viscous Damping

In the case of nonproportional damping, the vectors $\mathbf{b}_{i1}$ and $\mathbf{b}_{i2}$ are no longer collinear, and hence (3.4.6) does not satisfy (3.4.5) for the multiple inputs $\mathbf{u}$. This implies that the CBSI transformation (3.4.4) cannot exactly determine the desired second-order canonical basis variables η_i using the uncoupled complex modal variables z_i individually. In this case, it is possible to determine a basis using *quasi-normal* modal displacements $\tilde{\eta}_{di}$ and velocities $\tilde{\eta}_{vi}$ through the CBSI algorithm. The resultant CBSI transformation and basis is written as

$$\begin{Bmatrix} \tilde{\eta}_{di} \\ \tilde{\eta}_{vi} \end{Bmatrix} = \frac{1}{\bar{d}_i} \begin{bmatrix} 1 + 2\sigma_i e_i & -e_i \\ e_i(\sigma_i^2 + \omega_i^2) & 1 \end{bmatrix} \mathbf{z}_{ri} \tag{3.4.16}$$

and from (3.3.7) the error between the quasi-normal modal velocities and the time derivative of the quasi-normal modal displacements is

$$\dot{\tilde{\eta}}_{di} - \tilde{\eta}_{vi} = d_i \left(\mathbf{b}_{i1}^T + e_i \mathbf{b}_{i2}^T \right) \mathbf{u} \tag{3.4.17}$$

Thus, in order to minimize this error for arbitrary inputs $\mathbf{u}$, it is necessary to minimize the quantity J_u, where

$$J_u = d_i^2 \left(\mathbf{b}_{i1} + e_i \mathbf{b}_{i2} \right)^T \left(\mathbf{b}_{i1} + e_i \mathbf{b}_{i2} \right) \tag{3.4.18}$$

Since this is effectively a least-square criterion for e_i, the method is termed the Least-Square CSBI (CBSI-LS) algorithm.

At this point it might appear that (3.4.5) would yield the correct least-square solution for (3.4.18). However, in order to determine an optimal solution for e_i independent of the scaling parameter d_i, it is necessary to impose an additional scaling condition to constrain d_i. Otherwise, it would be necessary to minimize J_u with respect to both e_i and d_i. The optimal solution in that case, however, is trivial ($d_i = 0$), since J_u is quadratic. Therefore, if the CBSI-transformed input influence array is written as

$$\mathbf{V}_{i2}^{-1} \begin{bmatrix} \mathbf{b}_{i1}^T \\ \mathbf{b}_{i2}^T \end{bmatrix} = \begin{bmatrix} \tilde{\epsilon}_{ui}^T \\ \tilde{\phi}_{ui}^T \end{bmatrix} \tag{3.4.19}$$

then the transformation scaling can be controlled by requiring that

$$\tilde{\phi}_{ui}^T \tilde{\phi}_{ui} = \mathbf{b}_{i2}^T \mathbf{b}_{i2} \tag{3.4.20}$$

This implies that the norm of ϕ_{ui}, which is an estimate of the mode shape at the input locations, is constrained to the norm of $\mathbf{b}_{i2}$. From (3.4.20), d_i can be eliminated and J_u is a function strictly of e_i, viz.

$$J_u = \frac{S_{22} e_i^2 + 2 S_{12} e_i + S_{11}}{a_d e_i^2 + 2 b_d e_i + S_{22}} \tag{3.4.21}$$

where

$$
\begin{aligned}
S_{11} &= \mathbf{b}_{i1}^T \mathbf{b}_{i1} \qquad S_{12} = \mathbf{b}_{i1}^T \mathbf{b}_{i2} \qquad S_{22} = \mathbf{b}_{i2}^T \mathbf{b}_{i2} \\
a_d &= 4\sigma_i^2 S_{22} - 4\sigma_i(\sigma_i^2 + \omega_i^2) S_{12} + (\sigma_i^2 + \omega_i^2)^2 S_{11} \\
b_d &= 2\sigma_i S_{22} - (\sigma_i^2 + \omega_i^2) S_{12}
\end{aligned}
\tag{3.4.22}
$$

To minimize J_u, the necessary condition $\delta J_u = 0$ requires that

$$
\frac{dJ_u}{de_i} = 0 \tag{3.4.23}
$$

leading to the solution for e_i

$$
e_i = \frac{-b_e \pm \sqrt{b_e^2 - 4a_e c_e}}{2a_e} \tag{3.4.24}
$$

where

$$
\begin{aligned}
a_e &= b_d S_{22} - a_d S_{12} \\
b_e &= S_{22}^2 - a_d S_{11} \\
c_e &= S_{12} S_{22} - b_d S_{11}
\end{aligned}
\tag{3.4.25}
$$

The two solutions for e_i from (3.4.24) correspond to a minimum and maximum value of J_u. Applying the CBSI transformation (3.4.16) to (3.4.3), the CBSI realization for the nonproportional damping condition is

$$
\begin{aligned}
\begin{Bmatrix} \dot{\tilde{\eta}}_{di} \\ \dot{\tilde{\eta}}_{vi} \end{Bmatrix} &= \begin{bmatrix} 0 & 1 \\ -\tilde{\omega}_{ni}^2 & 2\tilde{\zeta}_i \tilde{\omega}_{ni} \end{bmatrix} \begin{Bmatrix} \tilde{\eta}_{di} \\ \tilde{\eta}_{vi} \end{Bmatrix} + \begin{bmatrix} \tilde{\epsilon}_{ui}^T \\ \tilde{\phi}_{ui}^T \end{bmatrix} \mathbf{u} \\
\mathbf{y}_d &= \sum_{i=1}^{n} \begin{bmatrix} \tilde{\phi}_{yi} & \tilde{\epsilon}_{yi} \end{bmatrix} \begin{Bmatrix} \tilde{\eta}_{di} \\ \tilde{\eta}_{vi} \end{Bmatrix}
\end{aligned}
\tag{3.4.26}
$$

where $\|\tilde{\epsilon}_{ui}\|_2$ has been minimized such that $\|\tilde{\phi}_{ui}\|_2 = \|\mathbf{b}_{i2}\|_2$. Note that the undamped natural frequency $\tilde{\omega}_{ni}$ and modal damping ratio $\tilde{\zeta}_i$ are now approximations because of the effects of nonproportional damping.

An alternate approach for determining the Least-Square CBSI transformation is through use of the damped mode shapes at the sensor locations, i.e. by use of $\mathbf{c}_{i1}$ and $\mathbf{c}_{i2}$ in (3.4.3). Recall from (2.1.35) the constraint relating the force input influence array $\mathbf{B}$ and the displacement output influence array $\mathbf{C}_d$, expressed in terms of the partitions of (3.4.1)

$$\mathbf{C}_d\mathbf{B} = \mathbf{c}_{i1}\mathbf{b}_{i1}^T + \mathbf{c}_{i2}\mathbf{b}_{i2}^T = 0 \tag{3.4.27}$$

This implies that the first-order delay term in the impulse response of force input-displacement output transfer function is zero, which in turn is a necessary condition for the impulse response behavior of a second-order system. Thus, an equivalent expression for e_i in terms of $\mathbf{c}_{i1}$ and $\mathbf{c}_{i2}$ is found by substituting the transformation constraint (3.4.4), viz.

$$(e_i\mathbf{c}_{i1} - \mathbf{c}_{i2})\,\mathbf{b}_{i2}^T = 0 \tag{3.4.28}$$

This relationship must hold for inputs at any physical degree of freedom spanned by the modal state space, i.e. for all $\mathbf{b}_{i2}$ in $\mathcal{R}^n$. Hence, an equivalent transformation constraint condition is given as

$$e_i\mathbf{c}_{i1} - \mathbf{c}_{i2} = 0 \tag{3.4.29}$$

This is the same condition claimed in (3.4.6), which is now proven to hold for both proportional and nonproportional damping. The remainder of the problem is basically equivalent to the optimal solution for e_i in terms of the

input matrix coefficients $\mathbf{b}_{i1}$ and $\mathbf{b}_{i2}$. Define

$$\begin{aligned}
\bar{S}_{11} &= \mathbf{c}_{i1}^T \mathbf{c}_{i1} \qquad \bar{S}_{12} = \mathbf{c}_{i1}^T \mathbf{c}_{i2} \qquad \bar{S}_{22} = \mathbf{c}_{i2}^T \mathbf{c}_{i2} \\
\bar{a}_d &= 4\sigma_i^2 \bar{S}_{11} + 4\sigma_i(\sigma_i^2 + \omega_i^2)\bar{S}_{12} + (\sigma_i^2 + \omega_i^2)^2 \bar{S}_{22} \\
\bar{b}_d &= 2\sigma_i \bar{S}_{11} + (\sigma_i^2 + \omega_i^2)\bar{S}_{12} \\
\bar{a}_e &= \bar{b}_d \bar{S}_{11} + \bar{a}_d \bar{S}_{12} \qquad \bar{b}_e = \bar{S}_{11}^2 - \bar{a}_d \bar{S}_{22} \\
\bar{c}_e &= -\bar{S}_{12}\bar{S}_{11} - \bar{b}_d \bar{S}_{22}
\end{aligned} \tag{3.4.30}$$

and the solution for e_i is given as

$$e_i = \frac{-\bar{b}_e \pm \sqrt{\bar{b}_e^2 - 4\bar{a}_e \bar{c}_e}}{2\bar{a}_e} \tag{3.4.31}$$

Recalling (3.4.24), the resultant CBSI realization using (3.4.31) minimizes $\|\tilde{\epsilon}_{yi}\|_2$ such that $\|\tilde{\phi}_{yi}\|_2 = \|\mathbf{c}_{i1}\|_2$.

A key motivation for the preceding derivation is that, for normal mode estimation in the presence of nonproportional damping, it is advantageous to use the maximum quantity of damped modal information available. Determination of the optimal e_i using $\mathbf{c}_{i1}$ and $\mathbf{c}_{i2}$ generally leads to a more balanced estimate of the normal modes. This comes from the observation that the solution for e_i can be heavily biased towards the phase quantities of a small number of measured degrees of freedom. So, although both the force input matrix coefficients $\mathbf{b}_{i1}$ and $\mathbf{b}_{i2}$ and the displacement output matrix coefficients $\mathbf{c}_{i1}$ and $\mathbf{c}_{i2}$ both express the values of the complex mode shapes at a number of physical degrees of freedom, the reality in modal testing is that there are a significantly larger number of measured sensors than force actuators. Furthermore, the test instrumentation may include driving point measurements, which are sensor collocated with the force inputs. In this case, the output matrix coefficients possess not only the mode shapes

at the numerous sensor locations, but also the mode shapes at the actuator locations.

The Least-Square CBSI methods can also be interpreted as solutions which seek to minimize the differences between the estimated Markov parameters $\mathbf{Y}$(k) and the reconstructed Markov parameters from the estimated normal modal parameters. Note that the violations of the second-order canonical transformation constraints (3.4.4) and (3.4.29) are exactly the residual quantities $\tilde{\epsilon}_{ui}$ and $\tilde{\epsilon}_{yi}$, i.e. the resultant matrix quantities in the CBSI-LS realization which do not fit the form of the MDV realization (3.2.9). The estimated normal modal model with proportional damping, however, is the CBSI-LS realization without these model residuals. The constraint violations, therefore, are a direct measure of the error between the system-identified Markov parameters and the reconstructed Markov parameters of the estimated normal modes model. For example, the error due to the omission of $\tilde{\epsilon}_{yi}$ is given as

$$\Delta\mathbf{Y}(k) = \sum_{i=1}^{n} [\,0 \quad \tilde{\epsilon}_{yi}\,] \begin{bmatrix} 0 & 1 \\ -\sigma_i^2 - \omega_i^2 & 2\sigma_i \end{bmatrix}^{k-1} \begin{bmatrix} \tilde{\epsilon}_{ui}^T \\ \phi_{ui}^T \end{bmatrix} \qquad k = 1, \ldots, \infty \tag{3.4.32}$$

Therefore, it is possible to directly evaluate the effect of the normal mode estimation accomplished using CBSI on the realization parameters which are intrinsic to the measured dynamics.

3.4.3 A Symmetrical CBSI Method

The final variant of the CBSI procedure to be presented determines a real-valued symmetrical companion form realization directly from the damped modal realization. In place of the second CBSI rotation, which

transforms the McMillan normal form realization, the Symmetrical CBSI (CBSI-SYM) method determines an objective normalization of the damped modes leading to a symmetrical form of the first-order realization, then applies a single transformation which preserves the symmetry of the matrix coefficients. The resultant CBSI realization is in a symmetrical companion form of the normal modal variables, viz.

$$\begin{bmatrix} \mathbf{\Xi} & \mathbf{I} \\ \mathbf{I} & 0 \end{bmatrix} \begin{Bmatrix} \dot{\eta} \\ \ddot{\eta} \end{Bmatrix} = \begin{bmatrix} -\mathbf{\Omega} & 0 \\ 0 & \mathbf{I} \end{bmatrix} \begin{Bmatrix} \eta \\ \dot{\eta} \end{Bmatrix} + \begin{bmatrix} \mathbf{\Phi}^T \hat{\mathbf{B}} \\ 0 \end{bmatrix} \mathbf{u}$$
$$\mathbf{y}_d = [\, \mathbf{H}_d \mathbf{\Phi} \quad 0 \,] \begin{Bmatrix} \eta \\ \dot{\eta} \end{Bmatrix} \tag{3.4.33}$$

A particular restriction on this method is that it requires the physically-based normalization of the damped modal coordinates as detailed in Chapter II, Section 2.3.3. This in turn requires driving point measurements (i.e. collocated sensors at the force inputs).

The equivalent normalized damped modal form of (3.4.33), as obtained from the driving point scaling (2.3.27)-(2.3.29), is given as

$$\begin{aligned} \dot{\mathbf{z}}_n &= \mathbf{\Lambda} \mathbf{z}_n + \mathbf{X}^T \hat{\mathbf{B}} \mathbf{u} \\ \mathbf{y}_d &= \mathbf{H} \mathbf{X} \mathbf{z}_n \end{aligned} \tag{3.4.34}$$

where

$$\begin{aligned} \mathbf{\Lambda} &= diag\{\sigma_i \pm \omega_i, i = 1, \ldots, n\} \\ \mathbf{X} &= \lfloor \ldots, \Re(\mathbf{X}_i) \pm \Im(\mathbf{X}_i), \ldots \rfloor \\ \sigma_i &= -\zeta_i \omega_{ni} \\ \omega_i &= \omega_{ni} \sqrt{1 - \zeta_i^2} \\ \Re(\mathbf{X}_i) &= \frac{1}{2\sqrt{\omega_1}} \phi_i \\ \Im(\mathbf{X}_i) &= -\frac{1}{2\sqrt{\omega_1}} \phi_i \end{aligned} \tag{3.4.35}$$

Therefore, we can define the second-order transformation as

$$\hat{\eta}_{di} = \mathbf{P}_i \mathbf{z}_{ni} = 1/\sqrt{2j\omega_i}\,[\,1 \quad j\,]\begin{Bmatrix} z_{ni} \\ \bar{z}_{ni} \end{Bmatrix} \tag{3.4.36}$$

such that the Symmetrical CBSI transformation is

$$\mathbf{V}_i = \sqrt{\frac{j}{2\omega_i}}\begin{bmatrix} j(\sigma_i - j\omega_i) & -j \\ -(\sigma_i + j\omega_i) & 1 \end{bmatrix} \tag{3.4.37}$$

and

$$\mathbf{V}_i^T \mathbf{V}_i = \begin{bmatrix} -2\sigma_i & 1 \\ 1 & 0 \end{bmatrix} \tag{3.4.38}$$

Then, applying the basis definition (3.4.36) to (3.4.34) and premultiplying by $\mathbf{V}_i^T$ to preserve symmetry, the resultant Symmetrical CBSI realization for nonproportional damping is given by

$$\begin{aligned} \begin{bmatrix} -2\tilde{\zeta}_i\tilde{\omega}_{ni} & 1 \\ 1 & 0 \end{bmatrix}\begin{Bmatrix} \dot{\hat{\eta}}_{di} \\ \dot{\hat{\eta}}_{vi} \end{Bmatrix} &= \begin{bmatrix} -\tilde{\omega}_{ni}^2 & 0 \\ 0 & 1 \end{bmatrix}\begin{Bmatrix} \hat{\eta}_{di} \\ \hat{\eta}_{vi} \end{Bmatrix} + \begin{bmatrix} \hat{\phi}_{ui}^T \\ \hat{\epsilon}_{ui}^T \end{bmatrix}\mathbf{u} \\ \mathbf{y}_d &= \sum_{i=1}^{n}[\,\hat{\phi}_{yi} \quad \hat{\epsilon}_{yi}\,]\begin{Bmatrix} \hat{\eta}_{di} \\ \hat{\eta}_{vi} \end{Bmatrix} \end{aligned} \tag{3.4.39}$$

In (3.4.39), because of the symmetry of the companion form realization, the relevant mode shapes at the inputs are given by $\hat{\phi}_{ui}$ in the upper partition of the input influence coefficient matrix, rather than the lower partition characteristic of the MDV realization.

The particular feature and potential advantage of the Symmetrical CBSI method is that the solution is not biased towards minimizing the residual quantities at particular input or output locations. Instead, the basis definition is "balanced" by the normalization of the damped modes, which leads to a realization with equivalent mode shape estimates and modal participation factors for the collocated input-output pairs independent of whether the damping is proportional or nonproportional. In fact, the symmetrical CBSI

realization follows as the only realization possessing the given symmetrical state coefficent matrices which allows the symmetry of the input and output influence matrices in (3.4.34) to be preserved. And, as demonstrated, the transformation does not consider the residual model quantities as in the Least Square CBSI, although the solution obtained in practice yields similar mode shape estimates, especially as compared to the CBSI-LS solution using the sensor matrix partitions $\mathbf{c}_{i1}$ and $\mathbf{c}_{i2}$. In the next section, the CBSI methods will be illustrated though numerical examples and contrasted with existing techniques.

3.4.4 Summary of CBSI Algorithm

For the basic CBSI (proportional damping):

Step 1 Determine the damped modal realization (see (2.3.25)) using an effective MIMO model estimation algorithm such as ERA or Polyreference.

Step 2 Apply McMillan transformation $\mathbf{V}_{i1}$ (3.2.11) to obtain the McMillan Normal Form realization (3.4.1).

Step 3 Compute e_i using (3.4.5) and scaling parameter d_i using (3.4.9)-(3.4.10).

Step 4 Apply the CBSI transformation $\mathbf{V}_{i2}$ (3.4.3) to obtain the CBSI realization (3.4.7).

Step 5 The normal modal parameters for mode i are given by ω_{ni}, ζ_i, ϕ_{ui} and ϕ_{yi} in the partitions of the CBSI realization matrices.

For nonproportional damping using Least-Squared CBSI:

Step 1 Determine the damped modal realization (see (2.3.25)) using an effective MIMO model estimation algorithm such as ERA or Polyreference.

Step 2 In the case of velocity or acceleration sensing, integrate once or twice (multiplying by $\mathbf{\Lambda}^{-1}$), respectively, to obtain the damped mode shape matrix $\mathbf{C}_z$. This allows the outputs to be treated as if they were measured displacements.

Step 3 Apply McMillan transformation $\mathbf{V}_{i1}$ (3.2.11) to obtain the McMillan Normal Form realization (3.4.1).

Step 4 Compute e_i using (3.4.30)-(3.4.31), taking advantage of the more spatially-extensive sensor data typically available.

Step 5 Apply the CBSI transformation $\mathbf{V}_{i2}$ (3.4.3) to obtain the CBSI-LS realization (3.4.26).

Step 6 The normal modal parameters for mode i are given by $\tilde{\omega}_{ni}$, $\tilde{\zeta}_i$, $\tilde{\phi}_{ui}$ and $\tilde{\phi}_{yi}$ in the partitions of the CBSI-LS realization matrices.

<u>For nonproportional damping using Symmetrical CBSI</u>:

Step 1 Determine the damped modal realization (see (2.3.25)) using an effective MIMO model estimation algorithm such as ERA or Polyreference.

Step 2 In the case of velocity or acceleration sensing, integrate once or twice (multiplying by $\mathbf{\Lambda}^{-1}$), respectively, to obtain the damped mode shape matrix $\mathbf{C}_z$. This allows the outputs to be treated as if they were measured displacements.

Step 3 Normalize the damped modes as in Chapter II, Section 2.3.3.

Step 4 Apply the CBSI-SYM transformation $\mathbf{V}_i$ (3.4.37) to obtain the CBSI-SYM realization (3.4.39).

Step 5 The normal modal parameters for mode i are given by $\tilde{\omega}_{ni}$, $\tilde{\zeta}_i$, $\hat{\phi}_{ui}$ and $\hat{\phi}_{yi}$ in the partitions of the CBSI-SYM realization matrices.

3.5 Numerical Examples

3.5.1 Mode Shape Collinearity Indicators

In order to evaluate the mode shape estimates given by various algorithms, it is helpful to define particular measures for modal parameter comparisons. The first of these, *Modal Phase Collinearity* (MPC) [23] is an indicator of the inherent degree of collinearity between the real and imaginary parts of the damped mode shapes. Modes with MPC values equal to 1.00 are effectively equivalent to normal modes, and the various methods of normal mode shape estimation should work equally well. Modes with MPC values of less than 0.90, on the other hand, do not possess unambiguous corresponding normal modes, and so the normal mode shape estimates will be sensitive to the methods used for their estimation. The MPC for damped mode shape $\mathbf{C}_{zi}$ is given as

$$\mathrm{MPC}_i = \frac{(S_{yy} - S_{xx})^2 + 4S_{xy}^2}{(S_{yy} + S_{xx})^2} \tag{3.5.1}$$

where

$$S_{xx} = \Re(\mathbf{C}_{zi})^T \Re(\mathbf{C}_{zi}) \quad S_{xy} = \Re(\mathbf{C}_{zi})^T \Im(\mathbf{C}_{zi}) \quad S_{yy} = \Im(\mathbf{C}_{zi})^T \Im(\mathbf{C}_{zi}) \tag{3.5.2}$$

Thus, the MPC is effectively a measure of the degree to which a damped mode is directly related to an undamped mode.

A second important indicator is the *Modal Assurance Criterion* (MAC), which is used to compare the relative collinearity of different normal mode shapes. The MAC is used, for example, to compare test-derived normal mode shapes to those predicted by finite element models. In the case of studying different normal mode estimation methods, the MAC can be used to evaluate the relative shape agreement between the exact normal mode shapes, given by known mass and stiffness matrices, and the estimated mode shapes. The MAC is generally defined as

$$\mathrm{MAC}_{jk} = \frac{(\phi_j^T \mathbf{Q} \phi_k)^2}{(\phi_j^T \mathbf{Q} \phi_j)(\phi_k^T \mathbf{Q} \phi_k)} \tag{3.5.3}$$

where ϕ_j and ϕ_k are corresponding mode shapes from models j and k, and $\mathbf{Q}$ is an optional weighting matrix. Note that both the MAC and the MPC measure the collinearity between two real vectors apart from the scaling, and so they are related quantities. They have been traditionally used for assessing different system properties, however. This thesis follows that convention by using the MPC to measure the inherent phase angle scatter of the damped modes, and using the MAC to compare the estimated normal mode shapes from different models or estimation methods. In addition, for mode shape comparisons herein, a weight matrix $\mathbf{Q} = \mathbf{I}$ will be used as opposed to a mass matrix, which is only critical for orthogonality measures.

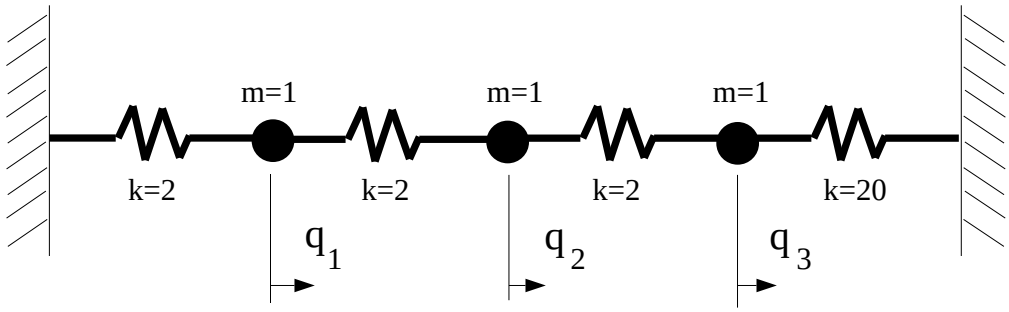

Figure 3.1: Spring-Mass Example Model

3.5.2 3-DOF Spring-Mass System with Proportional Damping

The first example, shown in Figure 3.1, is a simple 3 degree of freedom spring problem. As the CBSI algorithm does not require actuator input tests from all degrees of freedom, only one input will be used. The governing second-order differential equations are given as

$$\begin{Bmatrix} \ddot{q}_1 \\ \ddot{q}_2 \\ \ddot{q}_3 \end{Bmatrix} + \begin{bmatrix} .2 & -.1 & 0 \\ -.1 & .2 & -.1 \\ 0 & -.1 & 1.1 \end{bmatrix} \begin{Bmatrix} \dot{q}_1 \\ \dot{q}_2 \\ \dot{q}_3 \end{Bmatrix} + \begin{bmatrix} 4 & -2 & 0 \\ -2 & 4 & -2 \\ 0 & -2 & 22 \end{bmatrix} \begin{Bmatrix} q_1 \\ q_2 \\ q_3 \end{Bmatrix} = \begin{bmatrix} 0 \\ u \\ 0 \end{bmatrix}$$
$$\begin{Bmatrix} y_1 \\ y_2 \\ y_3 \end{Bmatrix} = \begin{bmatrix} 1 & 0 & 0 \\ 0 & 1 & 0 \\ 0 & 0 & 1 \end{bmatrix} \begin{Bmatrix} q_1 \\ q_2 \\ q_3 \end{Bmatrix} \tag{3.5.4}$$

The frequencies and normal mode shapes can be determined from the mass and stiffness as in (2.1.3). The mass-normalized mode shape matrix is then given as

$$\mathbf{\Phi}_{KM} = \begin{bmatrix} 0.6875 & -0.7261 & 0.0121 \\ 0.7226 & 0.6824 & -0.1104 \\ 0.0719 & 0.0847 & 0.9938 \end{bmatrix} \tag{3.5.5}$$

In the absence of noise, the damped modes of this simple system can be identified through modal testing and model estimation methods such as

Table 3.1
Notation Used in Example Problems

MPC	Modal Phase Collinearity
MAC	Modal Assurance Criteria
ST	Standard Technique modal estimate
MNF	McMillan Normal Form realization
CBSI	Basic CBSI Algorithm realization
CBSI-LS	Least-Square CBSI Algorithm realization
CBSI-SYM	Symmetrical CBSI Algorithm realization

ERA, leading to a damped modal realization, given in real block-diagonal form by

$$\dot{\mathbf{x}}_0 = \mathbf{A}_0\mathbf{x}_0 + \mathbf{B}_0 u$$
$$\begin{Bmatrix} y_1 \\ y_2 \\ y_3 \end{Bmatrix} = \mathbf{C}_0\mathbf{x}_0 + \mathbf{D}_0 u$$

where

$$\begin{aligned}
\mathbf{A}_0 &= \begin{bmatrix} -0.0475 & 1.3769 & 0 & 0 & 0 & 0 \\ -1.3769 & -0.0475 & 0 & 0 & 0 & 0 \\ 0 & 0 & -0.1470 & 2.4204 & 0 & 0 \\ 0 & 0 & -2.4204 & -0.1470 & 0 & 0 \\ 0 & 0 & 0 & 0 & -0.5556 & 4.6812 \\ 0 & 0 & 0 & 0 & -4.6812 & -0.5556 \end{bmatrix} \\
\mathbf{B}_0^T &= [\,0.4974\ -0.0362\ -0.6217\ 0.0455\ -0.1079\ 0.0134\,] \\
\mathbf{C}_0 &= \begin{bmatrix} -0.0525 & -0.7216 & -0.0240 & -0.3275 & -0.0003 & -0.0026 \\ -0.0552 & -0.7584 & 0.0225 & 0.3078 & 0.0030 & 0.0238 \\ -0.0055 & -0.0755 & 0.0028 & 0.0382 & -0.0266 & -0.2139 \end{bmatrix} \\
\mathbf{D}_0 &= [\,0.0000\ 0.0000\ 0.0000\,]^T
\end{aligned} \tag{3.5.6}$$

where the real and imaginary parts of the complex mode shapes $\mathbf{C}_z$ are given by alternating columns of $\mathbf{C}_0$. The first step in determining normal mode

estimates is to determine the MPC from (3.5.2), viz.

$$\text{MPC} = \begin{cases} 1.0000 & \text{Mode} \quad 1 \\ 1.0000 & \text{Mode} \quad 2 \\ 1.0000 & \text{Mode} \quad 3 \end{cases} \tag{3.5.7}$$

Therefore, the given system appears to be proportionally-damped, and normal mode estimation should be effective using either CBSI or the standard technique. First, applying the standard technique (ST), the mode shape matrix is

$$\mathbf{\Phi}_{ST} = \begin{bmatrix} 0.7235 & -0.3284 & 0.0026 \\ 0.7604 & 0.3086 & -0.0239 \\ 0.0757 & 0.0383 & 0.2156 \end{bmatrix} \tag{3.5.8}$$

Although from (3.5.5) and (3.5.8) $\mathbf{\Phi}_{KM}$ and $\mathbf{\Phi}_{ST}$ are not equivalent, the standard technique has not accounted for a mass-normalized type of scaling. Using the MAC from (3.5.3), however, the accuracy of the normal mode shapes from ST are apparent, viz.

$$\text{MAC}_{KM-ST} = \begin{cases} 1.0000 & \text{Mode} \quad 1 \\ 1.0000 & \text{Mode} \quad 2 \\ 1.0000 & \text{Mode} \quad 3 \end{cases} \tag{3.5.9}$$

Thus, as expected for proportionally-damped systems, the standard technique is effective for extracting the normal modal parameters, including the normal mode shapes.

Although CBSI was previously demonstrated to be exact for the general proportionally damped system, the basic method can be illustrated here. First, applying the transformation (3.2.11) to the complex form of (3.5.6), a McMillan normal form realization is given as

$$\begin{aligned} \dot{\mathbf{x}}_1 &= \mathbf{A}_1\mathbf{x}_1 + \mathbf{B}_1 u \\ \begin{Bmatrix} y_1 \\ y_2 \\ y_3 \end{Bmatrix} &= \mathbf{C}_1\mathbf{x}_1 + \mathbf{D}_0 u \end{aligned}$$

where

$$\mathbf{A}_1 = \begin{bmatrix} 0.0000 & 0.0000 & 0.0000 & 1.0000 & 0.0000 & 0.0000 \\ 0.0000 & 0.0000 & 0.0000 & 0.0000 & 1.0000 & 0.0000 \\ 0.0000 & 0.0000 & 0.0000 & 0.0000 & 0.0000 & 1.0000 \\ -1.8980 & 0.0000 & 0.0000 & -0.0949 & 0.0000 & 0.0000 \\ 0.0000 & -5.8798 & 0.0000 & 0.0000 & -0.2940 & 0.0000 \\ 0.0000 & 0.0000 & -22.222 & 0.0000 & 0.0000 & -1.1111 \end{bmatrix} \tag{3.5.10}$$

$$\mathbf{B}_1 = [0.4974\ -0.6217\ -0.1079\ -0.0734\ 0.2015\ 0.1227]^T$$

$$\mathbf{C}_1 = \begin{bmatrix} -0.0774 & -0.0439 & -0.0006 & -0.5241 & -0.1353 & -0.0006 \\ -0.0813 & 0.0412 & 0.0058 & -0.5508 & 0.1272 & 0.0051 \\ -0.0081 & 0.0051 & -0.0520 & -0.0548 & 0.0158 & -0.0457 \end{bmatrix}$$

Although by inspection (3.5.10) is not a correct second-order realization, it is still possible to extract mode shapes from either partition of $\mathbf{C}_1$. Because of the proportional nature of the damping, the normal mode shape estimate is insensitive to the basis definition, and so the mode shapes can be given as

$$\mathbf{\Phi}_{MNF} = \begin{bmatrix} -0.0774 & -0.0439 & -0.0006 \\ -0.0813 & 0.0412 & 0.0058 \\ -0.0081 & 0.0051 & -0.0520 \end{bmatrix} \tag{3.5.11}$$

and the resultant MAC values verify the mode shape accuracy, viz.

$$\mathrm{MAC}_{KM-MNF} = \begin{Bmatrix} 1.0000 & \text{Mode} & 1 \\ 1.0000 & \text{Mode} & 2 \\ 1.0000 & \text{Mode} & 3 \end{Bmatrix} \tag{3.5.12}$$

Applying the CBSI method to determine the correct second-order basis, the CBSI realization (which is a MDV realization) is given as

$$\dot{\mathbf{x}}_2 = \mathbf{A}_2\mathbf{x}_2 + \mathbf{B}_2 u$$

$$\begin{Bmatrix} y_1 \\ y_2 \\ y_3 \end{Bmatrix} = \mathbf{C}_2\mathbf{x}_2 + \mathbf{D}_0 u$$

where

$$\mathbf{A}_2 = \begin{bmatrix} 0.0000 & 0.0000 & 0.0000 & 1.0000 & 0.0000 & 0.0000 \\ 0.0000 & 0.0000 & 0.0000 & 0.0000 & 1.0000 & 0.0000 \\ 0.0000 & 0.0000 & 0.0000 & 0.0000 & 0.0000 & 1.0000 \\ -1.8980 & 0.0000 & 0.0000 & -0.0949 & 0.0000 & 0.0000 \\ 0.0000 & -5.8798 & 0.0000 & 0.0000 & -0.2940 & 0.0000 \\ 0.0000 & 0.0000 & -22.222 & 0.0000 & 0.0000 & -1.1111 \end{bmatrix} \tag{3.5.13}$$

$$\mathbf{B}_2 = [\,0.0000\ -0.0000\ 0.0000\ -0.7226\ 0.6824\ 0.1104\,]^T$$

$$\mathbf{C}_2 = \begin{bmatrix} -0.6875 & -0.7261 & -0.0121 & 0.0000 & 0.0000 & 0.0000 \\ -0.7226 & 0.6824 & 0.1104 & 0.0000 & -0.0000 & 0.0000 \\ -0.0719 & 0.0847 & -0.9938 & -0.0000 & 0.0000 & -0.0000 \end{bmatrix}$$

In addition to determining the second-order basis, as evidenced by the null partitions of the force input and displacement output influence arrays, the CBSI method also exploited the collocation between the single input u and output y_2 to determine an objective mass-normalization for the mode shapes. Thus, the CBSI mode shapes are given as

$$\mathbf{\Phi}_{CBSI} = \begin{bmatrix} -0.6875 & -0.7261 & -0.0121 \\ -0.7226 & 0.6824 & 0.1104 \\ -0.0719 & 0.0847 & -0.9938 \end{bmatrix} \tag{3.5.14}$$

and the MAC values are

$$\mathrm{MAC}_{KM-CBSI} = \begin{cases} 1.0000 & \text{Mode} \quad 1 \\ 1.0000 & \text{Mode} \quad 2 \\ 1.0000 & \text{Mode} \quad 3 \end{cases} \tag{3.5.15}$$

The above derivation used the basic CBSI method for proportional damping, but any of the CBSI variants presented in this chapter perform equally well on the general proportionally-damped system.

3.5.3 3-DOF Spring-Mass System with Nonproportional Damping

In the next example, the same 3-DOF mass-spring system as (3.5.4) will be used, but with significant nonproportional damping to demonstrate the effectiveness of CBSI in the general damping case, viz.

$$\mathcal{D} = \begin{bmatrix} 2 & -.1 & -.1 \\ -.1 & .2 & -.1 \\ -.1 & -.1 & 1.1 \end{bmatrix} \tag{3.5.16}$$

The degree of coupling between the normal modes can be seen by checking the orthogonality of the undamped mode shapes through the damping matrix:

$$\mathbf{T}^T \mathcal{D} \mathbf{T} = \begin{bmatrix} 0.9359 & -0.8991 & -0.0534 \\ -0.8991 & 1.2552 & 0.0562 \\ -0.0534 & 0.0562 & 1.1090 \end{bmatrix} \tag{3.5.17}$$

After determining the damped modal realization and the corresponding McMillan realization, CBSI can be applied. The results are summarized in Table 3.2, and the CBSI-LS realization which minimizes the output matrix partition $\tilde{\epsilon}_y$ is given by

$$\begin{aligned} \mathbf{A}_2 &= \begin{bmatrix} 0.0000 & 0.0000 & 0.0000 & 1.0000 & 0.0000 & 0.0000 \\ 0.0000 & 0.0000 & 0.0000 & 0.0000 & 1.0000 & 0.0000 \\ 0.0000 & 0.0000 & 0.0000 & 0.0000 & 0.0000 & 1.0000 \\ -2.5043 & 0.0000 & 0.0000 & -1.2281 & 0.0000 & 0.0000 \\ 0.0000 & -4.4578 & 0.0000 & 0.0000 & -0.9636 & 0.0000 \\ 0.0000 & 0.0000 & -22.216 & 0.0000 & 0.0000 & -1.1083 \end{bmatrix} \\ \mathbf{B}_2 &= [-0.3293 \ -0.2731 \ 0.0004 \ -0.7223 \ 0.9554 \ -0.1112]^T \\ \mathbf{C}_2 &= \begin{bmatrix} -0.7581 & -0.6847 & 0.0165 & 0.1263 & -0.3619 & -0.0039 \\ -0.7223 & 0.9554 & -0.1112 & -0.2346 & -0.1531 & 0.0004 \\ -0.0722 & 0.1215 & 0.9957 & -0.0312 & -0.0141 & 0.0001 \end{bmatrix} \end{aligned} \tag{3.5.18}$$

Table 3.2
Comparison of Normal Mode Shape Estimates for
3-DOF Nonproportionally Damped Model

Method	Indicator	Mode 1	Mode 2	Mode 3
	MPC	0.5573	0.1205	0.9987
ST	MAC	0.9793	0.9860	0.9998
MNF	MAC	0.8241	0.1434	0.9935
CBSI	MAC	0.9451	0.9261	1.0000
CBSI-LS	MAC	0.9976	0.9626	1.0000
CBSI-SYM	MAC	0.9986	0.9925	1.0000
Exact	Frequency	0.2193	0.3859	0.7503
Estimates	Frequency	0.2519	0.3360	0.7502
	% error	14.8649	-12.9281	-0.0150
Effective	Damping	38.8%	22.8%	11.8%

From this numerical example, the Symmetrical CBSI determines the closest estimate to the correct normal mode shapes known from the mass and stiffness. Note from the MPC that Mode 2 is most "complex" of the system modes and thus most sensitive to the mode shape estimation used, while Mode 3 is nearly uncoupled in a normal modal sense from Modes 1 and 2. Also, the McMillan normal form, because it lacks an objective basis definition, performs poorly as the MPC deviates from 1.0 as so is not recommended in general for mode shape estimation without an additional transformation such as rotating the damped modal realization or utilizing CBSI. Finally, note that, while mode shapes are generally more sensitive to the effects of nonproportional damping, the estimated frequencies can also be affected. In

this numerical example, the relatively large error in the frequency estimates is due in large part to a high degree of damping. It should be considered, however, that in the presence of significantly complex modes, even when the level of damping is low, the frequencies determined from normal mode estimation methods can vary from the true undamped frequencies of the mass and stiffness. This is because the estimation of the undamped frequencies is found by taking the magnitude of each complex eigenvalue, a process which inherently assumes a one-to-one relationship between the damped and normal modes. The non-collinearity of the damped modes, howver, is an indication that model equivalence does not hold on an individual modal level. A global method, such as UNDAMP presented in the next chapter, only assumes an equivalence between damped and normal modes models on a global level, and so is capable of improving these frequency estimates.

3.5.4 36-DOF Planar Truss with Light Nonproportional Damping

A more realistic space structure example, shown in Figure 3.2, is of a two-dimensional truss structure with 3 actuators and 18 sensors with fixed-fixed conditions. The structure exhibits relatively light damping averaging around 1% of critical, but possesses repeated frequencies which introduce the potential for modal coupling. The modal damping matrix, shown in Figure 3.3, is a perturbation on a proportional damping matrix such that some realistic degree of nonproportionality exists.

In Table 3.3, the accuracy indicators for the normal mode estimates are given for 13 modes possessing MPC values less than 0.99. Note in particular modes 27 and 28, which are more highly coupled. In Figures 3.4 and

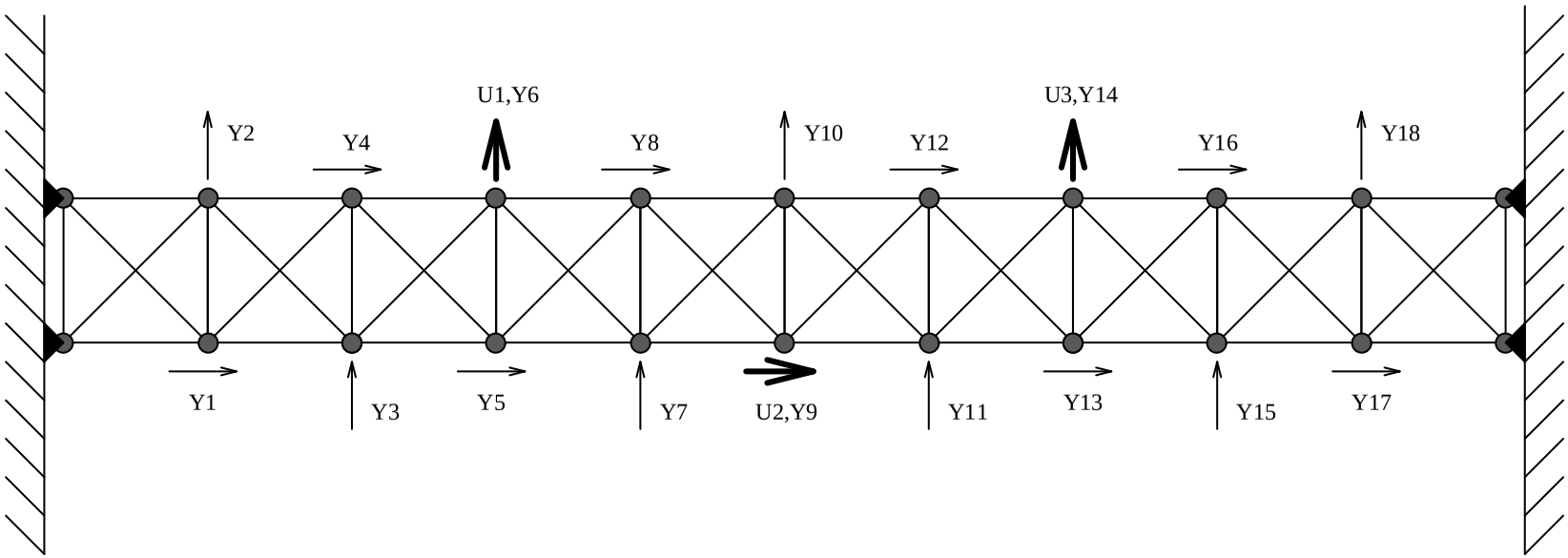

Figure 3.2: Planar Truss Example Model Showing Input Force and Output Displacement Locations

Table 3.3
Comparison of Normal Mode Shape Estimates for
36-DOF Nonproportionally Damped Truss

Mode	MPC	ST	MNF	CBSI	CBSI LS	CBSI SYM
16	0.9887	0.9993	0.1187	0.9995	0.9995	0.9995
17	0.9866	0.9993	0.2163	0.9994	0.9994	0.9994
19	0.9481	0.9983	0.0567	0.9982	0.9986	0.9986
20	0.9743	0.9991	0.0394	0.9995	0.9994	0.9994
22	0.9771	0.9617	0.0028	0.9446	0.9448	0.9444
23	0.9748	0.9617	0.0153	0.9402	0.9414	0.9410
25	0.9755	0.9998	0.0397	0.9999	0.9999	0.9999
26	0.8468	0.9934	0.0030	0.9977	0.9981	0.9980
27	0.5722	0.8755	0.0709	0.9058	0.9257	0.9241
28	0.5990	0.8896	0.0841	0.9236	0.9302	0.9299
29	0.9404	0.9964	0.0290	0.9985	0.9986	0.9986
30	0.9853	0.9996	0.1171	1.0000	1.0000	1.0000
31	0.9893	0.9998	0.1860	1.0000	1.0000	1.0000
Mean 1-36	0.9639	0.9909	0.3618	0.9918	0.9926	0.9926

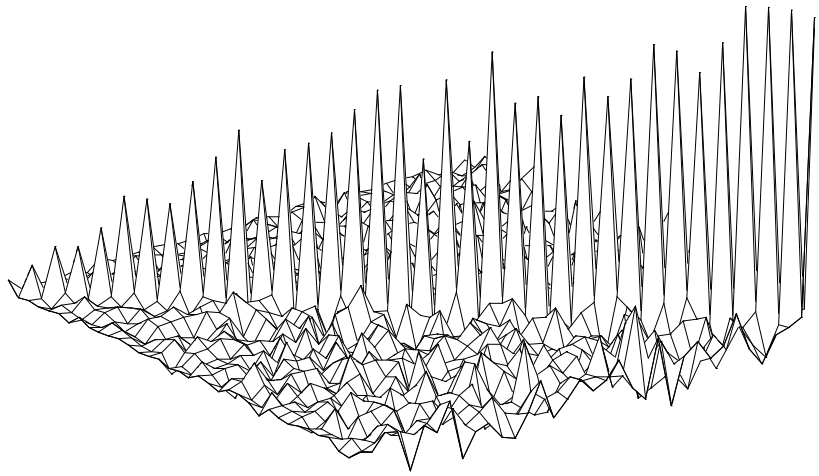

Figure 3.3: Modal Damping Matrix for Truss Example

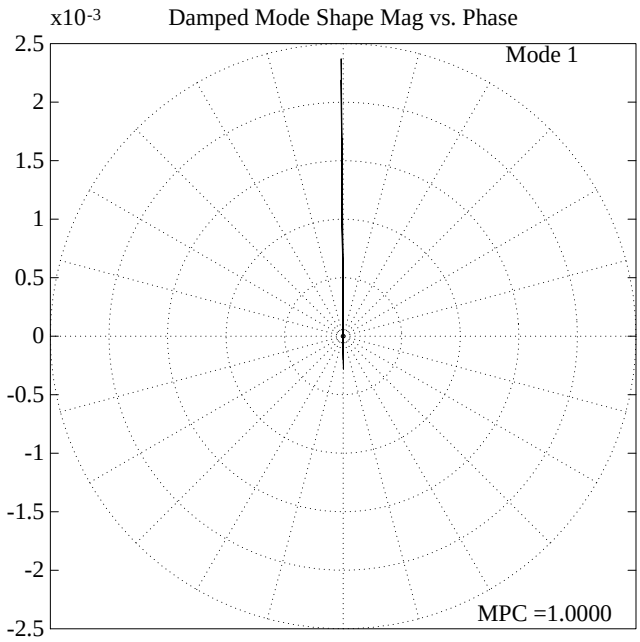

Figure 3.4: Complex Mode Shape with High Phase Collinearity

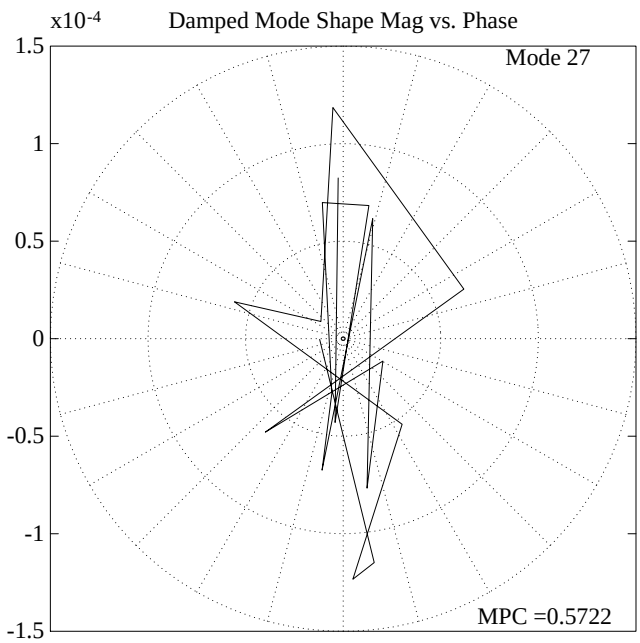

Figure 3.5: Complex Mode Shape with Poor Phase Collinearity

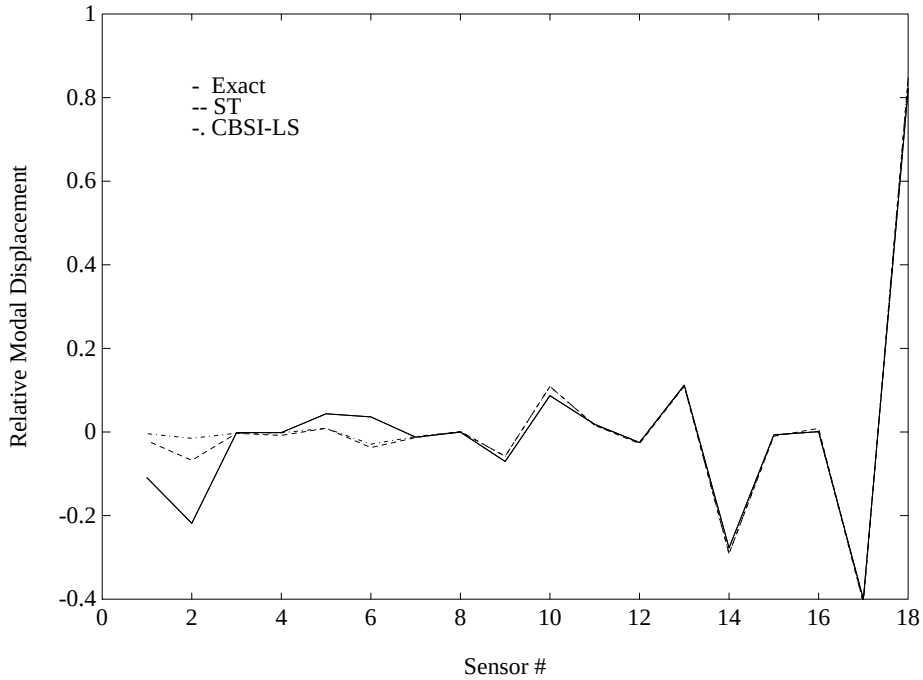

Figure 3.6: Comparison of Estimated Normal Mode Shapes for Planar Truss, Mode 23

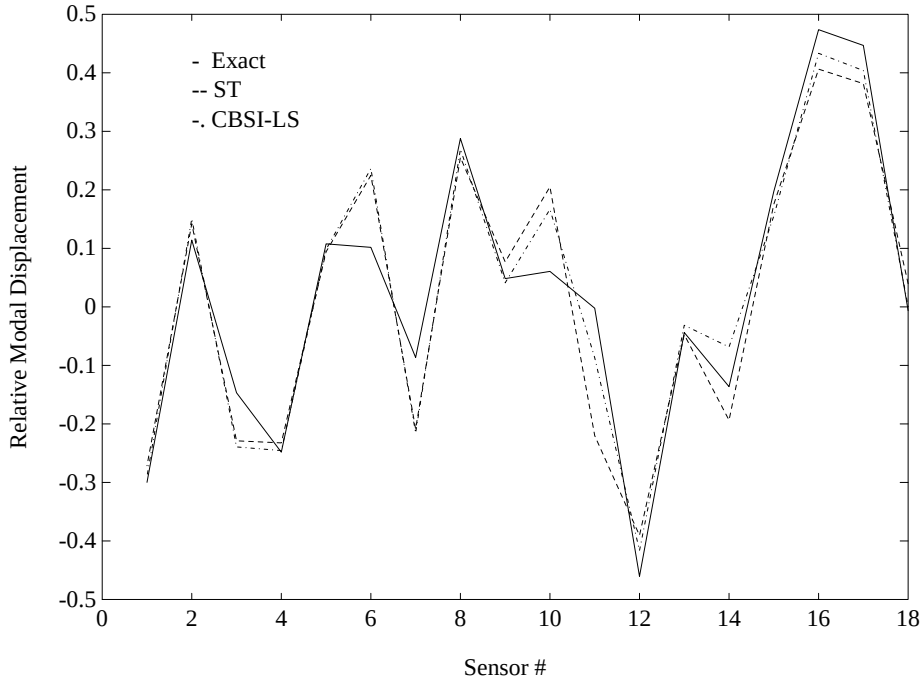

Figure 3.7: Comparison of Estimated Normal Mode Shapes for Planar Truss, Mode 27

3.5, the damped mode shapes for modes 1 and 27 are plotted in the complex plane. These plots show the poorer shape collinearity manifested as a wider dispersion of the phase angles for the largest relative magnitude displacements. Overall, the performance of CBSI-LS and CBSI-SYM, in terms of the MAC between the correct mode shapes and the CBSI estimates, are comparable. This is true for both the most complex of the modes, and also in terms of the mean indicator values over all 36 modes. Only in modes 22 and 23 does the ST approach identify a better estimated normal mode shape. Note also that in this general numerical example, the mode shapes obtained from the McMillan form realization, without the improvement of the second CBSI transformation, are quite poor as estimates of the normal modes, even for a lightly damped structure. Finally, Figures 3.6 and 3.7 illustrate the mode shape estimates from ST and CBSI-LS as compared to the exact mode shapes from the known mass and stiffness for modes 23 and 28.

Thus, as quantified through the MAC indicators with respect to the exact mode shapes, and as illustrated in the previous figures, application of the CBSI algorithm leads to a unique definition of the estimated normal mode shapes and shows a consistent improvement in accuracy over the standard technique for nonproportionally-damped systems.

3.6 Concluding Remarks

The present CBSI procedure offers a consistent link between the various system identification techniques and the second-order based equations of motion for structures. Utilizing the general transformation to second-order form, CBSI can determine an optimal estimate of second-order model states

which correspond individually to the damped modes of the given system realization. In the presence of strictly proportional viscous damping, the CBSI algorithm systematically determines the accurate normal modes in the form of the well-known second-order structural dynamics equations of motion.

For structures with nonproportional damping, the CBSI-LS or CBSI-SYM methods lead to generally accurate and reliable estimates of the normal modes and their mode shapes by transforming the given system realization to a "pseudo-normal" state variable basis. This pseudo-normal modes basis is defined by minimizing the difference between the estimated modal velocities and the time derivative of the estimated modal displacements. As the CBSI transformations are applied to the individual damped modes, however, its ability to determine the true normal modes is necessarily limited when the system damping is nonproportional. Therefore, in some cases where structures exhibit a high degree of modal energy coupling due to repeated frequencies and the presence of nonproportional damping, it is necessary to utilize a mode shape-damping decoupling method, which allows for the coupling of normal modes. This problem is addressed in the next chapter.

CHAPTER IV

EXTRACTION OF NORMAL MODAL PARAMETERS FOR NONPROPORTIONAL DAMPING

4.1 Introduction

This chapter presents a global transformation method for correcting the pseudo-normal modal basis of the CBSI realizations when the system damping is nonproportional. This is required because CBSI transforms the state space-based realizations as if they are proportionally damped structural systems. The transformation method is equivalent to the determination of mass, damping and stiffness through the direct solution of a damped inverse problem. The global transformation effectively isolates or extracts the damping attributes embedded in the mass and stiffness components due to the pseudo-normal mode characterization of the CBSI realization. Hence, the method is termed UNDAMP, for *uncoupled nonproportional damping.* In other words, CBSI masks the coupling of nonproportional damping which gives rise to violations of the identity relation of the velocity term in the second-order form of the structural dynamics equations and of the collinearity in the mode shapes corresponding to the displacement and velocity vectors. The present UNDAMP procedure is a global extension of the CBSI methods of Chapter III which is capable of extracting the true normal modes and nondiagonal modal damping matrix for systems with significantly complex modes.

Previous work in this area has focused on problems where the number of sensor measurements are equal to or exceed the number of identified modes. These methods share a common theoretical basis by implicitly solving the *inverse damped vibration problem* (IDVP) for generalized stiffness and mass, which then possess the correct normal modal parameters. Ibrahim's method [28] explicitly transforms the damped modes to a physical basis consisting of the measured coordinates, while Zhang and Lallement [30] iteratively determine a complex transformation to express the damped modes in a basis of estimated normal modes variables. Placidi et. al. [33] reviewed these existing methods and their deficiencies and proposed an improved approach by combining the best of the methods to develop an iterative algorithm which is independent of the mode shape normalization and allows for more sensors than measured modes. Minas and Inman [34] proposed a direct solution approach, but the system of equations is large in comparison to the dimension of the system, and the determinacy of the solution is not clearly apparent.

The UNDAMP algorithm presented herein is a transformation-based approach which can also be interpreted as solving the IDVP for generalized mass and stiffness matrices. Like the existing methods, UNDAMP assumes that there exists a underlying second-order system which is equivalent to the given realization. The UNDAMP algorithm, however, operates on the real-valued state space realization determined by CBSI, and explicitly defines a new set of generalized second-order displacement variables in terms of the existing state variables of the CBSI realization. This is in contrast to existing methods which typically operate on the complex-valued modal parameters and do not explicitly define the basis of the transformed model (except for Ibrahim, which uses the sensor degrees of freedom but requires the addition

of uncorrelated noise to handle indeterminacy created by a large number of sensors). The explicit basis definition of the UNDAMP algorithm leads to a direct transformation of the damped realization and allows the effect of coupling on the mass and stiffness matrices to be explicitly derived. Finally, the generalized displacement basis definition does not require that the number of sensor measurements be equal to or greater than the number of identified modes.

The UNDAMP algorithm is a second-order transformation method equivalent in form to CBSI, and constraints on the resulting second-order transformation are imposed so that the physical consistency of the resulting model is preserved. The necessary transformation and constraints thus derived allow for a direct solution of the well-determined and over-determined cases (where the number of sensors equal or exceed the number of modes) which requires only as many equations as the number of modes. An extension of the direct solution is also possible when the number of sensors is less than the number of modes. A scaling matrix is determined either directly or iteratively which augments a pseudo-inverse solution so as to satisfy the transformation constraints. For the underdetermined problem, an additional displacement consistency criterion is developed which projects the possible solutions to to exist in a physically consistent subspace. This displacement consistency criterion is automatically satisfied by the well-determined and over-determined solutions when the response characteristics of the given continuous-time state space realization are consistent with the second-order response behavior of a self-adjoint structural dynamic system.

The remainer of the chapter is organized as follows. Section 4.2 reviews the inverse damped vibration problem, which constitutes a theoretical

basis for the damping correction problem. The correctional basis transformation for nonproportional damping is then presented in Section 4.3. Section 4.4 details the implementation and performance of the damping correction algorithm on a series of numerical examples.

4.2 The Inverse Damped Vibration Problem

As noted previously, all methods for relating the nonproportionally damped and nominally undamped vibration modes are founded on the solution to the IDVP. In terms of a chosen set of n physical displacements $\mathbf{q}(t)$, the equations of motion are given as

$$\mathbf{M}\ddot{\mathbf{q}}(t) + \mathcal{D}\dot{\mathbf{q}}(t) + \mathbf{K}\mathbf{q}(t) = \hat{\mathbf{B}}\mathbf{u}(t) \tag{4.2.1}$$

where $\mathbf{M}$, $\mathcal{D}$ and $\mathbf{K}$ are the $n \times n$ inertia, damping and stiffness matrices, respectively, and $\mathbf{u}$ is a m-input force vector. When $\mathcal{D}$ is given as a general symmetric positive semidefinite matrix, a symmetrical first-order form of (4.2.1) can be written using a canonical form, viz.

$$\begin{bmatrix} \mathcal{D} & \mathbf{M} \\ \mathbf{M} & 0 \end{bmatrix} \begin{Bmatrix} \dot{\mathbf{q}} \\ \ddot{\mathbf{q}} \end{Bmatrix} = \begin{bmatrix} -\mathbf{K} & 0 \\ 0 & \mathbf{M} \end{bmatrix} \begin{Bmatrix} \mathbf{q} \\ \dot{\mathbf{q}} \end{Bmatrix} + \begin{bmatrix} \hat{\mathbf{B}} \\ 0 \end{bmatrix} \mathbf{u} \tag{4.2.2}$$

Thus, the generalized eigenproblem can be written in a symmetric form as

$$\begin{bmatrix} -\mathbf{K} & 0 \\ 0 & \mathbf{M} \end{bmatrix} \begin{bmatrix} \mathbf{X} \\ \mathbf{X}\mathbf{\Lambda} \end{bmatrix} = \begin{bmatrix} \mathcal{D} & \mathbf{M} \\ \mathbf{M} & 0 \end{bmatrix} \begin{bmatrix} \mathbf{X} \\ \mathbf{X}\mathbf{\Lambda} \end{bmatrix} \mathbf{\Lambda} \tag{4.2.3}$$

such that

$$\begin{gathered} \begin{bmatrix} \mathbf{X} \\ \mathbf{X}\mathbf{\Lambda} \end{bmatrix}^T \begin{bmatrix} \mathcal{D} & \mathbf{M} \\ \mathbf{M} & 0 \end{bmatrix} \begin{bmatrix} \mathbf{X} \\ \mathbf{X}\mathbf{\Lambda} \end{bmatrix} = \mathbf{I} \\ \begin{bmatrix} \mathbf{X} \\ \mathbf{X}\mathbf{\Lambda} \end{bmatrix}^T \begin{bmatrix} -\mathbf{K} & 0 \\ 0 & \mathbf{M} \end{bmatrix} \begin{bmatrix} \mathbf{X} \\ \mathbf{X}\mathbf{\Lambda} \end{bmatrix} = \mathbf{\Lambda} \\ \mathbf{\Lambda} = diag\{\sigma_i \pm j\omega_i, i = 1, \ldots, n\} \\ \mathbf{X} = [\ldots, \Re(\mathbf{X}_i) \pm j\Im(\mathbf{X}_i), \ldots] \end{gathered} \tag{4.2.4}$$

Here the columns of $\mathbf{X}$, are the complex damped mode shapes which may possess complicated phase relationships within each decoupled mode between spatially distinct points. If a proportionally damped system is expressed in this form, the relative phase relationships are either 0 or π radians, implying that the real and imaginary parts of $\mathbf{X}_i$ describe the same displacement shape; in other words the displacement and velocity mode shapes are equivalent. Otherwise, non-normal phase values indicate the presence of non-proportional damping, such that the mode shapes of the undamped system (given by the generalized eigenproblem of $\mathbf{K}$ and $\mathbf{M}$) and the damped system are distinctly different quantities.

The symmetric formulation (4.2.3)-(4.2.4) leads directly to a general solution for the inverse damped vibration problem when $\mathbf{\Lambda}$ and $\mathbf{X}$, measured at all n points in $\mathbf{q}$ and normalized as in (4.2.4), are known, viz.

$$\begin{aligned} \begin{bmatrix} \mathcal{D} & \mathbf{M} \\ \mathbf{M} & 0 \end{bmatrix} &= \left(\begin{bmatrix} \mathbf{X} \\ \mathbf{X\Lambda} \end{bmatrix} \begin{bmatrix} \mathbf{X} \\ \mathbf{X\Lambda} \end{bmatrix}^T \right)^{-1} \\ \begin{bmatrix} -\mathbf{K} & 0 \\ 0 & \mathbf{M} \end{bmatrix} &= \left(\begin{bmatrix} \mathbf{X} \\ \mathbf{X\Lambda} \end{bmatrix} \mathbf{\Lambda}^{-1} \begin{bmatrix} \mathbf{X} \\ \mathbf{X\Lambda} \end{bmatrix}^T \right)^{-1} \end{aligned} \tag{4.2.5}$$

which is equivalent to

$$\begin{aligned} \mathbf{K}^{-1} &= -\mathbf{X\Lambda}^{-1}\mathbf{X}^T \\ \mathbf{M}^{-1} &= \mathbf{X\Lambda X}^T \\ \mathcal{D} &= -\mathbf{M}\left(\mathbf{X\Lambda}^2\mathbf{X}^T\right)\mathbf{M} \end{aligned} \tag{4.2.6}$$

with the additional result that

$$\mathbf{XX}^T = 0 \tag{4.2.7}$$

The solution of the preceding inverse damped vibration problem yields two important results of interest to the nonproportional damping correction problem. First, it effectively decouples the influence of the general damping matrix $\mathcal{D}$ from the stiffness and mass, which in turn possess the properties of the normal undamped vibrational modes. Secondly, equation (4.2.7) provides a consistency indicator for the complex modes which can be used to evaluate the physical consistency of the non-normal phase quantities in the mode shapes.

The relevance of the consistency relationship (4.2.7) to the underlying physics of the second-order system can be understood in terms of the continuous-time Markov parameters. Recall from Chapter II the normalized damped modal realization given by

$$\begin{aligned} \dot{\mathbf{z}}_n &= \mathbf{\Lambda}\mathbf{z}_n + \mathbf{X}^T\mathbf{u} \\ \mathbf{y}_d &= \mathbf{X}\mathbf{z}_n \end{aligned} \tag{4.2.8}$$

where $\hat{\mathbf{B}}^T = \mathbf{H}_d = \mathbf{I}$ so that all independent transfer functions have been obtained. The solution in the Laplace domain for the output $\mathbf{y}$ can be written as

$$\mathbf{y}(s) = \sum_{i=1}^{\infty} \frac{1}{s^i}\mathbf{Y}(i)\mathbf{u}(s) \tag{4.2.9}$$

where the continuous-time Markov parameters $\mathbf{Y}(i)$ are defined as

$$\mathbf{Y}(i) = \mathbf{X}\mathbf{\Lambda}^{i-1}\mathbf{X}^T \tag{4.2.10}$$

Thus, (4.2.7) is the Markov parameter $\mathbf{Y}(1)$ of the continuous system realization relating applied force inputs to displacement outputs. In order for the outputs to be consistently identified as displacement quantities, the first-order delay term $\mathbf{Y}(1)$ must be equal to zero. Equation (4.2.7) then implies,

assuming that the feedthrough term (not given in (4.2.8)) is also zero, that the measured mode shapes are consistent with displacement quantities, and this consistency constraint must be satisfied in order for the solution to the inverse problem to be physically consistent with the resulting stiffness and mass. This is a key consideration in the damping correction problem. If the non-normal phase components of the normalized mode shapes $\mathbf{X}$ cannot satisfy (4.2.7d), then the inverse vibration solution (4.2.6) can introduce nonphysical quantities into the system stiffness and mass, thus adversely affecting the normal mode parameters that are being sought.

4.3 The UNDAMP Basis Correction Algorithm

Although the CBSI procedure yields a correct set of normal modes and mode shapes for proportionally-damped systems, it compromises the accuracy of the normal mode parameters for nonproportionally-damped cases. Hence, the CBSI-transformed system realization can be thought to give approximations of the undamped mode shapes, frequencies, and modal damping ratios while maintaining system equivalence. Specifically, the state space CBSI model retains the out-of-phase components of the damped modes as residual quantities in the input and output influence matrices. These perturbations of the idealized MDV model form can be used in defining basis corrections which adjust the mode shapes and frequencies and in the process fill in the off-diagonal terms of the modal damping matrix. Consequently, the non-normal complex mode shape phase components are systematically utilized to correct the deficiencies in the estimated normal modes of the second-order model.

4.3.1 Global UNDAMP Transformation to Second-Order Basis

We begin the present damping correction procedure with the nominal model resulting from the CBSI procedure. For clarity, the realization is transformed to a displacement-output equivalent form as detailed in Chapter II, Section 2.1.5. Then, using the general damping form of the CBSI realization from (3.4.26) and introducing tildes to denote the approximate nature of the modal parameters,

$$\begin{aligned} \begin{Bmatrix} \dot{\tilde{\eta}}_d \\ \dot{\tilde{\eta}}_v \end{Bmatrix} &= \begin{bmatrix} 0 & \mathbf{I} \\ -\tilde{\mathbf{\Omega}} & -\tilde{\mathbf{\Xi}} \end{bmatrix} \begin{Bmatrix} \tilde{\eta}_d \\ \tilde{\eta}_v \end{Bmatrix} + \begin{bmatrix} \tilde{\epsilon}_u^T \\ \tilde{\phi}_u^T \end{bmatrix} \mathbf{u} \\ \mathbf{y}_d &= [\, \tilde{\phi}_y \quad \tilde{\epsilon}_y \,] \begin{Bmatrix} \tilde{\eta}_d \\ \tilde{\eta}_v \end{Bmatrix} \end{aligned} \tag{4.3.1}$$

Observe that, if $\tilde{\epsilon}_u = 0$ and $\tilde{\epsilon}_y = 0$, then $\tilde{\eta}_d$ and $\tilde{\eta}_v$ represent the normal mode displacement and velocity, respectively. This is because $\tilde{\eta}_v = \dot{\tilde{\eta}}_d$ and the displacement outputs $\mathbf{y}_d$ are solely a function of $\tilde{\eta}_d$. Furthermore, if $\tilde{\mathbf{\Xi}}$ is diagonal (true if (4.3.1) is obtained from CBSI), the system is proportionally damped. However, if $\tilde{\epsilon}_u \neq 0$ and $\tilde{\epsilon}_y \neq 0$ due to nonproportional damping, $\tilde{\eta}_d$ and $\tilde{\eta}_v$ can be viewed as pseudo-normal modal displacement and velocity vectors, and the residual quantities $\tilde{\epsilon}_u$ and $\tilde{\epsilon}_y$ are a measure of the magnitude and spatial distribution of the nonproportional damping.

The preceding observation leads us to introduce a corrected displacement variable basis η_d as a linear combination of the approximate modal displacement and velocity variables $\tilde{\eta}_d$ and $\tilde{\eta}_v$, viz

$$\mathbf{T}_d \eta_d = \tilde{\eta}_d + \mathbf{V}_d \tilde{\eta}_v \tag{4.3.2}$$

Let us also define a new generalized displacement basis ξ in terms of η_d and $\mathbf{T}_d$ as

$$\xi = \mathbf{T}_d \eta_d = \tilde{\eta}_d + \mathbf{V}_d \tilde{\eta}_v \tag{4.3.3}$$

Thus, the problem of finding the generalized displacement basis ξ has been isolated from determining the corrected normal modal basis η_d. The criteria for selecting $\mathbf{V}_d$ can be developed independently of $\mathbf{T}_d$, and the resultant transformation applied, yielding a new generalized stiffness matrix $\mathbf{K}_\xi$ in the basis ξ, which is then diagonalized using $\mathbf{T}_d$ to yield the correct undamped eigenvalues $\mathbf{\Omega}$.

The transformation $\mathbf{V}_d$ can be termed a *coupling perturbation* matrix because it expressed the coupling effects of nonproportional damping on the pseudo-normal displacement variables $\tilde{\eta}_d$. Furthermore, substitution of (4.3.3) into (4.3.1) yields the damping correction transformation

$$\begin{Bmatrix} \xi \\ \dot{\xi} \end{Bmatrix} = \begin{bmatrix} \mathbf{I} & \mathbf{V}_d \\ -\mathbf{V}_d\tilde{\mathbf{\Omega}} & \mathbf{I} - \mathbf{V}_d\tilde{\mathbf{\Xi}} \end{bmatrix} \begin{Bmatrix} \tilde{\eta}_d \\ \tilde{\eta}_v \end{Bmatrix} = \mathbf{\Psi}_d \begin{Bmatrix} \tilde{\eta}_d \\ \tilde{\eta}_v \end{Bmatrix} \tag{4.3.4}$$

which is a perturbation through $\mathbf{V}_d$ on the identity matrix; i.e. $\mathbf{\Psi}_d \to \mathbf{I}$ as $\mathbf{V}_d \to 0$. Applying (4.3.4) to (4.3.1b), the output $\mathbf{y}_d$ in the corrected displacement basis becomes

$$\begin{aligned} \mathbf{y}_d &= [\, \tilde{\phi}_y \quad \tilde{\epsilon}_y \,] \begin{Bmatrix} \tilde{\eta}_d \\ \tilde{\eta}_v \end{Bmatrix} = [\, \tilde{\phi}_y \quad \tilde{\epsilon}_y \,]\, \mathbf{\Psi}_d^{-1} \begin{Bmatrix} \xi \\ \dot{\xi} \end{Bmatrix} \\ &= [\, \tilde{\phi}_y \quad \tilde{\epsilon}_y - \tilde{\phi}_y \mathbf{V}_d \,] \begin{Bmatrix} \xi \\ \dot{\xi} \end{Bmatrix} \end{aligned} \tag{4.3.5}$$

In order for $\mathbf{y}_d$ to become solely a function of the displacement variables ξ in the corrected model basis, we can identify the proper transformation constraint

$$\tilde{\epsilon}_y - \tilde{\phi}_y \mathbf{V}_d = 0 \tag{4.3.6}$$

such that

$$\mathbf{y}_d = [\, \tilde{\phi}_y \quad 0 \,] \begin{Bmatrix} \xi \\ \dot{\xi} \end{Bmatrix}$$

The constraint (4.3.6) ensures the output $\mathbf{y}_d$ for the new basis is independent of the new velocity variables $\dot{\xi}$. Note that the "mode shapes" with respect to the new basis are $\tilde{\phi}_y$. This does not imply, however, that the corrected normal mode shapes are equal to $\tilde{\phi}_y$ since we must still apply the re-diagonalizing transformation $\mathbf{T}_d$ to capture the corrected normal modes basis η_d. That is,

$$\begin{bmatrix} 0 & \mathbf{I} \\ -\mathbf{M}_\xi^{-1}\mathbf{K}_\xi & -\mathbf{M}_\xi^{-1}\mathcal{D}_\xi \end{bmatrix} = \mathbf{\Psi}_d \begin{bmatrix} 0 & \mathbf{I} \\ -\tilde{\mathbf{\Omega}} & -\tilde{\mathbf{\Xi}} \end{bmatrix} \mathbf{\Psi}_d^{-1} \qquad (4.3.7)$$
$$\mathbf{M}_\xi^{-1}\mathbf{K}_\xi\mathbf{T}_d = \mathbf{T}_d\mathbf{\Omega}$$

Thus, UNDAMP determines an MDV realization as

$$\begin{Bmatrix} \dot{\eta}_d \\ \ddot{\eta}_d \end{Bmatrix} = \begin{bmatrix} 0 & \mathbf{I} \\ -\mathbf{\Omega} & -\mathbf{\Xi} \end{bmatrix} \begin{Bmatrix} \eta_d \\ \dot{\eta}_d \end{Bmatrix} + \begin{bmatrix} 0 \\ \phi_u^T \end{bmatrix} \mathbf{u} \qquad (4.3.8)$$
$$\mathbf{y}_d = [\,\phi_y \quad 0\,] \begin{Bmatrix} \eta_d \\ \dot{\eta}_d \end{Bmatrix}$$

where

$$\begin{bmatrix} 0 & \mathbf{I} \\ -\mathbf{\Omega} & -\mathbf{\Xi} \end{bmatrix} = \begin{bmatrix} \mathbf{T}_d & 0 \\ 0 & \mathbf{T}_d \end{bmatrix}^{-1} \mathbf{\Psi}_d \begin{bmatrix} 0 & \mathbf{I} \\ -\tilde{\mathbf{\Omega}} & -\tilde{\mathbf{\Xi}} \end{bmatrix} \mathbf{\Psi}_d^{-1} \begin{bmatrix} \mathbf{T}_d & 0 \\ 0 & \mathbf{T}_d \end{bmatrix}$$
$$\begin{bmatrix} 0 \\ \phi_u^T \end{bmatrix} = \begin{bmatrix} \mathbf{T}_d & 0 \\ 0 & \mathbf{T}_d \end{bmatrix}^{-1} \mathbf{\Psi}_d \begin{bmatrix} \tilde{\epsilon}_u^T \\ \tilde{\phi}_u^T \end{bmatrix} \qquad (4.3.9)$$
$$[\,\phi_y \quad 0\,] = [\,\tilde{\phi}_y \quad \tilde{\epsilon}_y\,]\, \mathbf{\Psi}_d^{-1} \begin{bmatrix} \mathbf{T}_d & 0 \\ 0 & \mathbf{T}_d \end{bmatrix}$$

Note that the transformation (4.3.4) is a second-order canonical transformation consistent with (3.3.6) with a corresponding transformation constraint (4.3.6). As noted in Chapter III, the canonical transformation constraint may be written equivalently in terms of either the input influence matrix $\mathbf{B}$ or the displacement output influence matrix $\mathbf{C}_d$, as these quantities are constrainted as $\mathbf{C}_d\mathbf{B} = 0$ (see (3.4.29)). Thus, in the above development, the constraint in terms of the partitions of $\mathbf{C}_d$ is utilized, as the nonproportional damping is more clearly observed from a large number of sensors than from a small number of actuators.

4.3.2 Solution of $\mathbf{V}_d$ for Well and Overdetermined Constraint

The transformation constraint (4.3.6) provides a great deal of insight into the algorithmic nature of the damping correction problem. If we have n independent sensors (equal to the number of identified modes), $\tilde{\phi}_y$ is square and nonsingular and $\mathbf{V}_d$ is uniquely determined. Therefore

$$\mathbf{V}_d = \left(\tilde{\phi}_y\right)^{-1} \tilde{\epsilon}_y \tag{4.3.10}$$

For the overdetermined case, where the number of independent sensors is greater than n, we cannot completely account for the out-of-phase component measure $\tilde{\epsilon}_y$ using the transformation $\mathbf{V}_d$ over the n identified modes. We can, however, determine a least square solution using the pseudoinverse, which will minimize $\|\tilde{\epsilon}_y - \tilde{\phi}_y \mathbf{V}_d\|$. This is similar to the Least-Square CBSI presented in Chapter III, in which the solution for e_i is always overdetermined for MIMO systems. One crucial difference, however, is that an optimal value for $\mathbf{V}_d$ cannot be determined explicitly because $\mathbf{\Psi}_d$ does not lead directly to a normal modes basis.

An iterative approach to minimizing (4.3.6) can be implemented by successive application of UNDAMP using a least-squares solution to (4.3.6), viz.

$$
\text{while} \quad \|\mathbf{V}_d^{(k)}\| > \epsilon
$$

$$
\text{do} \quad \begin{cases}
(i) & \mathbf{V}_d^{(k)} = \left(\tilde{\phi}_y^{(k)T}\tilde{\phi}_y^{(k)}\right)^{-1}\tilde{\phi}_y^{(k)T}\tilde{\epsilon}_y^{(k)} \\
(ii) & \mathbf{\Psi}_d^{(k)} = \begin{bmatrix} \mathbf{I} & \mathbf{V}_d^{(k)} \\ -\mathbf{V}_d^{(k)}\tilde{\mathbf{\Omega}}^{(k)} & \mathbf{I} - \mathbf{V}_d^{(k)}\tilde{\mathbf{\Xi}}^{(k)} \end{bmatrix} \\
(iii) & \begin{bmatrix} 0 & \mathbf{I} \\ -\tilde{\mathbf{K}}_\xi & -\tilde{\mathcal{D}}_\xi \end{bmatrix} = \mathbf{\Psi}_d^{(k)} \begin{bmatrix} 0 & \mathbf{I} \\ \tilde{\mathbf{\Omega}}^{(k)} & -\tilde{\mathbf{\Xi}}^{(k)} \end{bmatrix} \mathbf{\Psi}_d^{(k)^{-1}} \\
(iv) & \tilde{\mathbf{\Omega}}^{(k+1)}\mathbf{T}_d = \mathbf{T}_d\tilde{\mathbf{K}}_\xi \\
(v) & \tilde{\mathbf{\Xi}}^{(k+1)} = \mathbf{T}_d\tilde{\mathcal{D}}_\xi\mathbf{T}_d^{-1} \\
(vi) & \begin{bmatrix} \tilde{\phi}_y^{(k+1)} & \tilde{\epsilon}_y^{(k+1)} \end{bmatrix} = \begin{bmatrix} \tilde{\phi}_y^{(k)} & \tilde{\epsilon}_y^{(k)} \end{bmatrix} \mathbf{\Psi}_d^{(k)^{-1}} \begin{bmatrix} \mathbf{T}_d & 0 \\ 0 & \mathbf{T}_d \end{bmatrix}^{-1} \\
(vii) & k = k+1
\end{cases}
\tag{4.3.11}
$$

4.3.3 Solution of $\mathbf{V}_d$ for Underdetermined Constraint

The underdetermined constraint problem, where the number of sensors is less than the number of modes, is much more difficult in that it admits an infinity of possible physical solutions which equally satisfy (4.3.6). An obvious choice is found using the uniquely-defined Moore-Penrose pseudoinverse of $\tilde{\phi}_y$ which yields a solution for $\mathbf{V}_d$ whose norm is minimized. This is attractive because the state transformation (4.3.4) is a perturbation through $\mathbf{V}_d$ of the identity matrix. Thus, if we wish to minimize (in some sense) the necessary change in the modal parameters while incorporating the mode shape phase relationships, it is logical to minimize the magnitude of $\mathbf{V}_d$, viz.

$$
\mathbf{V}_p = \tilde{\phi}_y^{+}\tilde{\epsilon}_y = \tilde{\phi}_y^T\left(\tilde{\phi}_y\tilde{\phi}_y^T\right)^{-1}\tilde{\epsilon}_y \tag{4.3.12}
$$

Unfortunately, the pseudoinverse solution for $\mathbf{V}_d$ lacks any physical insight into the general damping problem. For example, in the well-determined problem a unique solution for $\mathbf{V}_d$ exists because there is a sufficient number of displacement outputs to form a consistent basis of displacement variables. Finding a solution for $\mathbf{V}_d$ in the underdetermined case still implies certain characteristics of the unmeasured outputs within the space spanned by the state variables. The underdetermined constraint solution can be interpreted as equivalent to augmenting $\tilde{\phi}_y$ and $\tilde{\epsilon}_y$ with additional independent outputs; each of the possible solutions for $\mathbf{V}_d$ (including (4.3.12)) which satisfy the constraint (4.3.6) correspond to a different set of augmented outputs. It is therefore critical to consider the nature of these hypothetical augmented outputs and their consistency to the existing mode shapes represented by $\tilde{\phi}_y$ and $\tilde{\epsilon}_y$. Otherwise, the underlying physics of the damping problem is violated, generally leading to a stiffness operator possessing complex or negative eigenvalues. Recalling the inverse damped vibration problem, this is analogous to the displacement consistency constraint on the damped mode shapes $\mathbf{X}$ given by (4.2.7). Using these concepts, we can develop an equivalent criterion for $\mathbf{V}_d$ such that hypothetical outputs satisfy the same displacement consistency as the measured portions of the damped mode shapes. This is discussed below.

4.3.4 Displacement Consistency Criterion for $\mathbf{V}_d$

Let us examine solving the IDVP as in (4.2.6) from the CBSI-transformed model in terms of the complete generalized displacement basis

ξ. To determine an equivalent symmetric form of (4.3.1), we can multiply through by the modal form of the coefficient matrix in (4.2.2) to obtain

$$\begin{bmatrix} \tilde{\mathbf{\Xi}} & \mathbf{I} \\ \mathbf{I} & 0 \end{bmatrix} \begin{Bmatrix} \dot{\tilde{\eta}}_d \\ \dot{\tilde{\eta}}_v \end{Bmatrix} = \begin{bmatrix} -\tilde{\mathbf{\Omega}} & 0 \\ 0 & \mathbf{I} \end{bmatrix} \begin{Bmatrix} \tilde{\eta}_d \\ \tilde{\eta}_v \end{Bmatrix} + \begin{bmatrix} \tilde{\epsilon}_u^T \\ \tilde{\phi}_u^T \end{bmatrix} \mathbf{u}$$
$$\mathbf{y}_d = [\, \tilde{\phi}_y \quad \tilde{\epsilon}_y \,] \begin{Bmatrix} \tilde{\eta}_d \\ \tilde{\eta}_v \end{Bmatrix} \tag{4.3.13}$$

Then, converting to the corrected displacement velocity basis using the transformation given by (4.3.4), we have

$$\begin{bmatrix} \tilde{\mathbf{\Xi}} & \mathbf{I} \\ \mathbf{I} & 0 \end{bmatrix} \mathbf{\Psi}^{-1} \begin{Bmatrix} \dot{\xi} \\ \ddot{\xi} \end{Bmatrix} = \begin{bmatrix} -\tilde{\mathbf{\Omega}} & 0 \\ 0 & \mathbf{I} \end{bmatrix} \mathbf{\Psi}^{-1} \begin{Bmatrix} \xi \\ \dot{\xi} \end{Bmatrix} + \begin{bmatrix} \tilde{\phi}_u^T + \tilde{\mathbf{\Xi}}\tilde{\epsilon}_u^T \\ \tilde{\epsilon}_u^T \end{bmatrix} \mathbf{u} \tag{4.3.14}$$

Finally, in order to obtain symmetric coefficient matrices in the new basis, we can multiply through by $\mathbf{\Psi}^{-T}$, viz.

$$\mathbf{\Psi}^{-T} \begin{bmatrix} \tilde{\mathbf{\Xi}} & \mathbf{I} \\ \mathbf{I} & 0 \end{bmatrix} \mathbf{\Psi}^{-1} = \begin{bmatrix} \mathcal{D}_\xi & \mathbf{M}_\xi \\ \mathbf{M}_\xi & 0 \end{bmatrix}$$
$$\mathbf{\Psi}^{-T} \begin{bmatrix} -\tilde{\mathbf{\Omega}} & 0 \\ 0 & \mathbf{I} \end{bmatrix} \mathbf{\Psi}^{-1} = \begin{bmatrix} -\mathbf{K}_\xi & 0 \\ 0 & \mathbf{M}_\xi \end{bmatrix} \tag{4.3.15}$$

where $\mathbf{M}_\xi$, $\mathcal{D}_\xi$ and $\mathbf{K}_\xi$ are the generalized mass, damping and stiffness matrices with respect to the corrected generalized displacement basis ξ. Inverting (4.3.15a), we have

$$\begin{bmatrix} \mathcal{D}_\xi & \mathbf{M}_\xi \\ \mathbf{M}_\xi & 0 \end{bmatrix}^{-1} = \mathbf{\Psi} \begin{bmatrix} \tilde{\mathbf{\Xi}} & \mathbf{I} \\ \mathbf{I} & 0 \end{bmatrix}^{-1} \mathbf{\Psi}^T$$
$$\begin{bmatrix} 0 & \mathbf{M}_\xi^{-1} \\ \mathbf{M}_\xi^{-1} & -\mathbf{M}_\xi^{-1}\mathcal{D}_\xi\mathbf{M}_\xi^{-1} \end{bmatrix} = \mathbf{\Psi} \begin{bmatrix} 0 & \mathbf{I} \\ \mathbf{I} & -\tilde{\mathbf{\Xi}} \end{bmatrix} \mathbf{\Psi}^T \tag{4.3.16}$$
$$= \begin{bmatrix} \mathbf{I} & \mathbf{V}_d \\ -\mathbf{V}_d\tilde{\mathbf{\Omega}} & \mathbf{I} - \mathbf{V}_d\tilde{\mathbf{\Xi}} \end{bmatrix} \begin{bmatrix} 0 & \mathbf{I} \\ \mathbf{I} & -\tilde{\mathbf{\Xi}} \end{bmatrix} \begin{bmatrix} \mathbf{I} & -\tilde{\mathbf{\Omega}}\mathbf{V}_d^T \\ \mathbf{V}_d^T & \mathbf{I} - \tilde{\mathbf{\Xi}}\mathbf{V}_d^T \end{bmatrix}$$

which leads to the desired displacement consistency criterion by evaluating the upper left-hand submatrix of the right hand side of (4.3.16), as shown

$$\mathbf{V}_d + \mathbf{V}_d^T - \mathbf{V}_d\tilde{\mathbf{\Xi}}\mathbf{V}_d^T = 0 \tag{4.3.17}$$

This displacement consistency criterion implies that all mass, damping and stiffness models determined by the coupling perturbation matrix $\mathbf{V}_d$ through the generalized displacement basis ξ are symmetric (i.e. self-adjoint) structural dynamic models. This condition is expressed by the symmetric block matrix structure of the first-order physical coefficient matrices in (4.3.15).

This formulation also allows us to examine the effect of the coupling perturbation matrix $\mathbf{V}_d$ on the generalized mass and stiffness of the transformed model. Evaluating (4.3.15b), we have

$$\begin{aligned} \mathbf{K}_\xi^{-1} &= \tilde{\mathbf{\Omega}}^{-1} - \mathbf{V}_d \mathbf{V}_d^T \\ \mathbf{M}_\xi^{-1} &= \mathbf{I} - \mathbf{V}_d \tilde{\mathbf{\Xi}} - \tilde{\mathbf{\Xi}} \mathbf{V}_d^T - \mathbf{V}_d \left(\tilde{\mathbf{\Omega}} - \tilde{\mathbf{\Xi}}^2 \right) \mathbf{V}_d^T \end{aligned} \tag{4.3.18}$$

Thus, $\mathbf{V}_d$ leads to perturbations in the generalized stiffness and mass properties of the system. This is of critical concern to the damping correction problem, because if $\mathbf{V}_d$ is not consistent with the underlying second-order structural dynamic behavior, the resulting mass and stiffness and their normal modes and mode shapes will be inaccurate and may even lose the definiteness properties which are important to the structural model.

We can evaluate the displacement consistency of the measured outputs by either evaluating (4.2.7) with the damped modal model or by evaluating the CBSI-derived model using the equivalent expression

$$\tilde{\epsilon}_y \tilde{\phi}_y^T + \tilde{\phi}_y \tilde{\epsilon}_y^T - \tilde{\epsilon}_y \tilde{\mathbf{\Xi}} \tilde{\epsilon}_y^T = 0 \tag{4.3.19}$$

Satisfying (4.3.19) or (4.2.7) implicitly assumes that the complex damped modes have been correctly normalized relative to one another. Following the procedure outlined in Chapter II, Section 2.3.3, the damped modes can be effectively normalized using collocated actuator-sensor pairs to determine $\mathbf{X}$.

If the Symmetrical CBSI method of Chapter III is then applied to the normalized damped modal realization for which $\mathbf{X}$ satisfies (4.2.7), the resultant arrays $\tilde{\phi}_y$ and $\tilde{\epsilon}_y$ will be displacement consistent (i.e. satisfying (4.3.19)) and suitable for addressing the underdetermined constraint problem.

Thus, combining the displacement consistency criteria for the corrective transformation (4.3.17) with the transformation constraint (4.3.6), $\mathbf{V}_d$ can be determined such that the displacement sensor outputs are expressed solely as a function of the corrected modal displacements η_d and the unmeasured mode shape phase quantities are consistent with the modal displacement variable assumptions. This generalized, transformation-based algorithm is applicable to MIMO systems where the number of sensors is either greater than or less than the number of modes. As will be shown in the next section, the under-determined constraint poses the greatest challenge because additional physical constraints must be introduced in order to obtain a solution for $\mathbf{V}_d$.

4.4 Computational Considerations for Determining $\mathbf{V}_d$

For the well-determined and overdetermined cases of the constraint (4.3.6), there should be no need to impose the consistency criterion (4.3.17) if the criterion for the given measured outputs (4.3.19) is satisfied. This can be checked as follows,

$$\begin{aligned} \tilde{\phi}_y^+ \left(\tilde{\epsilon}_y \tilde{\phi}_y^T + \tilde{\phi}_y \tilde{\epsilon}_y^T - \tilde{\epsilon}_y \tilde{\mathbf{\Xi}} \tilde{\epsilon}_y^T \right) \tilde{\phi}_y^{+T} &= 0 \\ \tilde{\phi}_y^+ \tilde{\epsilon}_y + \tilde{\epsilon}_y^T \tilde{\phi}_y^{+T} - \tilde{\phi}_y^+ \tilde{\epsilon}_y \tilde{\mathbf{\Xi}} \tilde{\epsilon}_y^T \tilde{\phi}_y^{+T} &= 0 \\ \tilde{\phi}_y^+ &= \left(\tilde{\phi}_y^T \tilde{\phi}_y \right)^{-1} \tilde{\phi}_y^T \end{aligned} \tag{4.4.1}$$

But $\mathbf{V}_d = \tilde{\phi}_y^+ \tilde{\epsilon}_y$, hence (4.3.19) is equivalent to (4.3.17).

In the under-determined case of (4.3.6), however, it is necessary to explicitly satisfy (4.3.17). In addition, despite the apparent complexity of the resultant problem, it is likely that the solution for $\mathbf{V}_d$ is not unique. Therefore, we can either seek a general solution to minimize the magnitude of $\mathbf{V}_d$ while satisfying the constraint equations (4.3.6) and (4.3.17), or determine a particular solution which satisfies particular physical considerations. The particular solution is straightforward and will be detailed first.

4.4.1 Underdetermined Solution via Augmented Outputs

We shall augment $\mathbf{y}_d$ in (4.3.1) by additional hypothetical displacement outputs $\hat{\mathbf{y}}_d$ which are only a function of the approximate modal displacements $\tilde{\eta}_d$. In other words, from the point of view of the augmented outputs, the CBSI-derived system will appear to be proportionally damped, viz.

$$\begin{Bmatrix} \mathbf{y}_d \\ \hat{\mathbf{y}}_d \end{Bmatrix} = \begin{bmatrix} \tilde{\phi}_y & \tilde{\epsilon}_y \\ \phi_a & 0 \end{bmatrix} \begin{Bmatrix} \tilde{\eta}_d \\ \tilde{\eta}_v \end{Bmatrix} \tag{4.4.2}$$

Then, assuming $\tilde{\phi}_y$ and $\tilde{\epsilon}_y$ satisfy (4.3.19), the augmented portion of the mode shapes ϕ_a must satisfy

$$\tilde{\epsilon}_y \phi_a^T = 0 \tag{4.4.3}$$

in order for the displacement consistency criterion to hold for the complete set of measured and augmented outputs. This implies ϕ_a is in the null space of $\tilde{\epsilon}_y^T$. It can be verified that the particular solution is given by

$$\mathbf{V}_d = \left(\mathbf{I} - \mathbf{Q}_{n1}(\mathbf{Q}_{n2}^T \mathbf{Q}_{n1})^{-1} \mathbf{Q}_{n2}^T\right) \mathbf{V}_p \tag{4.4.4}$$

where

$$\mathbf{Q}_{n1} = null(\tilde{\phi}_y) \qquad \mathbf{Q}_{n1}^T\mathbf{Q}_{n1} = \mathbf{I}$$

$$\mathbf{Q}_{n2} = null(\tilde{\epsilon}_y) \qquad \mathbf{Q}_{n2}^T\mathbf{Q}_{n2} = \mathbf{I} \tag{4.4.5}$$

$$\mathbf{V}_p = \tilde{\phi}_y^+\tilde{\epsilon}_y = \tilde{\phi}_y^T(\tilde{\phi}_y\tilde{\phi}_y^T)^{-1}\tilde{\epsilon}_y$$

Therefore, by applying this particular physical condition on the augmented system, it is possible to obtain a unique solution for $\mathbf{V}_d$ which satisfies the displacement consistency constraint (4.3.17) and the transformation constraint (4.3.6).

While this approach is attractive because of its directness and clear physical interpretation, we are implicitly limiting the freedom we have to choose $\mathbf{V}_d$ and assuming that only the measured degrees of freedom have significant mode shape phase components to consider. This approach may therefore impose significant changes on the corrected modal properties, especially when the number of measured outputs l becomes significantly less than the number of identified modes n. Hence, it is necessary to consider a general optimization-based approach to minimize $\mathbf{V}_d$ subject to the given linear and nonlinear constraints (4.3.6) and (4.3.17).

4.4.2 Optimization-Based Underdetermined Solution

As noted previously, it is reasonable to seek a solution for $\mathbf{V}_d$ which incorporates the residual phase quantities $\tilde{\epsilon}_y$ into the second-order model form while attempting to minimize the change in the approximate modal parameters. This implies that, of the infinity of possible solutions for $\mathbf{V}_d$ in the underdetermined correction problem, we wish to find the resultant physical system which is close to the approximate proportionally damped system.

We can approach this numerical problem by noting that all solutions to (4.3.6) fit the form

$$\mathbf{V}_d = \mathbf{V}_p + \mathbf{Q}_{n1}\mathbf{S}_n^T \tag{4.4.6}$$

where $\mathbf{V}_p$ is the pseudoinverse solution given by (4.3.12), $\mathbf{Q}_{n1}$ is the orthonormal null space of $\tilde{\phi}_y$ and $\mathbf{S}_n$ is a scaling matrix to be determined. Note that (4.4.4) fits this form where $\mathbf{S}_n^T = \left(\mathbf{Q}_{n2}^T\mathbf{Q}_{n1}\right)^{-1}\mathbf{Q}_{n2}^T\mathbf{V}_p$.

We can further reduce the dimension of the constraint by utilizing the null space of $\tilde{\phi}_y$. The projection of (4.3.17) into the range space of $\tilde{\phi}_y$ becomes (4.3.19), which is automatically satisfied if the measured data is displacement-consistent. The projection of (4.3.17) into the null space of $\tilde{\phi}_y$ yields

$$\mathbf{S}_n^T\mathbf{Q}_{n1} + \mathbf{Q}_{n1}^T\mathbf{S}_n - \mathbf{S}_n^T\tilde{\mathbf{\Xi}}\mathbf{S}_n = 0 \tag{4.4.7}$$

which would be satisfied if $\mathbf{S}_n = 0$. However, the cross-projection of (4.3.17) onto the range and null spaces of $\tilde{\phi}_y$ leads to

$$\mathbf{Q}_{r1}^T\left(\mathbf{V}_p\mathbf{Q}_{n1} + \mathbf{S}_n - \mathbf{V}_p\tilde{\mathbf{\Xi}}\mathbf{S}_n\right) = 0 \tag{4.4.8}$$

where $\mathbf{Q}_{r1} = null(\mathbf{Q}_{n1}^T)$ is the range space of $\tilde{\phi}_y$. Therefore, satisfying (4.4.8) generally requires a nontrivial solution for $\mathbf{S}_n$ if $\mathbf{Q}_{r1}^T\mathbf{V}_p\mathbf{Q}_{n1} \neq 0$. Once again, we note that all solutions to (4.4.8) can be written as

$$\mathbf{S}_n = \left(\mathbf{I} - \mathbf{V}_p\tilde{\mathbf{\Xi}}\right)^{-1}\left[\mathbf{Q}_{n1}\mathbf{S}_{nn} - \mathbf{V}_p\mathbf{Q}_{n1}\right] \tag{4.4.9}$$

Substituting (4.4.9) into (4.4.7) leads to a reduced-order quadratic matrix problem, viz.

$$\mathbf{S}_{nn}^T\mathbf{N}_1 + \mathbf{N}_1^T\mathbf{S}_{nn} - \mathbf{S}_{nn}^T\mathbf{N}_2\mathbf{S}_{nn} + \mathbf{R} = 0 \tag{4.4.10}$$

where

$$
\begin{aligned}
\mathbf{N}_1 &= \mathbf{Q}_{n1}^T \left(\mathbf{I} - \mathbf{V}_p \tilde{\mathbf{\Xi}}\right)^{-T} \left(\mathbf{Q}_{n1} - \tilde{\mathbf{\Xi}} \mathbf{S}_n^{(0)}\right) \\
\mathbf{N}_2 &= \mathbf{Q}_{n1}^T \left(\mathbf{I} - \mathbf{V}_p \tilde{\mathbf{\Xi}}\right)^{-T} \tilde{\mathbf{\Xi}} \left(\mathbf{I} - \mathbf{V}_p \tilde{\mathbf{\Xi}}\right)^{-1} \mathbf{Q}_{n1} \\
\mathbf{R} &= \mathbf{S}_n^{(0)^T} \mathbf{Q}_{n1} + \mathbf{Q}_{n1}^T \mathbf{S}_n^{(0)} - \mathbf{S}_n^{(0)^T} \tilde{\mathbf{\Xi}} \mathbf{S}_n^{(0)} \\
\mathbf{S}_n^{(0)} &= -\left(\mathbf{I} - \mathbf{V}_p \tilde{\mathbf{\Xi}}\right)^{-1} \mathbf{V}_p \mathbf{Q}_{n1}
\end{aligned}
\tag{4.4.11}
$$

Thus we must solve for a scaling matrix $\mathbf{S}_{nn}$ of dimension $(n - l)$, where n is the number of measured modes and l is the number of measured sensors. Although this problem is reduced in scale as compared to (4.3.17), it is still difficult to solve in a direct fashion.

4.4.3 Two-Stage Iterative SQP Procedure for $\mathbf{S}_{nn}$

A two-stage iterative procedure has been developed to seek a solution to (4.4.10). Utilizing the *Sequential Quadratic Programming* (SQP) [68] method to handle the nonlinearity introduced by the constraint, we project (4.4.10) onto the singular values of the residual matrix $\mathbf{R}$ and determine the projection of $\mathbf{S}_{nn}$, a vector, which satisfies the scalar constraint and minimizes the norm of the solution vector. The solution for $\mathbf{S}_{nn}$ is then incorporated into $\mathbf{S}_n$ using (4.4.9) and new matrices $\mathbf{N}_1$ and $\mathbf{R}$ are found using (4.4.11a) and (4.4.11c). The two-stage procedure concludes when the norm of the residual $\mathbf{R}$ is effectively zero. For the inner stage, we first project (4.4.10) onto the singular values of the residual matrix $\mathbf{R}$, viz.

$$
\mathbf{R} = \sum_{i=1}^{n-l} s_i \mathbf{p}_i \mathbf{p}_i^T, \qquad \mathbf{p}_i^T \mathbf{p}_i = 1, \qquad \mathbf{p}_i^T \mathbf{p}_j = 0 \tag{4.4.12}
$$

$$\left.\begin{aligned} \mathbf{x}_i^T\mathbf{b}_i + \mathbf{b}_i^T\mathbf{x}_i - \mathbf{x}_i^T\mathbf{N}_2\mathbf{x}_i + s_i &= 0 \\ \mathbf{x}_i &= \mathbf{S}_{nn}\mathbf{p}_i \\ \mathbf{b}_i &= \mathbf{N}_1\mathbf{p}_i \end{aligned}\right\} \tag{4.4.13}$$

Then, for $i = 1 \quad \text{to} \quad (n-l)$, we minimize $\|\mathbf{x}_i\|$ subject to (4.4.13). Given the nonlinearity of the constraint, we can apply the (SQP) method

$$\begin{aligned} \min_{\mathbf{x}_i,\lambda} \bar{J} &= \frac{1}{2}\mathbf{x}_i^T\mathbf{x}_i - \lambda\Phi_i \\ \Phi_i(\mathbf{x}_i) &= \mathbf{x}_i^T\mathbf{b}_i + \mathbf{b}_i^T\mathbf{x}_i - \mathbf{x}_i^T\mathbf{N}_2\mathbf{x}_i + s_i \end{aligned} \tag{4.4.14}$$

leading to the system of equations

$$\begin{bmatrix} \mathbf{W}^{(k)} & -\left(\frac{\delta\Phi_i^{(k)}}{\delta\mathbf{x}_i}\right)^T \\ -\left(\frac{\delta\Phi_i^{(k)}}{\delta\mathbf{x}_i}\right) & 0 \end{bmatrix} \begin{Bmatrix} \delta\mathbf{x}_i \\ \lambda^{(k)} \end{Bmatrix} = \begin{bmatrix} -\mathbf{x}_i^{(k)} \\ \Phi_i^{(k)} \end{bmatrix} \tag{4.4.15}$$

where

$$\begin{aligned} \mathbf{W}^{(k)} &= \mathbf{I} + 2\lambda^{(k)}\mathbf{N}_2 \\ \frac{\delta\Phi_i^{(k)}}{\delta\mathbf{x}_i} &= 2\left(\mathbf{b}_i - \mathbf{N}_2\mathbf{x}_i^{(k)}\right)^T \\ \Phi_i^{(k)} &= \Phi_i(\mathbf{x}_i^{(k)}) \\ \mathbf{x}_i^{(k+1)} &= \mathbf{x}_i^{(k)} + \delta\mathbf{x}_i \\ \mathbf{x}_i^{(0)} = 0 \qquad\qquad & \qquad\qquad \lambda^{(0)} = 0 \end{aligned} \tag{4.4.16}$$

Each solution $\mathbf{x}_i$ is then projected back to form $\mathbf{S}_{nn}$, viz.

$$\mathbf{S}_{nn} = \sum_{i=1}^{n-l} \mathbf{x}_i\mathbf{p}_i^T \tag{4.4.17}$$

The procedure given requires an outer iterative stage since, in determining the ith projection of the solution $\mathbf{x}_i$, we do not constrain the projection vectors $\mathbf{p}_i$ to remain orthogonal through the matrix equation (4.4.8). Hence,

after determining $\mathbf{S}_{nn}$ from (4.4.17) at outer iteration j, we incorporate the solution using (4.4.9) to determine

$$\mathbf{S}_n^{(j+1)} = \mathbf{S}_n^{(j)} + \left(\mathbf{I} - \mathbf{V}_p\tilde{\mathbf{\Xi}}\right)^{-1} \mathbf{Q}_{n1}\mathbf{S}_{nn}^{(j)} \tag{4.4.18}$$

and form new matrices $\mathbf{N}_1$ and $\mathbf{R}$ using $\mathbf{S}_n^{(j+1)}$. The outer iteration concludes when the norm of the residual $\mathbf{R}$ is within a specified bound ϵ.

4.5 Summary of Damping Correction Algorithm

4.5.1 Well-Determined Transformation Constraint

For the well-determined problem (when the number of independent sensors equals the number of modes):

Step 1 Determine the damped modal realization (see (2.3.25)) using an effective MIMO model estimation algorithm such as ERA or Polyreference.

Step 2 In the case of velocity or acceleration sensing, integrate once or twice (multiplying by $\mathbf{\Lambda}^{-1}$), respectively, to obtain the damped mode shape matrix $\mathbf{C}_z$. This allows the outputs to be treated as if they were measured displacements.

Step 3 Apply CBSI algorithm (see Chapter III) to determine the approximate normal modal parameter realization (4.3.1). $\tilde{\phi}_y$ and $\tilde{\epsilon}_y$ are given by partitions of the $\mathbf{C}_d$ matrix in the CBSI realization.

Step 4 Solve for $\mathbf{V}_d$ using (4.3.10).

Step 5 Compute Ψ in (4.3.4) using $\mathbf{V}_d$ and the CBSI-estimated modal parameters $\tilde{\mathbf{\Omega}}$ and $\tilde{\mathbf{\Xi}}$. Apply the basis transformation to the CBSI

model and determine a new generalized stiffness matrix $\mathbf{M}_{\xi}^{-1}\mathbf{K}_{\xi}$ from the partitions of the transformed $\mathbf{A}$ matrix as in (4.3.7).

Step 6 Determine the eigenvectors of the new generalized stiffness and apply as a transformation to determine the corrected normal modes basis as in (4.3.8)-(4.3.9).

4.5.2 Over-Determined Transformation Constraint

For the over-determined problem (when the number of independent sensors exceeds the number of modes):

Steps 1-3 from well-determined procedure

Step 4 Iterate using the procedure outline in (4.3.11). This is equivalent to iteratng on Steps 4-6 from well-determined procedure until $\|\mathbf{V}_d^{(k)}\| < \epsilon$.

4.5.3 Under-Determined Transformation Constraint

For the underdetermined problem (when the number of sensors is less than the number of identified modes):

Steps 1-2 from well-determined procedure

Step 3 Normalize the damped modes as in Chapter II, Section 2.3.3. Check the displacement consistency criterion (4.2.7) using the complex normalized modes $\mathbf{X}$.

Step 4 Apply the symmetric CBSI algorithm as in Chapter III, Section 3.4.3. $\tilde{\phi}_y$ and $\tilde{\epsilon}_y$ are given by partitions of the $\mathbf{C}$ matrix resulting from CBSI-SYM.

Step 5 Solve for $\mathbf{V}_p$ using a pseudoinverse solution (4.3.12) to the transformation constraint (4.3.6).

Step 6 Compute an addition to $\mathbf{V}_p$ in the null space of $\tilde{\phi}_y$ either directly as in Section 4.4.1 or iteratively as in Section 4.4.2.

Step 7 Complete procedure by computing $\mathbf{\Psi}$ as in steps 5-6 for the well-determined problem.

4.6 Numerical Examples for the UNDAMP Algorithm

4.6.1 3-DOF Spring-Mass System with Nonproportional Damping

The first example, is a 3 degree of freedom mass-spring system with nonproportional damping. The system equations of motion are given as

$$\begin{Bmatrix} \ddot{q}_1 \\ \ddot{q}_2 \\ \ddot{q}_3 \end{Bmatrix} + \begin{bmatrix} 2 & -.1 & -.1 \\ -.1 & .2 & -.1 \\ -.1 & -.1 & 1.1 \end{bmatrix} \begin{Bmatrix} \dot{q}_1 \\ \dot{q}_2 \\ \dot{q}_3 \end{Bmatrix} + \begin{bmatrix} 4 & -2 & 0 \\ -2 & 4 & -2 \\ 0 & -2 & 22 \end{bmatrix} \begin{Bmatrix} q_1 \\ q_2 \\ q_3 \end{Bmatrix} = \begin{bmatrix} 0 \\ u \\ 0 \end{bmatrix} \tag{4.6.1}$$

The resultant undamped modal parameters are then given as the eigenvalues and eigenvectors of the mass and stiffness matrices, viz.

$$\mathbf{\Omega} = \begin{bmatrix} 1.8980 & 0 & 0 \\ 0 & 5.8798 & 0 \\ 0 & 0 & 22.222 \end{bmatrix}$$
$$\mathbf{T} = \begin{bmatrix} 0.6875 & -0.7261 & -0.0121 \\ 0.7226 & 0.6824 & 0.1104 \\ 0.0719 & 0.0847 & -0.9938 \end{bmatrix} \tag{4.6.2}$$

and the nonproportionality of the damping can be verified by computation of the modal damping matrix, given as

$$\mathbf{T}^T \mathcal{D} \mathbf{T} = \begin{bmatrix} 0.9359 & -0.8991 & -0.0534 \\ -0.8991 & 1.2552 & 0.0562 \\ -0.0534 & 0.0562 & 1.1090 \end{bmatrix} \tag{4.6.3}$$

Applying the symmetric form of CBSI to the normalized damped modal realization of (4.6.1) yields

$$\begin{aligned}
\tilde{\mathbf{\Omega}} &= \begin{bmatrix} 2.5043 & 0 & 0 \\ 0 & 4.4578 & 0 \\ 0 & 0 & 22.2155 \end{bmatrix} \\
\tilde{\mathbf{\Xi}} &= \begin{bmatrix} 1.2281 & 0 & 0 \\ 0 & 0.9636 & 0 \\ 0 & 0 & 1.1083 \end{bmatrix} \\
\tilde{\phi}_y &= \begin{bmatrix} 0.9252 & 0.7416 & -0.0165 \\ 0.9025 & -0.8288 & 0.1109 \\ 0.0907 & -0.1071 & -0.9937 \end{bmatrix} \\
\tilde{\epsilon}_y &= \begin{bmatrix} -0.1769 & 0.3085 & 0.0039 \\ 0.2784 & 0.2180 & -0.0004 \\ 0.0376 & 0.0225 & -0.0001 \end{bmatrix}
\end{aligned} \tag{4.6.4}$$

Using (4.3.19), we can verify that the displacement consistency criteria is satisfied. Then, assuming 3 sensors measure q_1, q_2 and q_3, the unique solution of $\mathbf{V}_d$ from (4.3.10) is found to be

$$\mathbf{V}_d = \begin{bmatrix} 0.0418 & 0.2907 & 0.0020 \\ -0.2907 & 0.0533 & 0.0027 \\ -0.0027 & -0.0018 & 0.0000 \end{bmatrix} \tag{4.6.5}$$

Completing the correction procedure by forming $\mathbf{\Psi}$ from (4.3.4), the new modal parameters are equivalent to (4.6.2)-(4.6.3).

For the underdetermined case, if we assume that only q_1 and q_2 are measured degrees of freedom, the pseudoinverse solution can be determined from (4.3.12), viz.

$$\mathbf{V}_p = \begin{bmatrix} 0.0405 & 0.2902 & 0.0020 \\ -0.2884 & 0.0542 & 0.0027 \\ 0.0255 & 0.0094 & -0.0001 \end{bmatrix} \tag{4.6.6}$$

If we apply the direct method of augmented inputs (4.4.4), we obtain

$$\mathbf{V}_d = \begin{bmatrix} 0.0418 & 0.2907 & 0.0020 \\ -0.2907 & 0.0533 & 0.0027 \\ -0.0027 & -0.0018 & 0.0000 \end{bmatrix} \tag{4.6.7}$$

Thus, the correct undamped modal parameters and nondiagonal modal damping matrix will be determined by completing the correction procedure summarized in Section 4.5.3. Note that this correction was accomplished using sensors only at q_1 and q_2.

If we restrict the problem further by using only the output at q_2, we find the direct solution leads to either complex undamped mode shapes or modes with inconsistent coefficients for the collocated input and output, which is a physically-irrelevant property given the real nature of the physical parameters and the reciprocity of the underlying physical system. Instead, applying the iterative minimization approach, we obtain

$$\mathbf{V}_d = \begin{bmatrix} 0.0413 & 0.2882 & -0.0188 \\ -0.2878 & 0.0524 & -0.0199 \\ 0.0233 & 0.0123 & 0.0004 \end{bmatrix} \tag{4.6.8}$$

and the resultant modal parameters are

$$\begin{aligned} \mathbf{\Omega} &= \begin{bmatrix} 1.8911 & 0 & 0 \\ 0 & 5.7811 & 0 \\ 0 & 0 & 22.6849 \end{bmatrix} \\ \mathbf{T}_m &= \begin{bmatrix} 0.7185 & -0.6854 & 0.1185 \end{bmatrix} \\ \mathbf{\Xi} &= \begin{bmatrix} 0.9394 & 0.8643 & -0.5025 \\ 0.8643 & 1.2076 & -0.4212 \\ -0.5025 & -0.4212 & 1.1530 \end{bmatrix} \end{aligned} \tag{4.6.9}$$

where $\mathbf{T}_m$ are the corrected measured mode shapes. By inspection, the damping correction using only one sensor was partially successful. The accuracy of the eigenvalues and eigenvectors for the lowest 2 modes was improved over the CBSI estimate (4.6.4), but the highest mode mode was somewhat adversely affected. This is because, as the number of measurements becomes

relatively small as compared to the number of measured modes, we have progressively less mode shape phase quantities to guide the damping correction, and the minimization approach may not yield the best solution.

An improved result can be obtained, however, by restricting the number of modes which are coupled through the UNDAMP transformation. For example, examining the Modal Phase Collinearity (reviewed in Chapter III, Section 3.5, Table 3.2), it is only the first two modes which can improved to any practical degree through the UNDAMP method, as mode 3 is already effectively uncoupled in a normal modes sense from modes 1 and 2. Therefore, using only the subspace spanned by damped modes 1 and 2, $\mathbf{V}_d$ is given as

$$\mathbf{V}_d = \begin{bmatrix} 0.0417 & 0.2904 & 0 \\ -0.2904 & 0.0532 & 0 \\ 0 & 0 & 0 \end{bmatrix} \tag{4.6.10}$$

and the resultant modal parameters are

$$\begin{aligned} \mathbf{\Omega} &= \begin{bmatrix} 1.8998 & 0 & 0 \\ 0 & 5.8761 & 0 \\ 0 & 0 & 22.2155 \end{bmatrix} \\ \mathbf{T}_m &= \begin{bmatrix} 0.7230 & -0.6818 & 0.1109 \end{bmatrix} \\ \mathbf{\Xi} &= \begin{bmatrix} 0.9365 & 0.8978 & 0 \\ 0.8978 & 1.2552 & 0 \\ 0 & 0 & 1.1083 \end{bmatrix} \end{aligned} \tag{4.6.11}$$

which leads to both a better approximation of the first two modes while not altering the reasonable estimate of mode 3 already obtained using CBSI.

4.6.2 36-DOF Planar Truss with Light Nonproportional Damping

A second numerical example, previously shown in Figure 3.2, is of a 36 d.o.f. planar truss with nonproportional damping. Using 18 sensors, the CBSI-estimated modal parameters were successfully corrected. Table 4.1 compares various implementations of UNDAMP using both modal set selection and the underdetermined constraint methods. The "best" solution is obtained through selection of the 12 modes possessing the lowest MPC measures, although reasonable and improved estimates were obtain when even fewer modes were considered.

For the underdetermined solutions which result from correcting the full space of modes, both the minimization and augmentation methods were applied, with the minimization approach yielding reasonable and improved modal estimates, while the augmentation approach lead to significant and unreasonable changes in the physical properties throughout the modal spectrum. Figure 4.1 illustrates how the iterative SQP-based minimization algorithm for the under-determined solution operates. In the minimization solution for correcting all 36 modes, the minimization procedure operated on a subspace of dimension 18 (36 modes minus 18 sensors) and drove the singular values of the quadratic constraint violation to within a specified tolerance in 2 iterations. Figure 4.2 shows the resultant nondiagonal modal damping matrix for the 12-mode overdetermined solution. The assumed proportional modal damping of the CBSI procedure has now been altered to accommodate the mode shape phase components originally expressed by the $\tilde{\epsilon}_y$ array. Figure 4.3 shows a comparison of the mode shapes for mode 27, which possessed the lowest phase collinearity.

Table 4.1

Comparison of Modal Assurance Criteria for Normal Modes Estimates Using the UNDAMP Algorithm on a 36-DOF Nonproportionally Damped Planar Truss

Mode Number	CBSI SYM	2 Modes O-D	12 Modes O-D	18 Modes W-D	28 Modes U-D Min	36 Modes U-D Aug	36 Modes UD Min
6	1.0000	1.0000	1.0000	1.0000	1.0000	0.7524	1.0000
7	1.0000	1.0000	1.0000	1.0000	1.0000	0.7134	1.0000
16	0.9995	0.9995	0.9998	0.9865	1.0000	1.0000	0.9994
17	0.9994	0.9994	0.9998	0.9937	1.0000	0.9995	0.9993
19	0.9986	0.9986	0.9993	0.9998	0.9999	0.9986	0.9994
20	0.9994	0.9994	1.0000	0.9999	1.0000	0.9982	0.9997
22	0.9444	0.9444	0.9996	0.7571	0.9964	0.8069	0.9947
23	0.9410	0.9410	0.9997	0.7451	0.9961	0.8050	0.9945
25	0.9999	0.9999	1.0000	0.0749	0.9995	0.0004	0.9992
26	0.9980	0.9980	1.0000	0.1055	0.9832	0.0027	0.9814
27	0.9241	0.9917	0.9999	0.9660	0.9822	0.4983	0.9786
28	0.9299	0.9957	0.9999	0.9849	0.9955	0.0491	0.9696
29	0.9986	0.9986	1.0000	0.9956	0.9946	0.0780	0.9697
30	1.0000	1.0000	1.0000	0.9969	1.0000	0.0041	1.0000
31	1.0000	1.0000	1.0000	0.9979	1.0000	0.2082	1.0000
32	1.0000	1.0000	1.0000	1.0000	0.9999	0.0008	1.0000
34	1.0000	1.0000	1.0000	1.0000	1.0000	0.7998	0.9999

O-D: Over-determined solution
W-D: Well-determined solution
U-D: Under-determined solution
Aug: Method of Augmented Outputs
Min: Iterative Minimization Method

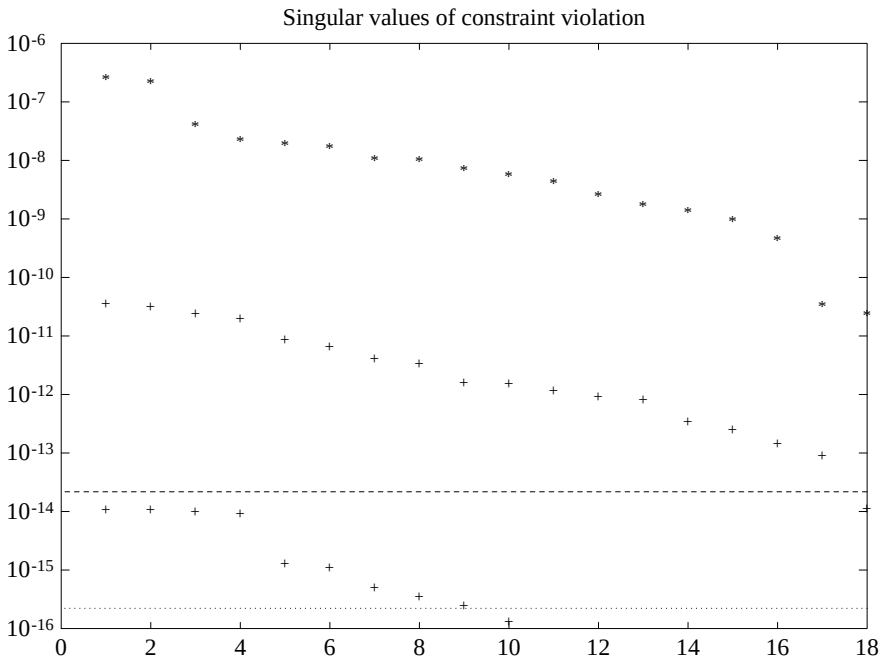

Figure 4.1: Example of Reduction in Quadratic Constraint Violation using the Iterative SQP-based Minimization Method for Underdetermined UNDAMP Problems

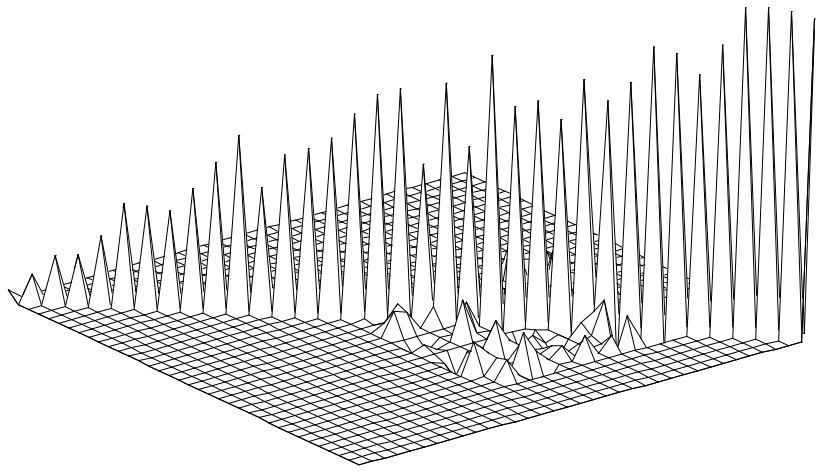

Figure 4.2: UNDAMP-derived Nondiagonal Damping Matrix for Nonproportionally Damped Planar Truss Problem

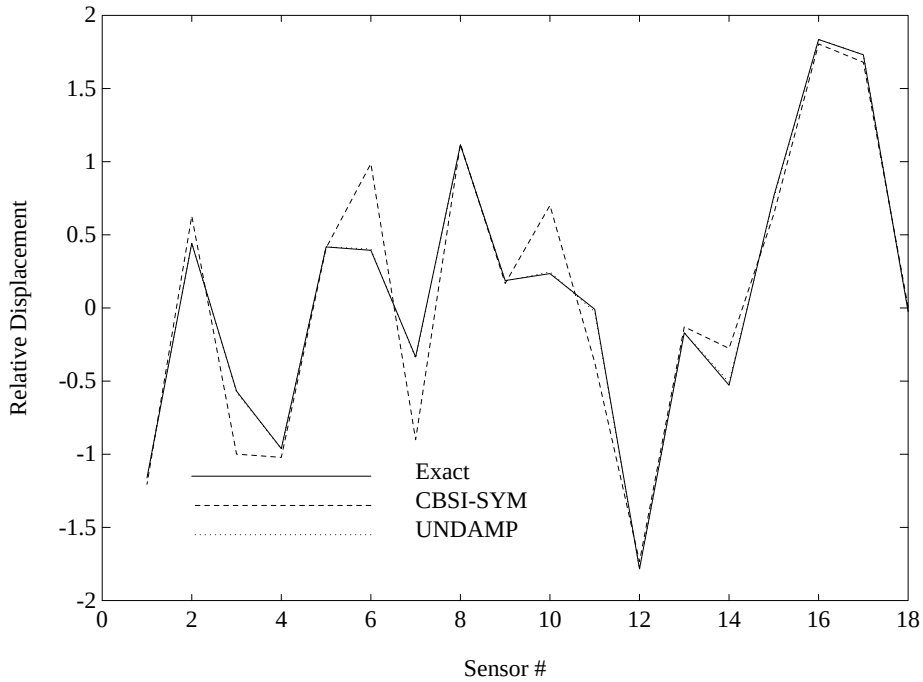

Figure 4.3: Improvement in Estimated Normal Mode Shape Using UNDAMP Corrective Transformation to the CBSI-derived Realization of the Planar Truss Problem

4.7 Concluding Remarks

A general damping correction procedure, termed UNDAMP, for determining the undamped modal properties from damped system realization parameters has been presented. The present procedure begins with the assumption that the system may be proportionally-damped and obtains estimated normal modes via the CBSI algorithm. If the displacement and velocity modes are different, the damping correction procedure is invoked to extract the normal modes and associated nonproportional damping matrix. This corrective transformation can be carried out in two distinct ways. If the number of sensors are at least equal to the number of identified modes, the direct transformation can be obtained by solving a linear constraint equation. If the number of sensors are less than the number of identified modes, the

linear constraint is underdetermined and the transformation must be determined either directly or iteratively such that a quadratic matrix consistency criterion is satisfied. The present damping correction procedure has been demonstrated through numerical examples.

CHAPTER V

MINIMAL-ORDER MASS AND STIFFNESS DETERMINATION

5.1 Introduction

The primary objective of modal testing of structures is to validate the homogeneous form of the governing linear differential equations of motion in terms of the dominant undamped modes of vibration. Naturally, there is only a finite number of points on the structure for which data can be collected, and these points are generally a small subset of the total degrees of freedom (d.o.f.) employed in the finite element modeling of the structure. In fact, the number of measurement points may also be typically small compared to the number of vibrational modes identified in the test, especially when utilizing modern instrumentation with high sampling rates and powerful, inexpensive scientific workstations for data analysis. Therefore, if l sensors are used to identify modal data for n modes, where $n > l$, there is not a unique model of the classical mass/stiffness form with physical d.o.f. which possesses order-n dynamics given only l spatial measurement points.

Much research in recent years has focused on methods for correlation or reconciliation of finite element models which inherently possess very large order dynamics to the limited sensor and frequency data obtained from modal testing. The primary advantage of this approach is that we can relate measured data back to physical design parameters of the system, resulting

in a model which not only possesses the observed modal characteristics, but will predict internal stress levels and sensitivity to further design changes as well. The drawback, however, is that these models must retain far higher numbers of degrees of freedom than can be correlated in test, and it is exactly the high-order localized uncorrelated behavior which is influential in specific model predictions such as stress distribution. Thus, while these models may be superior in most ways to unverified finite element models, there can be a tendency to trust their behavior in all cases when only their low-frequency global characteristics have been correlated.

An alternative approach is to directly calculate mass and stiffness from the modal parameters identified by test. The resulting matrices will then express only the behavior measured and not interpolate further degrees of complexity. This is sometimes referred to as the *inverse vibration problem* (IVP). The primary goal of the present paper is to investigate solutions to the IVP when the number of sensors l is less than the number of identified modes n. We will show that mass and stiffness matrices of dimension l, referring to the measured d.o.f., can be found from the n identified modes. These matrices are effectively reduced properties of the system, condensing n modal d.o.f. into l physical d.o.f., and the reduced matrices are directly related to classical model reduction, namely the so-called Guyan method.

One serious drawback of the reduced physical matrices is that they condense the identified dynamics from test into a smaller dimensional space. Thus, the measured eigenvalues and eigenvectors are not preserved by the resultant mass and stiffness matrices, and the model defined by the reduced matrices is not equivalent to the test in terms of the measured transfer functions. To address this issue, we endeavor to derive mass and stiffness matrices

which possess both the physical nature of the previous reduced parameters and yet preserve the full eigenspectrum as measured in test. If the mass and stiffness are determined strictly from test, as opposed to the common problem of large-order finite element model correlation, then the resultant matrices will be of *minimum order* to express the identified modes. In fact, these minimum-order coefficients for the second-order structural dynamic equations will, when cast into state space form, lead to a realization of the system transfer functions fully equivalent to the system realization used to derive the modal data.

The coordinate set chosen for the derivation of minimal-order mass and stiffness consists of the measured physical d.o.f. augmented by a set of generalized d.o.f which are specifically modal coordinates of the residual dynamics. The residual dynamic matrix is the difference between the measured modes and the projection of the reduced stiffness through the measured mode shapes. A singular value decomposition of the residual dynamic matrix is then used to determine the rank deficiency of the reduced stiffness, and a minimum order augmentation of the mode shapes using the orthonormal vectors of the singular values is performed to find the new minimal-order stiffness and mass matrices. Finally, the augmented portions of the new stiffness and mass matrices are diagonalized such that the augmented d.o.f. possess the desired modal orientation for the residual dynamics. This method of representation is similar to the the Craig-Bampton component mode synthesis (CMS) method for finite element models, which is popular among spacecraft dynamicists.

5.2 Reduced Mass and Stiffness from Normal Modal Parameters

Recent work in the area of structural identification has included the determination of mass and stiffness matrices directly from continuous time system realizations [37]. A major drawback to this approach, however, is that it requires the dimension of the physical model to be equivalent to the number of second-order states, implying that the number of independent sensors measured are equal to the number of identified modes. A more practical approach is to enrich the computed mass and stiffness matrices with the complete set of measured modes, independent of the number of sensors. This allows the resulting mass and stiffness to express contributions of all the modes observable from the available sensors. We begin by developing the concept of reduced mass and stiffness matrices, which are defined with respect to only the sensor DOF.

If we partition the DOF of a large-order structural dynamics model such as those obtained from finite element discretization into sets m and i, we have

$$\begin{aligned}\begin{bmatrix} \mathbf{M}_{mm} & \mathbf{M}_{mi} \\ \mathbf{M}_{mi}^T & \mathbf{M}_{ii} \end{bmatrix} \begin{Bmatrix} \ddot{\mathbf{q}}_m(t) \\ \ddot{\mathbf{q}}_i(t) \end{Bmatrix} + \begin{bmatrix} \mathcal{D}_{mm} & \mathcal{D}_{mi} \\ \mathcal{D}_{mi}^T & \mathcal{D}_{ii} \end{bmatrix} \begin{Bmatrix} \dot{\mathbf{q}}_m(t) \\ \dot{\mathbf{q}}_i(t) \end{Bmatrix} \\ + \begin{bmatrix} \mathbf{K}_{mm} & \mathbf{K}_{mi} \\ \mathbf{K}_{mi}^T & \mathbf{K}_{ii} \end{bmatrix} \begin{Bmatrix} \mathbf{q}_m(t) \\ \mathbf{q}_i(t) \end{Bmatrix} = \begin{bmatrix} \hat{\mathbf{B}}_m \\ \hat{\mathbf{B}}_i \end{bmatrix} \mathbf{u}(t)\end{aligned} \tag{5.2.1}$$

Here we can interpret the DOF sets m and i as the measured and unmeasured DOF from the experimental data. Then solving the static equations where no forces are applied to the $\mathbf{q}_i$ equations ($\hat{\mathbf{B}}_i\mathbf{u}(t) = 0$), we have

$$\mathbf{q}_i = -\mathbf{K}_{ii}^{-1}\mathbf{K}_{mi}^T\mathbf{q}_m \tag{5.2.2}$$

and a variable reduction operator is given as

$$\mathbf{q} = \begin{bmatrix} \mathbf{I} \\ -\mathbf{K}_{ii}^{-1}\mathbf{K}_{mi}^{T} \end{bmatrix} \mathbf{q}_m = \mathbf{\Phi}_c \mathbf{q}_m \tag{5.2.3}$$

In *component mode synthesis* (CMS) theory, $\mathbf{\Phi}_c$ are often termed the *constraint modes*, as they represent the displacement vectors of the internal degrees of freedom $\mathbf{q}_i$ with respect to the constraint modes, defined as the set of orthogonal unit displacements of the retained degrees of freedom $\mathbf{q}_m$. Applying the transformation (5.2.3) to $\mathbf{K}$, $\mathcal{D}$, and $\mathbf{M}$ in (5.2.1), the so-called *Guyan* reduced stiffness, damping, and mass are

$$\begin{aligned} \bar{\mathbf{K}} &= \mathbf{\Phi}_c^T \mathbf{K} \mathbf{\Phi}_c = \mathbf{K}_{mm} - \mathbf{K}_{mi}\mathbf{K}_{ii}^{-1}\mathbf{K}_{mi}^{T} \\ \bar{\mathcal{D}} &= \mathbf{\Phi}_c^T \mathcal{D} \mathbf{\Phi}_c \qquad \bar{\mathbf{M}} = \mathbf{\Phi}_c^T \mathbf{M} \mathbf{\Phi}_c \end{aligned} \tag{5.2.4}$$

The resultant model clearly no longer possesses the large order dynamics of $\mathbf{K}$ and $\mathbf{M}$, but preserves the general behavior of the larger eigenproblem for the lowest modes and modes which are strongly influenced by the retained degrees of freedom. In fact, this procedure is exactly correct for static analysis under the aforementioned assumptions, and for dynamic analysis in which the mass associated with the internal degrees of freedom is negligible. We further note that the Guyan reduction concept is really the idea of applying the static constraint modes transformation $\mathbf{\Phi}_c$ to reduce the mass and damping matrices, as the concept of static condensation of the stiffness was employed previously in static matrix structural analysis.

We now wish to show an alternative representation of the Guyan reduction in terms of the normal modes of the full-order system. We begin by assuming that the measured modes from test completely span the dynamics

of (5.2.1), such that the model representation in modal coordinates is a completely equivalent realization. Recalling (2.1.2)-(2.1.3), the corresponding normal modal equations of motion of (5.2.1) are given as

$$\ddot{\eta}(t) + \mathbf{\Xi}\dot{\eta}(t) + \mathbf{\Omega}\eta(t) = \mathbf{\Phi}_n^T \hat{\mathbf{B}}\mathbf{u}(t) \tag{5.2.5}$$

where $\mathbf{\Phi}_n$ are the mass-orthonormalized eigenvectors for the generalized undamped eigenproblem

$$\mathbf{K}\mathbf{\Phi}_n = \mathbf{M}\mathbf{\Phi}_n\mathbf{\Omega}$$

where

$$\begin{aligned} \mathbf{\Phi}_n^T\mathbf{M}\mathbf{\Phi}_n &= \mathbf{I} \\ \mathbf{\Phi}_n^T\mathbf{K}\mathbf{\Phi}_n &= \mathbf{\Omega} \\ \mathbf{\Phi}_n^T\mathcal{D}\mathbf{\Phi}_n &= \mathbf{\Xi} \end{aligned} \tag{5.2.6}$$

If we express the physical degrees of freedom $\mathbf{q}(t)$ in terms of the normal modal variables $\eta(t)$, we have the transformation

$$\mathbf{q}(t) = \mathbf{\Phi}_n\eta(t) = \begin{bmatrix} \phi_m \\ \phi_i \end{bmatrix} \eta(t) \tag{5.2.7}$$

where ϕ_m, ϕ_i are partitions of the eigenvectors at the measured and unmeasured (i.e. internal) degrees of freedom, respectively. Using (5.2.6) and assuming no rigid-body modes such that $\mathbf{\Omega}$ is nonsingular, the inverse vibration problem can be solved as

$$\begin{aligned} \mathbf{K}^{-1} &= \mathbf{\Phi}_n\mathbf{\Omega}^{-1}\mathbf{\Phi}_n^T \\ \mathbf{M}^{-1} &= \mathbf{\Phi}_n\mathbf{\Phi}_n^T \end{aligned} \tag{5.2.8}$$

Using the partitions of $\mathbf{K}$ as in (5.2.1), the inverse of $\mathbf{K}$ can be written symbolically as

$$\mathbf{K}^{-1} = \begin{bmatrix} \bar{\mathbf{K}}^{-1} & -\bar{\mathbf{K}}^{-1}\mathbf{K}_{mi}\mathbf{K}_{ii}^{-1} \\ -\mathbf{K}_{ii}^{-1}\mathbf{K}_{mi}^T\bar{\mathbf{K}}^{-1} & \mathbf{K}_{ii}^{-1}\left(\mathbf{I} + \mathbf{K}_{mi}^T\bar{\mathbf{K}}^{-1}\mathbf{K}_{mi}\mathbf{K}_{ii}^{-1}\right) \end{bmatrix} \tag{5.2.9}$$

where $\bar{\mathbf{K}}$ is the *Schur complement* of $\mathbf{K}_{ii}$ in $\mathbf{K}$ and is equivalent to the statically-condensed stiffness as given in (5.2.4). Furthermore, using the partitions of $\mathbf{\Phi}_n$ in (5.2.7) together with (5.2.8), we have

$$\mathbf{K}^{-1} = \begin{bmatrix} \phi_m \mathbf{\Omega}^{-1} \phi_m^T & \phi_m \mathbf{\Omega}^{-1} \phi_i^T \\ \phi_i \mathbf{\Omega}^{-1} \phi_m^T & \phi_i \mathbf{\Omega}^{-1} \phi_i^T \end{bmatrix} \tag{5.2.10}$$

Thus, comparing (5.2.9) and (5.2.10), the Guyan-reduced stiffness matrix with respect to the measured test degrees of freedom is found as

$$\bar{\mathbf{K}} = [\, \phi_m \mathbf{\Omega}^{-1} \phi_m^T \,]^{-1} \tag{5.2.11}$$

In order to determine the reduced mass, a slightly different calculation is required, as from (5.2.4) $\bar{\mathbf{M}}$ has combinations of mass and stiffness. We write the full-order mass $\mathbf{M}$ as

$$\mathbf{M} = \mathbf{K}\mathbf{K}^{-1}\mathbf{M}\mathbf{K}^{-1}\mathbf{K}$$

Then, expressing $\mathbf{K}^{-1}$ in modal terms from (5.2.8), grouping terms and applying the Guyan constraint mode transformation to both sides, we have

$$\begin{aligned} \mathbf{M} &= \mathbf{K}\mathbf{\Phi}_n \mathbf{\Omega}^{-1} \left(\mathbf{\Phi}_n^T \mathbf{M} \mathbf{\Phi}_n \right) \mathbf{\Omega}^{-1} \mathbf{\Phi}_n^T \mathbf{K} \\ &= \mathbf{K}\mathbf{\Phi}_n \mathbf{\Omega}^{-2} \mathbf{\Phi}_n^T \mathbf{K} \\ \bar{\mathbf{M}} &= \mathbf{\Phi}_c^T \mathbf{M} \mathbf{\Phi}_c = \mathbf{\Phi}_c^T \mathbf{K} \mathbf{\Phi}_n \mathbf{\Omega}^{-2} \mathbf{\Phi}_n^T \mathbf{K} \mathbf{\Phi}_c \end{aligned} \tag{5.2.12}$$

Noting that

$$\mathbf{K}\mathbf{\Phi}_c = \begin{bmatrix} \mathbf{K}_{mm} & \mathbf{K}_{mi} \\ \mathbf{K}_{mi}^T & \mathbf{K}_{ii} \end{bmatrix} \begin{bmatrix} \mathbf{I} \\ -\mathbf{K}_{ii}^{-1}\mathbf{K}_{mi}^T \end{bmatrix} = \begin{bmatrix} \bar{\mathbf{K}} \\ 0 \end{bmatrix}$$

the Guyan-reduced mass matrix is given as

$$\begin{aligned} \bar{\mathbf{M}} &= [\, \bar{\mathbf{K}} \quad 0 \,] \begin{bmatrix} \phi_m \\ \phi_i \end{bmatrix} \mathbf{\Omega}^{-2} [\, \phi_m^T \quad \phi_i^T \,] \begin{bmatrix} \bar{\mathbf{K}} \\ 0 \end{bmatrix} \\ \bar{\mathbf{M}} &= \bar{\mathbf{K}} \phi_m \mathbf{\Omega}^{-2} \phi_m^T \bar{\mathbf{K}} \end{aligned} \tag{5.2.13}$$

Therefore, $\bar{\mathbf{M}}$ as calculated in (5.2.13) possesses the qualities of the statically-condensed mass as opposed to $(\phi_m \phi_m^T)^{-1}$, which gives just the Schur complement of $\mathbf{M}_{ii}$ in $\mathbf{M}$. Note that when ϕ_m spans the modes completely (ϕ_m nonsingular, number of sensors equal to number of modes), (5.2.13) simplifies to

$$\begin{aligned} \bar{\mathbf{M}} &= \phi_m^{-T} \mathbf{\Omega} \phi_m^{-1} \phi_m \mathbf{\Omega}^{-2} \phi_m^T \phi_m^{-T} \mathbf{\Omega} \phi_m^{-1} \\ &= \phi_m^{-T} \phi_m^{-1} = (\phi_m \phi_m^T)^{-1} \end{aligned} \tag{5.2.14}$$

which is consistent with (5.2.8), since having a full space of sensors implies that $\phi_m = \mathbf{\Phi}_n$. Similarly, we can find the Guyan-reduced damping matrix $\bar{\mathcal{D}}$ as

$$\bar{\mathcal{D}} = \bar{\mathbf{K}} \phi_m \mathbf{\Omega}^{-1} \mathbf{\Xi} \mathbf{\Omega}^{-1} \phi_m^T \bar{\mathbf{K}} \tag{5.2.15}$$

Thus, the reduced system matrices given by (5.2.11), (5.2.13) and (5.2.15) are theoretically consistent with the Guyan reduction in the limit as the full eigen spectrum of (5.2.1) is measured. In addition, they are a function only of the partition of the mode shapes at the measured locations, and thus can be directly calculated from the measured test data.

Finally, the reduced stiffness $\bar{\mathcal{K}}$ is also an expression of the mobility curve-based stiffness parameters, the so-called system receptance. From (2.1.6), the frequency domain transfer function matrix $\mathcal{H}(\omega)$, where $\mathbf{y}(\omega) = \mathcal{H}(\omega)\mathbf{u}(\omega)$, is given for displacement sensing by

$$\mathcal{H}(\omega) = \mathbf{H}_d \left(\mathbf{K} + i\omega \mathcal{D} - \omega^2 \mathbf{M} \right)^{-1} \hat{\mathbf{B}} \tag{5.2.16}$$

Then, assuming actuators sensors at physical DOF $\mathbf{q}_m$, the receptance is found by the asymptotic limit of $\mathcal{H}(\omega)$ as $\omega \to 0$, viz.

$$\lim_{\omega \to 0} \mathcal{H}(\omega) = \mathbf{H}_d \mathbf{K}^{-1} \mathbf{H}_d^T = \bar{\mathbf{K}}^{-1} \tag{5.2.17}$$

We note here that $\bar{\mathbf{K}}$ is determined from the modes of the identified model which is generally a curve fit of much smaller dimension than is required to match the transfer function exactly. Thus, $\bar{\mathbf{K}}$ expresses the receptance of the approximate model, rather than the test-measured transfer function matrix.

5.3 Minimum-Order Mass and Stiffness from Normal Modal Parameters

As noted in the introduction, we base our method for a minimum-order equivalent mass and stiffness from test on the Craig-Bampton component mode synthesis method, which itself is related to the statically-condensed mass and stiffness of the Guyan reduction. Thus, we will use the method of determining the Guyan reduction from measured modes as reviewed in the preceding section to develop the equivalent minimum-order method. To begin, however, let us review the Craig-Bampton CMS method as applied to the finite element method. Recalling (5.2.2), in the Craig-Bampton method we represent $\mathbf{q}_i$ as

$$\mathbf{q}_i = -\mathbf{K}_{ii}^{-1}\mathbf{K}_{mi}^T\mathbf{q}_m + \mathbf{T}_\xi \xi \tag{5.3.1}$$

where ξ are augmented generalized degrees of freedom and $\mathbf{T}_\xi$ are the displacements of $\mathbf{q}_i$ with respect to unit displacements of ξ. Thus, the variable transformation is given as

$$\mathbf{q} = \begin{bmatrix} \mathbf{I} & 0 \\ -\mathbf{K}_{ii}^{-1}\mathbf{K}_{mi}^T & \mathbf{T}_\xi \end{bmatrix} \begin{Bmatrix} \mathbf{q}_m \\ \xi \end{Bmatrix} = \mathbf{T} \begin{Bmatrix} \mathbf{q}_m \\ \xi \end{Bmatrix} \tag{5.3.2}$$

and applying this to $\mathbf{K}$ gives

$$\hat{\mathbf{K}} = \mathbf{T}^T\mathbf{K}\mathbf{T} = \begin{bmatrix} \bar{\mathbf{K}} & 0 \\ 0 & \mathbf{T}_\xi^T\mathbf{K}_{ii}\mathbf{T}_\xi \end{bmatrix} \tag{5.3.3}$$

Thus, $\hat{\mathbf{K}}$ is block-diagonal, composed of the Guyan reduced stiffness and a residual symmetrical stiffness matrix. Note that we have not yet defined ξ as the modal coordinates of the residual structure; the form of $\hat{\mathbf{K}}$ is a consequence of (5.3.2), which basically defines ξ as a subspace orthogonal to $\mathbf{q}_m$ through $\mathbf{K}$. To uniquely define the direction of ξ, it is specified that $\mathbf{T}_\xi$ are the orthonormal eigenvectors of the generalized eigenproblem

$$\mathbf{K}_{ii}\mathbf{T}_\xi = \mathbf{M}_{ii}\mathbf{T}_\xi\mathbf{\Omega}_r$$

such that

$$\begin{aligned} \mathbf{T}_\xi^T\mathbf{K}_{ii}\mathbf{T}_\xi &= \mathbf{\Omega}_r \\ \mathbf{T}_\xi^T\mathbf{M}_{ii}\mathbf{T}_\xi &= \mathbf{I} \end{aligned} \tag{5.3.4}$$

Using (5.3.4) to fully define $\mathbf{T}_\xi$, the Craig-Bampton stiffness and mass matrices are given by

$$\begin{aligned} \hat{\mathbf{K}} &= \mathbf{T}^T\mathbf{K}\mathbf{T} = \begin{bmatrix} \bar{\mathbf{K}} & 0 \\ 0 & \mathbf{\Omega}_r \end{bmatrix} \\ \hat{\mathbf{M}} &= \mathbf{T}^T\mathbf{M}\mathbf{T} = \begin{bmatrix} \bar{\mathbf{M}} & \mathbf{M}_c \\ \mathbf{M}_c^T & \mathbf{I} \end{bmatrix} \end{aligned} \tag{5.3.5}$$

where

$$\mathbf{M}_c = \mathbf{M}_{mi}\mathbf{\Phi}_r - \mathbf{K}_{mi}\mathbf{K}_{ii}^{-1}\mathbf{M}_{ii}\mathbf{\Phi}_r \tag{5.3.6}$$

is a mass coupling between $\mathbf{q}_m$ and ξ and $\bar{\mathbf{M}}$ is the Guyan-reduced mass given by (5.2.12).

Starting from $\bar{\mathbf{K}}$, we can construct $\hat{\mathbf{K}}$ and $\hat{\mathbf{M}}$ from the measured modal test parameters ϕ_m and $\mathbf{\Omega}$ as follows. Partition the eigenvectors of $\hat{\mathbf{K}}$ and $\hat{\mathbf{M}}$ as

$$\begin{bmatrix} \bar{\mathbf{K}} & 0 \\ 0 & \mathbf{\Omega}_r \end{bmatrix} \begin{bmatrix} \phi_m \\ \phi_r \end{bmatrix} = \hat{\mathbf{M}} \begin{bmatrix} \phi_m \\ \phi_r \end{bmatrix} \mathbf{\Omega} \tag{5.3.7}$$

normalized such that

$$[\,\phi_m^T \quad \phi_r^T\,]\begin{bmatrix}\bar{\mathbf{K}} & 0\\ 0 & \mathbf{\Omega}_r\end{bmatrix}\begin{bmatrix}\phi_m\\ \phi_r\end{bmatrix} = \mathbf{\Omega} \tag{5.3.8}$$

Here, ϕ_r are the partition of the eigenvectors of $\hat{\mathbf{K}}$ and $\hat{\mathbf{M}}$ relating the augmented variables ξ to the normal modal variables of the global system η. Although ϕ_r and $\mathbf{\Omega}_r$ are unknowns, together they form a dynamic residual matrix $\Delta\mathbf{\Omega}$ which can be computed by the test-measured quantities ϕ_m, $\mathbf{\Omega}$ and $\bar{\mathbf{K}}$, viz.

$$\phi_r^T\mathbf{\Omega}_r\phi_r = \mathbf{\Omega} - \phi_m^T\bar{\mathbf{K}}\phi_m = \Delta\mathbf{\Omega} \tag{5.3.9}$$

Since $\bar{\mathbf{K}}$ is computed by (5.2.11), $\Delta\mathbf{\Omega}$ is a function solely of ϕ_m and $\mathbf{\Omega}$.

The required minimal rank augmentation of $\mathbf{q}_m$ is determined through the dynamic residual matrix $\Delta\mathbf{\Omega}$. In order to find the rank of $\mathbf{\Omega}_r$ and a vector basis for ϕ_r, we utilize a singular value decomposition of $\Delta\mathbf{\Omega}$, viz.

$$\mathbf{PSP}^T = svd\,(\Delta\mathbf{\Omega})$$

Examination of the singular values clearly indicates the required dimension of the augmented coordinates ξ. For example, with l independent spatial measurements, $\phi_m^T\bar{\mathbf{K}}\phi_m$ will be typically be of rank l, while $\mathbf{\Omega}$ is rank n, and $\phi_r^T\mathbf{\Omega}_r\phi_r$ is rank $(n-l)$. Therefore, the SVD should determine $(n-l)$ non-zero singular values for $\Delta\mathbf{\Omega}$. It is possible, however, for the reduced matrix to exhibit some rank deficiency (for example if flexibility mode contributions to $\bar{\mathbf{K}}$ are rank-updated to account for rigid-body modes), and so a rigorous approach is fully examine the singular values of $\Delta\mathbf{\Omega}$ to determine the correct rank p,

$$\Delta\mathbf{\Omega} = \mathbf{PSP}^T = \mathbf{P}_p\mathbf{S}_p\mathbf{P}_p^T \tag{5.3.10}$$

Having determined an basis $\mathbf{P}_p$ for the p augmented coordinates, we now augment ϕ_m by the rows of $\mathbf{P}_p^T$ which span the singular values, and solve the general inverse vibration problem:

$$\begin{aligned} \begin{bmatrix} \bar{\mathbf{K}} & 0 \\ 0 & \mathbf{K}_r \end{bmatrix} &= \begin{bmatrix} \phi_m \\ \mathbf{P}_p^T \end{bmatrix}^{-T} \mathbf{\Omega} \begin{bmatrix} \phi_m \\ \mathbf{P}_p^T \end{bmatrix}^{-1} \\ \begin{bmatrix} \bar{\mathbf{M}} & \tilde{\mathbf{M}}_c \\ \tilde{\mathbf{M}}_c^T & \mathbf{M}_r \end{bmatrix} &= \left[\begin{bmatrix} \phi_m \\ \mathbf{P}_p^T \end{bmatrix} [\, \phi_m^T \quad \mathbf{P}_p \,] \right]^{-1} \end{aligned} \tag{5.3.11}$$

Finally, the augmented d.o.f. are orthonormalized for consistency with the definition of ξ by solving the generalized eigenproblem

$$\begin{aligned} \mathbf{K}_r\mathbf{U} &= \mathbf{M}_r\mathbf{U}\mathbf{\Omega}_r \\ \mathbf{U}^T\mathbf{K}_r\mathbf{U} &= \mathbf{\Omega}_r \\ \mathbf{U}^T\mathbf{M}_r\mathbf{U} &= \mathbf{I} \end{aligned} \tag{5.3.12}$$

and performing a final transformation on the mass and stiffness matrices

$$\begin{aligned} \hat{\mathbf{K}} &= \begin{bmatrix} \mathbf{I} & 0 \\ 0 & \mathbf{U}^T \end{bmatrix} \begin{bmatrix} \bar{\mathbf{K}} & 0 \\ 0 & \mathbf{K}_r \end{bmatrix} \begin{bmatrix} \mathbf{I} & 0 \\ 0 & \mathbf{U} \end{bmatrix} = \begin{bmatrix} \bar{\mathbf{K}} & 0 \\ 0 & \mathbf{\Omega}_r \end{bmatrix} \\ \hat{\mathbf{M}} &= \begin{bmatrix} \mathbf{I} & 0 \\ 0 & \mathbf{U}^T \end{bmatrix} \begin{bmatrix} \bar{\mathbf{M}} & \tilde{\mathbf{M}}_c \\ \tilde{\mathbf{M}}_c^T & \mathbf{M}_r \end{bmatrix} \begin{bmatrix} \mathbf{I} & 0 \\ 0 & \mathbf{U} \end{bmatrix} = \begin{bmatrix} \bar{\mathbf{M}} & \mathbf{M}_c \\ \mathbf{M}_c^T & \mathbf{I} \end{bmatrix} \end{aligned} \tag{5.3.13}$$

Thus, in a mathematical sense, $\hat{\mathbf{K}}$ and $\hat{\mathbf{M}}$ are an equivalent measure of the normal mode parameters as observed from the physical DOF $\mathbf{q}_m$. Furthermore, this realization is unique from its definition in terms of the modal parameters of the system. This implies that, in an asymptotic sense, both the Guyan-reduced properties and the Craig-Bampton representation of (5.2.1) are intrinsic parameters of the physical system independent of the particular finite element representation. It is this intrinsic characteristic that we exploit for the derivation of augmented mass and stiffness matrices. Note also that the definition of $\hat{\mathbf{K}}$ and $\hat{\mathbf{M}}$ include as special cases both the modal model $[\mathbf{\Omega}, \mathbf{I}]$ and the physical model $[\mathbf{K}, \mathbf{M}]$ in the limits as the number of measured DOF varies from 0 to n.

5.4 Numerical Examples

5.4.1 3-DOF Undamped Spring-Mass System

In order to illustrate the mass and stiffness derivation methods presented in the preceding sections, the first example involves a simple undamped 3-DOF spring-mass system as shown in Figure 3.1. The undamped equations of motion are given as

$$\begin{Bmatrix} \ddot{q}_1 \\ \ddot{q}_2 \\ \ddot{q}_3 \end{Bmatrix} + \begin{bmatrix} 4 & -2 & 0 \\ -2 & 4 & -2 \\ 0 & -2 & 22 \end{bmatrix} \begin{Bmatrix} q_1 \\ q_2 \\ q_3 \end{Bmatrix} = \begin{Bmatrix} 0 \\ u \\ 0 \end{Bmatrix} \qquad (5.4.1)$$
$$y = q_2$$

The normal mode parameters of (5.4.1) are given as

$$\phi_m = [\,0.7226 \quad 0.6824 \quad -0.1104\,]$$
$$\mathbf{\Omega} = \begin{bmatrix} 1.8980 & 0 & 0 \\ 0 & 5.8798 & 0 \\ 0 & 0 & 22.222 \end{bmatrix} \qquad (5.4.2)$$

Thus, the reduced properties $\bar{\mathbf{K}}$ and $\bar{\mathbf{M}}$ from (5.2.11) and (5.2.13) are found to be

$$\bar{\mathcal{K}} = 2.8182 \qquad \bar{\mathcal{M}} = 1.2583 \qquad (5.4.3)$$

which are the correct Guyan-reduced stiffness and mass as given by (5.2.4). Note also that the Schur complement of $\mathbf{M}$ given by

$$\left(\phi_m \phi_m^T\right)^{-1} = 1.0000$$

is an incorrect expression for the Guyan-reduced mass as was shown analytically in Section 5.2.

To determine the minimum-order stiffness and mass, $\hat{\mathbf{K}}$ and $\hat{\mathbf{M}}$ respectively, we use the reduced stiffness $\bar{\mathbf{K}}$ above. Applying (5.3.9), we have

$$\Delta\mathbf{\Omega} = \begin{bmatrix} 0.4266 & -1.3896 & 0.2248 \\ -1.3896 & 4.5674 & 0.2123 \\ 0.2248 & 0.2123 & 22.188 \end{bmatrix} \tag{5.4.4}$$

Then the SVD of $\Delta\mathbf{\Omega}$ is found to be

$$\begin{aligned} \mathbf{P} &= \begin{bmatrix} 0.0096 & -0.2917 & -0.9565 \\ 0.0113 & 0.9565 & -0.2916 \\ 0.9999 & -0.0080 & 0.0125 \end{bmatrix} \\ \mathbf{S} &= \begin{bmatrix} 22.192 & 0 & 0 \\ 0 & 4.989 & 0 \\ 0 & 0 & 0.0000 \end{bmatrix} \end{aligned} \tag{5.4.5}$$

Finally, applying (5.3.11)-(5.3.13), the minimum-order properties are determined, viz.

$$\begin{aligned} \hat{\mathbf{K}} &= \begin{bmatrix} 2.8182 & 0 & 0 \\ 0 & 4.0000 & 0 \\ 0 & 0 & 22.0000 \end{bmatrix} \\ \hat{\mathbf{M}} &= \begin{bmatrix} 1.2583 & -0.5000 & 0.0909 \\ -0.5000 & 1.0000 & 0 \\ 0.0909 & 0 & 1.0000 \end{bmatrix} \end{aligned} \tag{5.4.6}$$

5.4.2 36-DOF Planar Truss with Light Nonproportional Damping

A second numerical example, previously shown in Figure 3.2, is of a 36 d.o.f. planar truss with nonproportional damping. Using 18 sensors, the minimal-order mass and stiffness can be determined. It was found in Chapter IV that using the UNDAMP algorithm, extremely accurate normal modal parameters could be obtained in the presence of nonproportional damping. Using these resultant modal properties, the reduced order stiffness was found and is illustrated in Figure 5.1. The minimal-order mass and stiffness matrices are then shown in Figures 5.2 and 5.3. In Figure 5.4, a plot

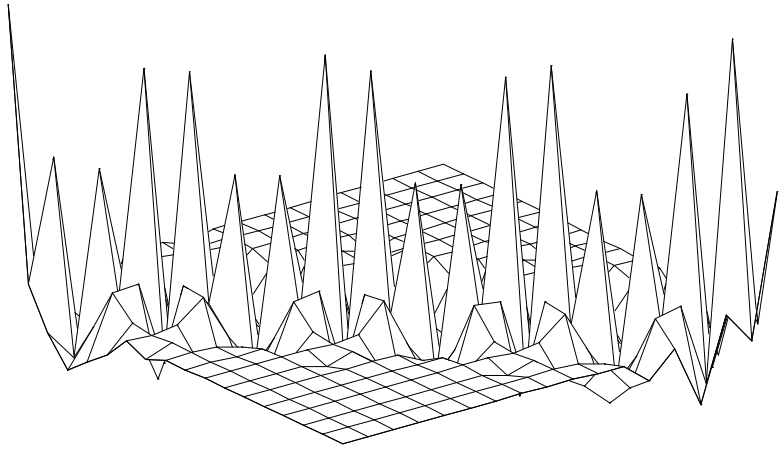

Figure 5.1: Measured Reduced Stiffness of Planar Truss

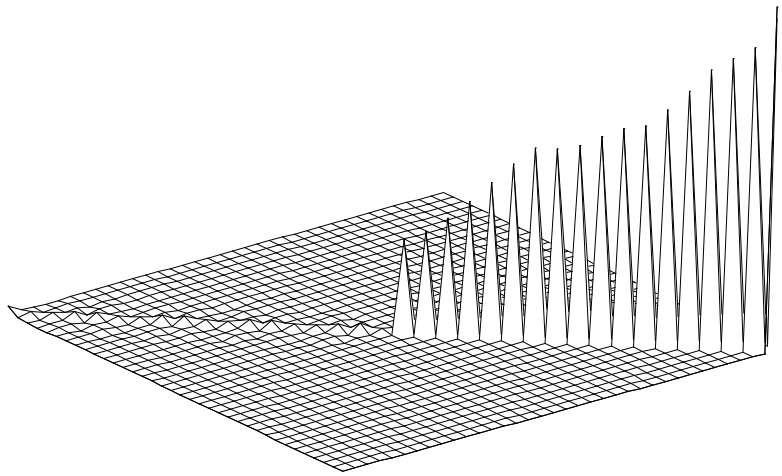

Figure 5.2: Minimal-Order (Craig-Bampton Basis) Measured Stiffness of Planar Truss

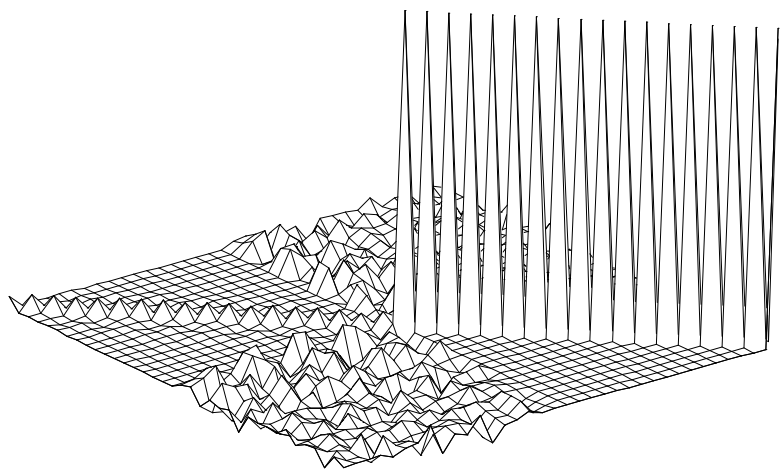

Figure 5.3: Minimal-Order (Craig-Bampton Basis) Measured Mass of Planar Truss

of the singular values of $\Delta\mathbf{\Omega}$ clearly shows the rank addition to the reduced stiffness required to obtain the equivalent minimal-order properties.

The convergence properties of the measured stiffness as a function of the number of identified modes is illustrated in Figure 5.5. The stiffness converges from a high value because it is defined as the inverse of the system flexibility at the measured degrees of freedom. Thus, when no modes are measured, the flexibility is zero and the stiffness approaches infinity. Then, as each mode contributes flexibility to the structure, the system stiffness quickly converges to its asymptotic form, the statically-condensed stiffness. Localized stiffnesses converge at a somewhat slower rate, however, depending on their strain energy contributions to the lower modes. In Figure 5.6, effective element stiffnesses in-line between longitudinal sensors are contrasted. Each stiffness is effectively that of two longerons in series, plus some influence

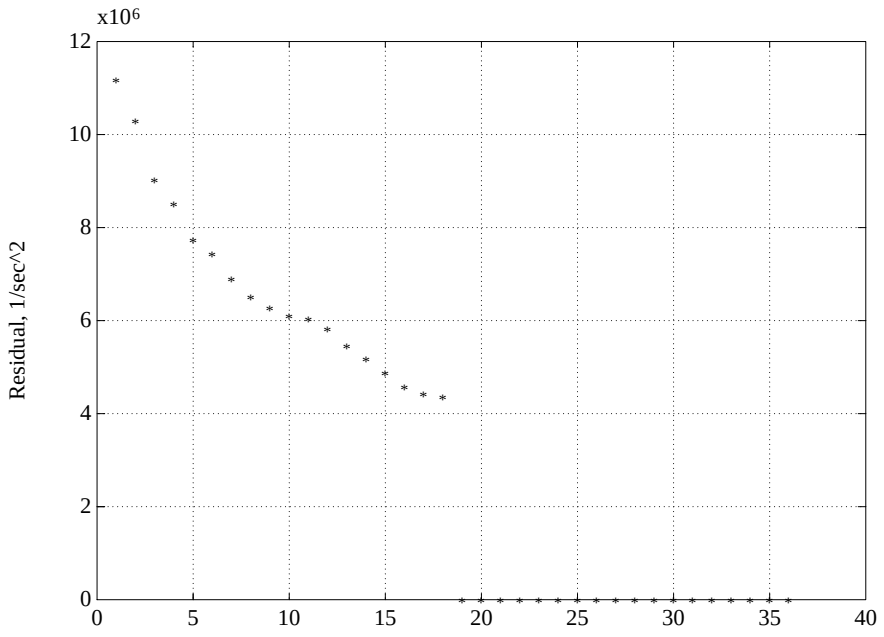

Figure 5.4: Singular Values of the Residual Stiffness

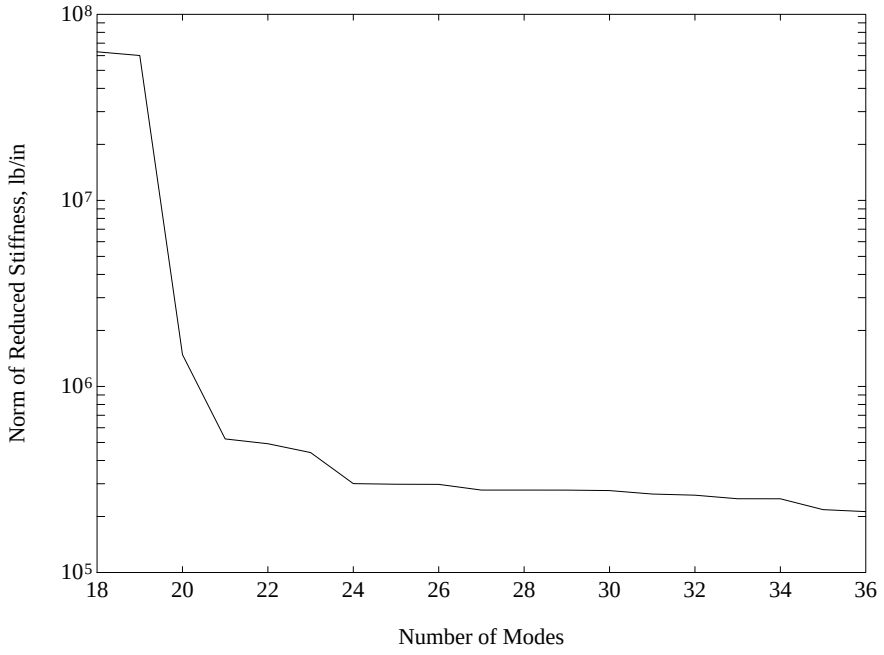

Figure 5.5: Convergence of the Reduced Stiffness Matrix

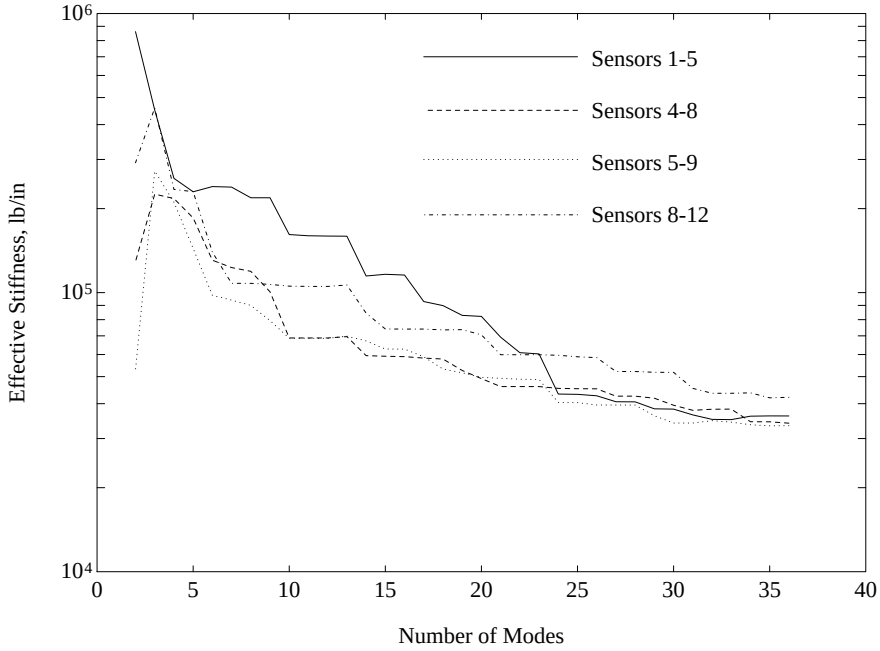

Figure 5.6: Convergence of Reduced Element Stiffnesses in Planar Truss

of the surrounding structure. The legend lists the sensor identification numbers from Figure 3.2 which are used to define the longeron "superelements". The stiffnesses are found by using only two sensor degrees of freedom in the reduced stiffness computation, then taking the negative off-diagonal term of the 2×2 reduced element stiffness matrix as the value of the stiffness coupling between the two degrees of freedom.

5.5 Conclusions

A generalized solution to the inverse vibration problem has been presented for systems with arbitrarily small numbers of discrete physical sensors and arbitrarily large numbers of inherent natural modes. A condensation solution results in reduced physical matrices which possess asymptotic equivalence to the Guyan method for finite element model reduction. An equivalent minimum-order solution is obtained by augmenting the physical

variable basis with generalized coordinates, resulting in a model which possesses the same topological properties as that obtained by the Craig-Bampton component mode synthesis method for dynamic finite element models. The resultant solutions have been applied successfully to numerical examples, and the convergence properties demonstrated. Application of the methods to experimental data will be presented in Chapter VI.

CHAPTER VI

IMPLEMENTATION AND APPLICATIONS

In this chapter the implementation of the CBSI, UNDAMP and minimal-order mass and stiffness methods is briefly presented. Then application of the algorithms to experimental data is presented through the use of FRF reconstructions, whereby it is seen that CBSI-based modal parameter estimation can improve the normal mode shapes in both numerical and experimental applications where nonproportional damping exists. Finally, the problem of damage detection from the examination of the computed reduced-order stiffnesses as presented in Chapter V is developed and applied to numerical and experimental data.

6.1 Implementation of Present Procedures

The second-order structural identification procedures presented herein have been implemented in the commercial Matlab^{TM} numerical analysis program [60] through a *Structural System Identification* (SSI) Toolbox. The SSI Toolbox consists of Matlab ".m" functions and is designed to interface smoothly with the *ModalID* system identification software package [61]. *ModalID* implements a family of efficient ERA-based system realization algorithms which identify discrete-time state space models from the Markov parameters of a linear MIMO system. *ModalID* can determine discrete-time realizations in either the nominal identified state basis (typically balanced

or cost-decoupled coordinates), or in the damped modal basis $\mathbf{z}$. The SSI Toolbox functions are designed to exploit the latter form if available in order to minimize the computations related to the conversion from discrete-time to continuous-time damped modes, at which point CBSI is applied. The following sections summarize the organization of the data and functions relevant to the SSI Toolbox.

6.1.1 Description of *ModalID* Data Blocks

The following standard data blocks are generated by the *ModalID* program and are subsequently used by the SSI Toolbox. *ModalID* allows for multiple identifications of the given Markov parameters per program execution based on different algorithmic parameters and model orders. The case number is given in each data block name (e.g. `A_1`).

`A` Discrete-time state transition matrix $\bar{\mathbf{A}}$ of the nominal identified realization.

`ABlk` $\bar{\mathbf{A}}$ of the damped modal realization in real block-diagonal form.

`B` Discrete-time input influence array $\bar{\mathbf{B}}$ of the nominal identified realization.

`BBlk` $\bar{\mathbf{B}}$ for the damped modal realization.

`C` Output influence array $\mathbf{B}$ of the nominal identified realization.

`CBlk` $\mathbf{C}$ for the damped modal realization.

`D` Input-output feedthrough matrix $\mathbf{D}$ of the realization. Equivalent to the first discrete Markov parameter $\mathbf{Y}(0)$.

`DBlk` Same as $\mathbf{D}$ which is independent of the basis definition for the realization.

`InID` Physical definition array for the force inputs. Includes a node identification number, global direction of the applied input (since force at a point is a vector quantity), input type (currently only applied external force is supported in the SSL Toolbox), and optionally the global geometric coordinates of the node location.

`OutID` Physical definition array for the sensor outputs. Same general organization as `InID`. Displacement, velocity and acceleration sensing are currently supported by the SSI Toolbox.

`f` Sample frequency of the discrete-time identified system. f is twice the Nyquist frequency, which is the highest frequency detectable from the sampled data. The sample rate Δt in seconds is equal to $1/f$.

In addition, the following data block is generated by and used commonly throughout the SSI Toolbox:

`CoID` Input-ouput collocation index. Used by many SSI functions for definition of both collocated input-output pairs and individual sensor derivative order with respect to displacement. Sensors with a relative order greater that zero (i.e. velocity or acceleration) can be integrated to determine displacement-equivalent output influence coefficients. Collocation is used for physical normalization of damped or normal mode shapes.

Because of the interactive nature of Matlab and the SSI Toolbox functions, users can individually control the data generated and choose appropriate

naming conventions. The SSI Toolbox functions are described in the next section.

6.1.2 SSI Toolbox Functions

smallskin The following Matlab functions have been developed to perform the second-order transformation methods presented in this thesis:

`era2mdk` A top-level function which determines an equivalent continuous-time realization in a second-order canonical modal or physical basis from the *ModalID* discrete-time realization using the CBSI, UNDAMP, and minimal-order mass-stiffness algorithms.

`era2mdv` Implementation of the CBSI algorithm. Transforms a discrete-time realization of arbitrary basis definition to the continuous-time normal modal canonical second-order basis. The basic CBSI, CBSI-LS and CBSI-SYM methods are supported.

`undamp` Implementation of the UNDAMP algorithm. Transforms the CBSI realization to a corrected second-order basis through a global second-order canonical transformation. Results in a normal modal second-order realization.

`mdv2cbm` Implementation of the minimal-order equivalent mass and stiffness method. Transforms the realization determined by CBSI or UNDAMP to an equivalent second-order physical or Craig-Bampton mixed physical-modal coordinate basis. From partitions of the resultant model the reduced stiffness and mass can be obtained.

`era2dmc` Transforms a discrete-time realization of arbitrary basis definition to the continuous-time damped modal coordinate basis.

`scaledmc` Physical normalization of the damped mode shapes using collocated inputs and outputs. Necessary when using the CBSI-SYM method and underdetermined conditions in the UNDAMP algorithm.

`dmc2mdv` Transforms a continuous-time damped modal coordinate basis to the normal modal canonical second-order basis using CBSI.

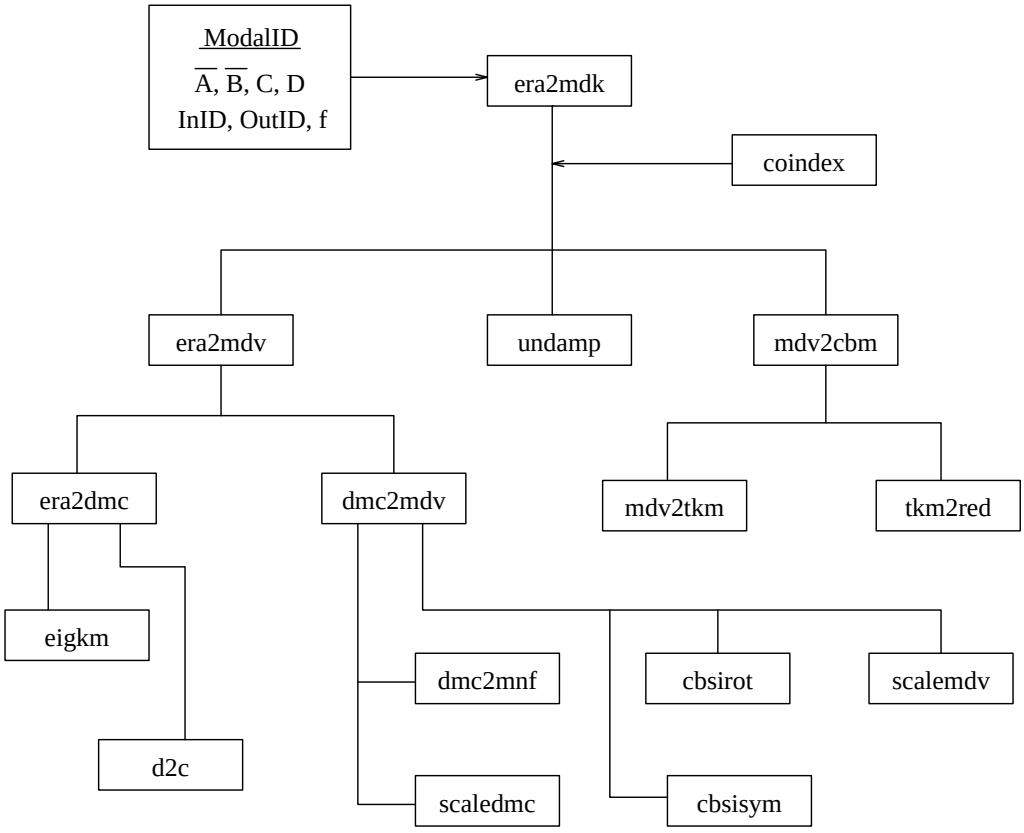

Figure 6.1: Hierarchical Organization of the SSI Toolbox

`scalemdv` Physical normalization of the normal mode shapes using collocated inputs and outputs. Necessary for determining mass-normalized modes for physical model derivation without a pre-existing mass model.

`mdv2tkm` Extracts the normal modal parameters from a second-order canonical modal (MDV) realization.

`tkm2red` Determines the reduced-order stiffness and mass matrices (asymptotically equivalent to Guyan-reduced) from the normal modal parameters.

`coindex` Forms the `CoID` data block from the information in `InID` and `OutID`.

There is a degree of redundancy in the above functions because the SSI Toolbox is designed in a hierarchical fashion as shown in Figure 6.1 The higher-level functions such as `era2mdk` will perform a sequence of model transformations based on user options using the lower-level SSI functions. For example, using defaults set in the functions, the reduced stiffness and mass can be obtained from the *ModalID* realization by simply writing:

```
[KRed_1,MRed_1] = era2mdk(A_1,B_1,C_1,InID,OutID,f);
```

Here the following defaults have been applied by the functions:

`blkflag = 0` The discrete-time realization matrices `A_1`, `B_1` and `C_1` are NOT assumed to be in block-diagonal form.

`basisflag = 0` Basis-dependent parameters are to be given in the physical (rather than modal) basis. There are output options specifically for the normal modal parameters and

reduced physical matrices `[KRed_1,MRed_1]` which are not affected by the selection (or default value of) `basisflag`. Other `era2mdk` outputs, however, including the generalized (Craig-Bampton) mass damping and stiffness, can be optionally given in a purely normal modal basis using `basisflag = 1`.

`cbsiflag = 1` Use the CBSI-LS method for normal mode shape estimation. Other options are:

- `cbsiflag = 0` Use basic CBSI for proportional damping (not recommended except for numerical problems).
- `cbsiflag = 2` Use symmetrical CBSI (CBSI-SYM).
- `cbsiflag = -1` Transform to McMillan normal form realization without using CBSI. Definitely not recommended unless the damped modal basis is specifically rotated and normalized to account for this transformation.

`undampflag = 0` Do not use UNDAMP corrective transformation. At this stage, the UNDAMP algorithm is not a "black box" and so requires careful attention.

6.2 Numerical Example of FRF Reconstruction

The CBSI procedure presented in Chapter III was evaluated through comparisons of the estimated mode shapes to the known exact normal mode shapes. In evaluating CBSI performance on real data, however, such comparisons are impossible as the exact mode shapes of the tested structure are unknown. It is possible to evaluate the normal modal estimates through reconstruction of the frequency response functions (FRFs) and comparison

to the FRFs of the state space realization. This reconstruction is standard practice and an essential verification of the measured data and the estimated model or modal parameters when performing model validation analyses. It must be noted that, in most finite element model correlation analyses, the actual measured structural response is disregarded for a number of practical reasons in favor of the estimated normal modal parameters of the estimated system realization. At each stage, therefore, some loss of information results, and this approximation can be quantified by reconstruction of the FRFs. Since the model correlation problem is generally underdetermined, it is often possible to exactly correlate the large-order finite element model to a small number of modal parameters. The adjusted finite element model will therefore exactly express the response characteristics of the estimated modal parameters, which together comprise the reconstructed FRF.

Consider first a numerical example for mode shape estimation and FRF reconstruction. In Chapter III, Section 3.5.3, a planar truss with light nonproportional damping was presented. In Figures 6.2 through 6.5 a series of displacement-force FRFs for Input 2 to Output 10 are shown. The solid line function is constructed from the exact known physical properties and sampled at 1000 Hz. The dashed and dotted line functions are reconstructions of exact realization utilizing the standard technique (ST) and CBSI methods of normal modal parameter estimation. These results demonstrate the superior accuracy of the CBSI estimated modes as compared to ST. In particular, CBSI-LS appeared to yield the best normal modal realization on the basis of this example problem as shown in Figure 6.5. Although ST also performed well in general over the test spectrum, there is clearly a loss a accuracy in the midrange frequencies due to the nonproportional damping

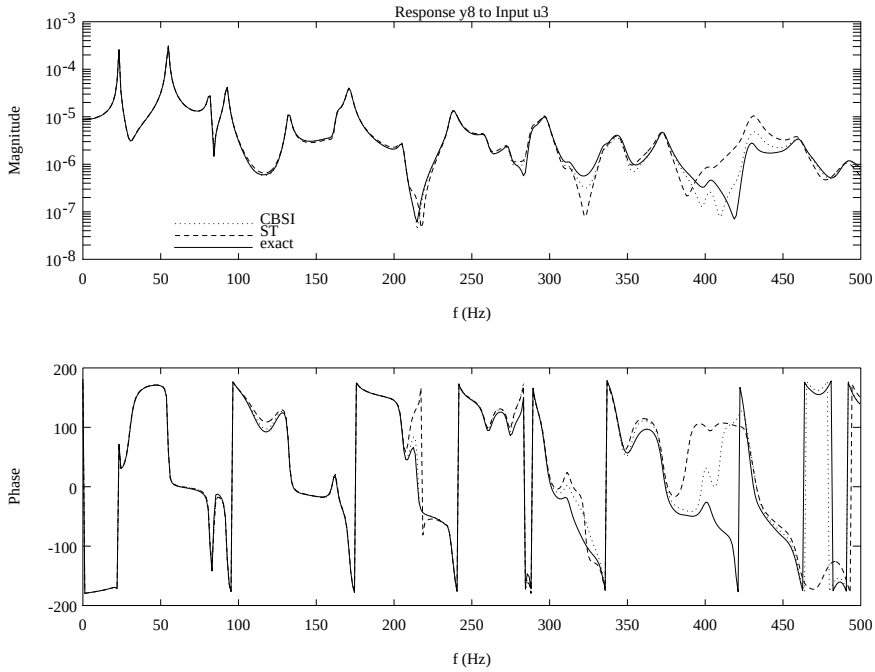

Figure 6.2: FRF Reconstruction for Planar Truss: ST vs. CBSI

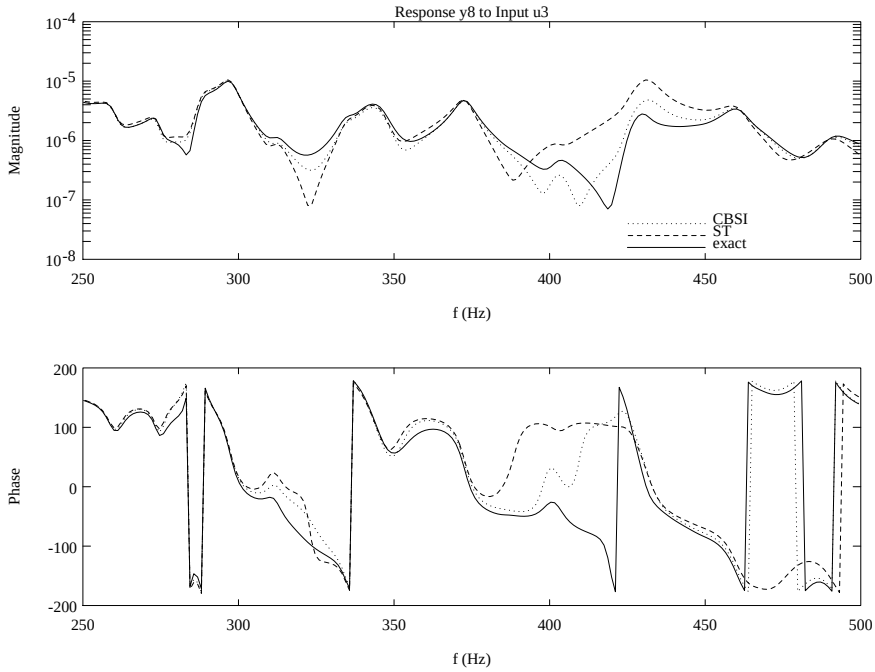

Figure 6.3: FRF Reconstruction for Planar Truss: ST vs. CBSI, Expanded View of Midrange Frequencies

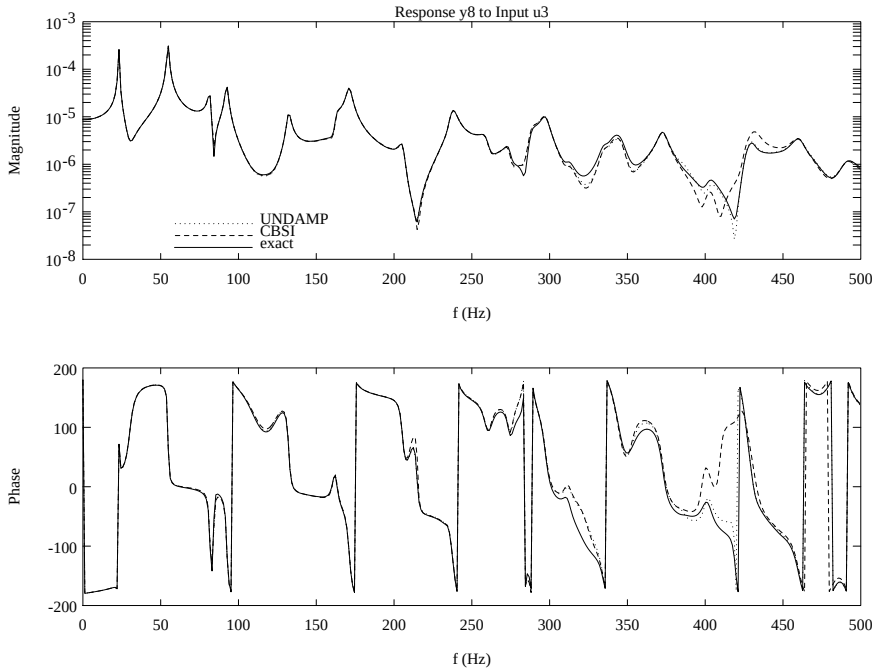

Figure 6.4: FRF Reconstruction for Planar Truss: CBSI vs. UNDAMP

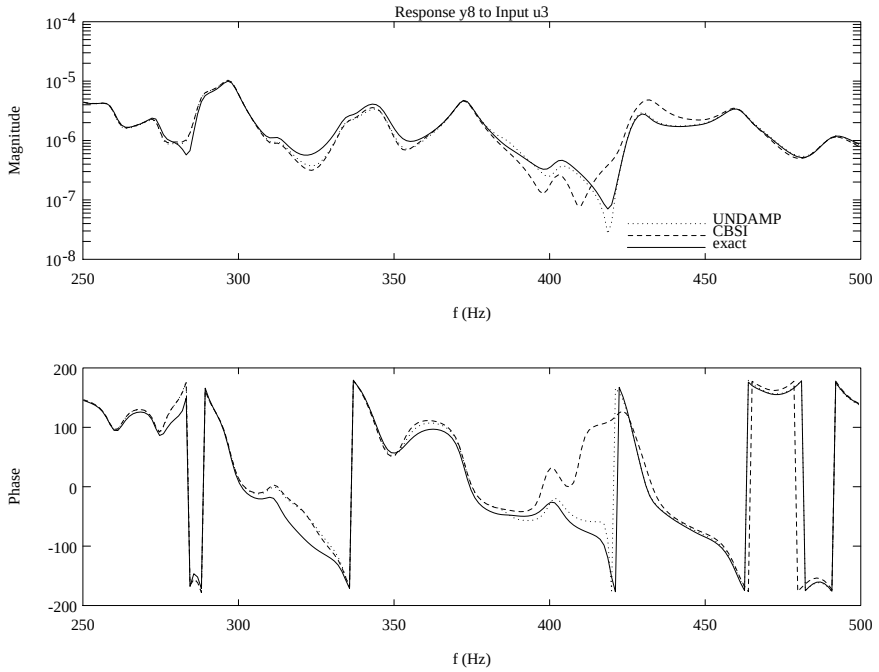

Figure 6.5: FRF Reconstruction for Planar Truss: CBSI vs. UNDAMP, Expanded View of Midrange Frequencies

effects on certain modes. The lower frequency modes, on the other hand, were ideally identified with high MPC values and hence were estimated with equal accuracy by both ST and CBSI.

6.3 FRF Reconstruction for Experimental Data

The ultimate test of analytical methods for system identification is application to real modal test data. The structure chosen herein is the *Model Update and Damage Detection Experiment* (MUDDE) testbed at the McDonnell Douglas Structural Dynamics and Controls Laboratory (SDCL) located at the University of Colorado, Boulder. The MUDDE structure, shown in Figure 6.6, is an 8-bay 1/10 scale model of the Space Station Freedom box truss configuration, representative of current and near-future flexible satellite platforms. The laboratory utilizes a CAMAC crate for data collection and Apple Macintosh^{TM} workstations with 40 MHz digital signal processors running the LabView^{TM} software environment for test control, DSP, and FRF computations.

6.3.1 Modal Testing and Data Collection

The specific modal testing performed was for the purpose of research into damage detection. The structure is unique amongst damage detection testbeds in that it is characterized principally by localized vibration modes rather than global mode shapes. The structure was designed for this feature by incorporating approximately half its total mass in a small number of lumped mass elements, as opposed to being uniformly distributed or cantilevered from a single interface. The dynamics are further complicated by testing in a suspended configuration with a low impedance support cable. As

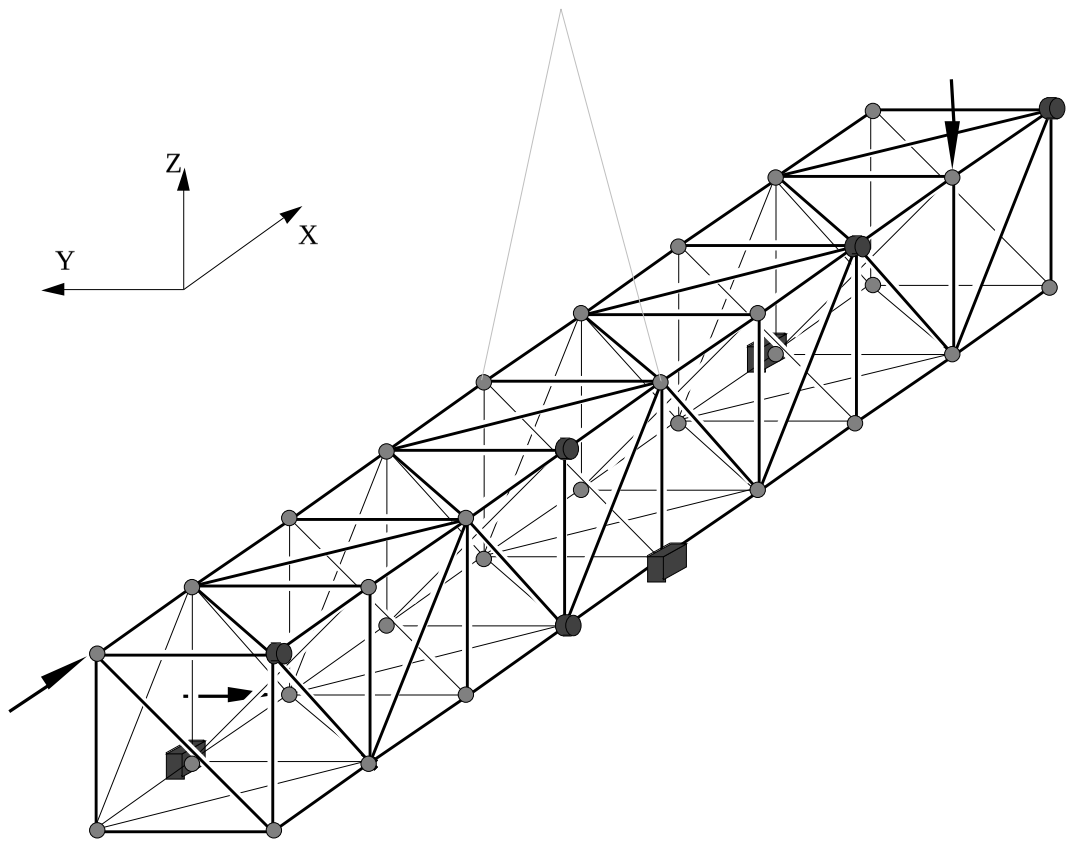

Figure 6.6: MUDDE Structure at the McDonnell Douglas Structural Dynamics and Controls Laboratory, University of Colorado, Boulder

a result, the lowest structural modes are localized movement of the lumped mass elements, and are closely followed by the lowest modes of individual truss members, leading to significant modal density and the potential for modal response coupling from closely spaced frequencies.

The dynamic behavior of the MUDDE structure poses a great challenge to both damage detection algorithms and more basic issues of structural modal identification. To more clearly discern this local behavior, a large array of spatial sensors were utilized. This allows for future research into sensor placement by studying partitions of the full collected data. Specifically, 108 sensor channels were recorded by locating a tri-axial block of accelerometers at each of the 36 structural joints on the truss as shown in Figure 6.7. Input forces at 3 spatially-distinct points were applied to excite the vibrational modes. Each input was paired with an additional collocated accelerometer to provide accurate driving point measurements for a total of 3 inputs and 111 outputs. The forces input to the structure were monitored at the shaker-structure interface by a piezo-crystal force transducer; the sensors used were piezo-film accelerometers.

Due to equipment limitations, it was necessary to apply each input in separate test trials, rather than simultaneously. Furthermore, only 36 sensors could be instrumented and measured at a time, making it necessary to "rove" a certain amount of equipment. Dummy masses were used to minimize the change in mass properties between differing configurations. The input signals were filtered at 180 Hz to minimize dynamic excitations above that level; anti-aliasing filters were set at 200 Hz and the data was sampled at 500 Hz, with a corresponding Nyquist frequency of 250 Hz. Each computed FRF was averaged over 30 trials with 8192 discrete frequencies. The 333

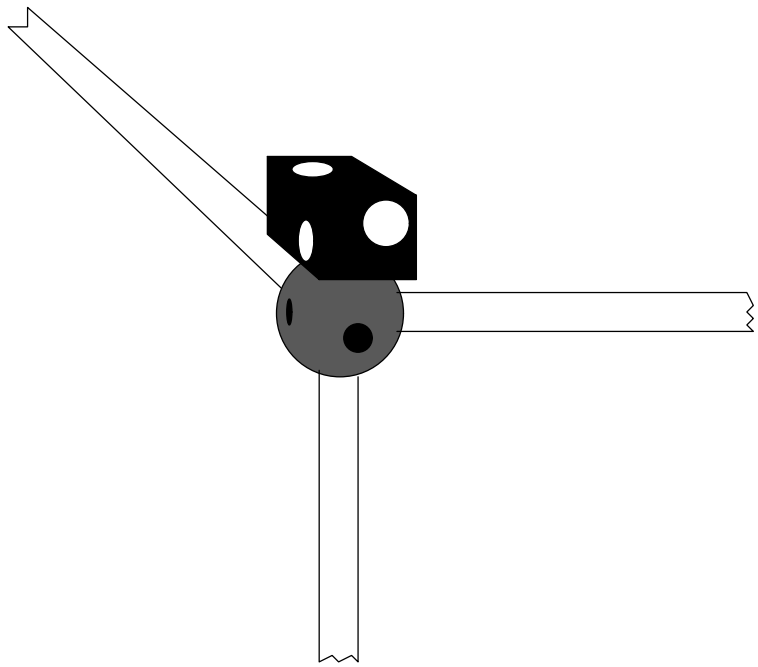

Figure 6.7: Tri-Axial Accelerometer Configuration on the MUDDE Structure

FRFs were then inverse-transformed into the discrete Markov parameters, assembled into a single data block, and written to a data file for use in model estimation analysis

6.3.2 System Realization and Normal Modal Estimation

A MIMO realization of the discrete system response from the 3 inputs to 111 outputs was obtained using the *ModalID* realization software program. A transpose formulation of the Hankel Q-Markov algorithm was utilized with q, the number of matched Markov and output covariance parameters, set to 40 and d, the number of data samples used for covariance computation, set to 1000. This formulation results in a 3000×3000 data matrix which is to be estimated by a finite-dimensional discrete-time state space realization. The determination of model order for such a complex structure remains a challenge for the structural dynamicist and it is difficult to separate the

apparent performance of analytical methods such as CBSI from the quality of the system realization. For this data, a state order of 500 was chosen, which provided a reasonably accurate estimate of the measured dynamics possessing much of the complexity exhibited by the measured FRFs. Initially, a 300 state realization was studied using various modal accuracy indicators and normal mode estimation with CBSI. The disappointing nature of the results lead to a reassessment of the model estimation and subsequently the new larger model order.

In the modal data analysis process on real data, it is typically necessary to discard some modes of the realization. Discriminating the modes which are mostly influenced by noise or the computational effects of the realization process remains yet another significant research challenge. While a number of studies exist [16, 23, 24], a lack of consensus remains, especially when the modes are complicated by nonproportional damping. In this analysis, the following modes were discarded:

- All real roots of the system realization.
- All modes with frequencies less than 2 Hz, because of the effects of low frequency sensor roll-off on FRF accuracy.
- All modes with Consistent Mode Indicator (CMI) values of less than 0.3. CMI is the product of the Extended Modal Amplitude Coherence (EMac) and the Modal Phase Collinearity (MPC) which was defined in Chapter III.

In addition, modes which could not accurately be mass-normalized from the 3 driving point measurements were discarded. These were modes for which the in-line modal amplitude coefficients for the collocated inputs and outputs did not possess a consistent direction. This is a physically-based modal selection

criterion made possible by the transformation-based CBSI algorithm. Figure 6.8 illustrates the two damped modes with the lowest and highest CMI values from the 500 state MUDDE modal test realization.

6.3.3 Results of FRF Reconstruction using Experimental Data

To fully study the implications of normal modal parameter estimation for frequency response function computation, it is necessary to utilize the normal nodal data for both sensor outputs and force inputs. In particular, collocated actuators and sensors should account for reciprocity, meaning the force influence coefficients and the displacement output coefficients are identical. Recall that, throughout the second-order structural identification procedures, this relationship was utilized to obtain normalized modal states. In reconstructing FRFs from experimental data, the estimated normal mode shapes were specifically normalized using the driving point measurements, then the mass-normalized modes were reconstructed into a purely second-order system, in effect by discarding the residual quantities of the displacement output equivalent influence array. In accordance with reciprocity relations, the input force coefficient array was reconstructed using the collocated sensor-measured mode shapes. The state transition matrix $\mathbf{A}$ was taken directly from the CBSI realization, and $\mathbf{A}$ and $\mathbf{B}$ were converted back to discrete time quantities at 500 Hz for impulse response computation. Finally, the feedthrough matrix $\mathbf{D}$ was taken as equivalent to the original quantity obtained by *ModalID*. This is because, although the feedthrough coefficient matrix is dependent on the modal parameters, the identified modal data is necessarily incomplete, and $\mathbf{D}$ is a purely physical quantity which can only be exactly expressed by the full modal spectrum.

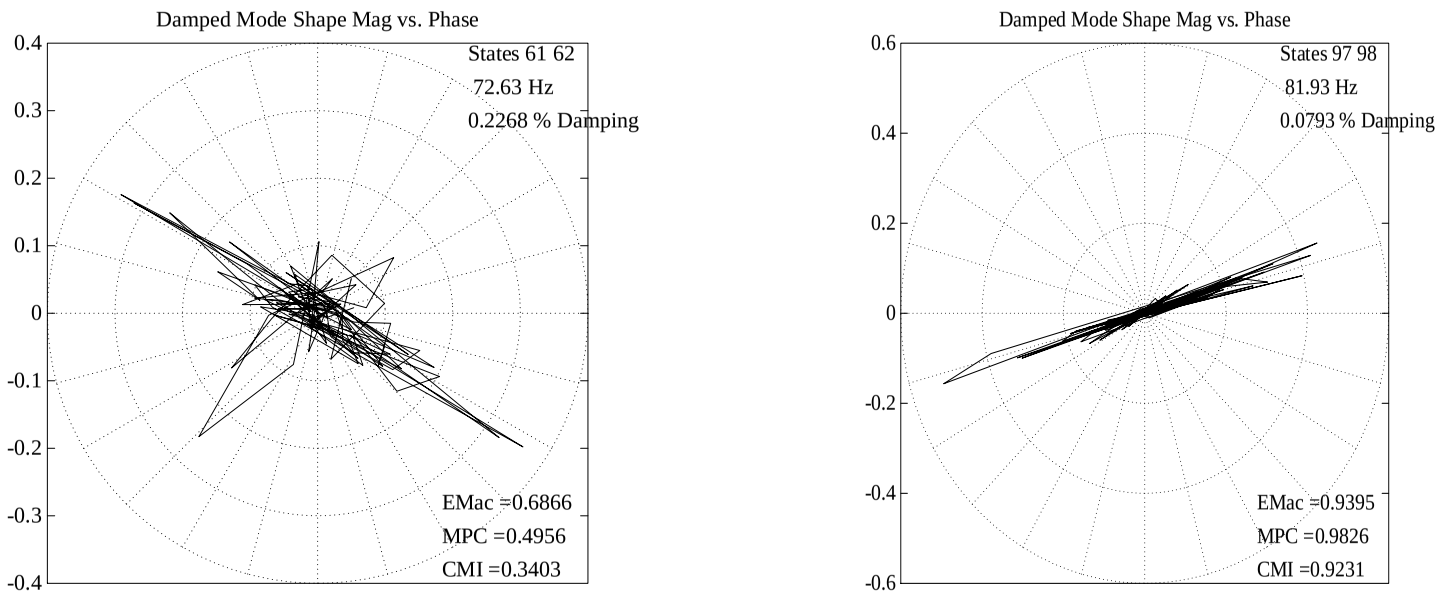

Figure 6.8: Complex Mode Shapes for MUDDE Modal Test Realization

The CBSI-SYM and CBSI-LS methods were evaluated through FRF reconstruction and contrasted with the standard technique (ST). Results for CBSI-SYM are illustrated in Figures 6.9 through 6.14. Because CBSI-LS and CBSI-SYM use different criterion for estimating the normal modes basis, there is a corresponding difference in mode shapes, although the FRF results are generally very similar. This difference also resulted in small differences in the modal selection due to scaling considerations. For example, CBSI-LS detected 144 acceptable second-order modes, while CBSI-SYM accepted 158 modes. The ST results shown were obtained using the same modes selected by CBSI-SYM for consistency in the comparisons. Finally, the solid line denoting the *ModalID* results was reconstructed again using only the modes selected by CBSI, but in contrast to CBSI and ST the complete first-order modal data was used, rather than the second-order normal mode estimates. The results shown are from the collocated sensors at input locations 2 and 3, relative to forces applied at input location 3. Thus, both a point and transfer inertance are presented.

It is difficult to draw a firm conclusion about the two methods by only studying the presented figures. There are particular frequency bands in which each method appears superior to the other. The damped modes obtained from *ModalID* are in general much more complex than the modes normally associated with such a lightly damped structure. It is possible, however, that the modal density through nonproportional damping is accountable for some of these characteristics. The modal density can also complicate the model order selection, and a number of the retained modes may not have yet converged to a more collinear phase distribution, even with a large state realization such as that used. Further studies of damped modal accuracy and

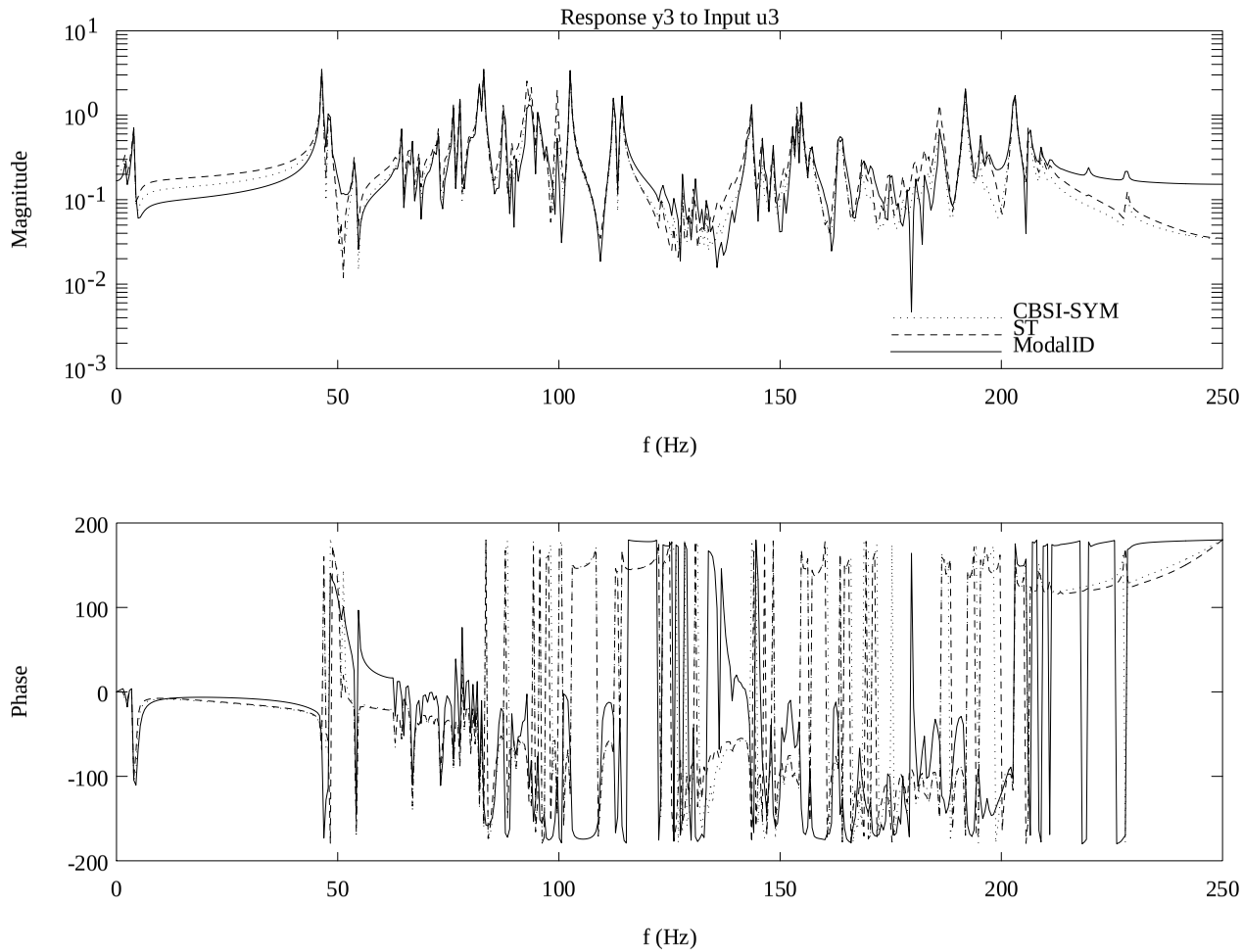

Figure 6.9: FRF Reconstruction for Experimental Data: CBSI-SYM vs. ST, Point Inertance for Input 3

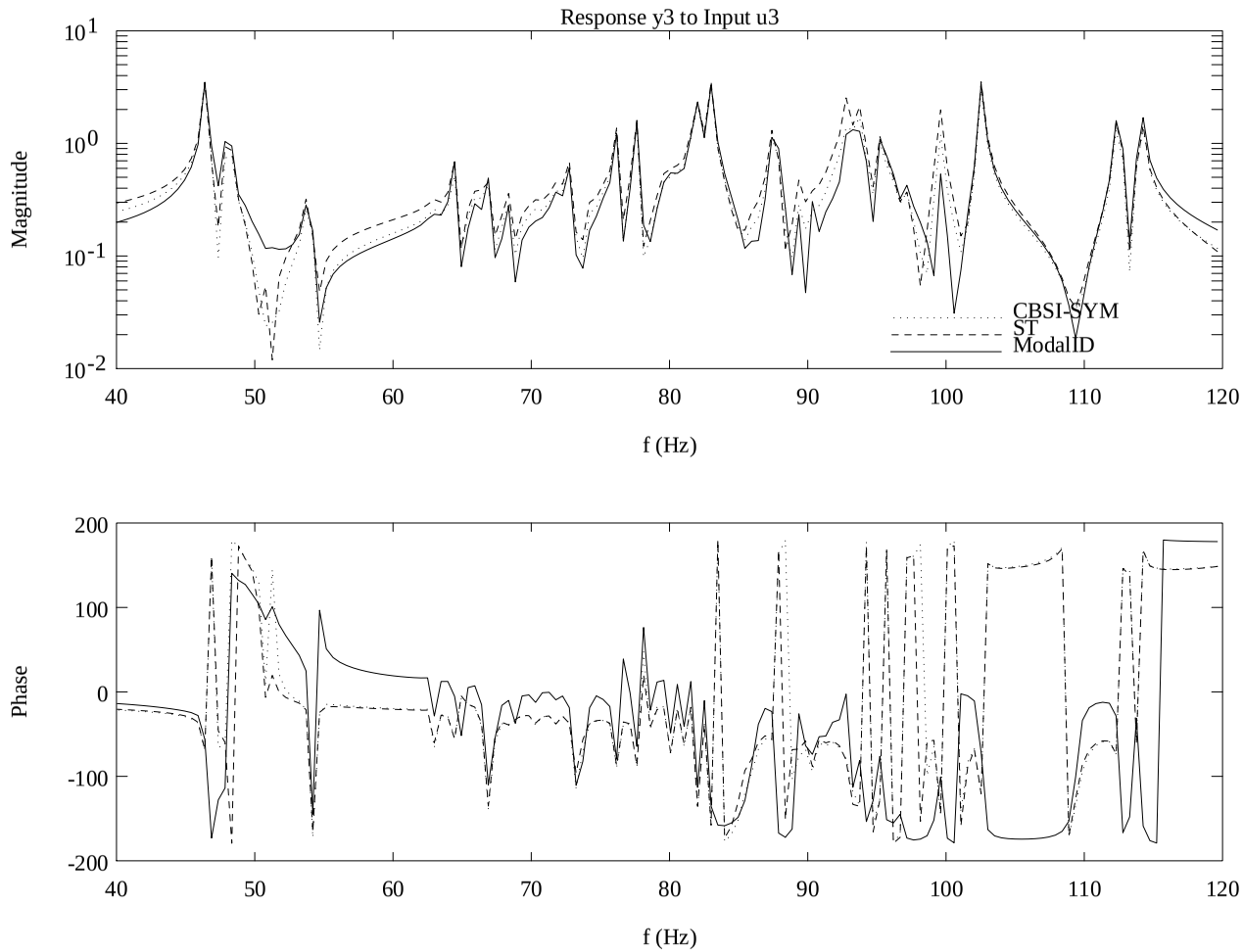

Figure 6.10: FRF Reconstruction for Experimental Data: CBSI-SYM vs. ST, Point Inertance for Input 3, Expanded View of Low-Midrange Frequencies

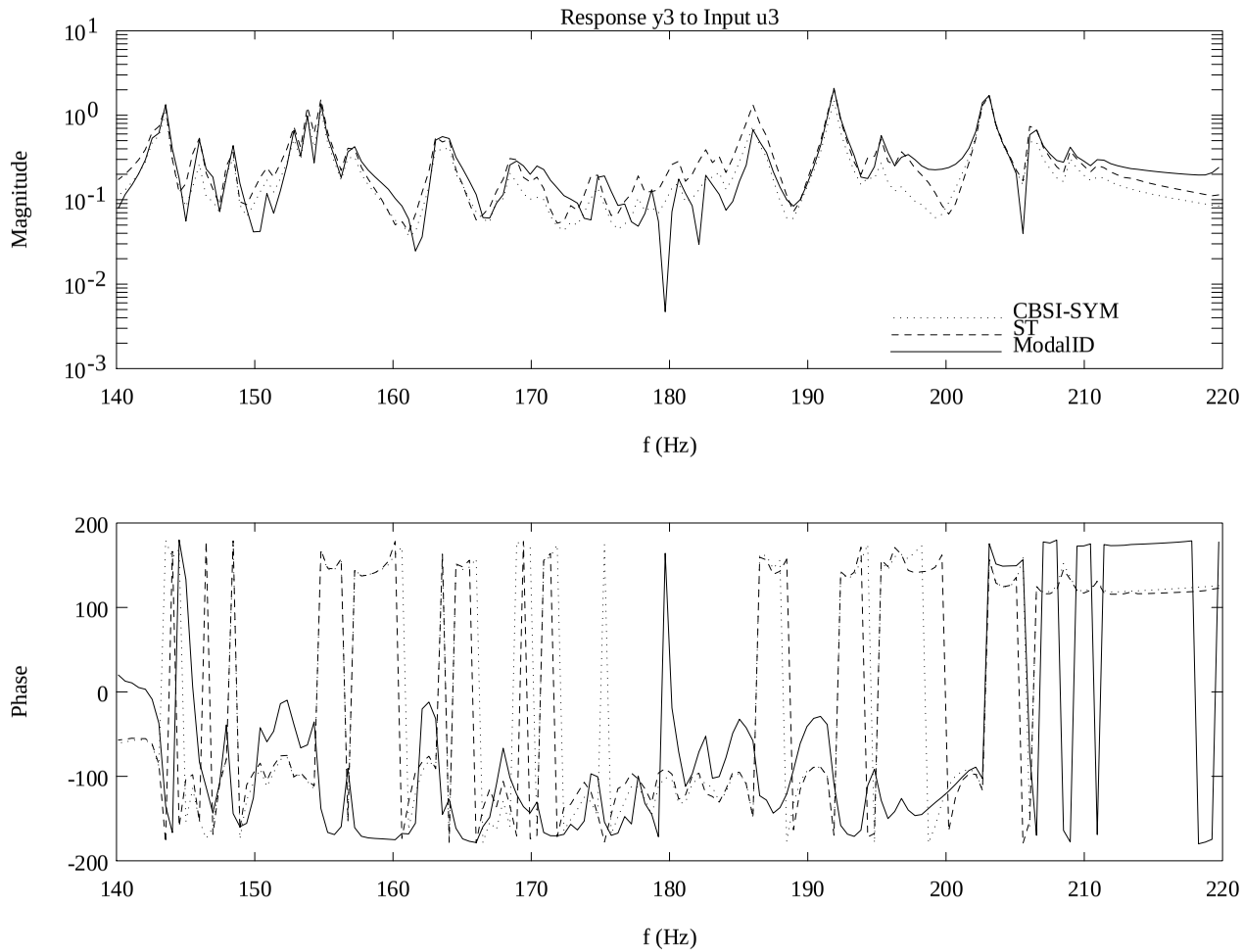

Figure 6.11: FRF Reconstruction for Experimental Data: CBSI-SYM vs. ST, Point Inertance for Input 3, Expanded View of Midrange-High Frequencies

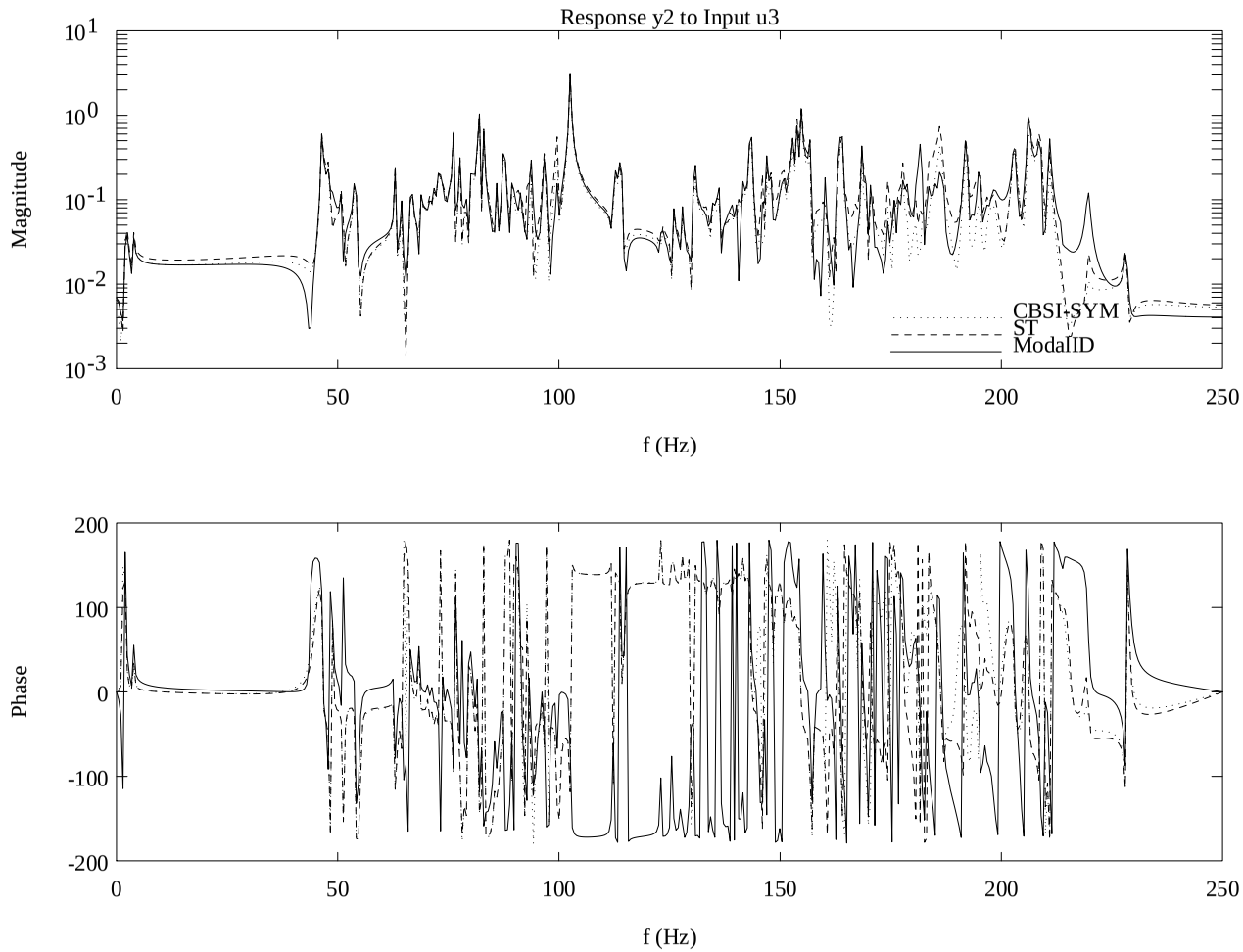

Figure 6.12: FRF Reconstruction for Experimental Data: CBSI-SYM vs. ST, Transfer Inertance from Input 3 to Input 2

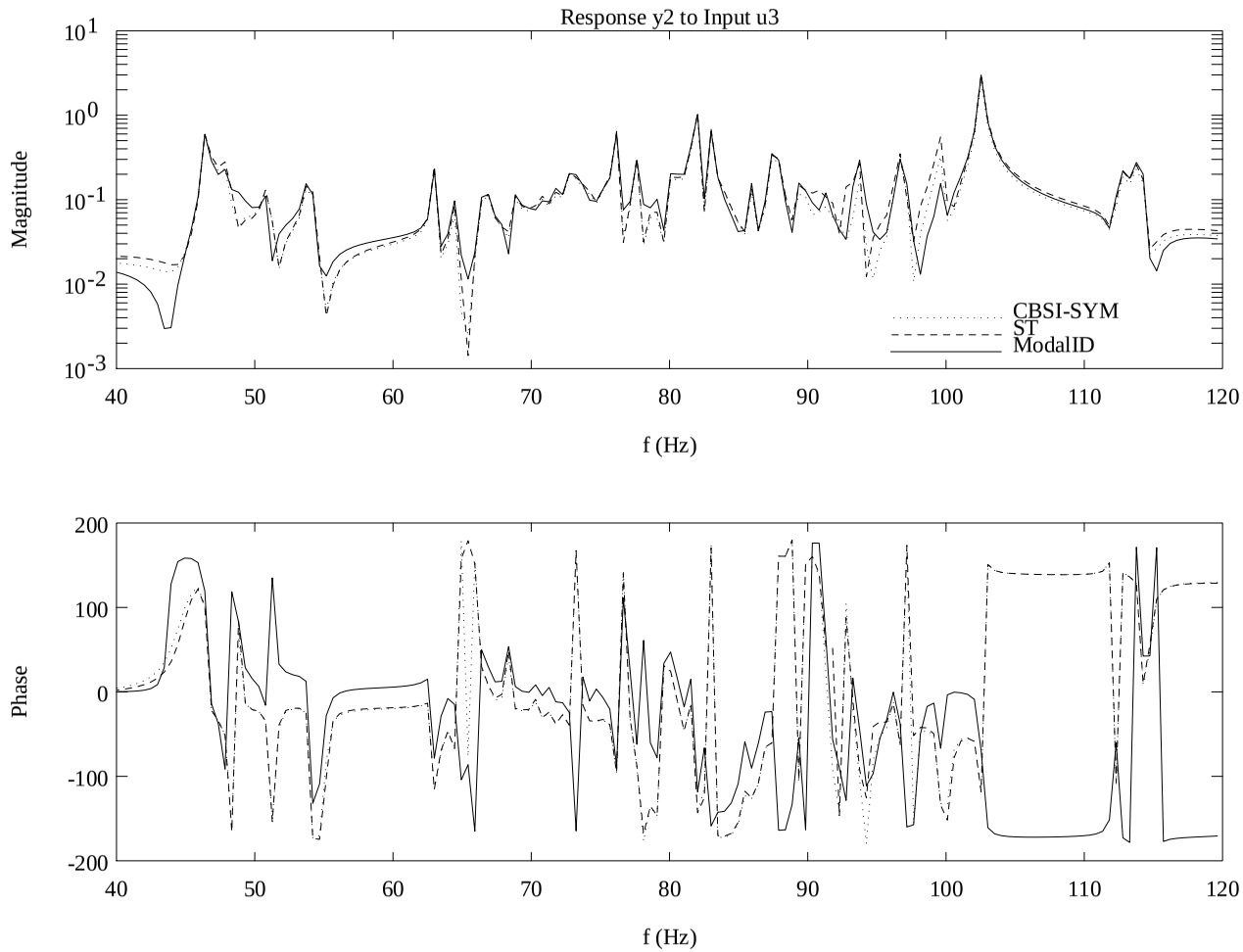

Figure 6.13: FRF Reconstruction for Experimental Data: CBSI-SYM vs. ST, Transfer Inertance from Input 3 to Input 2, Expanded View of Low-Midrange Frequencies

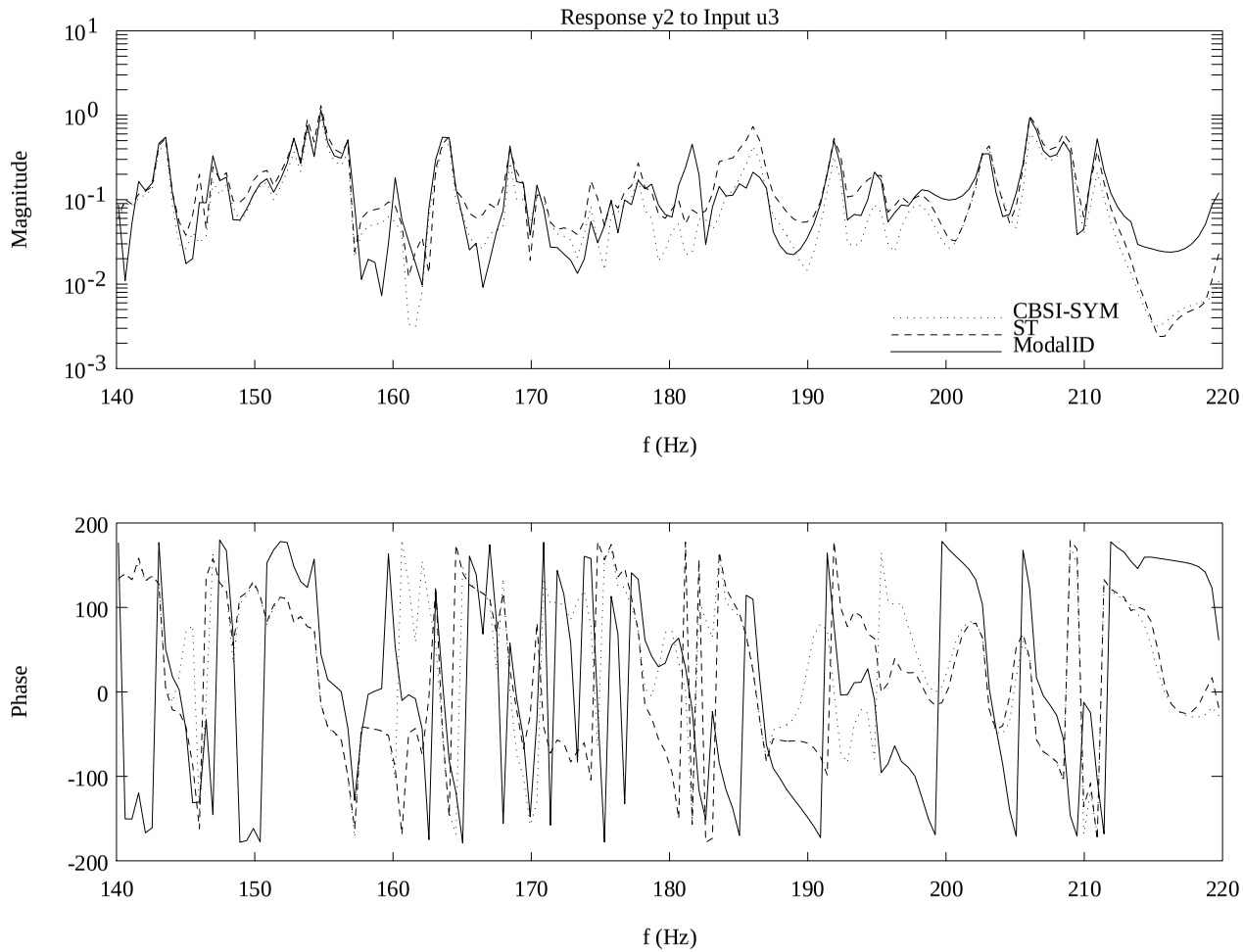

Figure 6.14: FRF Reconstruction for Experimental Data: CBSI-SYM vs. ST, Transfer Inertance from Input 3 to Input 2, Expanded View of Midrange-High Frequencies

convergence sensitivity on the realization analysis are necessary on this data, which is beyond the scope of the present work. A single quantitative measure of the response accuracy of the CBSI and ST methods can be computed using the Markov parameters. The impulse response for a single transfer pair is simply a response vector; a weighted measure of the response agreement can be found by computing the MAC between the exact (*ModalID*) response and the CBSI or ST time histories. The results for the driving point transfer functions previously illustrated are shown in Table 6.1.

Table 6.1

Output-Input	ST	CBSI-LS	CBSI-SYM
1-1	0.1679	0.2633	0.2300
1-2	0.1109	0.1580	0.1507
1-3	0.2581	0.3011	0.2853
2-1	0.1332	0.1890	0.1789
2-2	0.3176	0.3552	0.3438
2-3	0.3399	0.3933	0.3784
3-1	0.2314	0.2634	0.2573
3-2	0.3544	0.4015	0.3920
3-3	0.5455	0.6168	0.6050

Discrete Impulse Response Accuracy Indicators for
Second-Order Model Estimates of MUDDE Structural Dynamics

These methods were also applied to experimental data obtained for a modal testing and damage detection experiment on the prototype hex truss design for Space Station Freedom. The data was collected by McDonnell Douglas Corp. and provided to the SDCL organization at CU-Boulder.

Once again using *ModalID*, a 40 state discrete-time realization was obtained. By examination of the modal accuracy indicators and the general character of the modal density from the FRFs, the hex truss data is much simplier that the MUDDE structure. The results using CBSI show remarkable improvement in specific areas over the ST mode shapes in terms of FRF reconstruction. A sample result from the FRF reconstruction on the hex truss data is shown in Figure 6.15.

Early attempts at applying the UNDAMP procedure to experimental data have proven inconclusive. Among the problems encountered are difficulty in obtaining accurate driving point measurements for mode shape normalization, and the approximating effects of system realization theory. That is, ignoring the issues of sensor and actuator dynamics, for complex structures such as the MUDDE testbed and even the McDonnell Douglas Hex Truss, it is still a significant research challenge to accurately capture all of the dynamics within the test bandwidth using system realization algorithms. The inherent properties of the state space model obtained will include not only the structural modal properties, but also effects of the realization algorithm such as data window sizes and model truncation below the true system order. In addition, there may be slight nonlinearities in the structural dynamics which are averaged out by the curve-fitting properties of the realization algorithm. These various effects introduce various nonstructural behavior which the state space model can accommodate, but which do not fit the form of the second-order dynamics of a self-adjoint system. In other words, the model obtained from a system realization using CBSI will typically possess residual quantities which are *not* the result of

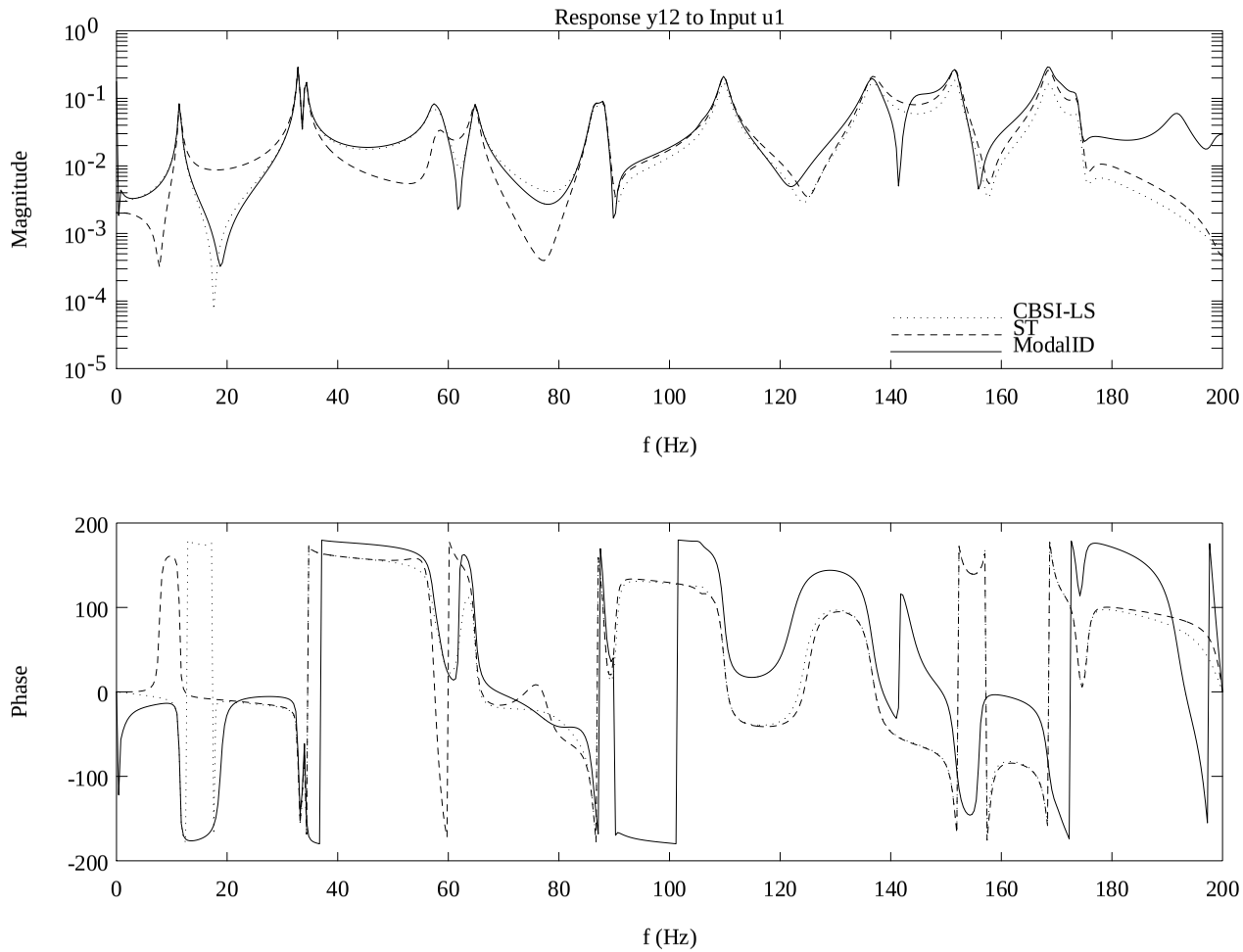

Figure 6.15: FRF Reconstruction for Hex Truss Experimental Data: CBSI-SYM vs. ST, Transfer Inertance from Input 1 to Input 12

nonproportional damping, and should therefore not be incorporated any further into the estimate of the undamped modal parameters identified through CBSI. There is a need for system realization algorithms which filter out nonstructural behavior and separately identify nonlinearities so that advanced analytical methods for structural identification can be practically applied.

6.4 Damage Detection Using Experimentally Measured Stiffness

An important new application of normal modal parameter identification and structural model correlation is the remote monitoring of the mechanical health of spacecraft structures. Such a capability implies the capability to detect damage or otherwise quantify significant changes in structural response characteristics such that adaptive components, including control systems, may respond to correct the problem and maintain mission performance. One class of damage detection algorithms infer damage from structural or modal parameters at a discrete number of measurement points, just as in modal testing and finite element modal correlation analyses. Thus, the CBSI and UNDAMP methods are relevant to the damage detection problem in that they are designed to improve the derivation of normal mode shapes from generally-damped structures. In addition, the method of minimal or reduced-order mass and stiffness matrices presented in Chapter V are relevant because they provide equivalent realization in a physical basis which naturally localizes physical changes in the identified dynamics. The resultant physical matrices can be either directly examined or efficiently manipulated to determine stiffness measurements for specific components or

substructures. This section examines the utility of measured stiffness matrices obtained from accurate CBSI-based modal realizations for detecting damage in structures.

6.4.1 Inverse Connectivity Algorithms

This damage detection procedure builds on the asymptotic Guyan stiffness method presented in Chapter V. Briefly, given an estimate of the normal mode shapes ϕ_m at the sensor locations for n modes, and the corresponding undamped eigenvalue matrix $\mathbf{\Omega}$, the Guyan-reduced stiffness is given as

$$\bar{\mathbf{K}} = \left(\phi_m \mathbf{\Omega}^{-1} \phi_m^T\right)^{-1} \tag{6.4.1}$$

In the limit that a large number of modes are retained in the model, this matrix converges to the Guyan-reduced stiffness for the structure in which the retained degrees of freedom are the displacements at the measurement output locations and directions. The modal parameters ϕ_m and $\mathbf{\Omega}$ are normal modal parameters obtained from partitions of the displacement output-equivalent realization extracted using CBSI or UNDAMP. The proposed method for detecting damage is to synthesize the reduced stiffness $\bar{\mathbf{K}}$ before and after damage, and *infer* the location and extent of damage by comparing the two. It is very important that the partition of the stiffness matrix has converged in the region being examined. This typically requires the accurate identification of a larger number of mass-normalized modes than might ordinarily be measured in a modal test.

Inferring the damage from the revised stiffness matrix is not as simple as directly examining the element of the difference matrix. Instead, it

requires a transformation of $\bar{\mathbf{K}}$ to extract elemental stiffnesses. To place this in a more general context, consider the structure and damaged substructure defined in Figure 6.16. The main structural DOF are $\mathbf{q}_A$, the damaged substructure DOF are $\mathbf{q}_I$, and the boundary DOF are $\mathbf{q}_B$. We suppose that the modal test has used sensor measurements corresponding to $\mathbf{q}_A$ and $\mathbf{q}_B$ but *not* $\mathbf{q}_I$. That is, we do not have any sensors within the damaged substructure, and must assess whether damage has occurred within the region bounded by $\mathbf{q}_B$. This is the most general formulation of the indirect damage detection problem.

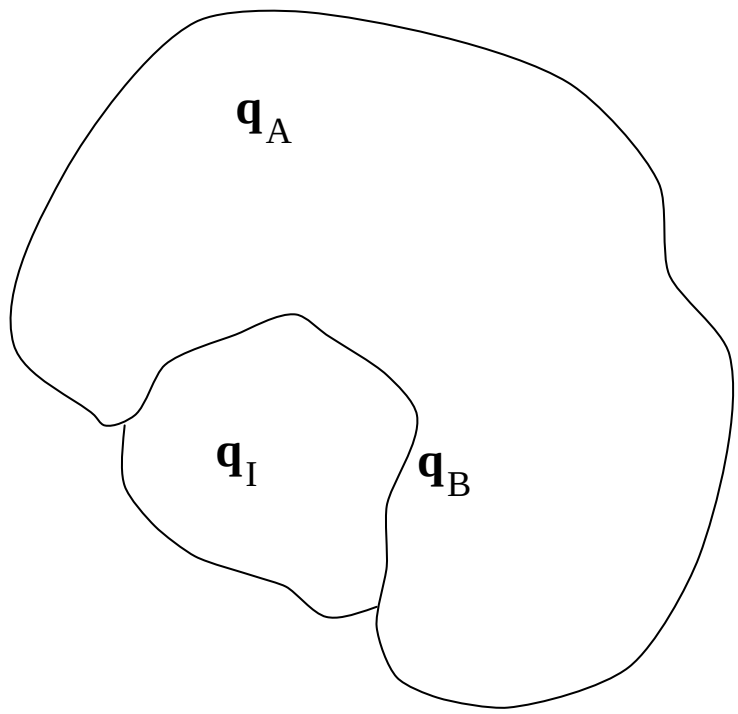

Figure 6.16: Structural Segmentation into Identified DOF, Boundary DOF, and DOF within a Damaged Substructure

The stiffness matrix for the main structure is defined to be

$$\mathbf{K}_A = \begin{bmatrix} \mathbf{K}_{AA} & \mathbf{K}_{AB} \\ \mathbf{K}_{AB}^T & \mathbf{K}_{BB}^A \end{bmatrix} \tag{6.4.2}$$

and the stiffness matrix for the substructure is defined to be

$$\mathbf{K}_I = \begin{bmatrix} \mathbf{K}_{II} & \mathbf{K}_{IB} \\ \mathbf{K}_{IB}^T & \mathbf{K}_{BB}^I \end{bmatrix} \tag{6.4.3}$$

in which the subscripts on the partitions refer to the corresponding structural DOF. The global stiffness matrix for the structure and substructure can then be constructed to be:

$$\mathbf{K}_{GG} = \begin{bmatrix} \mathbf{K}_{AA} & \mathbf{K}_{AB} & 0 \\ \mathbf{K}_{AB}^T & \mathbf{K}_{BB}^A + \mathbf{K}_{BB}^I & \mathbf{K}_{IB}^T \\ 0 & \mathbf{K}_{IB} & \mathbf{K}_{II} \end{bmatrix} \tag{6.4.4}$$

where the global DOFs have been ordered so that:

$$\mathbf{q}_G = \lfloor \mathbf{q}_A^T \quad \mathbf{q}_B^T \quad \mathbf{q}_I^T \rfloor^T \tag{6.4.5}$$

Note that there is presumed to be no direct coupling between $\mathbf{q}_A$ and $\mathbf{q}_I$.

This global stiffness matrix, however, is not the measured stiffness matrix. Instead, (6.4.1) effectively eliminates the unmeasured DOF $\mathbf{q}_I$ by a static condensation, by which:

$$\mathbf{q}_I = -\mathbf{K}_{II}^{-1}\mathbf{K}_{IB}\mathbf{q}_B \tag{6.4.6}$$

and defines the *measured* DOF vector to be:

$$\mathbf{q}_M = \lfloor \mathbf{q}_A^T \quad \mathbf{q}_B^T \rfloor^T \tag{6.4.7}$$

so that now the *Measured Stiffness Matrix* is:

$$\mathbf{K}_{MM} = \begin{bmatrix} \mathbf{K}_{AA} & \mathbf{K}_{AB} \\ \mathbf{K}_{AB}^T & \mathbf{K}_{BB}^A + \mathbf{K}_{BB}^I - \mathbf{K}_{IB}^T\mathbf{K}_{II}^{-1}\mathbf{K}_{IB} \end{bmatrix} \tag{6.4.8}$$

Notice that the damage in the substructure will be reflected in a change in the measured stiffness matrix by a change in the term:

$$\mathbf{K}_{BB}^{A} + \mathbf{K}_{BB}^{I} - \mathbf{K}_{IB}^{T}\mathbf{K}_{II}^{-1}\mathbf{K}_{IB} \tag{6.4.9}$$

It is critical to the success of the present damage detection algorithm that this partition of the measured stiffness matrix be converged. That is, attention must be given to the experimental measurement of modes which specifically contribute to this partition. The damage detection problem, then is: *"Given a measurement of the measured DOF stiffness matrix, determine the location and extent of the damage within the substructure enclosed by the boundary of the sensors."*

At this point, it is important to realize the advantage of the fact that this procedure generates an objective coordinate basis. Namely, the boundary DOF $\mathbf{q}_B$ are physical displacement DOF, as are typically used in a finite element model. Because of this objectivity, it is possible to apply *physical information* about the interconnectivity of the structure to directly infer the meaning of changes in the measured stiffness matrix. This physical interpretation is an important advantage of the algorithm. We have developed and studied two methods for deducing the location of stiffness damage of the structure from examination of the boundary stiffness matrix. These are referred to as the "pull test" and the "reduced element stiffness test." They are based on the knowledge that the data we will be analyzing is generated by the vibration of a truss structure measured by accelerometers located at nodes of the truss. We use this information to determine extensional stiffnesses between individual DOF known to lie at the ends of specific truss elements. It should be noted that the use of accelerometer measurements

will only allow us to examine the longitudinal or unidirectional stiffness of the truss members. If rotational DOF could also be measured, the bending stiffness of individual elements could be assessed using procedures similar to those described below.

Pull Test

The Pull Test (PT) algorithm imagines the following experiment is applied to the measured stiffness matrix of the structural model. To assess the local, longitudinal stiffness in the structure between two sets of sensors, two equal and opposite forces are applied between the sensors along a unit vector corresponding to the member in question, and the resulting strain is measured. In the context of the above analysis this is equivalent to defining the boundary DOF to be: In the context of the above analysis this is equivalent to defining the boundary DOF to be:

$$\mathbf{q}_B = \lfloor \mathbf{q}_1^T \quad \mathbf{q}_2^T \rfloor^T \tag{6.4.10}$$

where $\mathbf{q}_1$ are the three measured DOF at one end of the truss member, and $\mathbf{q}_2$ are the three measured DOF at the opposite end. Next, an internal longitudinal force vector is applied to the model between the boundary DOF along the member of the form:

$$\mathbf{Q} = \left\{ \begin{array}{c} 0 \\ -\hat{\mathbf{e}} \\ \hat{\mathbf{e}} \end{array} \right\} \tag{6.4.11}$$

in which the direction vector along the member is given by:

$$\hat{\mathbf{e}} = \frac{\mathbf{r}_2 - \mathbf{r}_1}{\|\mathbf{r}_2 - \mathbf{r}_1\|} \tag{6.4.12}$$

where $\mathbf{r}_1$ and $\mathbf{r}_2$ are the position vectors of the ends of the member. The resulting displacements are then computed according to:

$$\begin{Bmatrix} \mathbf{q}_A \\ \mathbf{q}_1 \\ \mathbf{q}_2 \end{Bmatrix} = \mathbf{K}_{MM}^{-1} \begin{Bmatrix} 0 \\ -\hat{\mathbf{e}} \\ \hat{\mathbf{e}} \end{Bmatrix} \tag{6.4.13}$$

The final step is to compute the *Pull Test Element Extensional Stiffness* given by:

$$k_{PT} = \frac{1}{(\mathbf{q}_2 - \mathbf{q}_1) \cdot \hat{\mathbf{e}}} \tag{6.4.14}$$

<u>Reduced Element Stiffness Test</u>

The Reduced Element Stiffness Test (REST) is a static condensation of the longitudinal element stiffness directly from the mass normalized modal vectors so that the resulting DOF include only the boundary DOF. For each modal vector, only the components contributing to the DOF at the boundary of the damaged element in the direction of $\hat{\mathbf{e}}$ are included to form the element stiffness matrix. These two scalar boundary DOF are defined by:

$$\begin{aligned} q_1 &= \mathbf{q}_1 \cdot \hat{\mathbf{e}} \\ q_2 &= \mathbf{q}_2 \cdot \hat{\mathbf{e}} \end{aligned} \tag{6.4.15}$$

The elemental stiffness matrix that we wish to find is

$$\mathbf{K}_{BB} = \begin{bmatrix} k_1 + k_2 & -k_2 \\ -k_2 & k_2 + k_3 \end{bmatrix} \tag{6.4.16}$$

where k_1 is the extensional stiffness from q_1 to ground, k_2 is the extensional stiffness of the member itself, and k_3 is the extensional stiffness from q_2 to ground. This means that the negative of the (2,1) element of $\mathbf{K}_{BB}$ is the extensional stiffness we wish to find to assess damage.

This element matrix can be found by static reduction of the $\mathbf{q}_A$ DOF. A more direct approach is to use the definition of the measured stiffness

matrix (6.4.1) and instead form the longitudinal element stiffness matrix mode-by-mode. If each modal vector is partitioned such that:

$$\phi^r = \begin{Bmatrix} \phi_A^r \\ \phi_1^r \\ \phi_2^r \end{Bmatrix} \tag{6.4.17}$$

in which ϕ_1^r are the 3-D components of mode r at node 1 on the truss element, and ϕ_1^r are the 3-D components of mode r at node 2 on the truss element, then the elemental DOF modal vectors can be defined by

$$\begin{aligned} \Phi_B &= [\,\cdots \quad \phi_B^r \quad \cdots\,] \\ \phi_B^r &= \begin{bmatrix} \phi_1^r \cdot \hat{\mathbf{e}} \\ \phi_2^r \cdot \hat{\mathbf{e}} \end{bmatrix} \end{aligned} \tag{6.4.18}$$

so that the longitudinal element stiffness matrix can be constructed directly from:

$$\mathbf{K}_{BB} = [\,\Phi_B \mathbf{\Omega}^{-1} \Phi_B^T\,]^{-1} \tag{6.4.19}$$

The *Reduced Element Extensional Stiffness*, then, is the negative of the (2,1) element of this matrix:

$$k_{REST} = -\mathbf{K}_{BB}(2,1) = k_2 \tag{6.4.20}$$

In this same notation of (6.4.16), the Pull Test extensional stiffness developed previously is given as

$$k_{PT} = k_2 + \frac{k_1 k_3}{k_1 + k_3} \tag{6.4.21}$$

which means that we expect the Reduced Element Stiffness Test to be more sensitive to damage in the extensional stiffness k_2 of the member.

6.4.2 Numerical Example: Planar Truss Structure

The 36-DOF planar truss structure studied previously and shown in Figure 3.2 was used to eveluate the effectiveness of damage detection using measured stiffnesses. The convergence property of the detection as a function of realization model order was also studied. The discrete displacement output Markov parameters for the undamaged structure were first simulated and a series of *ModalID* realizations were obtained, varying from 36 to 72 states. The 19 resultant realizations were then systematically processed using CBSI-LS and the longeron "superelement" stiffnesses were obtained for 7 localized areas using the REST stiffness formulation detailed above. The convergence of the element stiffnesses is shown in Figure 6.17. The analysis process was then repeated for the same structure with the stiffness of the longeron from node 6 to node 8 reduced to zero. The resultant stiffness convergence is shown in Figure 6.18. The damage is quite apparent at this point, given that nominally each element stiffness should converge to approximately the same value. The percentage difference in element stiffnesses is then shown in Figure 6.19. The damage detection procedure has clearly indicated a significant reduction in stiffness in the longeron superelement between nodes 4 and 8, thus localizing the model change to the extent possible given the sensor data available.

6.4.3 Application of Damage Detection to the MUDDE Testbed Structure

A similar analysis is now performed for the experimental modal testing of the MUDDE structure detailed in Section 6.3. Selection of the modes from the 500-state realization obtained by *ModalID* was done similarly to the FRF reconstruction problem, except that modes with low CMI values were

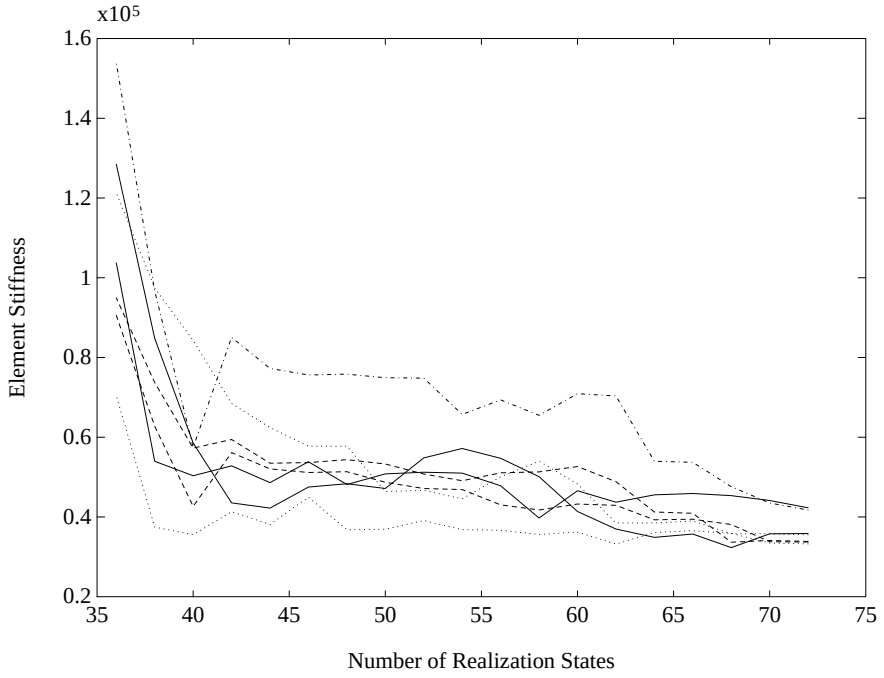

Figure 6.17: Convergence of Undamaged Element Stiffness for Numerical Planar Truss Example

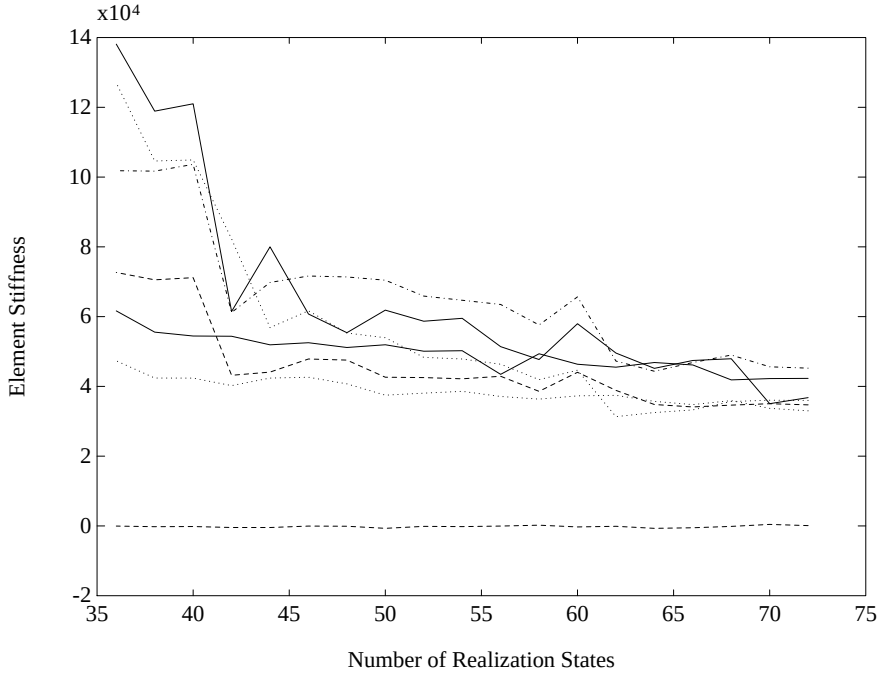

Figure 6.18: Convergence of Damaged Element Stiffness for Numerical Planar Truss Example

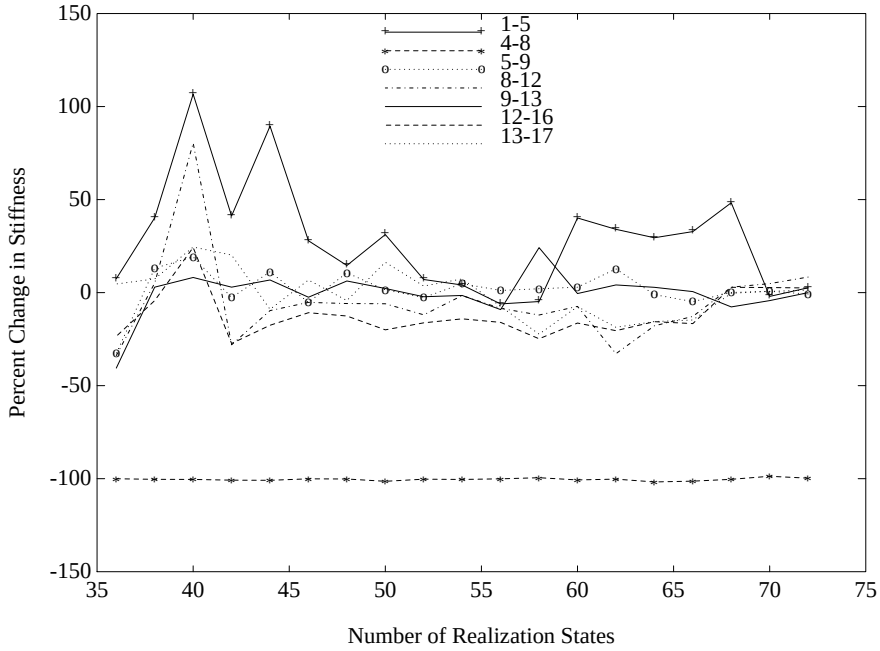

Figure 6.19: Convergence of Element Stiffness Changes for Numerical Planar Truss Example

retained if they could be consistently normalized by CBSI-LS. In addition, all the suspension modes were excluded from the stiffness analysis. This is because the reduced stiffness method is most sensitive to errors in low frequency modes, and it was judged that these modes, if accurately captured, should not contribute flexibility to the structure, even in the case of damage. In the modal testing and model estimation on the MUDDE structure, acceleration measurements were used, which generally have higher power in the higher frequency spectrum. The result of this on the model estimation process using system realization theory is that the observability of the higher frequency modes is enhanced, and those modes with the highest observability will typically converge earlier than modes with lower observability. Therefore, it is necessary to closely scrutinize the accuracy of the lower frequency

modes because of their relatively poorer convergence for acceleration sensing, and the sensitivity of the measured stiffness to their flexibility contributions.

Because of computational restrictions, the convergence of the measured stiffness as a function of model order was not obtained. Instead, the CBSI-estimated normal modes were ordered by their Modal Singular Values (MSV), which is a measure of the modal contribution to the measured response. Modes with high MSVs will typically converge to stable modal parameters at relatively lower model orders. The convergence of the longeron element measured stiffnesses as a function of the number of participating modes is shown in Figure 6.20. The trend is generally similar to the numerical example, except that the modes are ordered from high to low MSV, so the modes added later on are more poorly identified (in general). This is not a problem if the flexibility contribution from that mode is relatively small. Low frequency modes with low MSV values, on the other hand, can be problematic as seen in Figure 6.20. The significant drop in the stiffnesses of 4 longeron elements seen around 120 to 130 modes is due to the addition of flexibility from mode 2. This mode has not only a low MSV and low frequency (relative to the overall modal spectrum), but also possesses a low Modal Phase Collinearity (indicating mode shape complexity and sensitivity to the mode shape estimation problem) and a low relative modal displacement at the driving points (which can affect the accuracy of the driving point modal scaling employed in this procedure). Therefore, given the low confidence in this modal contribution, the final undamped longeron stiffnesses were computed without including mode 2. These final stiffnesses are highlighted at the right hand edge of Figure 6.20.

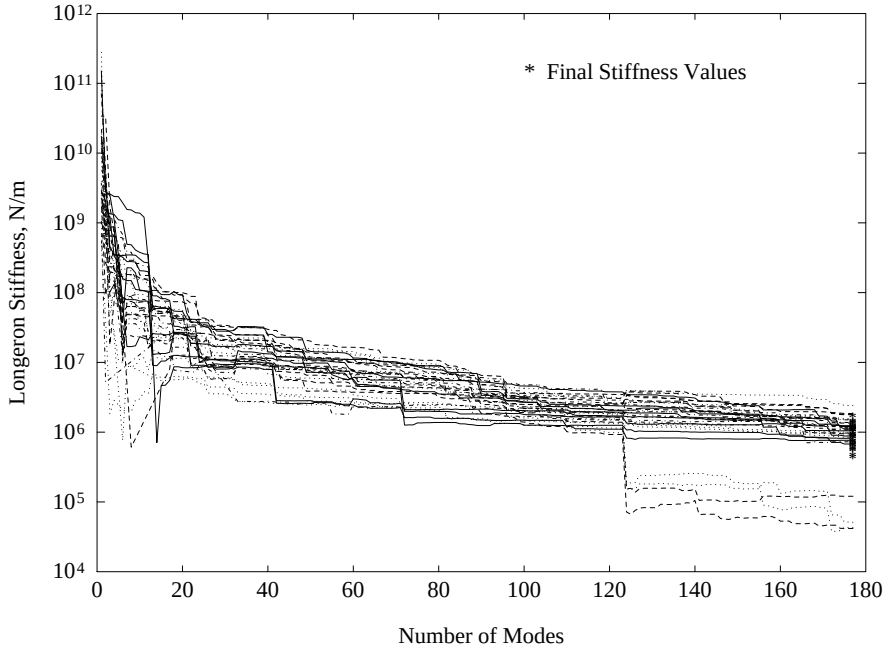

Figure 6.20: Convergence of Undamaged Longeron Stiffness for MUDDE Truss Modal Test

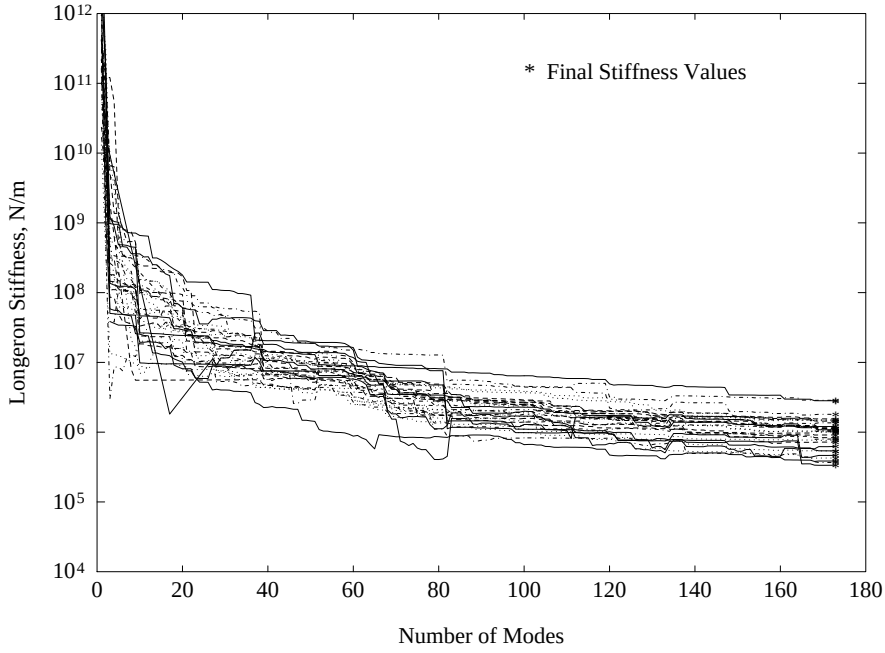

Figure 6.21: Convergence of Damaged Longeron Stiffness for MUDDE Truss Modal Test

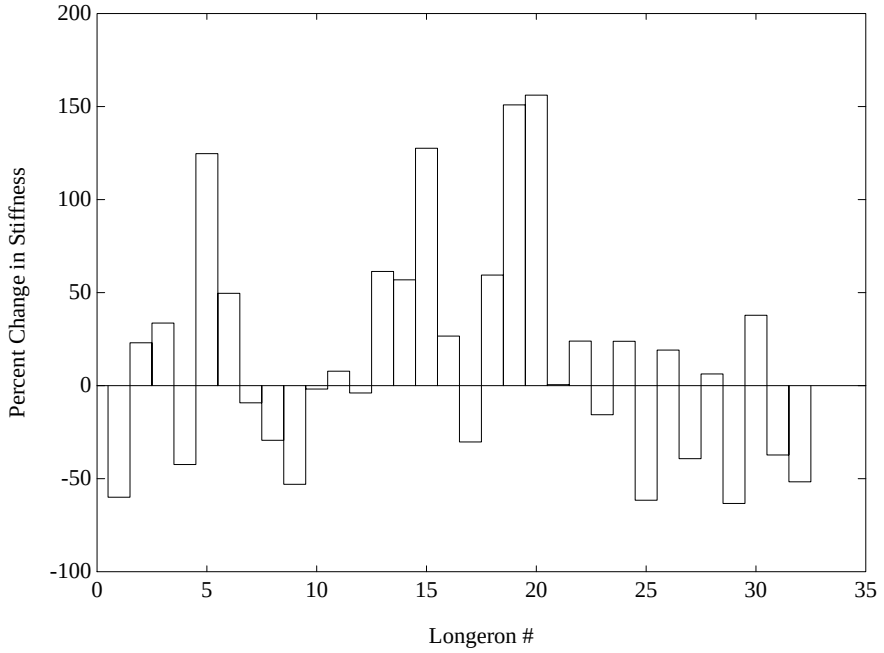

Figure 6.22: Resultant Changes in Longeron Stiffness for the MUDDE Structure: 173 Modes in Damaged Model

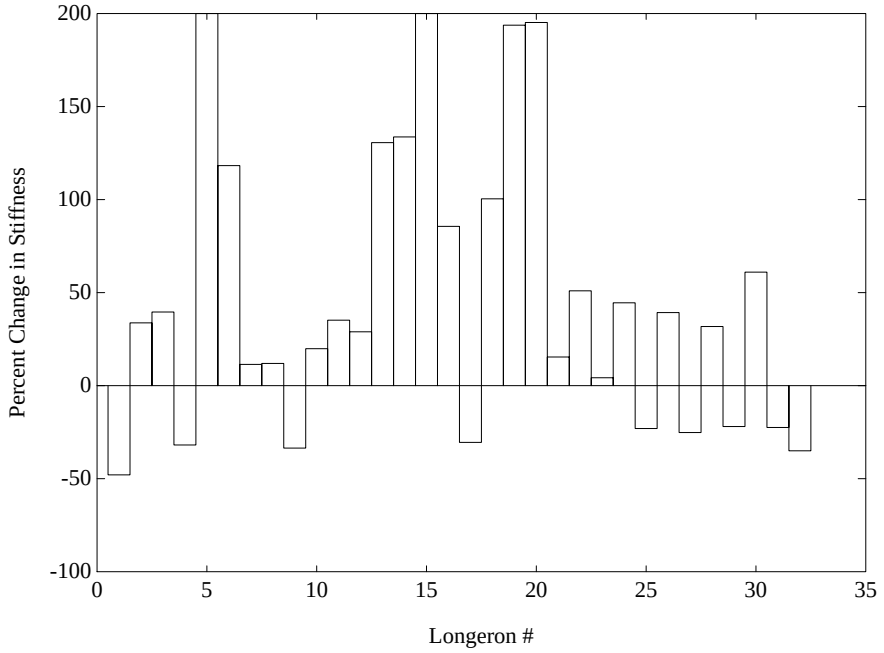

Figure 6.23: Resultant Changes in Longeron Stiffness for the MUDDE Structure: 140 Modes in Damaged Model

For the damaged structure, the same convergence study was performed, as shown in Figure 6.21. Two sets of stiffnesses were chosen for comparison, those using the full number of modes, and those using only the first 140 modal contributions (again ordered by MSV). The resultant change in stiffnesses is shown in Figures 6.22 and 6.23. In both cases, the results are somewhat ambiguous. There is a selection of elements displaying a significant reduction in stiffness, the greatest of which is Longeron 1. This is in fact the element which was removed in this damage case. It is not clear from these results, however, that it is the only damaged element. These mixed results could be attributed to many factors throughout the testing, realization and structural parameter identification process. While the measured stiffness damage detection method shows promise through both numerical and experimental demonstrations, much additional research is necessary to better determine realizations which converge to the important flexibility modes faster, along with reliable modal selection criteria and improved modal scaling via driving point measurements.

CHAPTER VII

CONCLUSIONS

7.1 Summary of Work

This dissertation has addressed three aspects of structural model synthesis from experimental data: construction of second-order structural dynamics models from state space-based system realizations, improved representations of normal modes and mode shapes for nonproportionally damped systems, and the rendering of enriched reduced-order mass and stiffness matrices from normal modes. Because state space realizations express the damped structural behavior and are not unique, the resulting models do not necessarily express the normal or undamped modal parameters of interest for structural model derivation. This thesis has therefore developed techniques for transforming state space realizations into desired second-order structural dynamics models from which the modal and physical parameters of interest can be obtained.

This research has uncovered a number of theoretical properties of structural dynamics within the context of system realization theory which are important to structural system identification techniques. For self-adjoint structural systems, driving point (or collocated) measurements are critical to modal state scaling, and indirectly to determining the consistency of physical measurements. This consistency arises directly from the nature

of the symmetrical second-order model and its characteristic modal parameters. Displacement consistency, such as the quadratic constraint criterion developed for the UNDAMP algorithm, becomes a critical issue when global transformations are applied to an assumed structural model, coupling the pseudo-displacement and velocity variables. This consistency ensures that the impulse response can be characterized in terms of displacement variables. Consequently, displacement consistency implies not only that the estimates of the measured impulse response functions are displacement quantities, but also that the "implied" but unmeasured impulse responses of the transfer functions *between outputs* are also displacement quantities.

Through numerical and experimental examples, the advantage of transformation-based methods for normal mode shape estimation has been demonstrated. The CBSI algorithm is particularly straightforward and efficient for transforming individual damped modes to optimal second-order state estimates. The UNDAMP algorithm has been shown to be effective in isolating the contaminations in the pseudo-normal modes and mode shapes due to nonproportional damping, resulting in improved normal modes and mode shapes. UNDAMP is applicable both to overdetermined as well as underdetermined systems, where the number of modes exceeds the number of measurements.

Finally, the normal modes and mode shapes obtained by CBSI or UNDAMP can be used to construct both reduced-order and minimal-order equivalent mass and stiffness matrices. The reduced-order properties have a asymptotic equivalence to the Guyan reduction for finite element models, and the minimal-order equivalent matrices are obtained through a minimum rank augmentation which has a corresponding relationship to the Craig-Bampton

component mode synthesis method. This procedure provides an alternative to finite element model correlation analysis for obtaining equivalent physical models for use in vibration control and damage detection for structures.

The major contributions of this work are summarized as follows:

a) A general transformation theory for determining second-order canonical bases from general state space realizations has been developed.

b) A similarity transformation-based method for optimally estimating the normal mode shapes of a structural dynamic system from the complex damped modes has been developed. The CBSI method is systematic and has been demonstrated to improve normal mode shape estimates even for nonproportionally damped systems as compared with existing techniques.

c) A global transformation method has been presented for the identification of true second-order state models of structures in the presence of significant nonproportional damping. The theoretical development leads to an important displacement consistency criterion for the damped realization and global transformation.

d) A particular direct solution for determining an equivalent physical model (i.e. mass and stiffness) from mass-normalized modal parameters has been derived. The resultant physical model has asymptotic equivalence to Guyan and Craig-Bampton-based finite element model reduction methods.

e) Numerical and experimental examples have been presented which illustrate the advantages of the second-order transformation-based methods developed herein. Applications to the problem of damage detection in space structures is detailed using both numerical and experimental data.

7.2 Directions for Future Research

7.2.1 System Realization

Structural identification can be enhanced by the incorporation of physical insight from the second-order synthesis to guide realization theory-based system identification. The primary goal is to separately characterize or isolate the influence of nonlinearities, gyroscopic damping and instrumentation dynamics on the modal test realization to be used for structural parameter derivation. This is not to suggest that these effects are immaterial to system performance. Instead, it is necessary to recognize the inherent qualities or assumptions governing the system being studied, and to determine appropriate empirical measures by which that system may be assessed. In particular:

a) Develop system realization methods which identify specific subclasses of state space realizations. For structures this would include reciprocal behavior and continuous-time impulse response characteristics.

b) Improve modal accuracy indicators via reciprocity and modal scaling considerations. It is necessary to develop a better understanding of the effects of noise, signal processing transforms and the inexact curve-fitting effects of the numerical algorithm.

7.2.2 Second-Order Models and Normal Modes Estimation

Applying these synthesis methods to real data has provided a healthy dose of reality (and humility) to this effort. There are specific technical areas where the CBSI and UNDAMP algorithms could be improved:

a) Improved modal scaling determination through multiple driving point measurements, use of modal Markov parameters and the force-acceleration feedthrough matrix.

b) Application of UNDAMP techniques to experimental data sets which do not satisfy the displacement consistency criterion. This may require the consideration of eigenvalue changes, what phase information should *not* be incorporated, and ways of allowing the analyst to control how different modes couple in physical or modal terms.

c) Convergence characteristics of estimated modal or physical parameters. This is not only an issue of mass and stiffness measures and their relation to modal truncation, but also for the characteristic damped modal parameters as a function of model order and data matrix construction.

7.2.3 Applications of Structural System Identification

a) Reduced-order model determination for structural vibration control using component-mode synthesis based techniques on test realizations.

b) Exploit the structural system characteristics to decentralize the system identification task for real-time control and health monitoring.

c) Substructure-based synthesis of subassembly testing into global dynamic models.

d) Use of second-order models and objective basis definitions for linearized identification of nonlinear phenomena.

e) The use of both measured modal and physical parameters and their confidence bounds in the problem of finite element model correlation.

REFERENCES

1. Ewins, D. J., *Modal Testing: Theory and Practice*, Research Studies Press Ltd., 1984.

2. Chen, J. C., "Evaluation of Spacecraft Modal Test Methods," *J. of Spacecraft and Rockets*, Vol. 24, No. 1, pp. 52-62, 1987.

3. Lewis, R. C. and Wrisley, D. L. (1950) "A System for the Excitation of Pure Natural Modes of Complex Structures." *J. of the Aeronautical Sciences*, Vol. 17, No. 11, pp. 705-722.

4. Klosterman, A. and Zimmerman, R. (1975) "Modal Survey Activity via Frequency Response Function," SAE Paper 751063.

5. Ibrahim, S. R. and Mikulcik, E. C., "A Method for the Direct Identification of Vibration Parameters from the Free Response," *Shock and Vibration Bulletin*, Vol. 47, Pt. 4, pp. 183-198, 1977.

6. Brown, D, Allemang, R., Zimmerman, R., and Mergeay, M., "Parameter Estimation Techniques for Modal Analysis," SAE Paper 790221, *SAE Transactions*, Vol. 88/1, 1979, pp. 828-846.

7. Vold, H., Kundrat, J., Rocklin, G. T. and Russell, R., "A Multiple-Input Modal Estimation Algorithm for Mini-Computers," SAE Paper 820194, *SAE Transactions*, Vol. 91/1, 1982, pp.815-821.

8. Juang, J. N. and Pappa, R. S., "An Eigensystem Realization Algorithm for Modal Parameter Identification and Model Reduction," *J. Guidance, Control, and Dynamics*, Vol. 8, No. 5, pp. 620-627, 1985.

9. Liu, K. T. and Skelton, R. E., (1993) "The Q-Markov COVER Algorithm for Flexible Structure Identification," *Journal of Guidance, Control and Dynamics*, Vol. , No. , pp. , 1993.

10. Juang, J.-N. (1987) "Mathematical Correlation of Modal Parameter Identification Methods via System Realization Theory," *Int. J. of Anal. and Expt. Modal Analysis*, Vol. 2, No. 1, pp. 1-18.

11. Leuridan, J. M., Brown, D. L. and Allemang, R. J., "Time Domain Parameter Identification Methods for Linear Modal Analysis: A Unifying Approach," *ASME J. Vibration, Stress and Reliability in Design*, Vol. 108, January 1986, pp. 1-8.

12. Skelton, R. E., *Dynamic Systems Control*, John Wiley and Sons, 1988.

13. Ho, B. L. and Kalman, R. E. (1965) "Effective Construction of Linear State-Variable Models from Input/Output Data," *Proceedings of the 3rd Annual Allerton Conference on Circuit and System Theory*, pp. 449-459; also, *Regelungstechnik*, Vol. 14, 1966, pp. 545-548.

14. Kung, S., "A New Identification and Model Reduction Algorithm via Singular Value Decomposition," *Proceedings of the 12th Asilomar Conf. on Circuits, Systems, and Computers*, Nov. 1978, pp. 705-714.

15. Wagie, D. A. and Skelton, R. E. (1986) "A Projection Approach to Covariance Equivalent Realizations of Discrete Systems," *IEEE Trans. Automatic Control*, AC-31, p. 1114.

16. Juang, J.-N. and Pappa, R. S., "Effects of Noise on Modal Parameters Identified by the Eigensystem Realization Algorithm," *Journal of Guidance, Control and Dynamics*, Vol. 9, No. 3, pp. 294-303, 1986.

17. Juang, J.-N., Cooper, J. E. and Wright, J. R., "An Eigensystem Realization Algorithm Using Data Correlations (ERA/DC) for Modal Parameter Identification," *Control Theory and Advanced Technology*, Vol. 4, No. 1, pp. 5-14, 1988.

18. Peterson, L. D. (1992) "Efficient Computation of the Eigensystem Realization Algorithm," *Proceedings of the 10th International Modal Analysis Conference*, February 1992, submitted for publication to *Journal of Guidance, Control and Dynamics.*

19. Meirovitch, L., *Analytical Methods in Vibrations*, McGraw-Hill, 1960.

20. Caughey, T. K. and O'Kelly, M. M. J., "Classical Normal Modes in Damped Linear Dynamical Systems," *Journal of Applied Mechanics*, Vol. 32, 1965, pp. 583-588.

21. Lang, G. F., "Demystifying Complex Modes," *Journal of Sound and Vibration*, Vol. 23, 1989, pp. 36-40.

22. Ljung, L., *System Identification: Theory for the User*, Prentice Hall, 1987.

23. Pappa, R. S., Elliot, K. B., and Schenk, A., "A Consistent-Mode Indicator for the Eigensystem Realization Algorithm," AIAA Paper 92-2136-CP, *Proceedings of the 1992 AIAA Structures, Structural Dynamics, and Materials Conference*, April, 1992, pp. 556-565.

24. Longman, R. W., Lew, J.-S., and Juang, J.-N., "Comparison of Candidate Methods to Distinguish Noise Modes from System Modes in Structural Identification," AIAA Paper 92-2518-CP, *Proceedings of the 1992 AIAA Structures, Structural Dynamics, and Materials Conference*, April 1992, pp. 2307-2317.

25. Imregun, M. and Ewins, D. J., "Realisation of Complex Mode Shapes," *Proceedings of the 11th Annual International Modal Analysis Conference*, February 1993, pp. 1303-1309.

26. Mayes, R. L., "A Multi-Degree-of-Freedom Mode Shape Estimation Algorithm Using Quadrature Response," *Proceedings of the 11th International Modal Analysis Conference*, February 1993, pp. 1026-1034.

27. Longman, R. W. and Juang, J. N. (1987) "A Variance Based Confidence Criterion for ERA-Identified Modal Parameters," Paper AAS 87-454, *AAS/AIAA Astrodynamics Specialist Conference*, Kalispell, MT, August, 1987.

28. Ibrahim, S. R. (1983) "Computation of Normal Modes from Identified Complex Modes," *AIAA Journal*, Vol. 21, No. 3, pp. 446-451.

29. Niedbal, N., "Analytical Determination of Real Normal Modes from Measured Complex Responses," *Proceedings of the 25th Structures, Structural Dynamics and Materials Conf.*, Palm Springs, CA, May 1984, pp. 292-295.

30. Zhang, Q. and Lallement, G. L. (1985) "New method of determining the Eigensolutions of the Associated Conservative Structure from the Identified Eigensolutions," *Proceedings of the 3rd International Modal Analysis Conference*, pp. 322-328.

31. Zhang, Q. and Lallement, G. L. (1987) "Comparison of Normal Eigenmodes Calculation Method Based on Identified Complex Eigenmodes," *Journal of Spacecraft and Rockets*, pp. 69-73.

32. Wei, M. L., Allemang, R. J., and Brown, D. L., "Real-Normalization of Measured Complex Modes," *Proceedings of the 5th International Modal Analysis Conference*, 1987, pp.708-712.

33. Placidi, F., Poggi, F. and Sestieri, A. (1991) " Real Modes Computation from Identified Modal Parameters with Estimate of Generalized Damping," *Proceedings of the 9th International Modal Analysis Conference*, pp. 572-579.

34. Minas, D. J. and Inman, D. J. (1991) " Identification of a Nonproportional Damping Matrix from Incomplete Model Information," *Journal of Vibration and Acoustics*, Vol. 113, No. 2, pp. 219-224.

35. Sestieri, A. and Ibrahim, S. R., "Analysis of Errors and Approximations in the Use of Modal Coordinates," *Proceedings of the 11th International Modal Analysis Conference*, 1993, pp. 425-433.

36. Hsu, C., Ju, M. S. and Tsuei, Y. G., "Extraction of Normal Modes from Experimental Data," *Proceedings of the 11th International Modal Analysis Conference*, 1993, pp. 1612-1617.

37. Yang, C.-D. and Yeh, F.-B. (1990) "Identification, Reduction, and Refinement of Model Parameters by the Eigensystem Realization Algorithm," *Journal of Guidance, Control and Dynamics*, Vol. 13, No. 6, pp.1051-1059.

38. Gladwell, G. M. L., *Inverse Problems in Vibrations*, Academic Press, 1986.

39. Baruch, M. and Bar Itzhack, I. Y., "Optimum Weighted Orthogonalization of Measured Modes," *AIAA Journal*, Vol. 16, No 4, pp. 346-351, 1978.

40. Berman, A. and Nagy, E. J., "Improvement of a Large Analytical Model using Modal Test Data," *AIAA Journal*, Vol. 21, No. 8, pp. 1168-1173, 1983.

41. Kabe, A. M., "Stiffness Matrix Adjustment Using Mode Data," *AIAA Journal*, Vol. 23, No. 9, pp. 1431-1436, 1985.

42. Smith, S. W. and Beattie, C. A., "Secant-Method Adjustment Using Modal Data," *AIAA Journal*, Vol. 29, No. 1, pp. 119-126, 1991.

43. Martinez, D., Red-Horse, J. and Allen, J., "System Identification Methods for Dynamic Structural Models of Electronic Packages," *Proceedings of the 32nd Structures, Structural Dynamics and Materials Conf.*, Baltimore, MD, 1991, pp. 2336-2346.

44. Roy, N. A., Girard, A. and Bugeat, L.-P., "Enhanced Updating of Finite Element Models Using an Energy Approach," *Proceedings of the 11th International Modal Analysis Conference*, Orlando FL, February 1993, pp. 655-660.

45. Farhat, C. and Hemez, F., "A Sensitivity-Based EBE Method for Updating Finite Element Dynamic Models," CSSC Report CU-CSSC-92-02, University of Colorado, Boulder, submitted to *AIAA Journal*, 1992.

46. Imregun, M. and Ewins, D. J., "An Investigation into Mode Shape Expansion Techniques," *Proceedings of the 11th International Modal Analysis Conference*, Orlando FL, February 1993, pp. 168-175.

47. Lancaster, P. and Maroulas, J., "Inverse Eigenvalue Problems for Damped Vibrating Systems," *Journal of Mathematical Analysis and Applications*, Vol. 123, No. 1, 1987, pp. 238-261.

48. Starek, L. and Inman, D. J., "On the Inverse Problem with Rigid-Body Modes," *ASME Journal of Applied Mechanics*, Vol. 58, December 1991, pp. 1101-1104.

49. Smith, S. W. and McGowan, P. E., "Locating Damaged Members in a Truss Structure Using Modal Data: A Demonstration Experiment," NASA Technical Memorandum 101595, April 1989.

50. Kashangaki, T. A-L., Smith, S. W. and Lim, T. W., "Underlying Modal Data Issues for Detecting Damage in Truss Structures," AIAA Paper 92-2264-CP, *Proceedings of the 33rd Structures, Structural Dynamics and Materials Conf.*, April, 1992.

51. Zimmerman, D. C. and Smith, S. W., "Model Refinement and Damage Detection for Intelligent Structures," book chapter in *Intelligent Structural Systems* (H. S. Tzou, editor), Kluwer Academic Publishers, 1992.

52. Zimmerman, D. C. and Kaouk, M., "Structural Damage Detection Using a Minimum Rank Update Theory," Submitted for publication to *ASME Journal of Vibration and Acoustics.*

53. Doebling, S. W., Hemez, F. M., Barlow, M. S., Peterson, L. D. and Farhat, C., "Damage Detection in a Suspended Scale Model Truss via Model Update," *Proceedings of the 11th International Modal Analysis Conference*, Orlando Fl, February 1993, pp. 1083-1094.

54. Hemez, F. and Farhat, C., "Locating and Identifying Structural Damage Using a Sensitivity-Based Model Updating Methodology," *Proceedings of the 34th Structures, Structural Dynamics and Materials Conf.*, La Jolla, CA, April, 1993.

55. Alvin, K. F., Park, K. C., and Belvin, W. K. (1992) "A Second-Order Structural Identification Procedure via State Space-Based System Identification," *Proceedings of the 1992 AIAA Guidance, Navigation and Controls Conference*, Hilton Head, SC, August, 1992, pp. 1600-1611., to appear in *AIAA Journal.*

56. Alvin, K. F., Park, K. C. and Peterson, L. D., "Extraction of Undamped Normal Modes and Nondiagonal Modal Damping Matrix from Damped System Realization Parameters," *Proceedings of the 34th Structures, Structural Dynamics and Materials Conf.*, La Jolla, CA, April 1993, AIAA Paper 93-1653.

57. Alvin, K. F., Peterson, L. D. and Park, K. C., "A Method for Determining Minimal-Order Mass and Stiffness Matrices from Modal Test Data," *Proceedings of the 11th International Modal Analysis Conference*, Orlando Fl, February 1993, pp. 1287-1293.

58. Guyan, R. J., "Reduction of Stiffness and Mass Matrices," *AIAA Journal*, Vol. 3, No. 2, p. 380, 1965.

59. Craig, R. R. and Bampton, M. C., "Coupling of Substructures for Dynamic Analyses," *AIAA Journal*, Vol. 6, No. 7, pp. 1313-1319, 1968.

60. *PRO-Matlab User's Guide*, The MathWorks, Inc., 1989.

61. Peterson, L. D., "ModalID User's Manual," 1992.

62. Peterson, L. D., Alvin, K. F., Doebling, S. W. and Park, K. C., "Damage Detection Using Experimentally Measured Mass and Stiffness Matrices," *Proceedings of the 34th Structures, Structural Dynamics and Materials Conf.*, La Jolla, CA, April, 1993.

63. Felippa, C. A. and Park, K. C. (1978) "Computational Aspects of Time Integration Procedures in Structural Dynamics. Part 1: Implementation," *Journal of Applied Mechanics*, Vol. 45, No. 3, pp. 595-602.

64. Park, K. C., Belvin, W. K., and Alvin, K. F., "Second-Order Discrete Kalman Filtering Equations for Control-Structure Interaction Simulations," to appear in *Journal of Guidance, Control and Dynamics*, 1993.

65. Brigham, E. O., *The Fast Fourier Transform and Its Applications*, Prentice Hall Inc., 1988.

66. Bendat, J. S. and Piersol, A. G., *Engineering Applications of Correlation and Spectral Analysis*, John Wiley and Sons, 1980.

67. Juang, J.-N., Phan, M., Horta, L. G., and Longman, R. W., "Identification of Observer/Kalman Filter Markov Parameters: Theory and Experiments," *Proceedings of the AIAA Guidance, Navigation and Controls Conference*, August 1991, pp. 1195-1207.

68. Fletcher, R. *Practical Methods of Optimization*, Second Edition, John Wiley and Sons, 1987.